12-2020

Seismic Loading Effects within Orthogonally Connected Steel Lateral Force Resisting Systems

Alhussin Faraj Aliwan
University of Arkansas, Fayetteville

Seismic Loading Effects within Orthogonally Connected Steel Lateral Force Resisting Systems

A dissertation submitted in partial fulfillment
of the requirements for the degree of
Doctor of Philosophy in Engineering

by

Alhussin Faraj Aliwan
University of Garyounis
Bachelor of Science in Civil Engineering
University of Tripoli
Master of Science in Construction Engineering

December 2020
University of Arkansas

The dissertation is approved for recommendation to the Graduate Council

_____
Gary Prinz, Ph.D.
Dissertation Chair

_____
Micah Hale, Ph.D.
Committee Member

_____
Shengfan Zhang, Ph.D.
Committee Member

_____
Cameron Murray, Ph.D.
Committee Member

ABSTRACT

Steel buildings located within seismically active regions require special design considerations to ensure public safety and prevent collapse during an extreme seismic event. Two commonly used steel systems are special moment frames (SMFs) and buckling-restrained braced frames (BRBFs). When two seismic systems share a common column in an orthogonal configuration (such as at a building corner), design specifications currently consider a 100+30 rule wherein the shared column is designed for 100% fuse demand in one direction, plus 30% fuse demand from the other direction. While this rule has been shown to be reasonable for elastic building response, a few studies performed on inelastic systems suggest that the 100+30 rule may not be reasonable for systems expected to experience significant inelastic response.

This study investigated nonlinear effects resulting from simultaneous earthquake loading of orthogonally oriented seismic systems. Detailed nonlinear time-history analysis of three-dimensional frame configurations was considered, addressing coupled and non-coupled orthogonal system effects on resulting shared column demands. Various seismic system pairs (sharing a column) are considered, including both moment frames and braced frames.

Results indicate that the current 100+30 rule is non-conservative for some frame-type combinations. Bidirectional seismic effects in coupled steel systems showed increased column axial demands over independent demand additions from un-coupled (unidirectional loading) analyses. Braced-frame-to–moment-frame configurations were more affected by bidirectional lateral forces than braced-frame-to-braced-frame orthogonal configurations. Additionally uncoupled steel systems experienced higher inter-story drift demands than the coupled frame configurations of the same geometry. A new approach to estimating shared column demands in orthogonal seismic systems was proposed herein.

ACKNOWLEDGMENTS

I gratefully acknowledge the funding support that made my Ph.D. work possible. I was funded by my country, Libya, which has a unique place in my heart. I am grateful to the people who have supported me throughout my academic study and research. I would first like to thank my adviser, Dr. Gary Prinz, who guided me in selecting the final theme for this research. I would not have been able to do the research and achieve the results presented here without his help and support. His recommendations and instructions were similarly essential to the writing of this dissertation. I would also like to thank the Committee Members: Dr. Micah Hale, Dr. Cameron Murray, and Dr. Shengfan Zhang, as well as all my instructors who throughout my educational career have encouraged me. Their direction made it possible for me to accomplish my highest academic goals. Finally, I would like to thank my family for their moral support during my college career and the completion of this dissertation.

To them, I am eternally grateful.

TABLE OF CONTENTS

LIST OF FIGURES

LIST OF TABLES

LIST OF TERMS

OMF	Ordinary Moment Frames
IMF	Intermediate Moment Frame
SMF	Special Moment Frame
RBS	Reduced Beam Sections
h	Distance between the centerline of the flanges
t	Column flange thickness
MF	Moment frame
BRBF	Buckling-restrained braced frames
BRB	Bucking-restrained brace
MCR_R	Maximum considered earthquake spectral response acceleration parameter
S_{D1}	Spectral response acceleration parameter at a period of 1 sec
S_{DS}	Spectral response acceleration parameter at short period
S_{MS}	the MCE_R,5% damping, spectral response acceleration parameter at short period
S_{M1}	the MCE_R,5% damping, spectral response acceleration parameter at a period of 1 sec
Cs	Seismic response coefficient
R	Response modification factor
V	Seismic base shear
W	Effective seismic weight of the building
ZRBS	Section Modulus of Reduced Beam Section
Zx	Plastic Section Modulus of a member
Z_e	Effective plastic modulus of a section at the location of a plastic hinge

V_{RBS}	Larger of the two values of shear force at the center of the reduced beam section at each end of a beam
h_i, h_x	the height above the base to the level *i* or *x*
W_i, W_x	Portion of W that is located at or assigned to level *i* or *x*
M_{pc}	Moment capacity at the column face
M_{pb}	Plastic moment
M_f	Moment beam demand at the column face
Mpr	Moment capacity at the column face
VP	Plastic Shear at reduced beam section location
a	Horizontal distance between a column flange and the start of the reduced beam section.
b	Length of an RBS cut
c	Depth of cut at the center of the reduced beam section
K_e	Effective stiffness
K_i	Effective stiffness ai level *i*
E	Models of elasticity
I_c	Moment of inertia of the column
I_b	Moment of inertia of the beam
Δ	Inter-story drift
Δ_a	the available inter-story drift by AISC provisions
C_d	Deflection amplification factor
$I_{req.}$	Required moment of inertia
A_{cor}	the cross-sectional areas of the BRBs

F_b	the axial force of the BRBs
Fy	the yield strength of the BRBs
$F_{b,\,ULT}$	ultimate strengths of the BRBs
β	the compression strength adjustment factor
ω	strain-hardening adjustment factor
Ry	material over strength factor
α	the uniaxial stress
α_0	the yield stress
ε_0	the yield strain
ε_r	the strain at the last load reversal
Lc	the length of the restrained yielding piece of BRB
Lt	Restrained non-yielding piece of BRB
Lj	Unrestrained non-yielding segments piece of BRB
$L_{br,Yield}$	Restrained yielding part of BRB
E_{eff}	Effective modulus of elasticity
T_A, T_B	Lower and upper response periods, (0.2T) and (1.5T) respectively
S_a^{target}	the target acceleration response spectrum
S_a^{actual}	the acceleration response spectrum of the actual acceleration time history
V	Story shear force
Ve	Elastic story shear force from equivalent lateral force procedure
(V/Ve)	the normalized base shear under the equivalent lateral forces
PGA	Peak ground acceleration

CHAPTER 1: INTRODUCTION

1.1 Introduction

Steel buildings located within seismically active regions require special design considerations to ensure public safety and prevent collapse during an extreme seismic event. Two common steel systems used to provide sufficient stiffness and ductility for earthquake force dissipation are special moment frames (SMFs) and buckling-restrained braced frames (BRBFs). SMFs rely on rigid beam-to-column connections and special connection detailing to provide lateral stiffness and create highly ductile frame regions for damage control, while BRBFs use special brace elements to dissipate seismic energy through stable tension-compression brace yielding. In both system types, damage is intended to be controlled within highly ductile components (acting as a sort of structural fuse) while surrounding building structural systems remain mostly un-damaged.

Controlling damage in the structural fuse regions is typically achieved by using a capacity-based-design approach, wherein surrounding frame demands are determined from the fully strain-hardened capacity of the structural fuse element of the seismic system (SMF, BRBF, etc.). For example, in capacity based design of BRBFs, the brace of a BRBF is proportioned to resist the applied seismic demand, while the surrounding beams and columns in the BRBF are proportioned based on demands from the fully strain-hardened brace capacity (ensuring the brace as the "weakest-link").

When two seismic systems share a common column in an orthogonal configuration (such as at a building corner), it is unreasonable to expect the shared column to carry 100% of each fuse demand (due to earthquake directionality effects). In such shared column orthogonal

configurations, design specifications currently consider a 100+30 rule wherein the shared column is designed for 100% fuse demand in one direction, plus 30% fuse demand from the other direction.

The 100-30 percent rule has appeared in design recommendations since the late 1970's (ATC, 1978). The perceived theoretical basis for the 100+30 rule likely originated from work by Newmark (1975) and by Rosenblueth and Contreras (1977). Menun and Der Kiureghian (1999) demonstrated that the 100+30 rule, 100+40 rule, and square root sum of the squares (SRSS) rule for orthogonal combinations are special cases of a complete quadratic combination (CQC3) rule. The accuracy of the 100+30, 100+40, and SSRS for elastic systems depends on the reference system of the building relative to the "principle directions" of the earthquake loading. While these rules have been shown to be reasonable for elastic building response, limited studies performed on inelastic systems suggest that the 100+30 rule may not be reasonable for systems expected to experience significant inelastic response. For example, in MacRae and Mattheis (2000) near-fault ground motions applied to a 3-story steel moment frame building resulted in column demands (resulting from large drifts in two orthogonal directions) that exceeded those determined using the 100+30 rule.

The work presented herein aimed to provide guidance on nonlinear effects resulting from simultaneous earthquake loading of orthogonally oriented seismic systems (of differing type and geometry). Detailed nonlinear time-history analyses of three-dimensional frame configurations were considered herein, addressing coupled and non-coupled orthogonal system effects on the resulting shared column demands. Earthquake incident angle was varied to identify any coupled system effects (as compared to the un-coupled analyses) and various seismic-system pairs (sharing a column) were considered, including both moment frames and braced frames.

The following section presents an outline of the dissertation organization, describing the relevant background literature, analysis methodology, research approach, results and conclusions on shared column effects in orthogonally connected seismic systems.

1.2 Organization of the Dissertation

This research dissertation is divided into six chapters describing the relevant background, seismic system design, analysis approach (involving both coupled and uncoupled orthogonal systems), relevant results, and conclusions.

The following chapter, Chapter 2, presents relevant background on orthogonality considerations in connected seismic systems, and describes the creation of current rules for seismic system demand estimations used in design. Additionally, Chapter 2 provides a summary of steel seismic systems considered in this research (including common moment and braced frame systems).

Chapter 3 presents design considerations for the special moment frames (SMF) and buckling-restrained braced frames (BRBFs) to be analyzed herein, which are developed for two different seismic hazard levels (representing two different seismic zones). The two zones considered are located within Los Angeles, CA, and Salt Lake City, UT. To investigate orthogonality effects and the applicability of the considered 100+30 design rule, frame designs consider orthogonal connections between two frame types: special moment frame with buckling-restrained braced frame (SMF-BRBF), and buckling-restrained braced frame with buckling-restrained braced frame (BRBF-BRBF).

In Chapter 4, orthogonality effects for uncoupled and coupled steel seismic configurations are analyzed using advanced, dynamic, time-history simulations. Time-history analyses in Chapter

4 are all performed using the Open System for Earthquake Engineering Simulation (OpenSees). Two seismic systems in multiple building-height configurations were considered in Chapter 4: 1) special moment frames (SMFs) in 6- and 9-story configurations, and 2) buckling-restrained braced frames (BRBFs) in 6-, 9-, and 12-story configurations. Each configuration is dynamically loaded under ten scaled ground motions in two combinations (BRBF-BRBF and SMF-BRBF). Column demand comparisons with current design provisions are made for all configurations. In addition, mean maximum inter-story drift of the shared column is investigated to identify interaction effects.

Chapter 5 investigates the influence of dynamic loads on uncoupled and coupled steel frames using more detailed finite element analyses capable of identifying local damage. The commercial finite element software ABAQUS is used for all analysis configurations of Chapter 5. 6-story coupled and uncoupled steel configurations considered. Due to the computational cost of more detailed finite element simulations, only one of the ten scaled earthquakes used in the Chapter 4 time-history analysis, is considered.

Chapter 6 provides a summary of the orthogonality effects resulting from different seismic system configurations and presents key conclusions for improved estimation of shared-column demands.

CHAPTER 2: OVERVIEW OF BI-DIRECTIONAL EARTHQUAKE EXCITATION RULES FOR AND RELEVANT SEISMIC SYSTEM OVERVIEW

2.1 Introduction

Internal forces in structural elements commonly develop due to the combined effects of seismic loading. The seismic regulations and guidelines for buildings and bridges prescribe combination rules to estimate the maximum structural response under simultaneous earthquake excitation and multi-directional seismic loads. Bi-directional effects of seismic loads can be considered using the spectrum intensity concept. According to the Pacific Earthquake Engineering Research (PEER) ground motion data base every earthquake exhibits three response spectra: acceleration, displacement, and velocity. Every response shows three directions: two are horizontally perpendicular and one is vertically perpendicular (two in the horizontal plane and one in the vertical direction).

To prevent plastic strain, structural members should be designed to withstand seismic loads from all orientations. Insufficient element sizes could result by following the structural design based on considering the orthogonal seismic effects separately and then inappropriate axial force distribution in the members could develop due to the combined effects of earthquakes [2]. A skew seismic shaking, for instance, may induce large column moments under simultaneous yielding of the beam at the same level. Therefore, the elasticity of columns under uniaxial forces and bending moments can become inelastic due to biaxial force and bending moments.

In practice, the principle axes of seismic design are not known, therefore, it is common to design for the worst case [i.e. for that direction of the principal axes that yields the maximum response (PGA)].

2.2 Current Multicomponent Combination Rules

The bi-directional effects of lateral loads were investigated and introduced to design structures in seismic areas. Current regulations address multicomponent effects by combining the orthogonal effects of seismic loading using a percentage rule or square root of sum of squares (SRSS) rule. Two sets of axes are assumed for the multicomponent combination effects: the first one defines the principal orientation of the seismic loads, while the other specifies the building model as shown in Figure 1. The two coordinate systems are related, horizontally, by θ, and the third direction is vertical for the both coordinate systems. The *X* and *Y* symbolize the configuration axes, while X_1 and Y_1 show the principle axes of ground motion. The seismic design rules assumed θ is moving counterclockwise and the location of the earthquake and building principle axes have harmonic motion (symmetrical movement).

2.2.1 The Concept of Percentage Rules

Two percentage rules were presented to determine the response quantity from the orthogonal components of seismic loading by Newmark (1979). The rule assumed the result of orthogonal effects (R) is 100% of the response from one orientation plus a percentage (α) of the response from the other two directions as illustrated by Equations 2.1 to 2.3, where R_1, R_2, and R_3 are the seismic response from the orthogonal component of an earthquake. Summarizing, three cases are considered, and the biggest response should be used in the design.

$$R = R_1 + \alpha R_2 + \alpha R_3 \qquad \text{Eq. 2. 1}$$

$$R = \alpha R_1 + R_2 + \alpha R_3 \qquad \text{Eq. 2. 2}$$

$$R = \alpha R_1 + \alpha R_2 + R_3 \qquad \text{Eq. 2. 3}$$

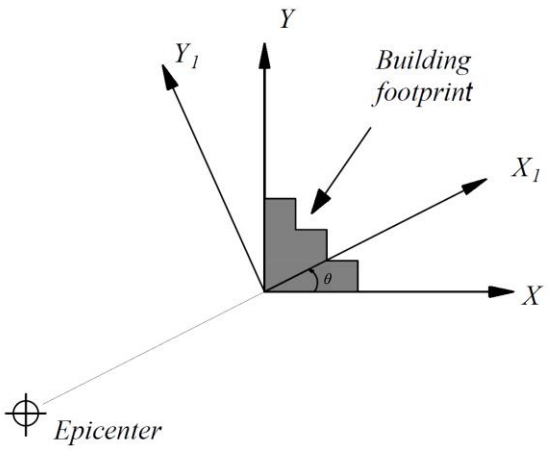

Figure 1. Interaction between the principal axes of structure and an earthquake (Definition of θ in the horizontal coordinates).

The contribution of the other component (α) was assumed to be 30% by Bosenblueth and Contreras in (1977) and adopted by the Uniform Building Code (UBC 1997) and Caltrans bridge design specifications (Caltrans, 1990) with some modifications. They used two horizontal components (R1, R2) (Equation 2.1, 2.2) and neglected the vertical direction (R3=0). Newmark (1975) suggested using 40% as a contribution of the orthogonal effects of seismic loading.

2.2.2 The Concept of the square-root of sum of squares (SRSS) rule

The concept of the SRSS rule is similar to the percentage rules; however, this rule assumes the three responses (R1, R2, and R3) are statically independent, and the overall response equals the square-root sum of squared individual components as illustrate in Equation 2.4.

$$R = \sqrt{R_1^2 + R_2^2 + R_3^2} \qquad \text{Eq. 2.4}$$

The rule does not consider interactions between the structure and earthquake and would only be valid when principle earthquake axes coincide with the assumed ground motion components. According to the Caltrans Specifications for Bridges (Caltrans, 1995), principle

earthquake axes cannot be assumed to coincide with the axes of the building. Therefore, the earthquake components could be correlated, and this correlation is not taken into account by the SRSS rule.

2.3 Degree of Freedom of Structures under the Orthogonal Effects of Earthquakes

2.3.1 Single Degree of Freedom Systems

Peak ground acceleration is used to evaluate the intensity of an earthquake, and the maximum elastic deformation in a building through the seismic loading indicates the significant ground motion intensity. Figure 2 shows a single degree of freedom system subjected to bi-directional seismic loading. The strong acceleration (based on PGA) is assumed to be in the x-axis, which maximizes axial force in the system; whereas, the other horizontal seismic acceleration affects the y-axis. The resultant direction of the two horizontal orientations is illustrated in Figure 2. These accelerations were conducted by using Beverly Hills-12520 Mulhol strong motion record, which is considered to be representative of motions experienced by structures during the Northridge earthquake (see Table.1).

According to the percentage rules, the maximum axial force expected in the structural element under these combined accelerations could be estimated by considering internal forces developed in the principal orientation (x) plus a percentage of the other direction's contribution (y). For design purposes, only the strong horizontal acceleration (the principle component) is considered as illustrated in Equation 2.5. Most current building codes use this procedure to evaluate the effect of bi-directional components, and then the factor (α) is an essential percentage to specify the combination rules [2].

$$R_{xy} = R_x + \alpha R_x \qquad \text{Eq. 2.5}$$

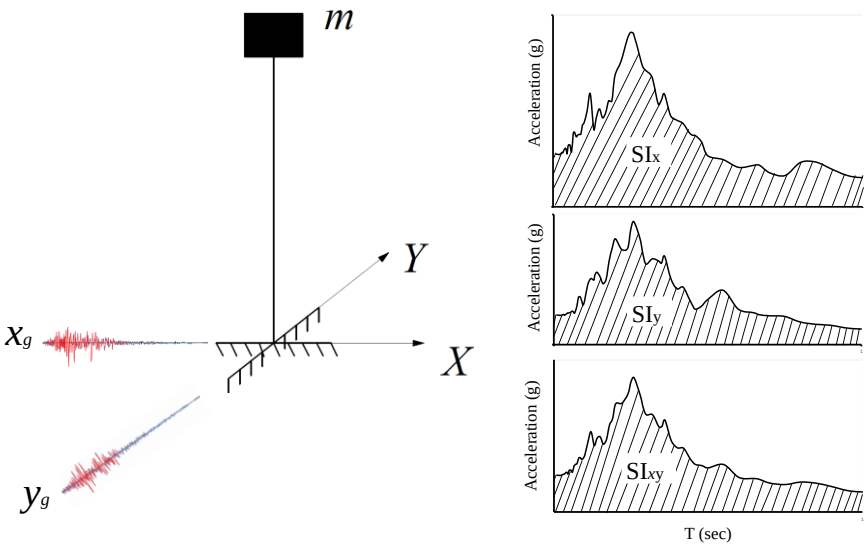

Figure 2. Bi-directional earthquake excitation and spectrum intensities for individual component and results for single degree of freedom.

2.3.2 Two Degree of Freedom Systems

The fundamental concept of this dynamic system is structures have two independent coordinates to describe their movement. The motion may or may not be in the same coordinate direction. The two degree of freedom (D.O.F) system has displacement (Δ) and rotation (θ). The displacement could be in one direction (Δ_x) or two orientations (Δ_x, Δ_y), and the same is true for rotation (θ_x) or (θ_x, θ_y).

In this study, to investigate the bi-directional seismic loading on configurations, uncoupled steel frames were modeled under the concept of two D.O.F dynamic systems in two directions (Δ_x, Δ_y, θ_x, and θ_y) using OpenSEES and ABAQUS software. Figure 3 shows a 6-story unjointed SMF, which represents two degrees of freedom under the combined coordinates. The x-, and y-axis are the principle orientations of the SMF and BRBF respectively; whereas, the X_1, and Y_1 are the assumed principle components of an earthquake. For uncoupled models, the principle directions of the structures and earthquakes were assumed to coincide; therefore, α in Equation 1.5 equals zero.

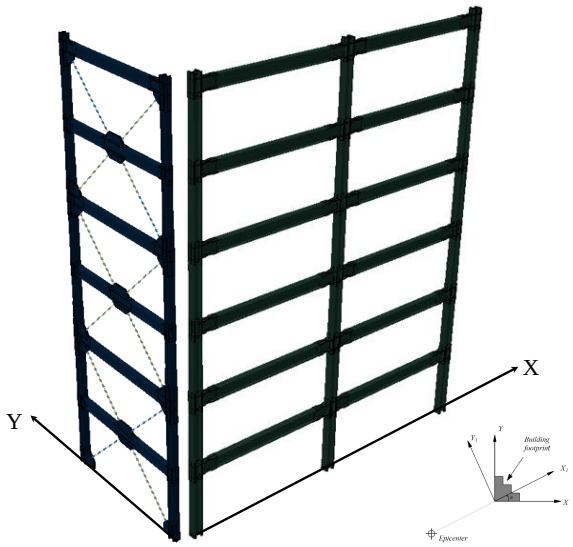

Figure 3. Bi-directional earthquake excitation for two degree of freedom (Uncoupled frames).

2.3.3 Three Degree of Freedom Systems

A vertical component (z-direction) is now taken into account. Dimensional movements and rotations are resolved into six components (Δ_x, Δ_y, and Δ_z) and (θ_x, θ_y, and θ_z) respectfully. This system is useful for investigating orthogonal effects of lateral loads on structures and determining the comprehensive behavior of the system.

Figure 4 shows a 3-dimentional system for SMF and BRBE under coupled steel systems, which is one of the models used for this project research. All the SMFs were in the x-direction, while the BRBFs are assumed in the y-direction; these axes picture the bi-directional components of the building. To investigate the orthogonal effects of an earthquake on a structure, the coefficient (α) was considered to be 30%; therefore, earthquake directions are skewed 30% counterclockwise to the building components. More specifically, 100% of the resultant force in the strong components plus 30% of the resultant force from the second horizontal direction are used for structural design.

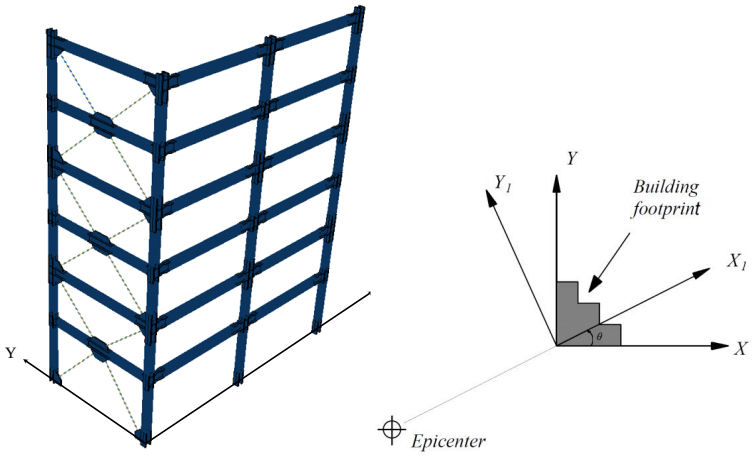

Figure 4. Bi-directional earthquake excitation for three degree of freedom (Coupled frames).

2.4 Overview of Steel Seismic Systems

Moment frame and braced frames are the primary framing systems for steel construction in seismically active areas. Braced frames show a higher lateral stiffness for drift control compared to moment configurations.

2.4.1 Steel Moment Frames

In the past years, moment frames commonly have been used in order to rsist high lateral forces when big openings are required. The strength and flexibility of steel structures are based on the connections between their beams and columns. Ordinary Moment Frames (OMFs), Intermediate Moment Frames (IMFs) and Special Moment Frames (SMFs) are the three types of steel moment frames used. Each kind of frame forms a system of columns and beams that are coupled together with partly or fully restrained moment joints. The differences among the three types account for each one's ability to resist ground motion shaking.

2.4.1.1 Ordinary Moment Frame (OMFs)

This kind of frame is formed from beams and columns that are connected by bolts and welds to form rigid joints. They resist the lateral loads through the bending in the beams and columns, and their ductility is small where the seismic reduction factor (R) equals 3.5. The OMFs are also expected to sustain limited inelastic deformations and are used in regions where there is no or low seismic ground shaking.

2.4.1.2 Intermediate Moment Frame (IMFs)

The IMFs are the next level up, designed to resist limited inelastic deformations as the result of lateral forces. As per the AISC, they must use pre-qualified connections or have passed a qualifying cyclic test, proving their ability to sustain inter-story drift angle of up to 0.02 radians. Thus, IMF's are only installed in low- to mid-seismic regions.

2.4.1.3 Special Moment Frame (SMFs)

The SMFs are commonly used configurations in seismically active areas, where they are designed to withstand dramatic inelastic deformation in both their members and connections when subjected to lateral forces. They also require the use of pre-qualified connections that have passed a qualifying cyclic test. These connections must sustain an inter-story drift angle of up to 0.04 radians (AISC) (ANSI/AISC 341-16) [1]. The SMFs are used in regions with mid- to high-seismic activity. A properly detailed SMF is one of the most ductile lateral-force resisting systems. A steel frame designed and detailed as a Special Steel Moment Frame (SMF) must meet all the AISC 341 requirements for beams, columns, and connections. Since the SMF is more ductile than an OMF, ASCE 7-16 assigns it an R factor of 8.0 versus an R factor of 3.5 for an OMF.

2.4.1.3.1 Reduced Beam Sections (RBS) in SMFs

Reduced beam section moment connections have become common in regions that have high seismic demands. The geometry of these connections is created by decreasing the dimensions of the beam flange as shown in Figure 5. The general concept of the RBS is to reduce the cross-section of the beam flange near the columns. This reduction causes an increase in enhancement balanced yielding and a decrease in the negative effects of seismic lateral forces on steel structures [45] [62].

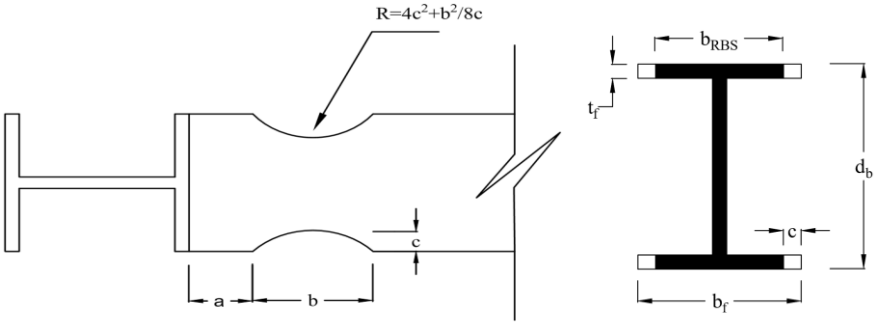

Figure 5**.** Typical geometry of radius-cut reduced beam section

A study was conducted by Kildashti et al. (2012) [8] to investigate the effect of the RBS in moment resisting frames. They concluded that there is a strong relationship between using these connections and the effects of P-Δ on the drifts, where they keep the best distribution of stresses and the flexibility along the height of the building can be achieved, which leads to a decrease in the value of P-Δ and then reduction of drifts. Moreover, in non-RBS moment frames, the deformation in top stories is based on the drift in ground stories; these values are small in RBS frames compared to non-RBS steel moment frames.

Steel structures without RBS are susceptible to cracking at the bottom of the flange weld, while structures with RBS have the ability to sustain the drift until 0.02 radians without disadvantages as shown by Swati and Gaurang [9]. Using RBS minimizes the stress concentration

at penal zones and gives these zones the ability to resist or reduce seismic influence on structures. Rahnavard et al. (2015) [4] concluded that steel structures with RBS are more ductile than other steel connections. A parametric study by Domingues, D. (2020) [54] on the effect of skew angle on the SMFs concluded that the size of columns has considerable effect on the column yielding. The deep and medium columns with considerable skew angles are expected to have more column twist than shallow columns, and the flexural capacity at the connection of special moment frames is reduced by increasing the skew angle. The local damage of RBS is reduced when the axial load of columns is increased; however, increasing the skew angle has the opposite effect.

An experimental and numerical study [9] concluded that the cyclic behavior with RBS connections reached 0.02 radians without any cracks in the welds, unlike beams without RBS moment connections. Chi and Uang (2002) [72] tested RBS moment connections with deep columns. They concluded that the ratio of the distance between the centerline of the flanges to the cubic column flange thickness (h/t_{cf}^3) has the largest effect on the torsion of columns, which increases in tandem with this ratio. Using more lateral bracing close to the RBS zone improves the strength against lateral torsional buckling, which comes from bending and warping stresses.

There is no doubt that reducing steel beam flanges leads to reducing the stiffness of connections and thus focuses the stresses in these components. The target region of the flanges is defined by reducing the moment capacity by about 10%, compared to the yielding moment (plastic moment). Therefore, the yielding will appear in this area instead of the zone around the field weld. An experimental study by Chen et al. (1996) [11] showed that only 3% of the stiffness value is wasted compared to non-cut beam flanges. This percentage is small and can be taken into consideration when calculating the required moment capacity.

2.4.1.3.2 Panel Zones in SMFs

Beam-column connections in SMFs develop inelasticity (plasticity) in beams and panel zones. The effectiveness of moment connections is dependent upon their ability to transfer shear forces and moments, which are developed in beams, to columns. Considerable shear forces and moments at moment connections lead to various failure modes such as fracture at their sides. Significant ductility could be achieved from panel zone deformation, and then inelastic deformation for the steel building is controlled by the high ductility potential of the panel zone.

Panel zones with balanced strength in connections give the structures more stability. The strong panel zones are designed so that the yielding happens in the beams. The weak panel zones are selected to raise the inelastic distortion of the panel zone. Increased ductility can be achieved by using weak panel zones rather than strong panel zones. Using strong panel zones in deep column connections is more effective when a lower probability of torsion and twist exists, as stated by Zhang, and Ricles (2006) [37] and Shin and Engelhard (2013) [38]. The ratio of story drift can also be increased when deep beams are used, as Hsiao et al [40] pointed out.

Using weak panel zones close to the beam strength with reduced beam-section moment connections can provide a better (more stable) hysteric response compared to the strong and balanced panel zones. The beams then have the ability to withstand lateral torsional buckling in the presence of the slab (Jones et al. 2002) [42].

2.4.1.3.3 Doubler and Continuity Plates in SMFs

Doubler and continuity plates are significant parts for getting a better performance of beam-column connection in SMFs. These elements are welded to column web and flanges in order to transfer the forces from beams to columns through the panel zone, preventing deformations.

Doubler plates are required to increase the shear strength of the column panel zone and to prevent it from yielding under the given loading, when the column web thickness is inadequate to resist the compressive and tensile flange force. Continuity plates, also known as panel zone horizontal stiffeners or column transvers stiffeners, are placed between column flanges to support transfer forces from beam flanges through the entire connection to the column. Providing these elements to the panel zone is essential when the column flange thickness is not enough to resist compressive and tensile forces.

A parametric study was carried out by Norwood and Prinz (2019) [44] on the effect of increasing the level of eccentricity between the beam flanges and continuity plates on the capacity of welded beam-to-column moment connections. A total of 12 beam-to-column connection frames considering two column sizes and six various levels of connection eccentricity, ranging from 0 to 6 in, were investigated. Norwood and Prinz concluded that the efficiency of continuity plates to transfer forces from beam flanges through the panel zone decreases whenever the eccentricity between beam flange and continuity plates has increased, and a new design equation was introduced to determine the capacities of beam-to-column connection at eccentricities 0 to 4.5 in. Berde et al (2017) [63] pointed out that using continuity plates with half the thickness of beam flanges could be enough instead of employing one that has the same thickness as the beam flange, based on an analytical study including frames with half and full thickness of beam flanges.

More details about designing the penal zones, doubler plates, continuity plates, and the AISC provisions and requirements for these elements are explained throughout the coming chapters.

2.4.2 Braced Steel Frames

2.4.2.1 Concentric Braced Frames

In this case, steel frames are provided by diagonal braces in their planes, where both ends are connected with beam-column joints to form a truss and create a stiff frame. Different configurations of concentric braced frames have been used such as V, X or one directional diagonal bracing as shown in Figure 6. The braces can act as tension and compression members that provide stability for the structure. The bracing is commonly used for mid-sized and high buildings because it provides strength in both directions. However, frames that are supported concentrically are less efficient terms of energy dissipation.

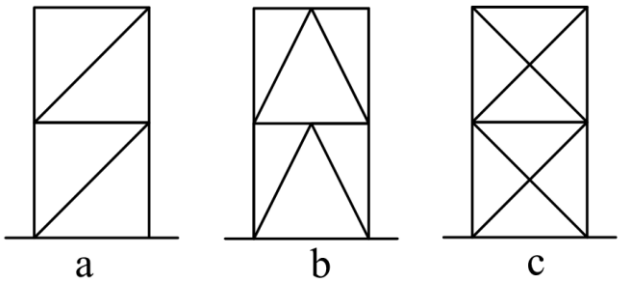

Figure 6. Typical concentric braced frames (a) diagonal bracing, (b) V bracing, (c) X bracing.

2.4.2.2 Eccentric Braced Frames

In addition to the beams and columns, eccentric braced frames consist of in-plane braces where one or both of the ends of the members are not touching the beam-column joint. Examples of various forms of these frames are shown in Figure 7. Braces have the ability to disperse the seismic loads (shear force) by transferring these forces to the columns of other braces. These frames have more ductility with greater energy dissipation proficiencies than the concentric braced configurations using the same materials.

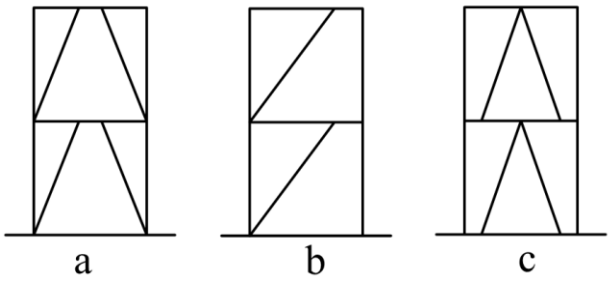

Figure 7. Typical Eccentric Braced Frames.

2.4.2.3 Buckling-Restrained Braced Frames

Buckling-restrained braced frames (BRBFs) are new systems used as fundamental lateral load-resisting systems for configurations in regions that are seismically active. The buckling-restrained braces form the substantial elements to enhance stability against lateral loads and are connected to the main frame via gusset plates. An experimental and numerical study by Prinz et al. [33] on BRBF behavior concluded that using top-flange beam splices leads to transfer of considerable axial forces and is effective at demands in the connection zones of these steel systems, where the gusset connection zone remained undamaged during cyclic loading until 0.06 rad. The performance of buckling-restrained braced frames with eccentric frames was tested under seismic loading by Prinz et al. (2011) [15]. They concluded that the maximum story drifts in these frames are almost the same as in eccentrically braced frames and have considerable residual drifts compared to similar eccentrically braced frames

2.4.2.3.1 Buckling-restrained Braces

Bucking-restrained braces (BRBs) offer stable and predictable hysteretic behavior, as they yield in tension and compression and provide considerable energy dissipation capacity and ductility, which makes them an appealing alternative to conventional compression-buckling braces. Figure 8 shows the general shape, composition installation, and the high performance in

tension and compression capacity for the BRBs compared to the traditional braces respectively. The steel core consists of three parts: restrained non-yielding segment at the middle, restrained non-yielding segment behind the yielding part, and unrestrained non-yielding segment at the ends.

A new type of BRBs was introduced by Qu et al. (2018) [61] that contains steel angle fuses. According to this study, considerable fuse strain levels and stable behavior were achieved under seismic loading. Morteza and Tremblay (2018) [71] investigated twelve full-scale BRBs with bolted steel restrained systems to evaluate their inelastic behavior. The proposed connection of BRBs showed considerable energy dissipation and high ductility capacity through the large amplitude cyclic loading. Also, considerable ductility was shown for the BRB system under the repeated fast-rate seismic deformation history, and then it could be qualified for long duration loading such as is found in seismic areas.

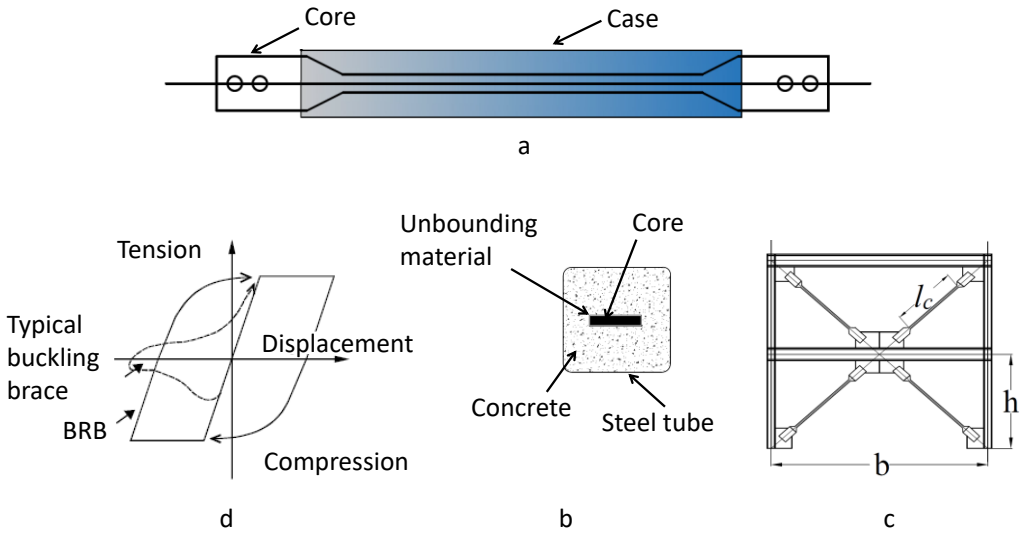

Figure 8. Buckling Restrained Braces a: General form. b. Cross-Section. c. Installation. d. Behavior under Cyclic Loads.

2.4.2.3.2 Gusset Plates

Gusset plate connections are either welded or bolted to the diagonal members and the framing elements of steel braced frames. Relying on the type of bracing systems, gusset plates are subjected to axial forces (tension or compression) from the braces. The axial loads transferred from the braces produce normal forces, shear and bending in these connections. The AISC Seismic Provisions (AISC 2016) dictate the design of brace frame gusset plates in seismic areas, a topic which is given more attention in the following tasks (ABAQUS).

CHAPTER 3. DESIGN OF PROTOTYPE SPECIAL MOMENT FRAME AND BUCKLING-RESTRAIND BRACED FRAME CONFIGURATIONS

3.1 Introduction

In this research, coupled and uncoupled SMFs and BRBFs with 6- and 9-story structures as shown in Figure 9 were designed to evaluate frame orthogonality effects during seismic loading. Additionally, 12-story BRBFs are considered to cover the highest elevation permitted for BRBFs in seismic areas. Each frame configuration was loaded using 10 earthquake ground motions in four different orientations 0, 30, 60, and 90 degrees as shown in Figure 10.

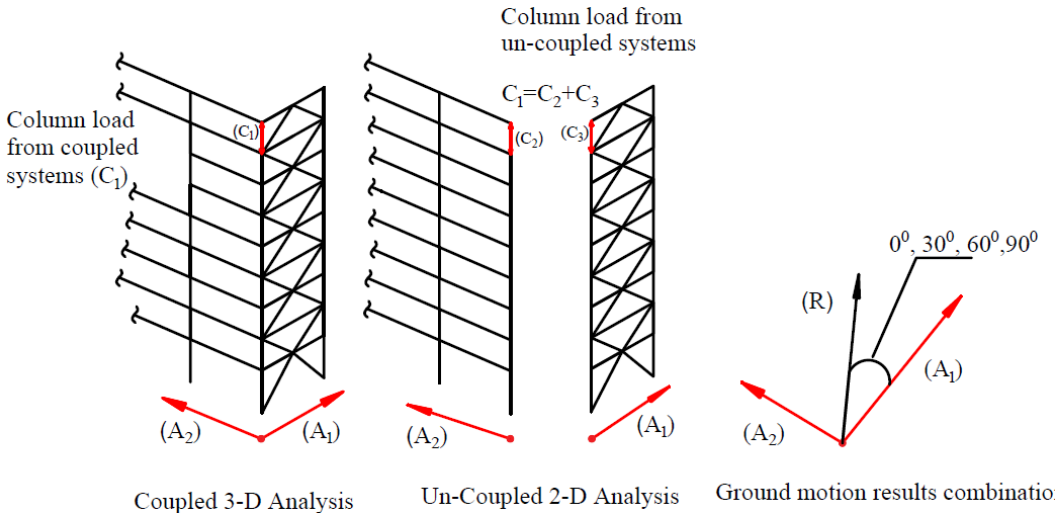

Figure 9. Investigation into interaction using un-coupled 2- and 3-D analysis.

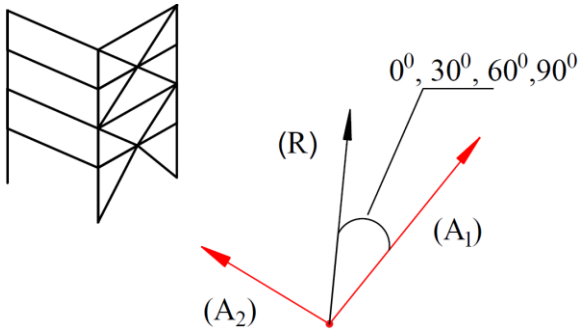

Figure 10. Application of ground motion resultant at 0, 30, 60, and 90 degrees.

To investigate the orthogonal effects on seismically loaded steel configurations in a 2-dimentional system, two types of steel systems have been designed. Models with 6- and 9-story levels were selected for the moment frames while frames with 6-, 9-, and 12-story levels were chosen for the braced frames. All structures were four bays wide and six bays deep with every bay being 30 feet long. The first story was 18 feet while the remaining stories were 13 feet in height. The SMFs and the BRBFs were investigated as moment frame coupled with moment frame (MF-MF), braced frame coupled with braced frame (BF-BF), and moment frame coupled with braced frame (MF-BF) as shown in Figure 9. To achieve better results and comparisons, the frames were designed considering two places with different seismic acceleration parameters: Los Angeles, CA, and Salt Lake City, UT.

Figure 11 shows multiple configuration shapes with various steel systems. It provides diversity of the configurations that will lead to a comprehensive study of the orthogonal effects of seismic loads on columns and an evaluation of their demands. Because of symmetry, one quarter of the building plan view is considered, and the lateral forces, bay dimensions and floor masses are taken from a SAC study [28].

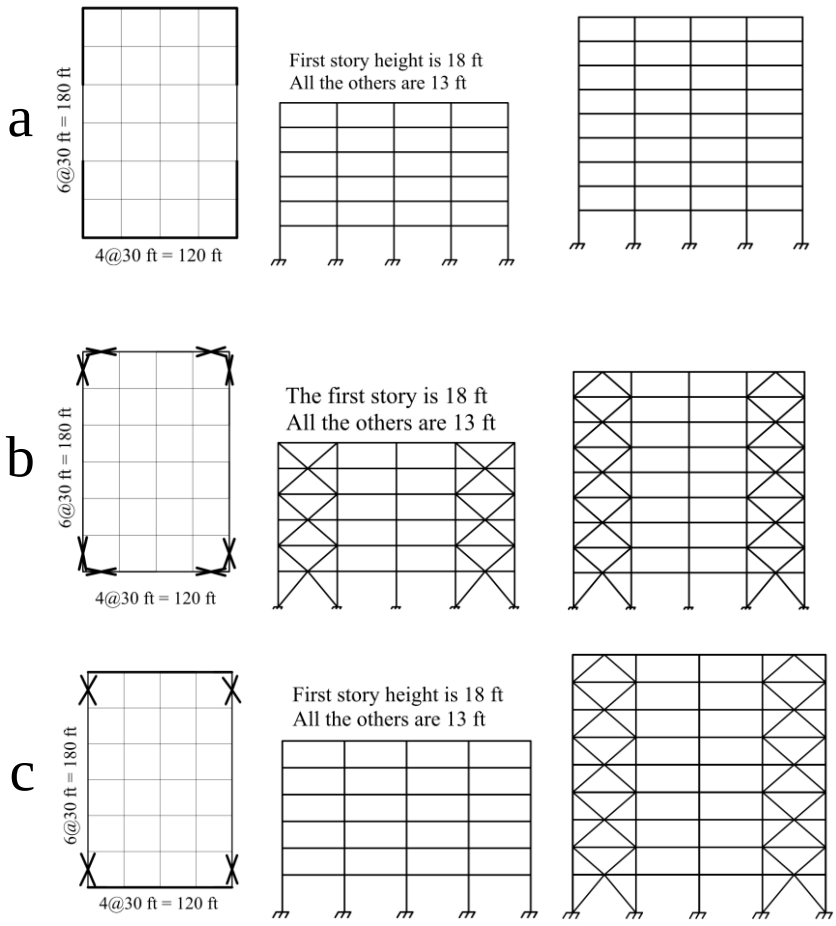

Figure 11. The 6- and 9-story moment and braced frames (a) MF-MF; (b) BF-BF; (c) MF-BF.

3.2 Seismic Design of Special Moment Frames

Special moment frames (SMFs) have been created to cover not only architectural needs, but also seismic requirements. Various forces, such as axial, shear and bending moments appear in the structure due to the lateral loads as shown in Figure 12. The SMFs are designed in accordance with AISC standards to withstand the seismic loads in addition to the gravity loads. Additional requirments are explained in AISC 341 for columns that are not designed as part of a seismic force-resisting structure.

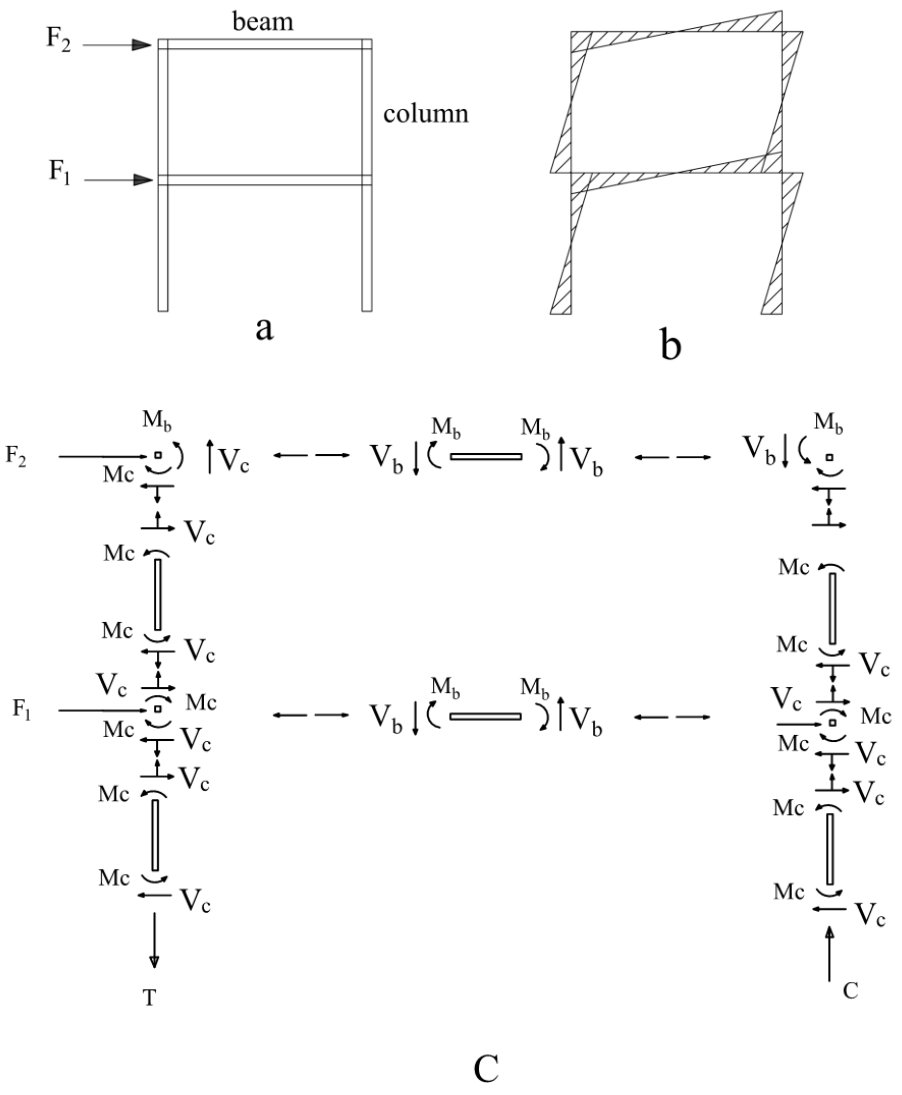

C

Figure 12. (a) Geometry of a moment frame; (b) The shape of moment diagram of lateral loads; (c) The force in columns, beams and panel zones.

3.2.1 Considering of Seismic Force

The guidelines outlined in ASCE 7-10 [1] were followed to design the special moment frames. Drift requirements of each story are the guidance to determine the beam and column design sizes for SMFs by design code. To determine the lateral forces caused by earthquakes, the spectral response acceleration parameter S_{D1} at a period of 1 sec and at short period S_{DS} can be determined

by following the equations 1 and 2 where they are equal to 0.820 and 1.560 for the Los Angeles site while 0.98 and 0.539 for the Salt Lake City site, respectively, as shown in Figure 13.

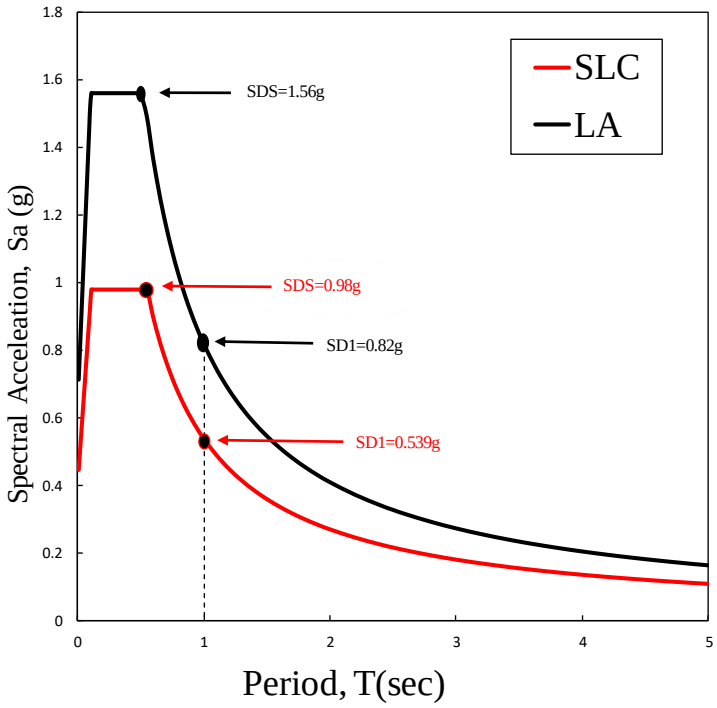

Figure 13. Design acceleration spectrums for LA and SLC.

$$S_{DS} = \frac{2}{3} S_{MS} \qquad \text{Eq. 2-1}$$

$$S_{D1} = \frac{2}{3} S_{M1} \qquad \text{Eq. 2-2}$$

Equation 2.3 illustrates how the seismic response coefficient (*Cs*) is calculated and (R) has been defined in ASCE-7 as 8.

$$C_S = \min\left(\frac{S_{DS}}{R} I, \frac{S_{D1}}{T}\frac{I}{R}\right) \geq 0.044\, S_{Ds} \geq 0.01 \qquad \text{Eq. 2-3}$$

The seismic base shear, V, and the vertical distribution of seismic force are defined according to the following equations:

$$V = C_s . W \qquad \text{Eq. 2-4}$$

Where

$$C_{vx} = \frac{W_x.h_x^k}{\sum_{i=1}^{n} W_i.h_i^k} \quad \text{Eq. 2-5}$$

h_i, h_x are the height above the base to level i or x, respectively

W_i, W_x are portion of W that is located at or assigned to Level i, or x, respectively

k is distribution exponent

The force at each level is calculated as:

$$F_x = C_{vx}.V \quad \text{Eq. 2-6}$$

3.2.2 Reduced Beam Section Design

Reduced beam sections are utilized to design the SMFs, where the beam flanges are trimmed off before the beam ends to specific dimensions. Using the RBS cuts in steel beams ensures that the maximum stress, caused by earthquakes, will occur away from the beam-column conections. The main goal for using RBS is to keep the high stresses away from columns that might cause failure. Dimensions of RBS are related to the cross-section of the beams and columns around it. Compared to welded unreinforced flange connections, using the RBS decreases the possible ductile fractures due to a significant reduction of plastic strain, which develops near the column face at RBS connection zones [4, 10, 12, 29, 37, 42].

Based on the size of beam and columns, the dimensions of the RBS are defined as shown in Figure 14. The dimensions of the RBS are calculated according to equations 7, 8 and 9. These specifications are defined in AISC-358 [1].

$$0.5\ b_f \leq a \leq 0.75\ b_f \quad \text{Eq. 2-7}$$

$$0.65\ d \leq b \leq 0.85\ d \quad \text{Eq. 2-8}$$

$$0.1\ b_f \leq c \leq 0.25\ b_f \qquad \text{Eq. 2-9}$$

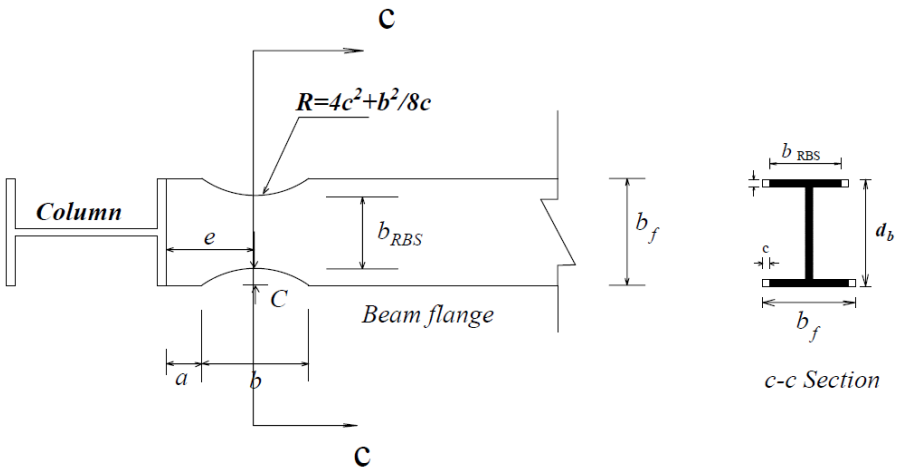

Figure 14. Typical geometry of radius-cut reduced beam section.

In this research, the values of a, b, and c are assumed to equal $0.75b_f$, 0.65d, and $0.2\ b_f$ respectively. In addition, AISC 358 formulations have been used to determine the moment at the column face and the moment capacity of the column where the ratio (M_{pc}/M_{pb} >1.0) between both is used to satisfy the strong column-weak beam criterion. The RBS is placed at a distance x from the column in order to prevent the stress from reaching the column, as shown in Figure 15. The dimensions of all RBS for 6- and 9-story SMFs are listed in Table 1 and 2.

$$M_f = M_{pr} + V_p(X) \qquad \text{Eq. 2-10}$$

$$M_c = M_{pr} + V_p\left(X + \frac{d_c}{2}\right) \qquad \text{Eq. 2-11}$$

The capacity of the column face is:

$$M_{pe} = R_y . Z_b . F_y \qquad \text{Eq. 2-12}$$

Where

$$X = a + \frac{b}{2} \qquad \text{Eq. 2.13}$$

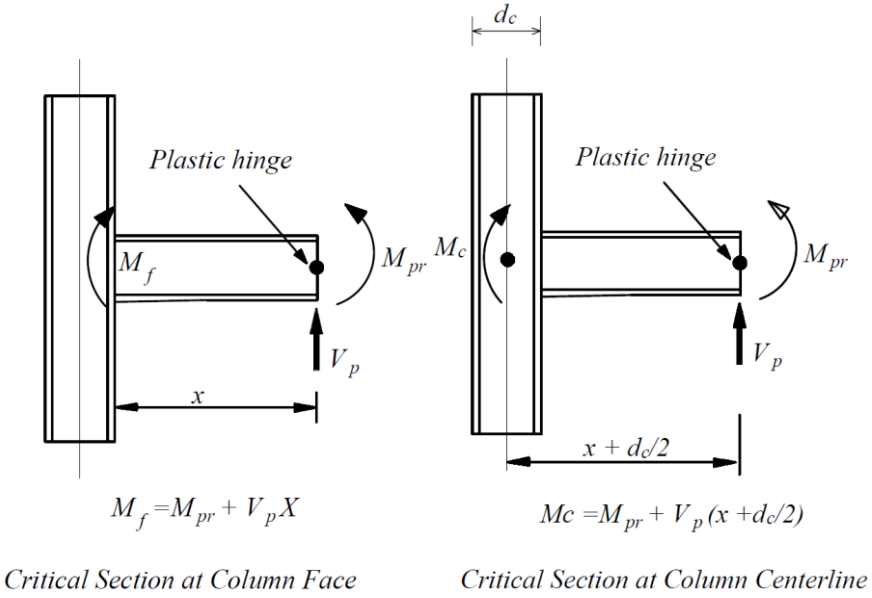

Figure 15. Calculation of demands at critical sections.

Table 1. Summary of RBS Dimensions for 6-Story SMF Beams.

Story	RBS Dimensions (in)							
	Los Angeles				Salt Lake City			
	A	B	c	$\frac{M_{pe}}{M_f}$ ratio	A	b	c	$\frac{M_{pe}}{M_f}$ ratio
1&2	9	17	2.5	1.04	9	15	2.5	1.09
3&4	9	16	2.5	1.09	6	15	1.5	1.02
5&6	9	16	2.5	1.08	6	15	1.5	1.01

Table 2. Summary of RBS Dimensions for 9-Story SMF Beams.

Story	RBS Dimensions (in)							
	Los Angeles				Salt Lake City			
	a	b	c	$\frac{M_{pe}}{M_f}$ ratio	a	b	c	$\frac{M_{pe}}{M_f}$ ratio
1&2	10	17	2.5	1.07	9	15	2.5	1.08
3&4	9	17	2.5	1.08	6	15	2.5	1.09
5&6	9	17	2.5	1.08	9	15	2.5	1.08
7&8	9	16	2.5	1.09	9	15	2.5	1.01
9	6	14	1.5	1.04	7	10	2	1.1

The seismic base shear was defined based on the seismic response coefficient C_s and the weight of the whole building, where C_s was calculated based on S_{D1}, S_{DS}, T, and R. To define the required moment of inertia, the stiffness, internal and external forces, and the drift were calculated based on equations 3-1 to 3-6. An example is provided in Appendix A. The member sizes of the beams and columns for 6- and 9-story SMFs in both locations, LA and SLC, are introduced in Tables 3 and 4.

$$k_e = \frac{6E}{h^2}\left[\frac{1}{\frac{h}{2I_C}+\frac{L}{I_b}}\right] \quad \text{Eq.2-14}$$

$$k_i = \frac{12E}{h^2}\left[\frac{1}{\frac{h}{I_C}+\frac{L}{I_b}}\right] \quad \text{Eq.2-15}$$

$$\Delta = \frac{V_{e.Avg}\,.h^2}{6E}\left[\frac{h}{2I}+\frac{L}{I}\right] \quad \text{Eq.2-16}$$

$$\Delta_a = 0.02\,h_{sx} \quad \text{Eq.2-17}$$

$$\Delta_{ae} = \frac{\Delta_a}{C_d} \quad \text{Eq.2-18}$$

$$I_{req.} = \frac{\Delta_a}{\Delta_{ae}} \quad \text{Eq.2-19}$$

Table 3. Summary of 6-Story SMF Members Sizes for Prototype Frames.

Story	**Size of the Sections**			
	Los Angeles		**Salt Lake City**	
	Beam	Column	Beam	Column
1	W24×279	W14×550	W24×131	W14×311
2	W24×279	W14×550	W24×131	W14×311
3	W24×192	W14×426	W24×103	W14×233
4	W24×192	W14×426	W24×103	W14×233
5	W24×162	W14×342	W24×84	W14×193
6	W24×162	W14×342	W24×84	W14×193

Table 4. Summary of 9-Story SMF Members Sizes for Prototype Frames.

Story	Size of the Sections			
	Los Angeles		**Salt Lake City**	
	Beam	Column	Beam	Column
1	W24×279	W14×550	W24×192	W14×398
2	W24×279	W14×550	W24×192	W14×398
3	W24×229	W14×455	W24×162	W14×342
4	W24×229	W14×455	W24×162	W14×342
5	W24×207	W14×426	W24×146	W14×311
6	W24×207	W14×426	W24×146	W14×311
7	W24×176	W14×398	W24×117	W14×283
8	W24×176	W14×398	W24×117	W14×283
9	W18×97	W14×145	W16×77	W14×132

3.3 Considering Seismic Design of Buckling-Restrained Braced (BRBF) Frames

The capacity-based method was followed to design 6-, 9- and 12-story level BRBFs, where the designed braces are considered as the weakest members in the configurations. This is carried out by designing the beams and columns of each bay to withstand maximum brace forces [5, 13, 66]. Figure 16 shows the analysis of the BRBs based on their locations and on the point of the intersection, either at the ends or the middle of the beams.

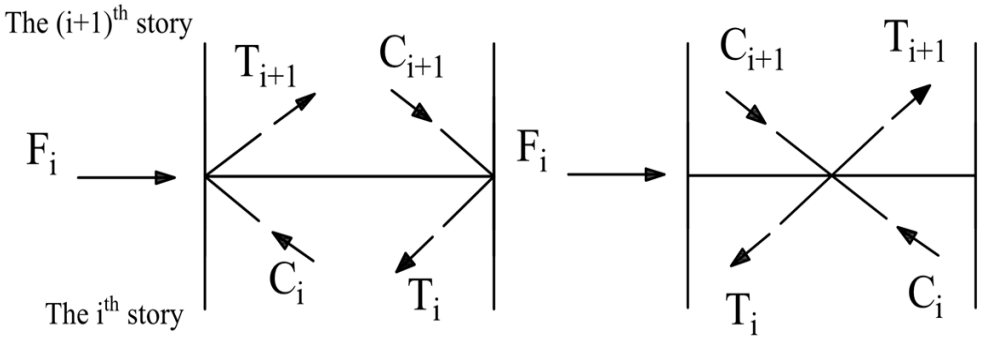

Figure 16. Typical analysis for 2-story X-bracing configurations.

The cross-sectional areas of the BRBs in the BRBFs are determined using Eq. 2-20, where the axial forces in the BRBs are calculated based on the forces obtained from the lateral loads analysis over the height of BRBFs

$$A_{cor} = \frac{F_b}{\emptyset F_y} \quad \text{Eq. 2-20}$$

Where A_{cor} is the cross-section area of core braces, F_b and F_y are the axial force and the yield strength of the BRBs respectively. Eq. 2-21 was used to determine the expected yield and ultimate strengths of the BRBs.

$$F_{b\_ULT} = \beta . \omega . R_y . F_y . A_{cor} \quad \text{Eq. 2-21}$$

Where β is the compression strength adjustment factor, ω is the strain-hardening adjustment factor, and R_y is the material overstrength factor. In this study, the coefficients $\beta, \omega,$ and R_y are estimated based on the properties of the BRBs presented by Star Seismic Inc. The value of the buckling-restrained brace overstrength factors ($\beta . \omega . R_y$) is 1.8 [15, 22]. Table 5 lists the cross-sectional area of the BRB yielding parts in both sites LA and SLC for 3-, 6-, and 12-story BRBFs. Member sizes for 6-, 9-, and 12-story BRBFs in the LA and SLC sites are listed in Table 6 through 8 respectively.

Table 5. Cross-sectional areas of the BRB yielding segments (in^2).

Floor	LA			SLC		
	6-Story	9-Story	12-Story	6-Story	9-Story	12-Story
1	19.54	22.56	27.86	12.84	15.19	18.86
2	18.76	22.28	23.51	12.34	14.05	18.77
3	17.17	21.63	23.23	11.29	13.72	18.55
4	14.64	20.52	22.72	9.62	13.12	18.15
5	11.06	18.87	21.94	7.26	12.18	17.53
6	6.37	16.62	20.83	4.19	10.83	16.64
7	-	15.34	19.35	-	9.02	15.46
8	-	10.1	17.46	-	6.7	13.95
9	-	5.67	15.11	-	3.81	12.07
10	-	-	12.26	-	-	9.8
11	-	-	8.88	-	-	7.1
12	-	-	4.93	-	-	3.94

Table 6. Summary of 6-Story BRBF Members Sizes.

Floor	Los Angeles		Salt Lake City	
	Beam	Column	Beam	Column
1	W21×44	W14×176	W21×44	W14×132
2	W21×44	W14×176	W21×44	W14×132
3	W21×44	W14×82	W21×44	W14×68
4	W21×44	W14×82	W21×44	W14×68
5	W21×44	W14×48	W21×44	W8×48
6	W21×44	W14×48	W21×44	W8×48

Table 7. Summary of 9-Story BRBF Members Sizes.

Story	Size of the Sections			
	Los Angeles		Salt Lake City	
	Beam	Column	Beam	Column
1	W21×93	W14×283	W21×44	W14×233
2	W21×44	W14×283	W21×44	W14×233
3	W21×44	W14×159	W21×44	W14×132
4	W21×44	W14×159	W21×44	W14×132
5	W21×44	W14×132	W21×44	W14×109
6	W21×44	W14×132	W21×44	W14×109
7	W21×44	W14×53	W21×44	W14×48
8	W21×44	W14×53	W21×44	W14×48
9	W21×44	W14×53	W21×57	W14×48

Table 8. Summary of 12-Story BRBF Member Sizes.

Story	Size of the Sections			
	Los Angeles		**Salt Lake City**	
	Beam	Column	Beam	Column
1	W21×93	W14×426	W21×44	W14×283
2	W21×44	W14×426	W21×44	W14×283
3	W21×93	W14×311	W21×68	W14×193
4	W21×44	W14×311	W21×44	W14×193
5	W21×93	W14×193	W21×44	W14×145
6	W21×44	W14×193	W21×44	W14×145
7	W21×44	W14×145	W21×44	W14×132
8	W21×93	W14×145	W21×44	W14×132
9	W21×44	W14×68	W21×44	W14×68
10	W21×93	W14×68	W21×44	W14×68
11	W21×44	W14×48	W21×44	W14×48
12	W21×44	W14×48	W21×68	W14×48

CHAPTER 4. DYNAMIC TIME-HISTORY DETERMINATION OF SHARED COLUMN DEMANDS IN ORTHOGONALLY CONNECTED SEISMIC SYSTEMS CONSIDERING COUPLED AND UNCOUPLED CONFIGURATIONS

4.1 Introduction

The Open System for Earthquake Engineering Simulation (OpenSEES) was used to model the SMFs and BRBFs in 2-dimensional systems [49]. The gravity loads are assigned to the beam-column joint nodes. A Giuffre-Menegotto-Pinto material model was taken as a reference to model all the members (Steel02 and F_y=50 ksi) [28] [46]. The beams and columns have been modeled as non-linear beam-column members with inelastic fiber sections, and all base columns are considered as fixed connections.

Another column is added to each model to consider P-delta effects, which represents one-quarter of the building gravity columns, connected with the main frames. The representative column is rigidly constrained to have the same deformation as the main model at each floor where the gravity loads were applied to each node corresponding to its story load. It has the same properties, strength, and stiffness as the gravity columns, and its base is modeled as a pinned connection. This approach is followed by several publications [28, 27, 26], which considered non-linear investigations.

4.2 Computer Modeling of Uncoupled Frames

4.2.1 Computer Modeling of SMFs

Four special moment frames (SMFs) were modeled as a moment frame with a reduced beam section and panel zone, as shown in Figure 17. The reduced beam section was modeled as rotational spring that followed a bilinear hysteretic response based on the modified Ibarra

Krawinkler deterioration model [47, 48]. The cyclic deterioration of the stiffness and strength can be determined using this model.

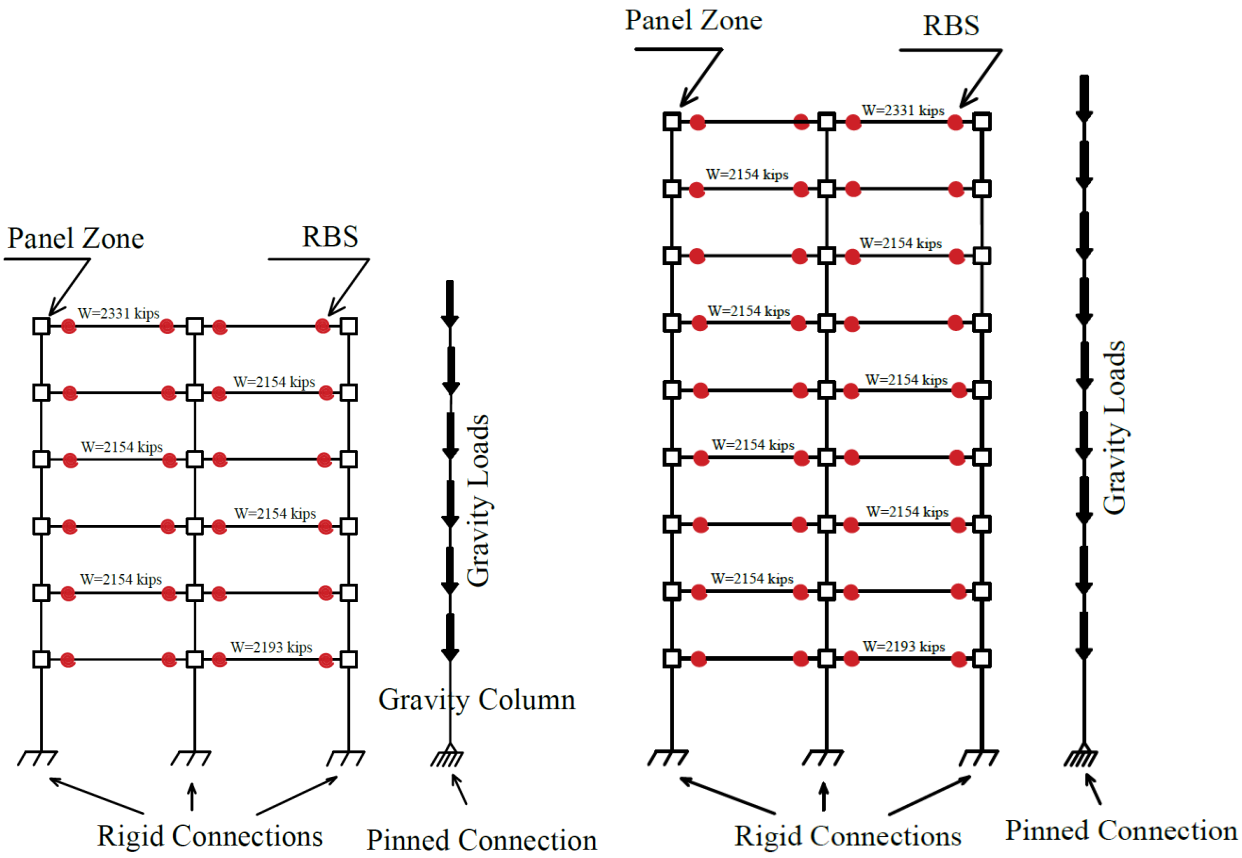

Figure 17. The OpenSees models for 6- and 9-Story SMFs.

4.2.1.1 Modeling of the Beams and Columns

Modeling beams, columns and bracing in OpenSees has two approaches using the physical theory model. The first method is distributed plasticity where the plasticity is spread along the element. The second one is lumped plasticity where plasticity is focused at the ends over an identified length and inside the element where it behaves elastically. The first approach is followed in this study where it allows a more realistic modeling of the elements (progressive yielding in the cross-section and along the element) and also allows for natural modeling of the interaction between bending and axial forces.

In this study, the moment at yield at RBSs of models is defined depending on the properties of the reduced section, and all the plastic hinges are modeled using rotational springs for the OpenSEES models. In addition, the part of the beam between the column and the RBS is modeled as an elastic beam-column element.

The webs and flanges of beams and columns are divided into small isolated elements. The flanges of the W-sections are divided into 16×4 fibers, while the web is divided into 16×2 fibers as shown in Figure 18. This division was based on the estimated direction of bending in the plane of frames. The beams and columns were modeled using non-linear beam-column elements with fiber discretization of the cross section.

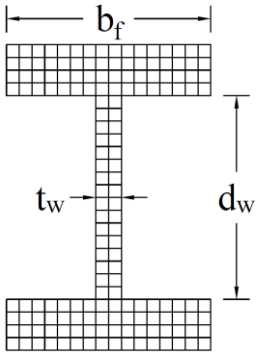

Figure 18. Fiber details of a W-section (beams and columns).

4.2.1.2 Modeling of the Panel Zone

The panel zone was modeled using an approach similar to those employed for the beams and columns where it primarily deforms in shear due to the opposing moments in the columns and beams. The model had a rectangular shape with two points at each corner, one of which had a rotational spring to represent shear distortions in the panel zone as shown in Figure 19. The four elements were modeled as elastic beam column elements. The gravity column was loaded by floor weights and linked to the main model to simulate P-Δ effects. Since loads cannot be

applied at the center of the beam-column joint, floor masses were lumped at the top node of the panel zone (node xy7). The lateral loads were applied at the centerline of the floor level along the right side of the panel zone (node xy05) [49].

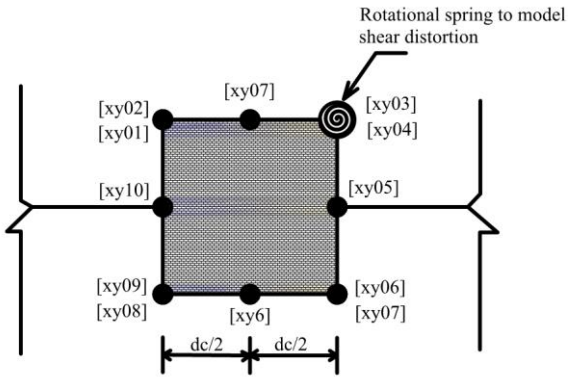

Figure 19. Nodes on the panel zone model.

4.2.1.3 Modeling of Buckling-Restrained Braced Frames BRBFs

Buckling-restrained braces have the ability to resist lateral loads. As a result, beams, columns and connections are not principally affected by the inelastic deformations. Six buckling-restrained braced frames with 6-, 9-, and 12-story structures were modeled as a truss frame where the buckling-restrained braces resist the tension and compression forces as shown in Figure 20.

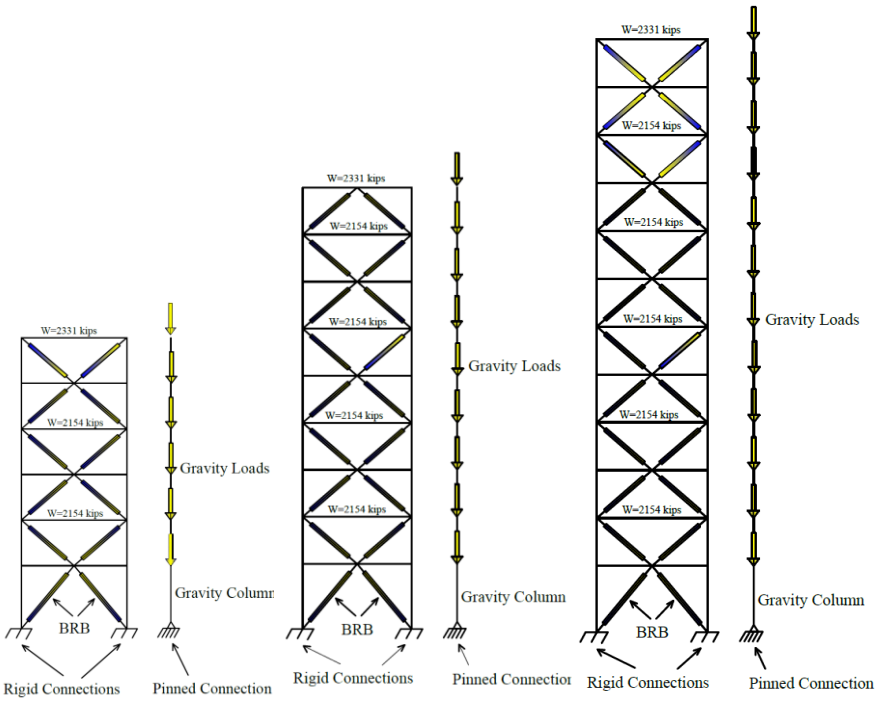

Figure 20. The OpenSEES models for 6-, 9-, and 12-Story BRBFs.

The buckling-restrained braces were modeled using the approach presented by Gupta and Krawinkler [28, 46, 50]. According to these publications, during shaking, the stresses and strains change constantly in accordance with equations 3-1 and 3-2, where R represents the parameter that controls the cyclic curve and is considered to change as a function of the plastic excursion ζ of the earlier loading. The modulus of elasticity and the transition of the slope change are based on the stresses in the braces, as shown in Figure 21.

$$\sigma^* = \frac{\varepsilon^*}{(1+\varepsilon^{*R})^{\frac{1}{R}}} \qquad \text{Eq. 3-1}$$

$$R = R_0 - \frac{a_1 \xi}{a_2 + \xi} \qquad \text{Eq. 3-2}$$

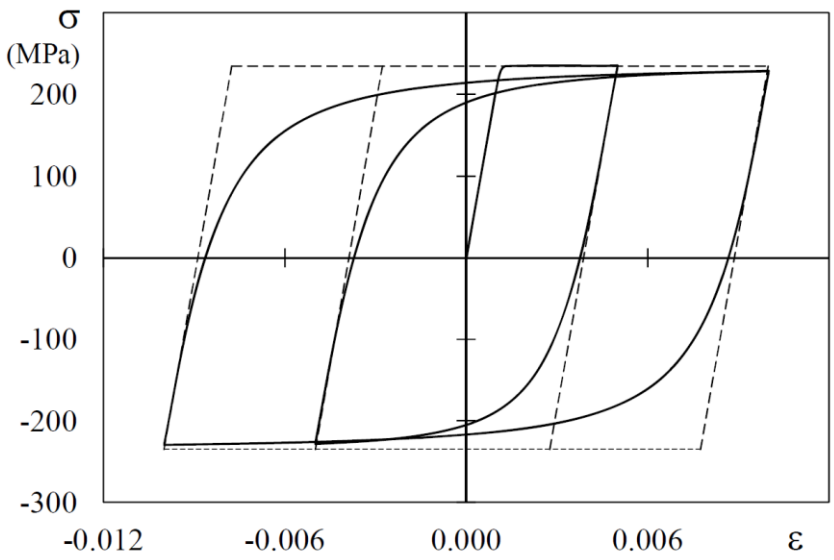

Figure 21. Stress-strain curve of Giuffrè and Pinto model.

The previous model was improved by Menegotto and Pinto [46] by adding the kinematic hardening, and the new relationship between the stress and the strain is as followed in Eq. 3.3 to 3-5. Figure 22 illustrates the change of the parameters σ_0 , σ_r, ε_0, ε_r and R that are updated when the strain is reflected and the change in the behavior of the axial force from negative to positive is based on the axial force in the brace.

$$\sigma^* = b\varepsilon^* + \frac{(1+b)\varepsilon^*}{(1+\varepsilon^{*R})^{\frac{1}{R}}} \quad \text{Eq. 3-3}$$

$$\sigma^* = \frac{\sigma-\sigma_r}{\sigma_0-\sigma_r} \quad \text{Eq. 3-4}$$

$$\varepsilon^* = \frac{\varepsilon-\varepsilon_r}{\varepsilon_0-\varepsilon_r} \quad \text{Eq. 3-5}$$

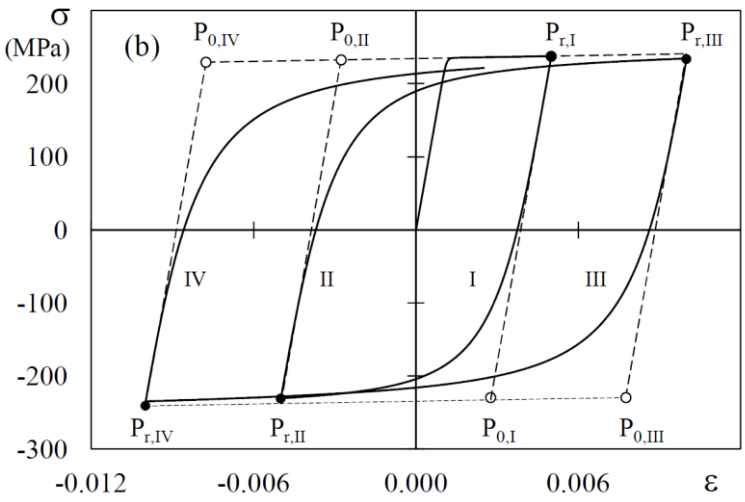

Figure 22. Suggested model by Menegotto and Pinto.

Buckling-restrained braces are originally made of three parts: yielding steel cores (typically 38-46 ksi yield strength), the buckling-restraint mechanism, and the unbonding mechanism. The steel core forms the significant part of BRB where it consists of three pieces with different areas: a restrained yielding piece, a restrained non-yielding piece, and an unrestrained non-yielding piece as presented in Figure 23.

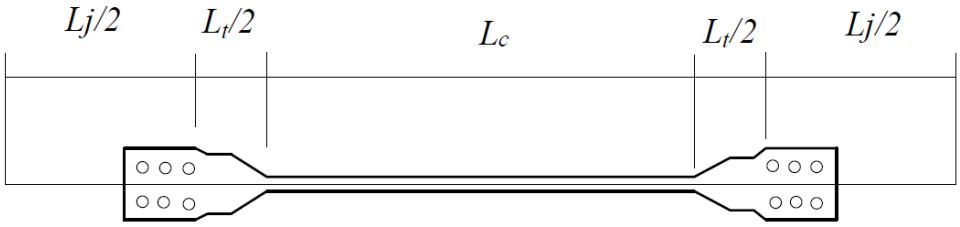

Figure 23. Dimensions of buckling-restrained braces.

Where *Lc* is the length of the restrained yielding piece, *Lt* is the restrained non-yielding piece and *Lj* is the unrestrained non-yielding segments piece. Reducing the yielding of the steel core (*Lc*) would have one of two consequences: increasing the effective stiffness or reducing the

BRB fatigue life [13, 33]. The length of the restrained yielding part, $L_{br.Yield}$, is calculated using the following equation (3-6):

$$L_{br.Yield} = \left[L_t - 2\left(\frac{L_t}{h} * d_b + 24\right)\right] * 0.85 \quad \text{Eq. 3-6}$$

Where L_t is the total length of the BRBs, h is the height of the floor, d_b is the beam depth and the ends of the BRBs were assumed to be 2 ft (24 in) as depicted in Figure 24.a. In this study, where the buckling-restrained braced frames (BRBFs) are 2-story X-BRBFs, the length of the brace is calculated using Eq. 3.7, where *b* denotes the horizontal extension of the brace.

$$L_1 = \sqrt{b^2 + h^2} \quad \text{Eq. 3-7}$$

The two elements between the two end nodes of the BRBs are modeled as elastic elements (rigid elements), while the middle part (*lc*) is modeled as plastic elements as shown in Figure 24.b. Due to the difference of sections along the steel core, the effective stiffness varies from one portion to another. The effective modulus of elasticity, E_{eff}, is calculated using the following equation 3.8.

$$E_{eff} = \frac{L_1 * E}{L_{br.Yield}} \quad \text{Eq. 3-8}$$

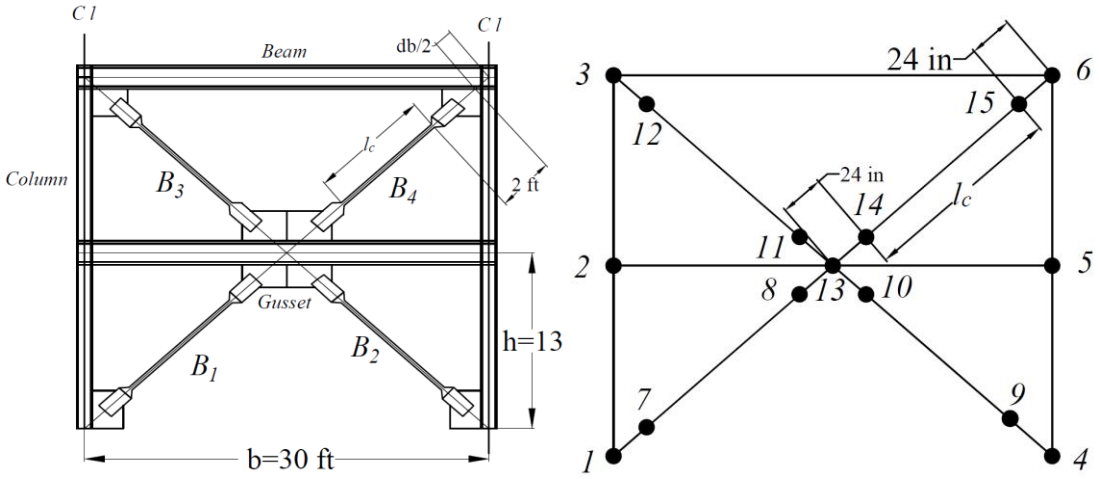

Figure 24. (a) 2-story X BRBF; (b) OpenSEES model.

The BRBs exhibit higher strength in compression than tension, which affects the cyclic behavior of the BRBs during the seismic loading. Considerable numbers of the BRBs were experimentally tested to investigate their strain hardening values in tension and compression [CoreBrace]. Based on these tests, backbone curves were carried out to define the strain hardening ratios in tension and compression. The BRBs were modeled as truss elements having steel02 (Giuffre-Menegotto-Pinto model with kinematic and isotropic strain hardening) hysteric model with properties selected to represent characteristics of the BRBs perceived in CoreBrace tests [55]. In this research project, the difference in strain hardening values in tension and compression is taken into account based on the backbones of the BRBs shown in Figure 25.

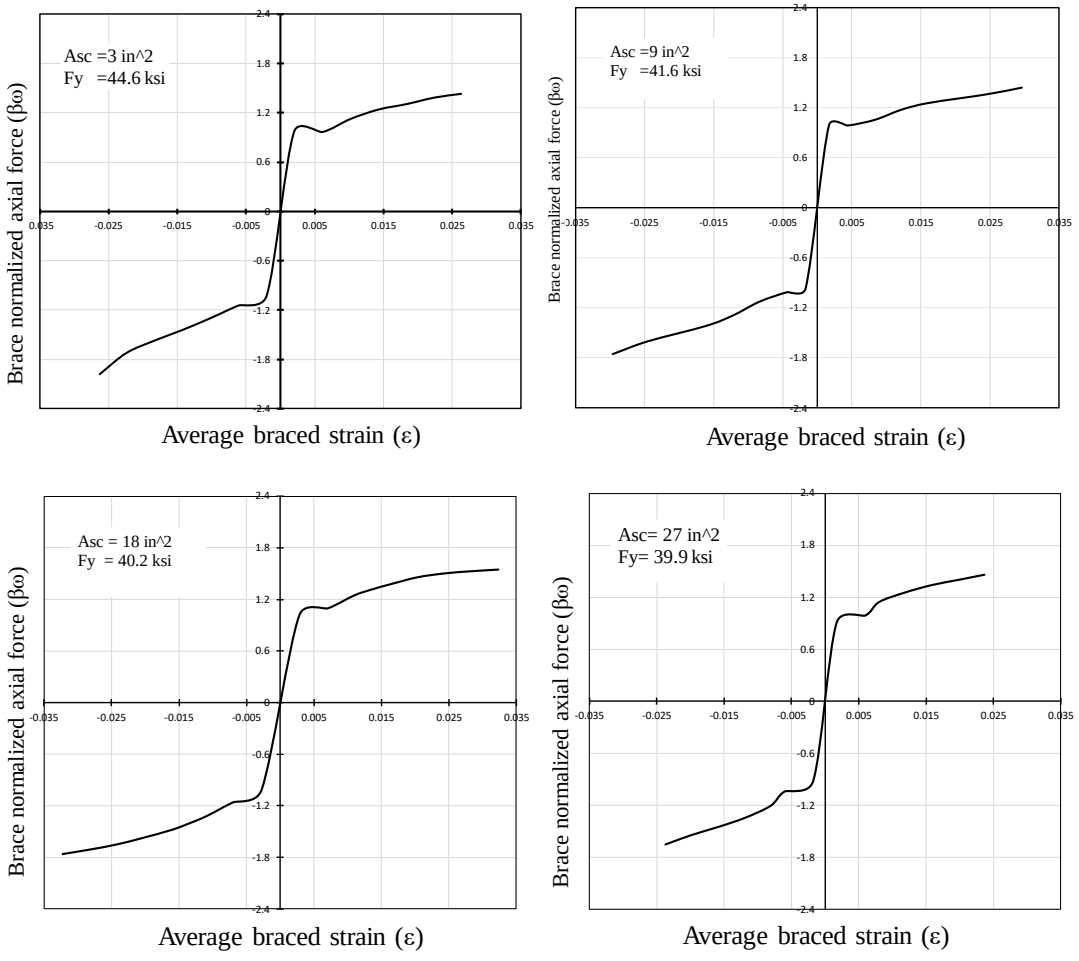

Figure 25. Backbone Curves at various yield stresses (F_y) and areas of braces (A_{sc}).

4.3 Computer Modeling of Coupled Frames

To consider the non-linear effects resulting from simultaneous earthquake loading of orthogonally oriented seismic systems, 3-D configurations were modeled in various forms. Multiple joined steel frames with various compositions are considered to evaluate column demands. The models include MF-MF, BF-MF, and BF-BF combinations. Figure 26 shows two coupled modes of 14 configurations under the investigation including 6-, 9- and 12-story frames.

Modeling of beams, columns, braces, reduced beam sections and panel zones was done following the same approach used to model the uncoupled systems.

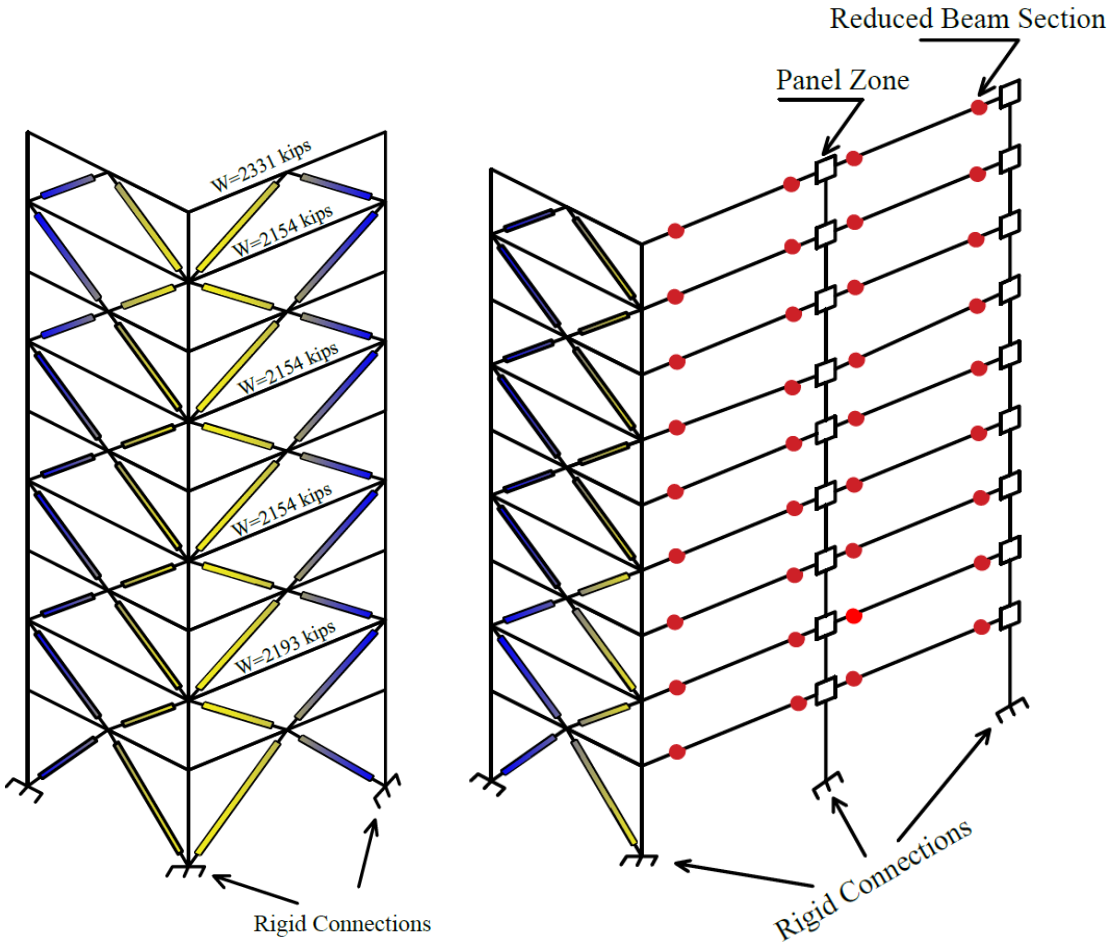

Figure 26. The OpenSEES models for 9-Story coupled BF and MF.

To investigate the difference in forces resulting from seismic loading and column demands, 6- and 9-story coupled BF-MFs were modeled. The BRBF was modeled as a truss frame with one bay in the Z-direction, while the MF included two bays in the X-direction with widths of 30 feet each, as shown in Figures 2.3 and 3.10. The gravity loads were pointed at the joints at each level of the configuration.

4.4 Non-Linear Analysis

Non-linear seismic analysis is used in structural engineering to design steel configurations for moderate to powerful earthquakes. The time history performance of the SMFs and BRBFs models is mainly applied to the coupled and uncoupled steel frames to evaluate the axial forces in the corner columns along the previous suggested frames, which are 20 models, by changing the interaction between the frames and the earthquakes. Each building of the 20 frame configurations is dynamically loaded by ten ground motions oriented at four resultant incident angles (0, 30, 60, 90 degrees), which are listed in Table 9. These records were chosen from PEER strong motion database [22, 68], and some properties of these accelerations are illustrated next to each acceleration. Earthquake shaking mostly occurs in three directions, two horizontal components and one vertical component. The strength of an earthquake is defined by the absolute value of the peak ground acceleration (PGA), which is equal to the maximum ground acceleration that occurred at a location. Figure 27 Shows North-South, East-West, and the upper components of acceleration history for Loma Prieta, station Gilroy Array, which is one of the earthquakes listed below. In this research the PGA has been determined for the ten earthquakes, and based on the maximum absolute value of the PGA, the component of acceleration has been chosen. Figure 28 shows the design and individual earthquake spectrum in both sites, LA and SLC.

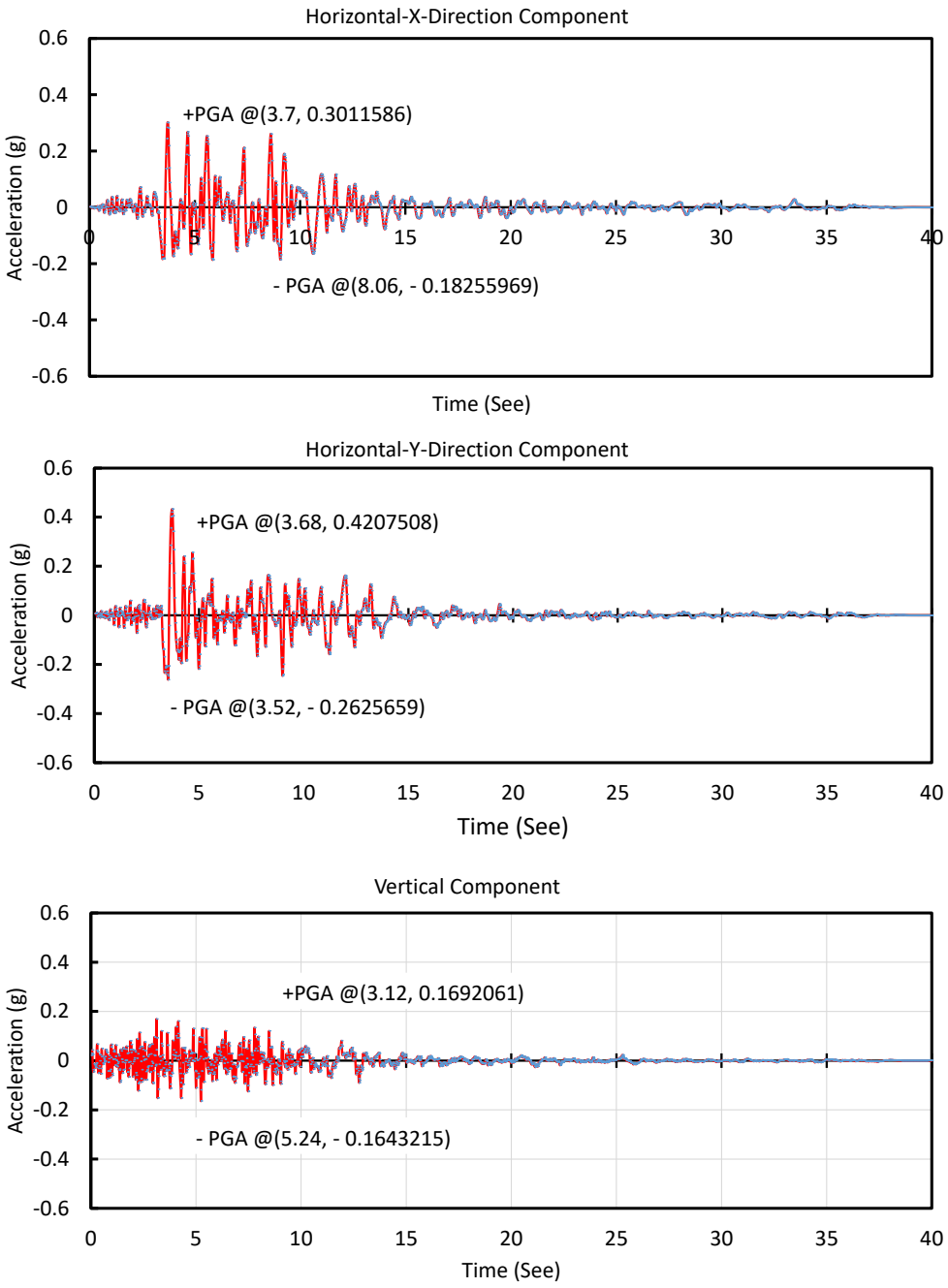

Figure 27. Fault-normal components of the acceleration time histories recorded for Loma Prieta, North-South, East-West, and Upper Fault-normal components of the acceleration.

Table 9. Summary of seismic records.

No.	RSN	Earthquake	Record	Magnitude	PGA(g)	Rrup (km)	Station
1	767	Loma Prieta	G03090	6.93	0.536	14.40	Gilroy Array #3
2	768	Loma Prieta	G04090	6.93	0.411	16.10	Gilroy Array #4
3	777	Loma Prieta	HCH090	6.93	0.242	28.20	Hollister City Hall
4	778	Loma Prieta	HDA255	6.93	0.27	25.80	Hollister Differential Array
5	806	Loma Prieta	SVL360	6.93	0.207	25.80	Sunnyvale-Colton Ave.
6	959	Northridge	CNP196	6.69	0.383	15.80	Canoga Park-Topanga Can
7	952	Northridge	MU2125	6.69	0.621	20.80	Beverly Hills-12520 Mulhol
8	963	Northridge	ORR090	6.69	0.57	22.60	Castaic-Old Ridge Route
9	1052	Northridge	PKC360	6.69	0.42	8.20	Pacoima Kagel Canyon
10	998	Northridge	WST000	6.69	0.43	29.00	LA-N Westmoreland

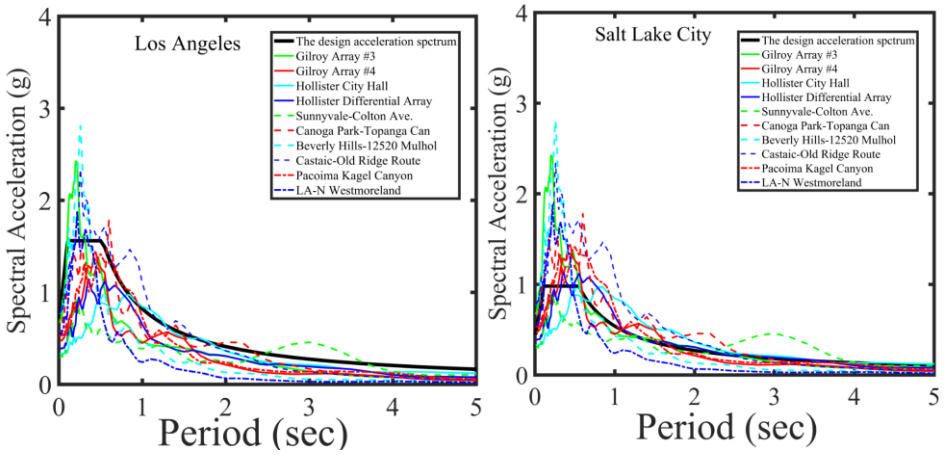

Figure 28. Design spectra and individual earthquake spectram: (a) L A; (b) SLC.

4.5. Scaling of the Ground Motions

Scale factors have been considered in order to match the seismic acceleration with the design spectural curve. In this research, the procedure to define the scale factors is the same as that followed by Makrup & Jamal, (2016) [51]. The equation 3.7 illustrates the method of matching the ten selected ground motions with the design response spectrums for the two sites (Los Angeles and Salt Lake City) where α is the scale factor.

$$\alpha = \frac{\sum_{T=T_A}^{T_B} S_a^{actual} . S_a^{target}}{\sum_{T=T_A}^{T_B} (S_a^{actual})\text{^}2} \qquad \text{Eq. 3-7}$$

Where T_A and T_B are the lower and upper response periods, (0.2T) and (1.5T) respectively.

S_a^{target} is the target acceleration response spectrum.

S_a^{actual} is the acceleration response spectrum of the actual acceleration time history.

The response period of a structure depends on many factors, including the stiffness and the height of the structure. Structures with higher stiffness have a lower fundamental period compared to buildings with lower stiffness while the taller configurations have a period larger than the short structures.

The design spectral response acceleration parameter at short periods, S_{DS}, and the design spectral response acceleration parameter at a period of one sec, S_{D1} , are defined using USGS. These values are equal to 1.56 g and 0.82 g respectively for the Los Angeles site, while they are equal to 0.980 g and 0.539 g respectively for Salt Lake City. The period range was taken between 0.2 T to 1.5 T for scaling [18]. The fundamental periods of the structures are listed in Table 10 and 11 using the eigenvalue analysis (OpenSEES). Details of the earthqukes utilized along with the scale factors for each structure are listed in Tables 12 to 15.

Table 10. Summary of the fundamental Periods (T) for the uncoupled frames (Sec).

Frame	**Site**			
	Los Angeles		**Salt Lake City**	
	SMF	BRBF	SMF	BRBF
6-Story	1.51	1.17	2.73	1.45
9-Story	2.23	1.79	3.35	2.03
12-Story	-	2.41	-	2.93

Table 11. Summary of the fundamental Periods (T) for the coupled frames (Sec).

Frame	Site			
	Los Angeles		Salt Lake City	
	BF-BF	BF-MF	BF-BF	BF-MF
6-Story	1.07	2.01	1.24	3.05
9-Story	1.47	3.00	1.72	3.73
12-Story	1.97	-	2.35	-

Table 12. Earthquake Scale Factors for 6-, 9-,and 12-Story Uncoupled SMFs and BRBFs (LA).

Earthquake	Station	SMFs		BRBFs		
		6-Story	9-Story	6-Story	9-Story	12-Story
Loma Prieta	Gilroy Array #3	1.68	1.35	1.3	1.55	1.74
	Gilroy Array #4	1.56	1.31	1.24	2.06	1.79
	Hollister City Hall	0.91	1.01	1.59	1.16	0.96
	Hollister Differential Array	1.41	1.39	1.49	1.11	1.27
	Sunnyvale-Colton Ave.	1.21	1.96	2.51	2.09	1.21
Northridge	Canoga Park-Topanga Can	1.53	1.25	1.29	1.29	1.46
	Beverly Hills-12520 Mulhol	1.83	2.05	1.69	1.88	1.88
	Castaic-Old Ridge Route	0.82	0.98	0.93	0.82	0.77
	Pacoima Kagel Canyon	1.33	1.71	1.14	1.08	1.18
	LA-N Westmoreland	2.88	3.55	1.97	2.05	3.24

Table 13. Earthquake Scale Factors for 6-, 9-,and 12-Story Uncoupled SMFs and BRBFs (SLC).

Earthquake	Station	SMFs		BRBFs		
		6-Story	9-Story	6-Story	9-Story	12-Story
Loma Prieta	Gilroy Array #3	0.92	0.83	1.09	0.89	1.09
	Gilroy Array #4	0.89	1.22	1.38	1.06	0.83
	Hollister City Hall	0.69	0.69	0.98	0.66	0.74
	Hollister Differential Array	0.94	0.84	0.79	0.73	1.09
	Sunnyvale-Colton Ave.	1.32	1.05	1.71	1.05	1.06
Northridge	Canoga Park-Topanga Can	0.85	0.59	0.69	0.72	0.77
	Beverly Hills-12520 Mulhol	1.39	2.05	0.89	1.07	1.63
	Castaic-Old Ridge Route	0.67	0.68	0.64	0.43	0.69
	Pacoima Kagel Canyon	1.16	0.94	0.67	0.61	0.91
	LA-N Westmoreland	2.49	3.35	2.15	2.09	2.58

Table 14. Earthquake Scale Factors for 6-, 9-,and 12-Story Coupled SMFs and BRBFs (LA).

Earthquake	Station	BF-SMF		BRBFs		
		6-Story	9-Story	6-Story	9-Story	12-Story
Loma Prieta	Gilroy Array #3	1.31	1.67	0.74	0.8	1.03
	Gilroy Array #4	1.11	1.49	1.63	1.75	1.35
	Hollister City Hall	2.05	1.79	0.92	2.13	1.69
	Hollister Differential Array	1.57	1.47	1.34	1.62	1.65
	Sunnyvale-Colton Ave.	1.98	2.82	1.77	1.88	2.03
Northridge	Canoga Park-Topanga Can	1.14	1.21	1.04	1.31	1.27
	Beverly Hills-12520 Mulhol	1.17	1.7	0.88	0.63	0.77
	Castaic - Old Ridge Route	0.93	0.95	1.04	0.83	0.78
	Pacoima Kagel Canyon	1.35	1.18	0.72	1.6	1.2
	LA-N Westmoreland	1.16	2.49	1.12	0.98	0.93

Table 15. Earthquake Scale Factors for 6-, 9-,and 12-Story Coupled SMFs and BRBFs (SLS).

Earthquake	Station	BF-SMF		BRBF-BRBF		
		6-Story	9-Story	6-Story	9-Story	12-Story
Loma Prieta	Gilroy Array #3	0.74	1.04	0.46	0.61	0.79
	Gilroy Array #4	0.75	1.03	0.95	1.08	0.77
	Hollister City Hall	1.12	1.06	1.28	1.54	1.42
	Hollister Differential Array	1.11	0.89	1.41	1.10	0.87
	Sunnyvale-Colton Ave.	1.56	1.68	1.15	1.22	1.28
Northridge	Canoga Park-Topanga Can	0.76	0.51	0.69	0.68	0.84
	Beverly Hills-12520 Mulhol	1.01	1.25	0.52	0.38	0.55
	Castaic-Old Ridge Route	0.63	0.60	0.62	0.44	0.51
	Pacoima Kagel Canyon	0.7	0.68	1.09	0.88	0.94
	LA-N Westmoreland	1.08	1.84	0.67	0.68	0.63

4.6 Analysis and Results

Two approaches of analysis are followed in this study: the static pushover analysis and the time history analysis. The static pushover analysis compares the elastic behavior of the structures while the time history analysis measures the inelastic behavior of the building under dynamic loading. The seismic analysis is typically a dynamic analysis that could be linear or non-linear, whereas the pushover is a non-linear static analysis. In pushover, the capacity of the structure for the maximum displacement is studied, while in the time history analysis the displacements from

the shaking should meet code standards. The dynamic analysis is used to determine torsional effects because the pushover analysis is not accurate.

4.6.1 Pushover Analysis

To compare the strengths of the two frame systems, the pushover analysis was completed for the SMFs and BRBFs at both sites, Los Angeles and Salt Lake City. Figures 29 and 30 show the results of this analysis for the SMFs and BRBFs. The pushover analysis is defined based on the story shear forces (V) and the elastic story shear forces from equivalent lateral force procedure (Ve). The normalized base shear was investigated as a function of the roof drift where (V/Ve) represents the frame drift under the equivalent lateral forces. The resemblance of the yield for the SMFs and BRBFs indicates that a similar design strength for all models was developed ranging from 2.4 to 2.7 for SMFs and 1.8 to 2.1 for BRBFs at a roof drift of 0.06 rad.

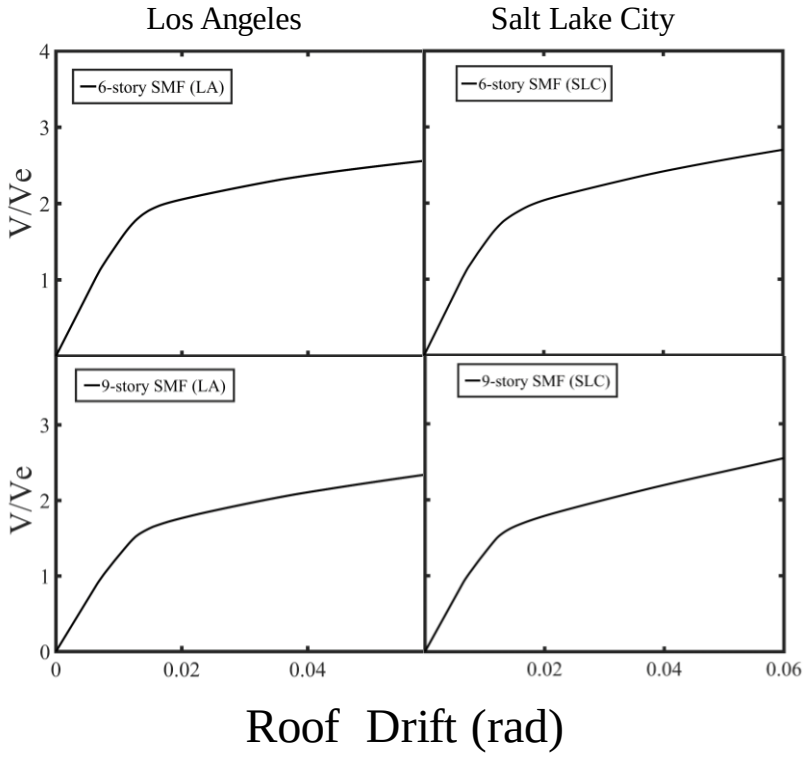

Figure 29. Pushover analysis results for SMFs.

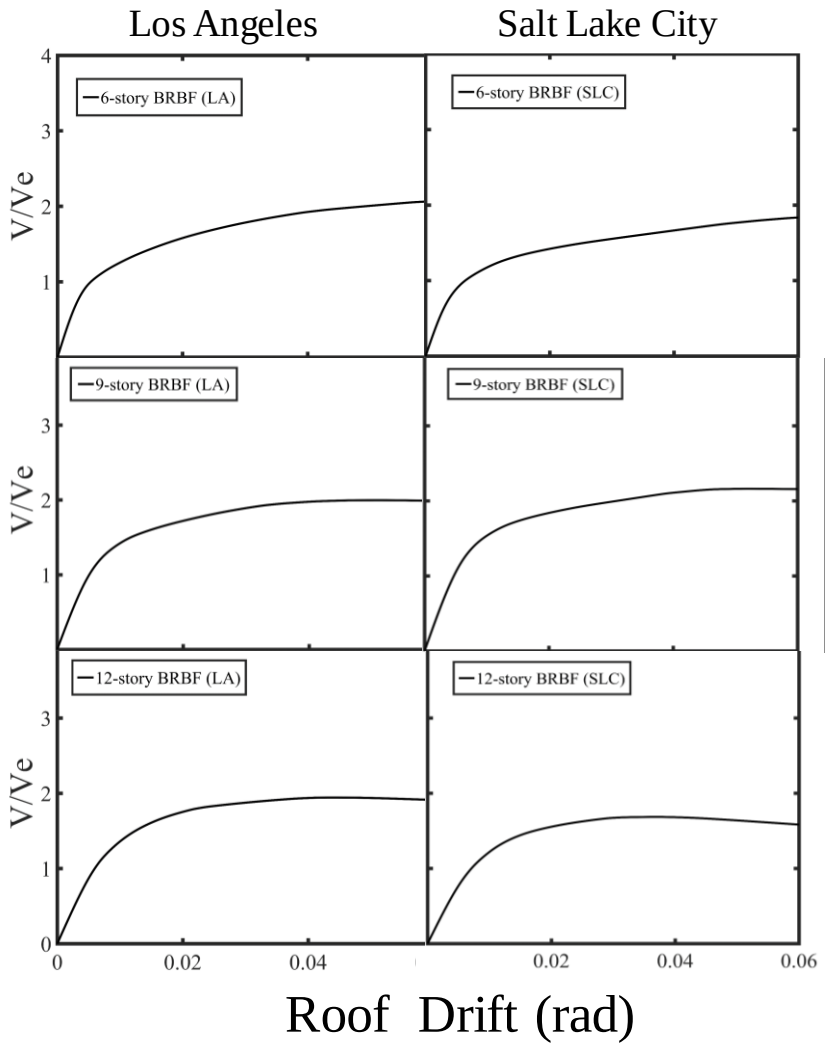

Figure 30. Pushover analysis results for BRBFs.

4.6.2 Time History Analysis

The time history analysis was performed to investigate the seismic response of the frames under dynamic loading of typical earthquakes. Ten scaled earthquake ground motions were chosen from the Pacific Earthquake Engineering Research Center (PEER Ground Motion Database) to accomplish the dynamic analysis resulting in 800 analyses.

The two most common measures of ground motion are peak ground acceleration (PGA) and peak ground velocity (PGV), measured in the north-south (N-S), east-west (E-W) , and vertical

(UP) directions. Based on the strongest PGA of the earthquake, the acceleration was selected to be in the E-W direction when θ equal to 0^0, which is along the *x*-axis. The directions of the other attack angles are considered to be perpendicularly related counter-clockwise from the *x*-axis directed to the (N-S) direction until an orientation of 90^0, which represents the *y*-direction. The 30^0 and 60^0 orientations are added to the previous directions to cover all the potential seismic loads on the construction and their orthogonal effects in seismically loaded steel systems. By assuming the (E-W) direction is the reference axis (the strongest PGA of the ten earthquakes are slected to represent the E-W), the orthogonal effects of seismic accelerations are estimated based on the earthquake strike-normal attack angles.

4.6.2.1 Results of the Time History Analysis for Uncoupled Frames

For the dynamic analysis, the uncoupled special moment frames (SMFs) and the buckling-restrained braced frames (BRBFs) were inelastically loaded using the ten scaled earthquake ground motions with directions $\theta = 0^0$, $\theta = 30^0$, $\theta = 60^0$, and $\theta = 90^0$. For the uncoupled BRBF_SMF steel systems, the SMFs are assumed to be located in the E-W orientation, while the BRBFs are in the N-S direction. Figure 31 includes four charts that present the change in the column forces affected by seismic shaking at the previous orintations for 6- and 9-story structures in the LA and SLC sites. The attack angle 30^0 to the structure axes considerably increased the force in the columns along the frames for the both the 6- and 9-story uncoupled frames in the two sites. Increasing the oriented angle to the N-S direction, where the orientation is assumed to be 60^0, aises the column forces more than the previous orientation. The corner columns are more affected by the simulataneous bidirectional horizontal vibration and the increased effect of the large stike-normal component of the seismic shaking relative to the BRBF. The BRBs directaly transfer the lateral

seismic loads to the columns based on the assumption that the BRBF works as a truss frame. In the *y*-direction, which represents the attack angle of 90^0, the columns undergo only the single directional horizontal shaking. This effect represents shaking the BRBF in the N-S direction and exhibits a lower increase of force in the column along the buiding compared to the two previous bidirectional movements.

Figure 32 shows the orthogonal effects of the seismic loading on the corner columns for uncoupled frames under the combinations of BF with BF in 6-, 9-, and 12-story structures in the LA and SLC sites. The bidirectional horizontal attack angle of 30^0 has the same effect of 60^0 on the corner columns along the buiding as the frame periods in each orientation are similar. The single horizontal attack angles 0^0 and 90^0, which represent the E-W direction and N-S direction, respectively, show the same results for the same reason. The simulataneous shaking of the two bidirectional horizontal attack angles caused considerable increase for the axial forces in columns along the uncoupled BF-BF systems.

The uncoupled steel frames for the combination of BF-BF are significantly affected by the bidirectional attack angles of 30^0 and 60^0, and the axial forces increased and had almost the same percentages of the forces in the columns along the configuration. These percentages ranged an average of 64.8%, 61.5% and 40.2% for the 6-, 9- and 12-story uncoupled BF-BF in the LA site respectively. The force increases ranged an average of 64.5%, 37.8% and 36.6% for 6-, 9- and 12-story uncoupled BF-BF respectively in the SLC site.

From the same figure (Figure 32), it is clear that the upper levels of the frames were significantly affected by the combined shaking force resulting from the bidirectional attack angles, which exceeded the design loads. More specifically, the upper columns are more likely to experience forces than the lower columns when the BRBs at the highest level of the building are

connected directaly to the column. The brace creates forces in the top column that are transmitted to the lower columns, as shown in 6- and 12-story frames of the Figure. Designing the top columns of the braced frames based on the maximum tensile axial forces in the BRBs gives these columns more capability to resist strong seismic loads.

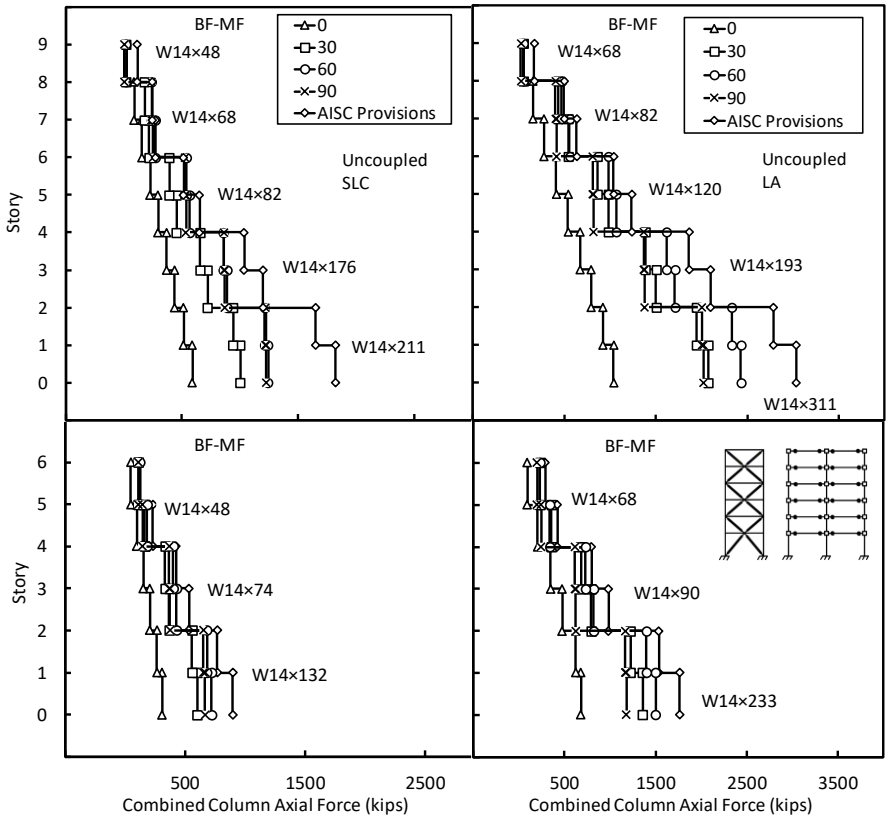

Figure 31. Seismic Forces in the Columns with the Column Demands for 6- and 9-Story Uncoupled Frames (BF-MF).

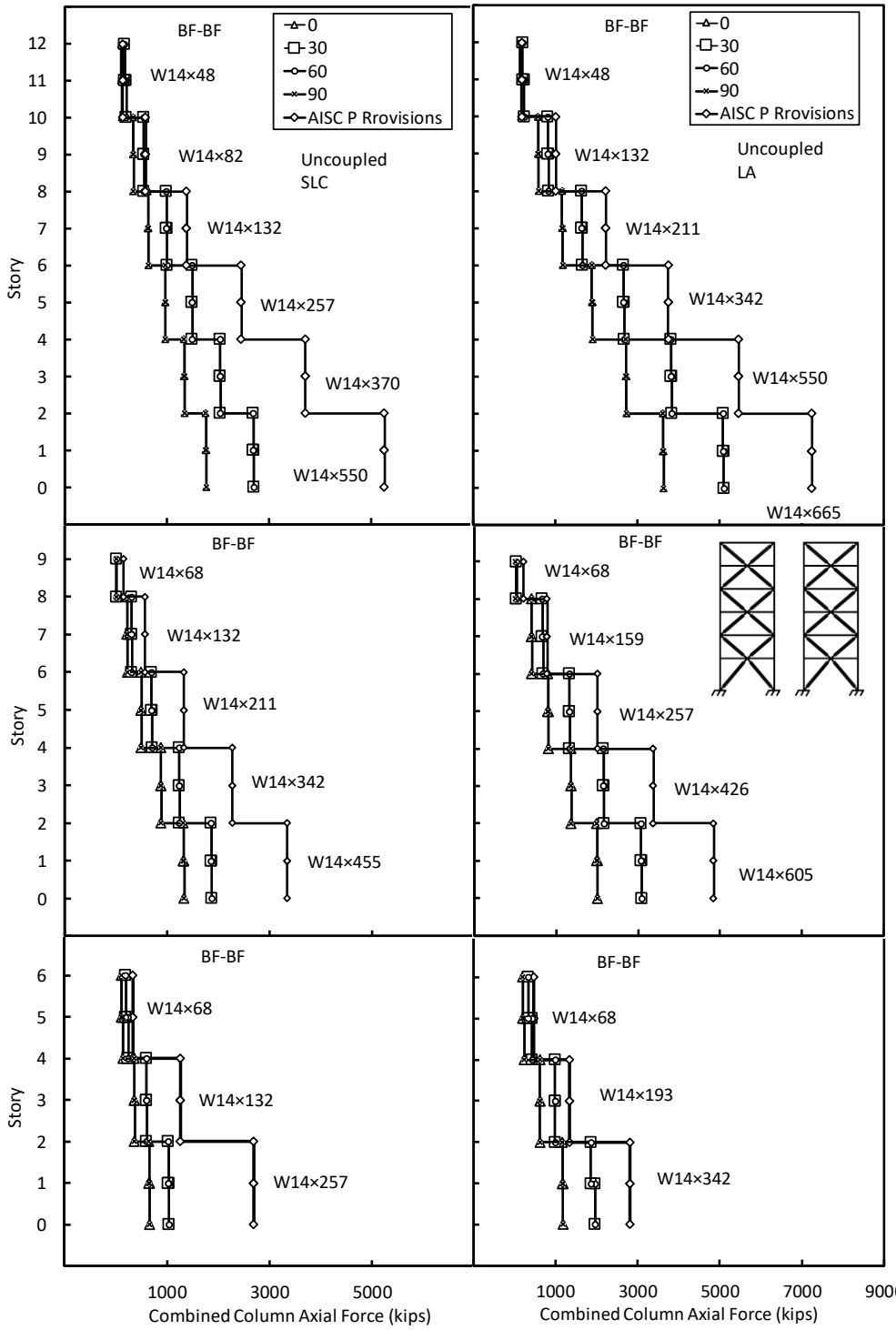

Figure 32. Seismic Forces in the Columns with the Column Demands for 6-, 9- and 12-Story Uncoupled Frames (BF-BF).

4.6.2.2 Results of the Time History Analysis for Coupled Frames

The orthogonal effects of seismic shaking on the corner columns in the coupled steel systems differ based on the seismic attck angle. Figure 33 shows four graphs that illustrate the changes in steel columns according to the direction of the eathquake attack angle for the composition (installation) BF-MF. The orientation (direction) of angles is assumed to be the same as for the previous analysis (uncoupled steel systems), where the angles 0^0 and 90^0 represent the E-W direction and N-S direction (i.e., in the *x*- and *y*-directions), respectively. The forces in columns in the 3D steel frames subjected to shaking in the principal and orthogonal directions produced almost the same response as in the equivalent 2D configurations that were used previously. The simultaneous bidirectional horizontal seismic loading of 30^0 caused a considerable increase in the axial forces in corner columns compared to the principal axes x-direction for the both 6- and 9-story steel systems. The columns in the 9-story steel frames in both the LA and SLC sites experienced a greater impact than the 6-story frame; the tall structures under the seismic shaking experience show more drifts than the short ones, which increases forces in the structural elements. When the direction of the earthquake attack is increased to 60^0 , the bidirectional load produces more forces in the columns than the 30^0 orientation, where the BRBF becomes more effective. The maximum force of the orthogonal effects of seismic loading was at an attack angle of 90^0, which represents the N-S direction. The inelastic behaviour of the BRBs gives a greater stiffness and flexibility to the braced frame and the whole structure. Configurations with these properties have the ability to resist significant shaking without failure and then produce considerable tension and compression forces in the columns.

Figure 34 shows six graphs that illustrate the impact of seismic shaking for 6-, 9- and 12-story coupled steel configurations under the combination of BF-BF in the LA and SLC sites.

Because of the similarty in composition for the steel systems, which are BRBFs in the E-W direction and N-S direction, the orthogonal effects of the ten earthquakes at 0^0 show the same response as 90^0, and 30^0 appears to have the same reaction as 60^0. By considering the change of the forces in the columns, it is concluded that the attack angle of 0^0 created the same magnitudes of forces as the orientation of 90^0 and 30^0 is similar to 60^0. The compound seismic shaking of 30^0 and 60^0 inceased the forces by an average of 49.7% and 48.6% for the 6-story configuration, 44.2% and 43.5% for the 9-story frames, and 43.2% and 37.9% for the 12-story frames in the LA and SLC sites, respectively. These persentages indicate that the simultaneous bidirectional horizontal shaking in seismically active areas leads to forces that exceed the strength of the columns. Significantly, following the 100+30% rule for designing the columns underestimates the combined shaking. This rule has been based on the assumption that orthogonal effects may be satisfied by designing such elements for 100% of the expected seismic force in one direction plus 30% of the expected seismic force in the perpendicular direction. The combination requiring the greater component strength is used for design.

As expected, depending on the previous results related to the uncoupled braced frames, the coupled configurations for the BF-BF composition showed that simultaneous bidirectional horizontal shaking causes axial forces in the upper columns to exceed the maximum column axial demands from the analysis. Therefore, following the current provisions in design, the BRBFs with 2-story X-bracing leads to columns inelastically loaded with more than the maximum expected limit, which could affect the other structure elements. Alternative provisions in designing these steel systems should be considered to estimate the axial forces in columns resulting from the tension and compression forces in the BRBs. For example, columns could be designed based on the full tensile capacity of the BRBs, where the compression braces carry no axial force after

buckling, representing a conservative bound on the amplification of the column axial loads immediately after buckling. On the other hand, the lower columns in the 12-story BRBFs are too conservatively designed, which leads to increasing the size of the columns and the costs of construction. Using reduced values for the ratio between expected and normal material strength factor (Ry), compression strength factor (β), and strain hardening factor (ω) to estimate the ultimate axial strengths of braces will lead to a more economical column design. More figures related to the column design, column demand and Individual Seismic Forces are presented in Appendix C. (See Figures, Appendix C).

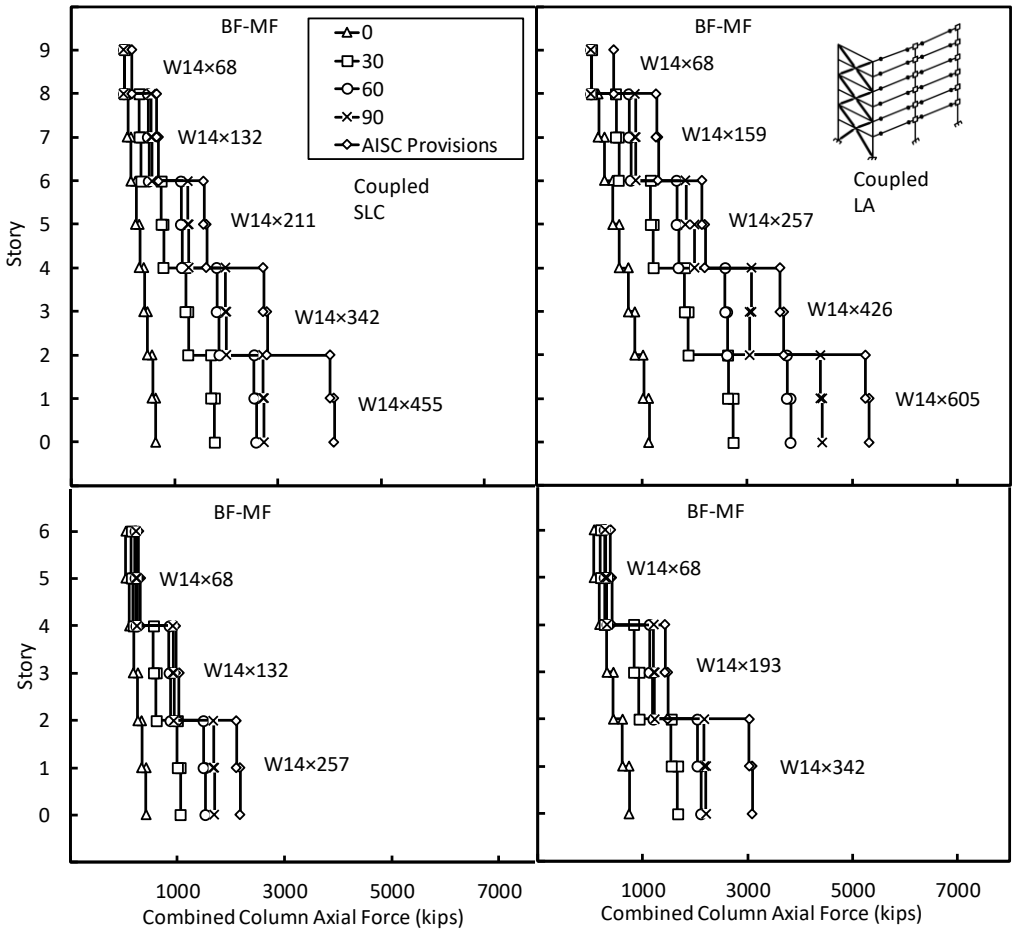

Figure 33. Seismic Forces in the Columns with the Column Demands for 6- and 9-Story Coupled Frames (BF-MF).

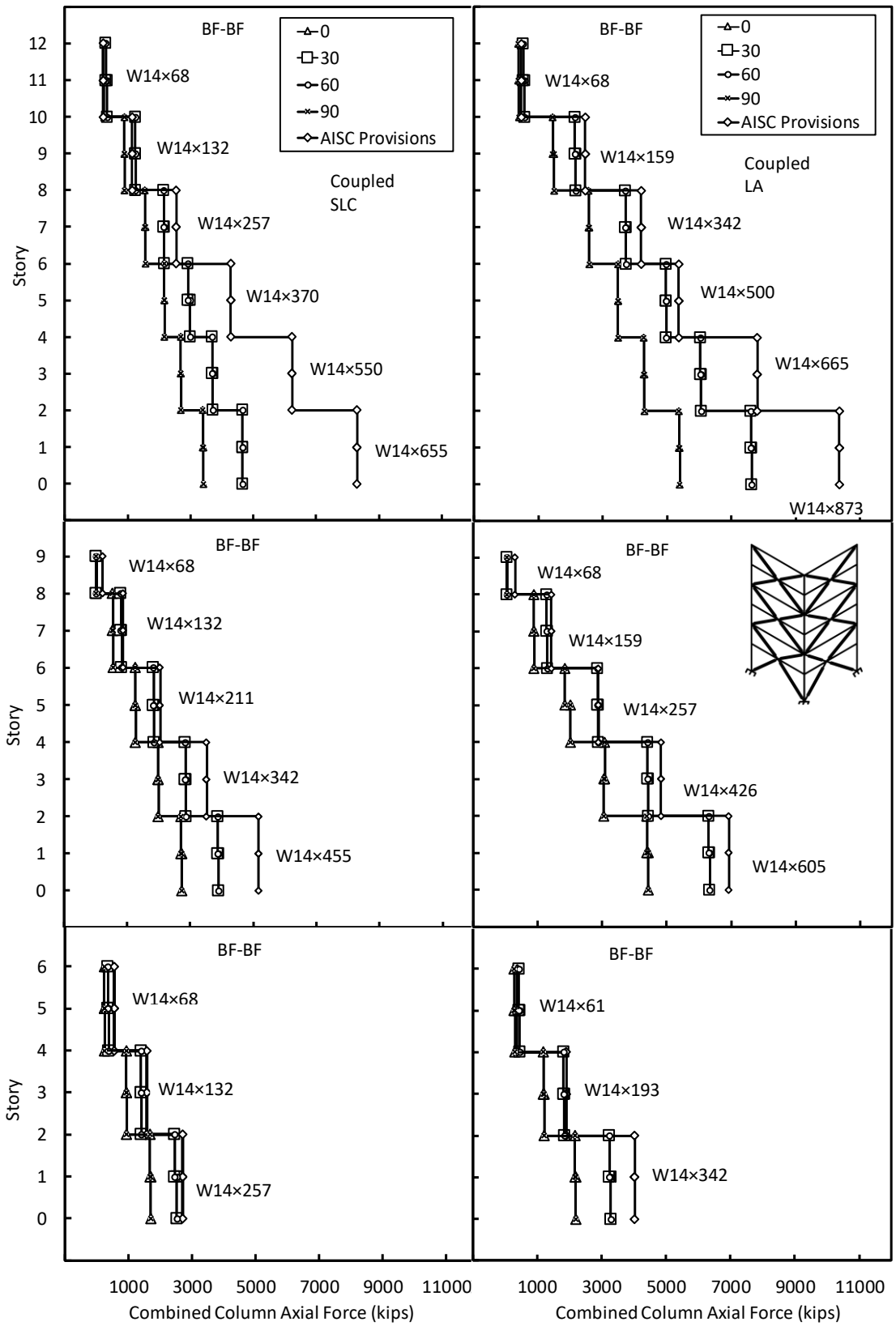

Figure 34. Seismic Forces in the Columns with the Column Demands for 6-, 9- and 12-Story Coupled Frames (BF-BF).

4.6.3 Column Demands

Normalization of the forces gives a clear picture for comparison between column demands and column design. In this part, the mean maximum column axial load at each level, Pu, resulting from the time history analysis using the ten scaled earthquakes is normalized by the design axial column demands, Pd, following the current design provisions for steel systems in the seismic active areas. The normalized axial column demands (Pu/Pd) are provided for coupled and uncoupled steel configurations with different levels that are under investigation. The charts' profiles are almost identical with respect to the changing of normalized values based on the seismic angle attack.

Figure 35 shows the average normalized column demands for 6- and 9-story isolated and connected steel buildings under the compositions (BF-MF). In some columns, the average column demands exceeded the design demands, which means that these elements are under considerable inelastic behavior through the cyclic loading. Reaching this stage of yielding could lead to the unyielding (elastic) elements (column, beams, and braces) being loaded higher than they were designed for, reaching significant plastic behavior. As can be seen in the mentioned figure, at the seismic attack angle of zero degrees, the columns along the structures for the four compositions are still in elastic behavior (Pu/Pd<1). Because the main purpose of this research is investigating the orthogonal effects of seismic loads on the corner columns, the (Pu/Pd) will be considered as a percentage. The maximum percentage of average normalized column demands for the 6-story uncoupled frames were 74%, 65%, and 92% at the orientations of 30^0, 60^0, and 90^0 respectively, whereas the 6-story structure recorded 58.2%, 82%, and 84%, respectively (where the *x*-axis was taken as the reference direction, which represent a 0^0 angle). The peak percentage of (Pu/Pd) for the 9-story uncoupled building recorded 57.9%, 64.9, and 42% at the directions of 30, 60, and 90

degrees, respectively. These values result from the SMF being located in the *x*-direction (E-W direction), while the BRBF is along the *y*-axis (N-S direction).

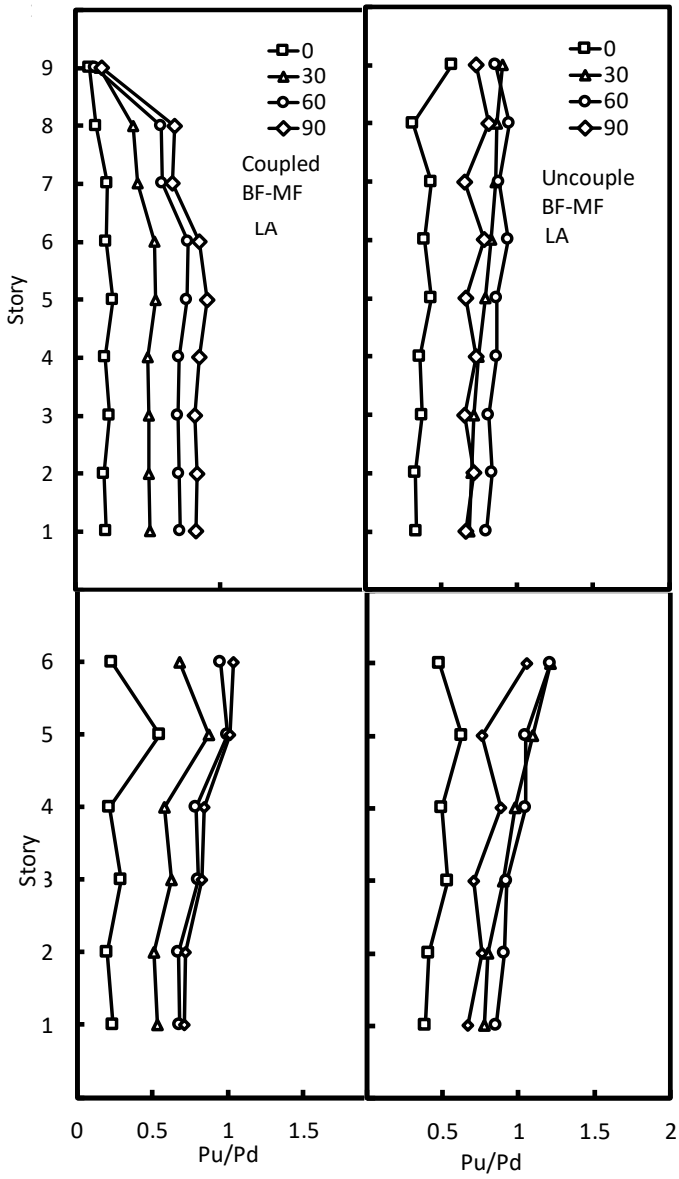

Figure 35. Normalized average maximum column demands for 6- and 9-story frames.

Figure 36 illustrates the normalized average maximum column demands for 12-story uncoupled and connected frames under the composition (BF-BF). The maximum (Pu/Pd) value was 0.96 at the level two for the angles of 0^0 and 90^0, which means that all the columns are still

within the elastic behavior. This value increased and reached 1.33 at the same level for the 30^0 and 60^0 angles. The column (and possibly the upper and lower columns) reached the plastic behavior with a considerable concentration of stresses for this area. As a percentage, this incrimination is equivalent to 38.5 %. The 12-story steel frame followed the procedure and had almost the same values, where (Pu/Pd) values were 0.83 for 0^0, and 90^0 angles, whereas 1.21 for 30^0, and 60^0, with the increasing percentage equivalent to 46.7%. The same procedure has been followed to consider the normalized average maximum column demands for the steel systems in the SLC site. The results are asymptotic and close to the outcomes of the LA site.

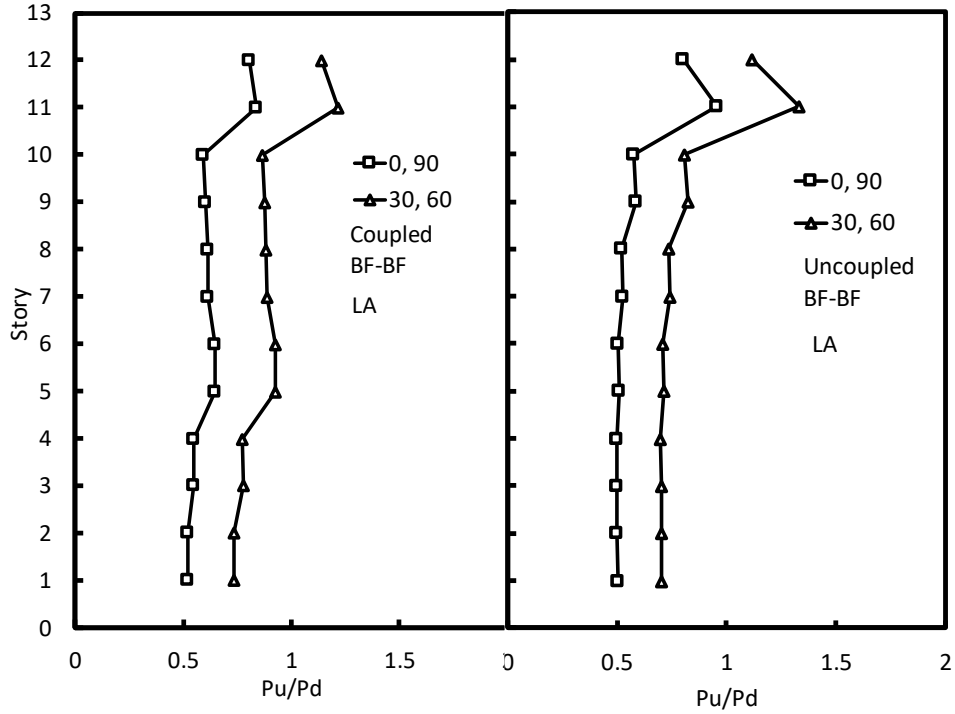

Figure 36. Normalized average maximum column demands for 12-story frames.

4.6.4 Mean of Maximum Inter-Story Drifts for Coupled and Uncoupled Frames (LA)

The other method to evaluate the stiffness of structures is the inter-story drift where it is an important damage demand parameter of configurations under earthquake loading. This parameter

is the relative displacement of one level to the others and it could result from axial deformation in the columns or global foundation settlement. Consequently, accurate evaluation of the maximum inter-story drift is significant to seismic analysis and structural design. Many publications presented mixed results about inter-story drifts, and the majority of them disregarded the orthogonal effects of seismic loading on the displacements and drifts of columns along the structure [10, 14, 21, 27, 41, 39, 52, 53].

In this research, the distributions of the mean peak drift ratios along the configuration height for the 6-, 9-, and 12-story frames were considered under the dynamic analysis by using the ten ground motions listen in the Table 9. These records were applied to coupled and uncoupled frames under the compositions BF-MF and BF-BF for the LA site to investigate the behavior of steel structures and calculate the mean maximum inter-story drifts under the time history analysis at different orientations. The peak responses were investigated to examine and evaluate the dynamic performance of the frame models in seismically active areas. The following figures show an example of the corner columns with seismic loads at the angles of 0^0, 30^0, 60^0 and 90^0 to quantify the effect of coupled axial load on the cyclic behavior of the steel columns before defining the maximum inter-story drifts (ISD) at each level.

The procedure of equivalent lateral design in SEI/ASCE 7-10 requires that the inelastic displacements of the building can be estimated through the amplification of elastic displacements, which could be obtained from the linear analysis. According to a study by Ariyaratana and Fahnestock 2010 [43], the peak story drift response depends on the type of connections, either moment-resisting or non-moment-resisting, and the type of system if the frame employs isolated BRBFs or a BRBF-SMF dual system. Using moment-resisting connections in the isolated BRBFs leads to a reduction in the maximum story drift compared to non-moment resisting connections.

Considerable reduction of the maximum story drift is achieved by using isolated BRBFs compared to the corresponding BRBF-SMF dual systems, which increases the ISDs.

Figure 37 summarizes the mean maximum absolute peak story drifts along the height of the 6- and 9-story isolated and coupled BRBFs and BRBF-SMF systems. In general, the story drifts for these systems are similar, although some stories had different values based on the seismic attack angles. The values of the ISDs of the isolated BRBFs systems are likely the outcomes of a time history analysis similar to those identified in analysis by previously listed publications. However, considerable differences can be shown by changing the seismic attack. The four charts in Figure 37 show that the drift profiles along the height of the structures have a similar general shape but with the middle levels exhibiting considerably higher inter-story drifts than the lower and upper levels. It was noticed that the peak inter-story drifts mostly existed at the first or second stories, which means the inelastic deformations of the configuration elements focused at the lower levels during the peak seismic loading.

The 2D models have ISDs slightly greater than the 3D models, which could be dependent on the type of connections [39]. All the models had maximum ISD values less than 0.02 rad at the 0^0 orientation, whereas these ratios increase based on the seismic angle attack. The maximum ISD recorded was at the second story for all attack angles for 6-story coupled and uncoupled steel systems under the combination (BF-MF). However, a slight difference was noticed for 9-story frames, where the maximum ISD was located at the second and third stories. The seismic attack angle of 90^0 (y-direction, which means 100% of the seismic load orientated to the braced frame) recorded the minimum ISD values, compared to the other directions at the same levels, which ranged from 0.0066 to 0.0183 rad and 0.0056 to 0.0125 rad for 6- and 9-story uncoupled and coupled frames respectively. Generally, the seismic attack angle of 30 degrees caused less ISD in

most levels than the angle of 60^0. The maximum ISD values of the 6-story isolated systems at the 30^0 and 60^0 angles were 0.023 and 0.021 rad, which are equivalent to 41.1% and 28.8% compared to y-axis. These values were 0.0215 and 0.0175 rad for dual systems, which are equivalent to 58.1% and 28.7% rad respectively. The 9-story steel frames showed almost the same value as the previous ones. The peak ISD values of the uncoupled systems at the 30^0 and 60^0 orientations were 0.0217 and 0.0207 rad, which are equivalent to 41.4% and 36.2% compared to the reference direction (x-axis). These values reached 0.0241 and 0.0214 rad for coupled configurations, which are equivalent to 45.4% and 40.1%, respectively.

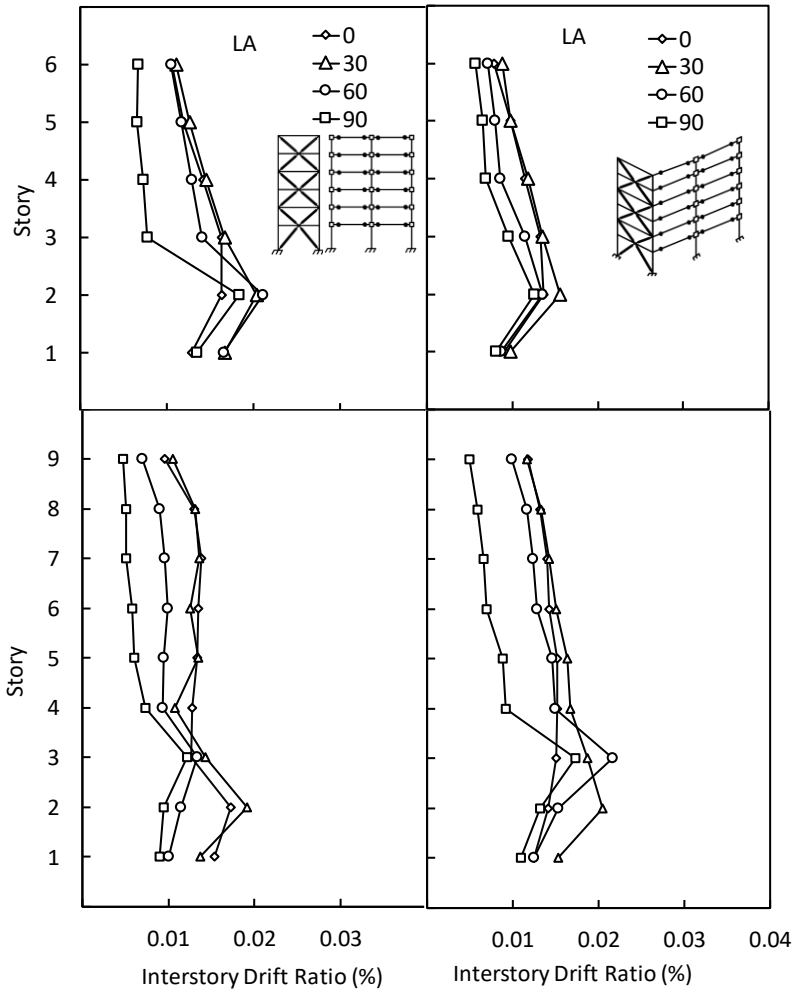

Figure 37. Average maximum inter-story drift for 6- and 9-story coupled and uncoupled frames (BF-MF combination).

Figure 38 illustrates the ISDs for the coupled and uncoupled eccentrically braces steel systems in 6- and 9-story configurations. Because of the similar composition of the frames (BF-BF) at the two coordinates that represent the E-W and N-S directions (X- and Y-directions), the two ISDs of 0^0 and 90^0 orientations will have the magnitudes for the angles of 30^0 and 60^0. The four charts in this figure showed very similar profiles with some differences in the values and the concentration of the plastic deformation. The ISDs for 6-story uncoupled frames ranged between 0.067 and 0.0183 rad for the X- and Y-direction, while ranged between 0.0077 and 0.0231 rad for the orientations 30 and 60 degrees. This increase is equivalent to 26.2% and 22.2% respectively. These values differ slightly for the 9-story steel systems where 0.0173 and 0.0224 rad were exhibited for isolated systems, whereas 0.0122 and 0.0143 rad for were exhibited for coupled configurations, respectively.

The 12-story buckling-restrained braced models had the same general shape for both the uncoupled and coupled composition as shown in Figure 39. The maximum ISD appeared at the third floor for all cases, which means the inelastic behavior will likely happen in the elements at this region. The peak ISDs for the seismic attack angles ($30^0 = 60^0$) reached 0.0355 and 0.0161 rad, which is equivalent to 46.1% and 30.9% for uncoupled and coupled systems respectively.

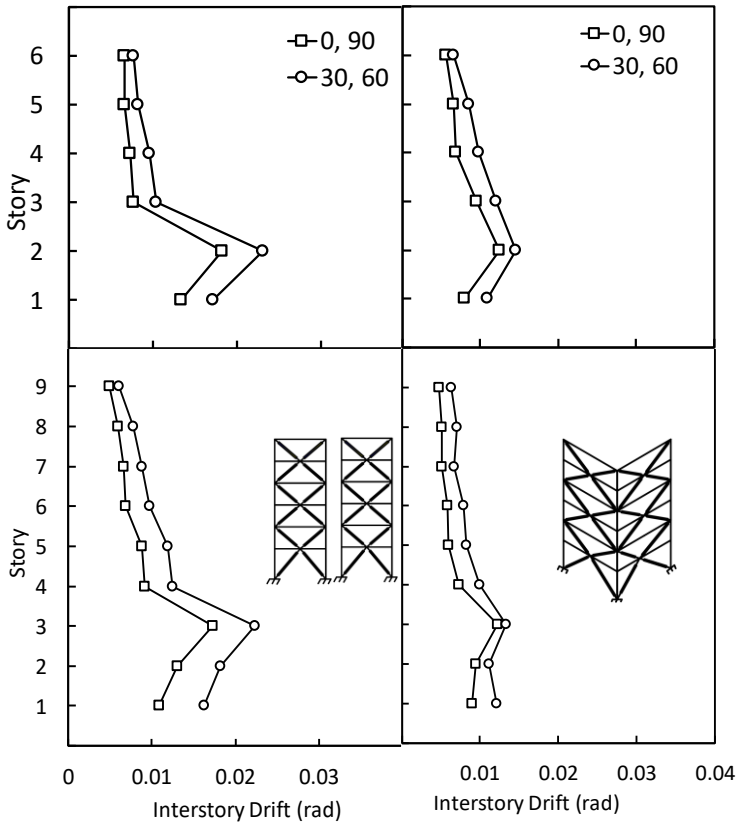

Figure 38. Average maximum inter-story drift for 6- and 9-story coupled and uncoupled frames (BF-BF combination).

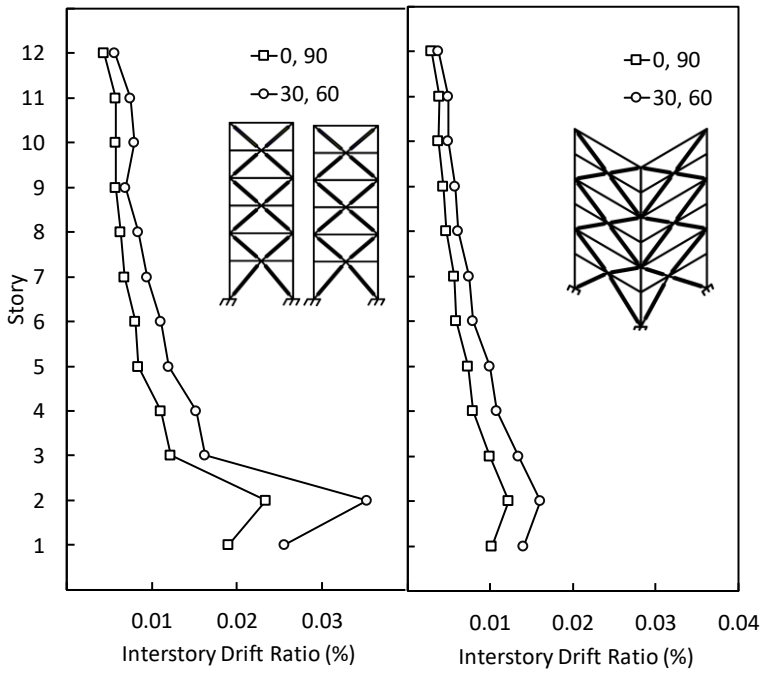

Figure 39. Average maximum inter-story drift for 12-story coupled and uncoupled frames (BF-BF combination).

4.7 Conclusions from Time-History Analysis Investigations

In this study, the orthogonal effects of seismic loads and column demands were investigated in 20 uncoupled and coupled configurations representing two steel systems (SMFs and BRBFs), three heights (6-, 9- and 12-story frames), and two compositions (SMF-BRBF and BRBF-BRBF) using time history analysis (ten scaled earthquakes), which were orientated to four angles (0^0, 30^0, 60^0, and 90^0) in two sites (LA and SLC). The SMFs were designed according to the equivalent lateral force method outlined in ASCE-7-10, where the member sizes for the special moment frame bays were governed by drift requirements. The RBSs were used in the special moment frame design so that the yielding and plastic hinge occurs within this zone, which is at a short distance from column face. The BRBFs were designed as truss frames according to current provisions to resist the lateral seismic loads along the structure.

The maximum column axial forces caused by the orthogonal effects of seismic loads were calculated on the four previous orientations and compared to the E-W direction, which represents the x-axis, to evaluate the current design rules and introduce a new rule to enhance steel systems under inelastic behavior. Conclusions from this study are as follows:

1- The axial force in the corner columns in steel configurations increases according to the attack angle. This effect of combined seismic shaking is impacted by increasing the orientation of the BRBFs; the attack angle of 60^0, which is close to the BRBF, produces higher forces in the corner columns than the attack angle 30^0.

2- The buckle of braces in the 2-story X-braced BRBFs leads to redistribution of the tension and compression loads, resulting in an increase in the axial column force.

3- Estimating bidirectional demands in shared columns based on the 100+30 rule was inadequate in the upper building stories, where orthogonal effects exceeded code

demand estimations by near 50% on average. Column demands for the BRBFs with 12 stories at the top levels exceeded those used in the design at the top levels by between 40 to 75%, whereas the column demands in the bottom stories were considerably lower than code demand estimations.

4- Structures of the composition BF-BF are more affected by simultaneous bidirectional shaking than MF-BF configurations, where the BRBs in the coupled BRBFs cause an increase in shared column demands due to the bidirectional effect of the normal bracing components.

5- Demands from coupled BRBF system analyses indicate that the 100+30 rule results in conservative demand estimations for the lower building stories having higher lateral seismic demands. In lower building stories, estimated demands exceeded measured demands by more than 40% for the coupled BRBF-BRBF configurations. Measured column demands from the addition of uncoupled BRBF analyses indicates less conservancy in code demand estimations for the lower building stories, suggesting load redistribution benefits in actual coupled building systems.

CHAPTER 5: THREE-DIMENSIONAL FINITE ELEMENT INVESTIGATIONS INTO EARTHQUAKE-INDUCED FRAME ORTHOGONALITY EFFECTS

5.1 Introduction

Special moment frames (SMFs) and buckling-restraint braced frames (BRBFs) are the most popular steel systems for resisting seismic loads. The research in this chapter focuses on the response of SMFs and BRBFs under the seismic (frequent) behavior of vibration caused by an earthquake. Coupled and un-coupled steel configurations in six levels are modeled using ABAQUS [58]. The inelastic behavior of the SMFs is taken over (dominated) by reduced beam sections (BRBs), which are located away from the column flanges to keep the column from plastically deforming. The inelastic behavior of BRBFs is controlled by buckling of braces, yielding and post-buckling behavior. Due to the variation of compressive and tensile strengths of steel braces, the non-linear performance of these elements is nonsymmetrical. This dilemma has been solved by surrounding the brace with a tube and filling it with a structural material with a high compressive strength, which results in equivalent strengths in both tension and compression as well as symmetric response. The braces are generally designed as truss elements, which means they can only carry axial forces, and are connected to column and beam flanges by gusset plates.

Two steel systems that include SMF and BRBF combinations of coupled and uncoupled configurations are considered here to evaluate the orthogonal effects of seismic loads on the corner column of a building. Because the building under investigation is symmetric, one-fourth of the configuration is taken to account, which requires less computational time for analysis. Therefore, the seismic masses for each floor are calculated based on this assumption and lumped at the column as shown in Figure 40 (red dots) to simulate the physical structure conditions through the seismic incident.

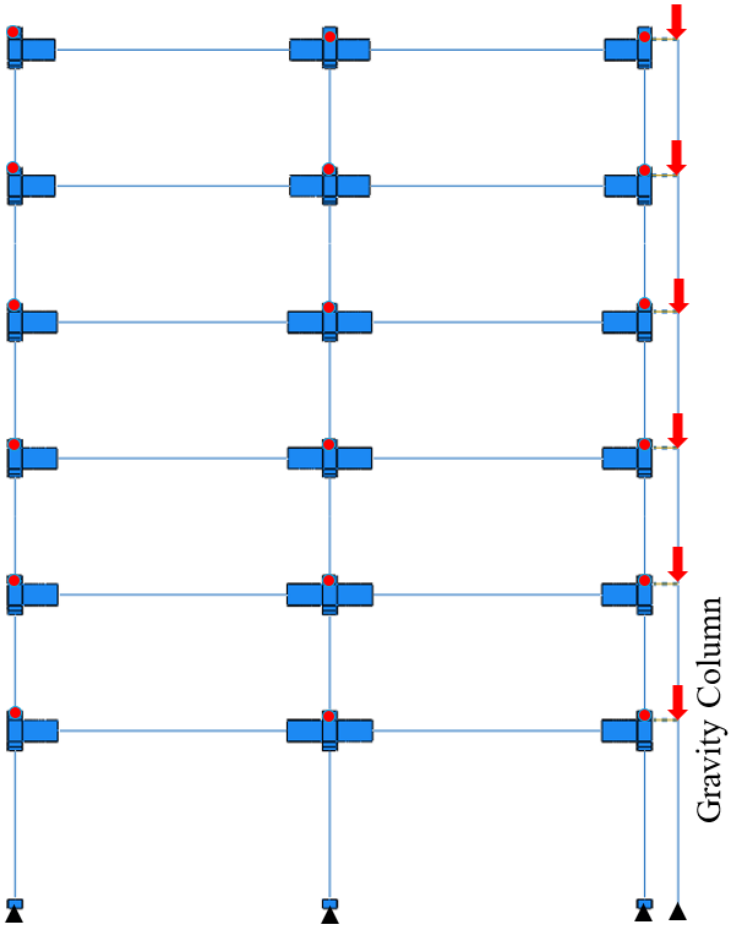

Figure 40. ABAQUS finite element model for 6-story SMF.

The model elements of SMF and BRBF (beams, columns, continuity plates, doubler plates, and gusset plates) were modeled as shell elements of type of S4R, which stands for Shell, 4-nodes, and reduced integration elements, respectively. Six degrees of freedom (three displacements and three rotations) are at each node of this element as is beneficial for computational efficiency. In addition, more accurate results and significantly reduced running time can be achieved by using reduced integration, which has been used by previous studies for modeling [6, 7, 12, 54].

The beams and columns are cut at a distance of $d_b/2$ beyond the RBS cut for beams and $d_c/2$ for columns (above and lower the beam flanges) for the SMFs, while they are cut at the same distance beyond the gusset plates for the BRBFs. Rigid body nodes were created at the center of

each cross-section of the beams and columns, and then connected with a beam wire element as shown in Figure 41. Following this procedure leads to decreased analysis running time especially for huge structures modeled in three dimensions (as presented in this study).

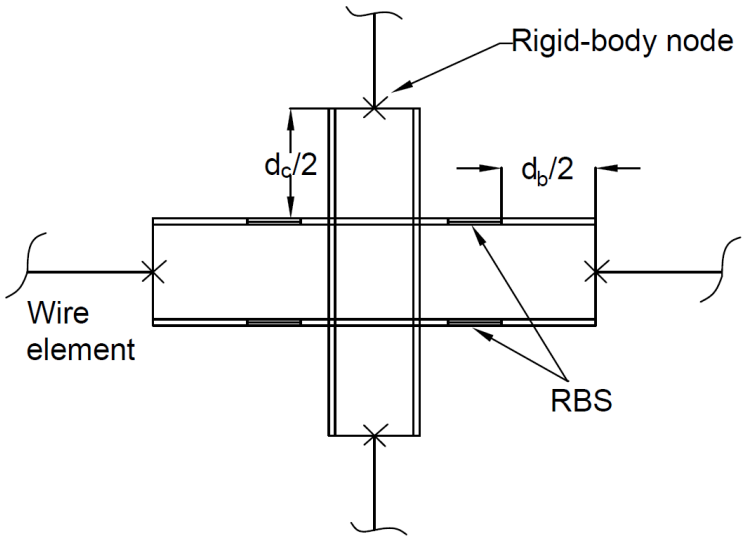

Figure 41. Details of structural elements in ABAQUS.

5.2 Properties of Materials

The material properties used for the time history analysis were calibrated from cyclic coupon testing of A572 Gr 50 steel [14], which is used for dynamic analysis in OpenSees models. This type of steel is similar to A992 steel, which is commonly used for rolled wide flange shapes. Many previous studies used the steel for plastic analysis, and the results were naturalistic (reasonable results) [6, 7, 54]. This research focused on the non-linear behavior of the structural members so that a combined non-linear isotropic and kinematic material model was used in ABAQUS [65] for material hardening during plastic strain using Equation 5.1 The kinematic hardness parameter (c) equals 406.18 while the gamma is 37.175; whereas α_1 is considered to be zero and the mass density is 0.2838 Ib/in^3. Table 16 lists some other properties for the steel. These

values have been used by some previous finite element models [5, 6, 7, 12, 54] with reasonable results for plastic strain.

$$\alpha = \frac{C}{\gamma}\left(1 - e^{-\gamma\varepsilon^{pl}}\right) + \alpha_1 e^{-\gamma\varepsilon^{pl}} \quad \text{Eq. 5.1}$$

Table 16. Properties of A572 steel used in the finite element models.

Material	Young's model (ksi)	Yield stress (ksi)	Poison's ratio
Steel	29000	63.5	0.3

5.3 Element Mesh Size

Choosing the mesh size is extremely important for capturing the critical stresses, strains, and local buckling. Because the connections are the most critical parts in the models, the mesh size is smaller than the other regions. In this research study, four-node quadrilateral elements were used, and a mesh size of 0.5 in×0.5 in was applied for the connections that include the length of $d_b/2$ beyond the RBS cut for the beams, or $d_c/2$ after the beam flanges for the columns. All continuity plates, doubler plates, and gusset plates were meshed by the same mesh size (0.5 in). A general mesh size of 2-inch squares was applied for the rest of structural elements (beams and columns). This technique is similar to previous dynamic analysis [6, 7, 54].

The capacity of the structural elements could be affected by the initial deformations. Therefore, these initial imperfections should be taken into account through the dynamic analysis. In this research project, the mode shape for each model was obtained using the frequency analysis (linear perturbation analysis) in ABAQUS, and then composed on the dynamic models as initial distortion. The initial geometry imperfections were scaled by the straightness tolerance limit of L/1000 [(AISC 2010a [7] [10] [54] where L is clear column length (the column's unbraced length).

5.4 Damping and Modeling of the SMF and BRBF Systems

The Rayleigh damping for all ABAQUS models matched the OPENSEES models presented in chapter 4, which equals five percent (5%). Frequency models have been created for SMF and BRBF to determine the first and third vibration modes. The Rayleigh damping parameters (α and β) were calculated by following Equation 5.2 [13, 54]. Table 17 summarizes the damping parameter that was acquired from the frequency analysis and which was used for running the time history analysis in ABAQUS.

$$\zeta_i = \frac{\alpha}{2\omega_i} + \frac{\beta\omega_i}{2} \qquad \text{Eq. 5.2}$$

Table 17. Damping parameters for the structures.

Model	ω_1 (rad/s)	ω_2 (rad/s)	α	B
SMF	5.0486	5.3356	0.260341	0.009597
BRBF	3.5444	4.6011	0.200193	0.12278

5.4.1 Modeling the Reduced Beam Section (RBS)

Using deep columns in the SMF (with RBS connections) could lead to column twisting due to the eccentric forces at beam flanges, which is caused by the distortion at the SMF RBS connections under the plastic strain (lateral torsional buckling) [22]. Moreover, lateral torsional buckling for deep columns has a higher probability of occurring than in medium and shallow columns [23]. To avoid this phenomenon, shallow columns were used throughout both the SMF and BRBF, as listed in Table 18. To keep the stresses away from the columns, Reduced Beam Section (RBS) connections were created at a distance of (a) from the column flanges, as shown in Figure 42. The RBS designed by following AISC 385-16 [1], and the RBS flange-cut dimensions at each story (b, c) are listed in Table 4.3 An example of the RBS calculations is available in Appendix A.

Table 18. Beam-column size and the beam RBS flange-cut dimensions.

Level	Column	Beam	Beam RBS dimensions (in)		
			A	b	C
1&2	W14×550	W24×279	9	17	2.5
3&4	W14×426	W24×192	9	16	2.5
5&6	W14×342	W24×162	9	16	2.5

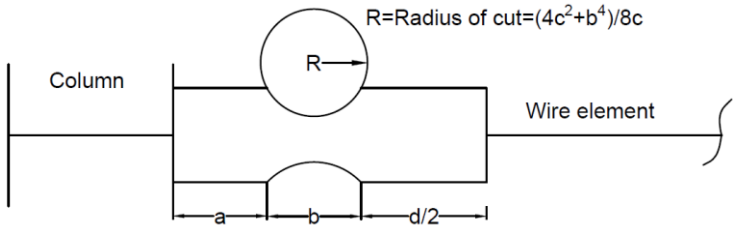

Figure 42. Geometry and dimensions of reducer beam section details.

5.4.2 Modeling the Gravity Column for SMF and BRBF

In multistory structures, the impacts of gravity load through the structural displacements are expressed as P-Δ effect. The response of this effect increases (expands) under the static lateral loads, whereas it depends on the dynamic load (based on the natural period of the building) for the time history analysis. This variation in response could be negligible for elastic frames; however, it is substantial for inelastic structures [24].

In this study, to consider the P-Δ effect, a gravity column was added to the main models at distance of 30 feet from the uncoupled SMF and BRBF with a gravity column density of 2.836E-010 as shown in Figure 40. By considering the weak axis bending, the P-Δ gravity column strength and stiffness corresponds to the sum of the individual gravity columns (one quarter of the structure at each story). This approach is similar to previous dynamic analysis [6, 22, 25, 27]. The gravity column was modeled as wire element and has the same height as the original model; its properties are listed in Table 19. To prevent the movement of the moments and to provide the same displacements and rotations as the main models, rigid links with pin connections were used to

connect the gravity column to the models. One quarter of the gravity loads, including the dead load, live load and seismic load under the factored load combination of (1.2DL+0.5 LL+E) [1], were applied to the gravity column at each level (vertical red arrow) as shown in Figure 40.

Table 19. Properties of the gravity column for SMF and BRBF.

Level	**Area (in^2)**	**I_{xx} (in^4)**	**I_{xy} (in^4)**	**I_{yy} (in^4)**	**J (in^4)**
1&2	1000	3124.47	3000	3124.47	6248.94
3&4	9000	1543.4	1000	1543.4	3086.94
5&6	8000	598.26	400	598.26	1196.52

I_{xx}. the moment of inertia around *X*-axis.
I_{yy}. the moment of inertia around *Y*-axis.
I_{xy}. the moment of inertia around *X*- and *Y*-axis.
J. the polar moment of inertia.

5.4.3 Modeling the Continuity and Doubler Plate

Panel zones have considerable effect for transferring the lateral loads to other elements, and through their ductile behavior can significantly enhance the overall ductility of the SMFs. In steel moment configurations, columns experience unbalanced moments, which are transmitted to the panel zone through the forces at the centroid of the beam flanges. When the moment generated via the tension and compression forces is higher, utilizing continuity plates is required.

AISC provisions require that continuity plates are needed when column flange thickness is lower than one-sixth of the beam flange depth *($t_{cf} < b_f/6$).* The minimum thickness of the plates must be at least equal one-half (50%) of the thickness of the beam flange for one-sided connections and equal three-quarters (75%) of the beam flange thickness for two-sided connections. A design example for continuity plates is presented in Appendix A. Table 20 shows the geometric dimensions for continuity plates used in ABAQUS, and the installation of the continuity plate in The SMF is illustrated in Figure 43.

Table 20. Dimensions of continuity plates used in SMFs.

Level	t_{cf}	$b_f/6$	one-sided connections	two-sided connections	w_p
1&2	4.16	2.9	1.14	1.71	5.4
3&4	3.5	2.87	0.865	1.28	5.25
5&6	3.04	2.8	0.785	1.18	5.2

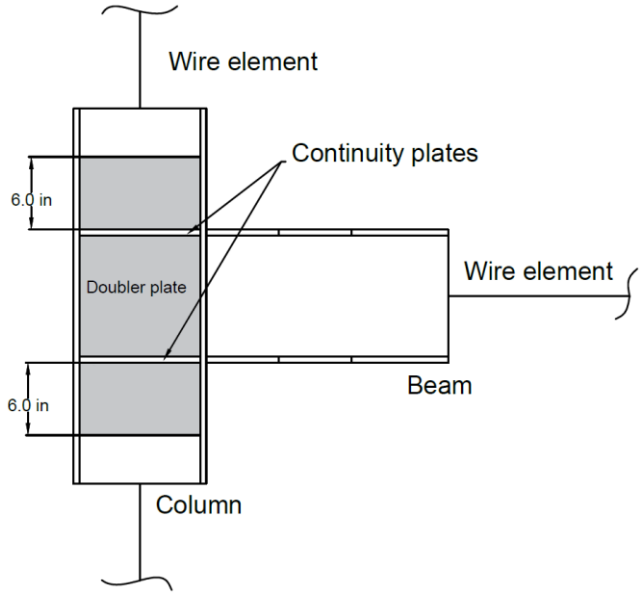

Figure 43. Instillation of the continuity and doubler plates in SMFs.

Through the cyclic behavior, significant ductility could be obtained by using stable panel zones [56] [57]. To prevent using thin plates, AISC limits the minimum thickness of the doubler plate to ¼ in, and it requires the plate to be in contact with the column web. The extension of these structural elements must be at least 6 inches above and below the top and bottom of the moment frame beams as shown in Figure 43. The doubler plate design calculations for the SMF are shown in Appendix A, and the geometric dimensions used in ABAQUS are presented in Table 21.

Table 21. Geometry of the doubler plates.

level	width	high	T_p required	T_p used	T applied in ABAQUS
1&2	12.56	32.2	1.69	2	4.38
3&4	12.62	30.7	1.14	1.5	3.38
5&6	12.56	29.5	1.41	1.5	3.04

5.4.4 Gusset plates Modeling in BRBFs

The overall seismic performance of BRBFs depends on the precise design of the connections that join the braces to the main frame. The object of seismic design is to reach the ultimate system ductility before the fracture of braces. To achieve the maximum ductility, the braces are able to yield and buckle, carrying considerable displacements, dissipating much seismic energy, and finally withstanding seismic loads through ductility and flexibility. In the BRBFs, the BRBs are attached to the columns and beams through gusset plate connections, and these plates are connected to the configuration via fillet welds as shown in Figure 45. The axial forces in the braces, tension or compression, are transferred to the main frame by these plates; thus, they must have appropriate strength and stiffness to transfer the expected loads. Inadequate gusset plates lead to a significant loss of stiffness and strength of the BRBs and negatively affects the whole structure. Using gusset plates in the BRBFs leads to an increase in the flexural stiffness of the connections and decreases the BRBs length.

The AISC seismic design provisions require that the axial capacity of gusset plates should exceed the ultimate compressive force of BRBs and provide connection design equations to ensure that this occurs. According to the AISC code, due to the out-of-plane buckling of these plates that could occur before the ultimate load of BRBs, based on some tests, the instability of the plates should also be considered. The prospective axial forces in the BRBs vary from tension and compression, and brace resistance is estimated based upon yield stress of the material. The shear fracture of the gusset plate must not occur prior to the brace fracture so that the inelastic behavior of the brace can be reached. Table 22 summarizes the geometric dimensions of the gusset plate for the 6-story uncoupled BRBF that is used in ABAQUS models.

Table 22. Geometry of the gusset plates.

Level	Dimensions (in)				Thickness
	Edge plates		Middle plates		
	Length	Width	Length	width	
6&5	30	21.44	60	15.525	3
4&3	30	21.44	60	15.525	2.5
2&1	30	21.44	60	15.525	2

5.4.5 Geometry and Modeling of Buckling-Restrained Braces

Buckling-restrained braces are structural elements added to steel configurations and designed to allow them to resist cyclical lateral loads. The comprehensive process of design for the BRBs is not specific in the current codes; some data is available based upon some of the experimental tests of the BRB specimens, which is only feasible for design of similar buildings. The BRBs are made of two main parts: the steel core and the external jacket as shown in Figure 8. The steel core is subjected to inelastic deformations due to the cyclic behavior caused by seismic loading, while the external jacket restrains against any buckling of the steel core bar. The BRBs are supposed to yield in both tension and compression with balanced behavior due to the lateral restraint provided by the jacket. The steel core is divided into three zones: the yielding region, transition region, and connection region. The yielding segment has the smallest cross-sectional area and is totally restrained to ensure compressive and tensile yielding. The transition segments are directly on either side of the yielding area, and they have a similar constraint but a larger cross-section than the yielding zone. The connection segments are the zones of the brace that extend beyond the restraining components and have the largest cross-section area, which is used to connect the brace to the gusset plates at the corner of beams and columns.

Figure 44 shows the three typical core parts. Determining the flexural stiffness of each segment is important. Equation 4.3 is used to estimate the axial stiffness of an individual section where k_i, A_i, and L_i are stiffness, area, and length at the level (i) [50]. The effective stiffness of the

three springs as a series can be calculated using Equation 4.4; and the effective stiffnesses of BRBs for 6-story uncoupled BRBF are listed in Table 23. In the case of the lower stiffness, modifying the BRB could be done by shortening the yielding core length. The BRB was modeled as non-linear-spring (a connector section assignment with only an axial load) as shown in Figure 45. The springs are connected to the gusset plates at each level and work axially from work-point to work-point in the 2-X-story BRBF. This approach simulates the real-life behavior of the structures under seismic shaking.

$$k_i = \frac{A_i + E}{L_i} \qquad \text{Eq. 4.3}$$

$$k_{eff} = \frac{1}{(\frac{1}{k_{YC}} + \frac{1}{k_{TR}} + \frac{1}{k_{CR}})} \qquad \text{Eq. 4.4}$$

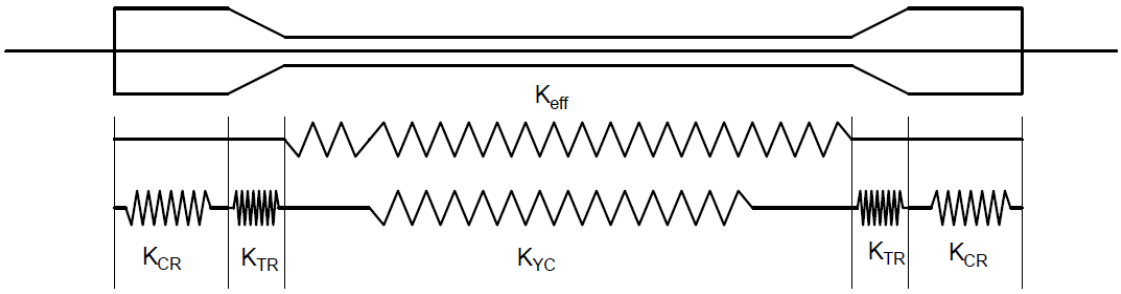

Figure 44. Schematic diagram of the BRB components with axial their stiffness.

Table 23. Spring stiffness for 6-story BRBF (ksi).

level	P_u (kips)	K			$K_{eff.}$
		K_{yield}	$K_{transition}$	$K_{connection}$	
6	583.1	1948.2	39258.8	16920.4	1485.6
5	986.7	3357.9	66446.2	28631.9	2514.1
4	1345.5	4578.9	90625	39038.5	3222.5
3	1524.9	5189.5	102732.2	44247.3	3885.5
2	1704.3	5800	114767.5	49445	4342.5
1	1794	4957.3	120857.5	20758.1	3178.4

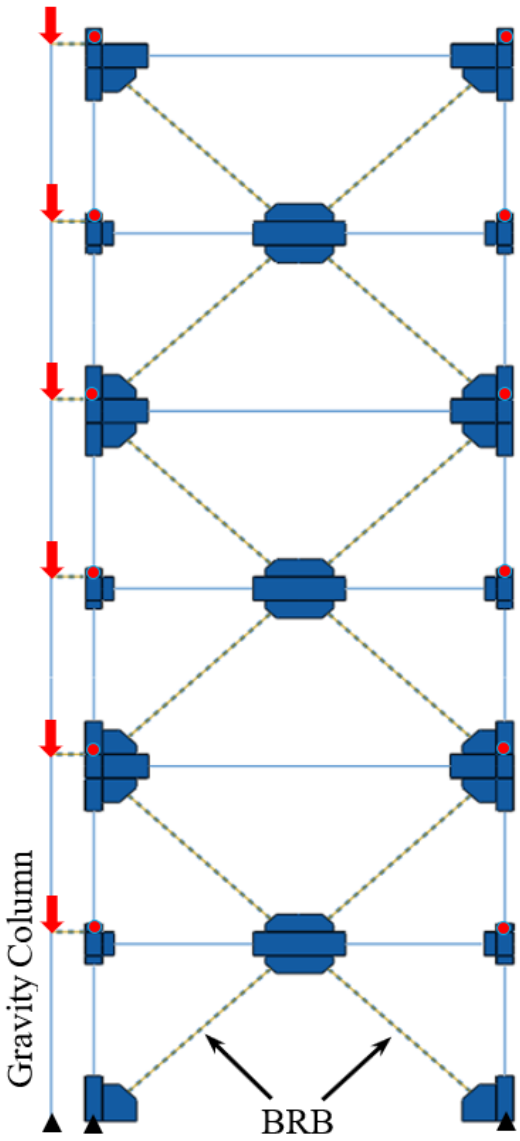

Figure 45. ABAQUS finite element model for 6-story BRBF.

5.5 Boundary Conditions for the SMF and BRBF

Numerical simulations are a suitable method for considering the structural response under seismic shaking, and the fabricated boundary conditions have significant effects on the accuracy of the results. In this study, the boundary conditions used for prototype models describe the real-life conditions under the seismic loading as shown in Figure 46. Two types of boundary conditions

were applied to the models; the first was for the gravity analysis (BC. Gr), and the second was for the dynamic analysis (BC. EQ). All boundary conditions were considered at reference points (RP) that were located at the center of the cross-section (X-sign), and each RP is rigidly tied to its cross-section in which it works as a full section. In other words, applying the BC at the RP gives uniform distribution for the BC within its cross-section. The bases of the main model and gravity column are pin connections in which some movement is allowed at the seismic load direction (x-axis), and rotation perpendicular on this direction (y-axis). The lateral beam support was considered to control the rotation and lateral motion of the beams. The gravity column has the same BCs as the main model based on where they are applied.

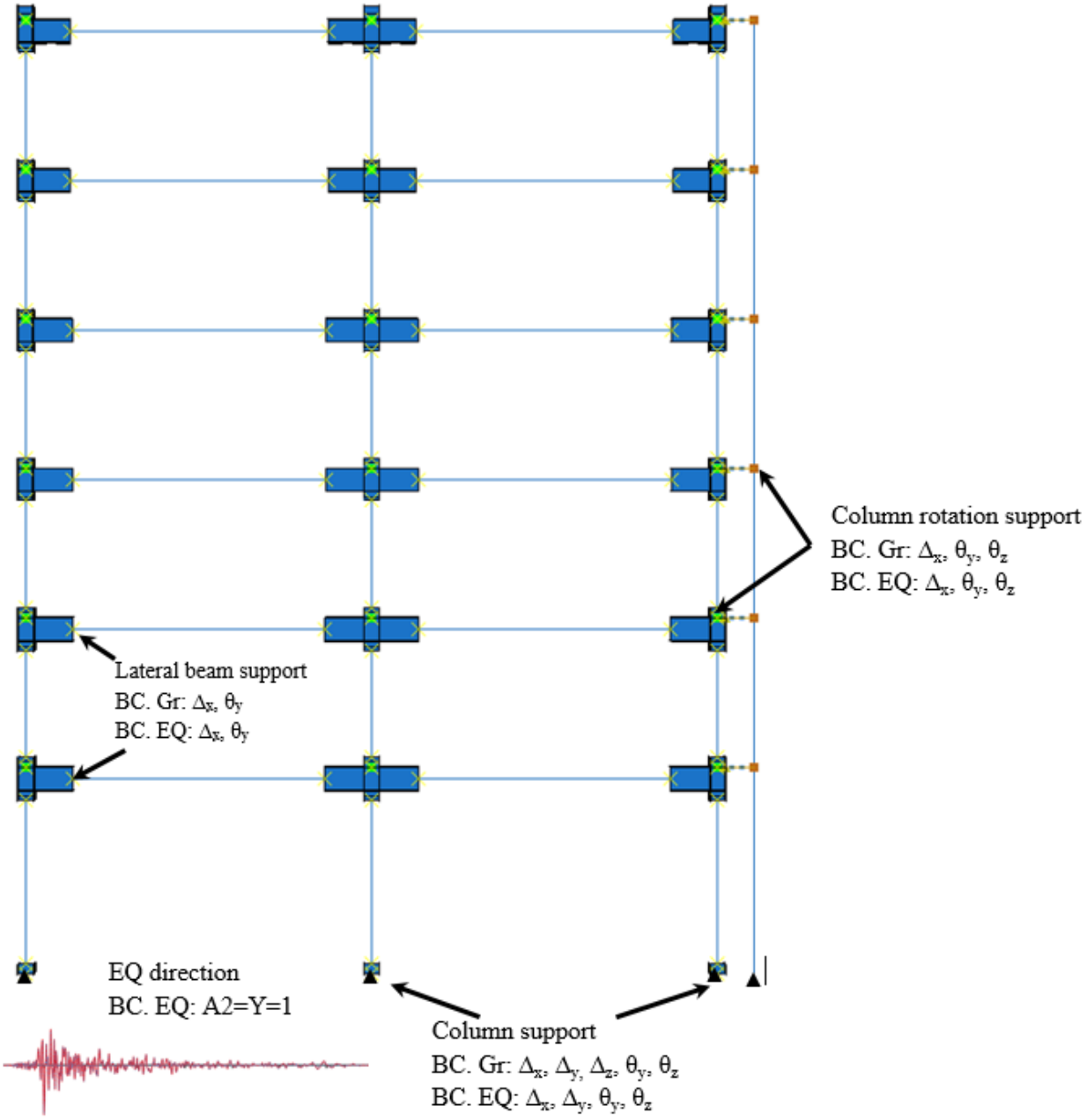

Figure 46. Boundary conditions and applying the earthquake for 6-story uncoupled model.

5.6 Results and Discussion

A static analysis (self-weight) followed by a dynamic analysis were carried out separately to investigate the orthogonal effects of seismic loads on steel structures in seismically active areas.

In such cases, the deformed geometry and stress state of the gravity analysis are imported before the dynamic analysis is run.

5.6.1 Gravity Analysis

Four models have been tried out, which include coupled and uncoupled frames for the combinations of BRBF with 2-story X-configuration and SMF, to consider the uniform acceleration under the gravity loads. One quarter of the structure mass was distributed (as a lumped mass) to each column, at each story height level.

The fundamental frequencies for the four various model geometries were obtained, and the values of alpha (α) and peta (β) were calculated and considered in the dynamic analysis. Table 17 lists the alpha and beta values for 6-story SMF and BRBF.

5.6.2 Time History Dynamic Analysis and Results of SMF and BRBF

Time history analyses of the models based on the assumptions described previously were conducted by using the Pacoima Kagel Canyon strong motion record that is considered to be representative of motions experienced by structures during the Northridge earthquake; some of the properties of the record are presented in Table 9. The Peak Ground Acceleration (PGA) was used to identify and define the strong component of the earthquake. The powerful seismic direction was assumed to be in the east-west direction (which represents the *x*-axis) for two-dimensional analysis; by contrast, the three-dimensional analysis had E-W and N-S components, which symbolizes the *y*-axis, applied simultaneously.

The key goal of this chapter is to establish the previous results (using OpenSEES) and compare them with ABAQUS results. The results from the inelastic dynamic analysis of the 6-

story uncoupled frames are shown in Figure 47. In general, it is concluded that the seismic attack angle (the interaction between the earthquake and the building) has considerable effect on the seismic column demands. The redistribution of axial loads based on the attack angles within the columns of interest exhibit significant variation with increasing axial loads, where this rise refers to the effect of simultaneous bidirectional horizontal shaking. The attack angle of 0.0^0, which represents the E-W direction and *x*-axis, was considered as a reference to evaluate biaxial shaking that moves counter-clockwise. The column axial load increased at the angle of 30^0 where it produced simultaneous trembling for both the SMF and BRBF, and had significantly more trembling at 30^0 vs. 0.0^0 for both the SMF and BRBF. The local axial column load showed various reactions where the lower columns were more affected by the biaxial movement than the upper columns. The simultaneous shaking at the angle of 60^0 had more effect on the column steel configuration than the previous attack angle, an increase that was expected because of increasing the effects of buckling restrained braces in the BRBF, which are located in the N-S direction.

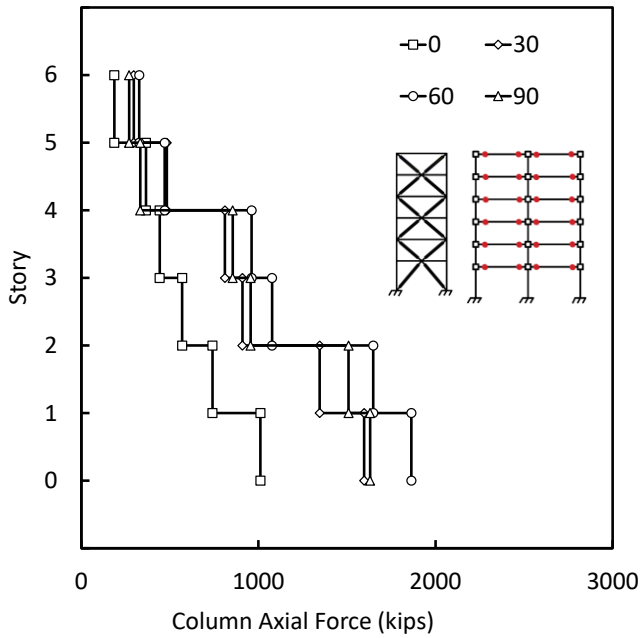

Figure 47. Seismic Forces in the Columns for 6- Story Uncoupled Frames (BF-MF).

Figure 48 includes four charts that show the comparison of results at four directions of lateral seismic loads based on two finite element simulations OpenSEES and ABAAQUS. The profiles illustrate the close match of results between the two-time history dynamic analyses for the SMF and BRBF, which investigated the effect of seismic loading at the proposed orientations. The difference between the two analyses ranged an average of 9.65 %. This compatibility indicates that structures under bidirectional lateral loads (angles of 30^0 and 60^0) are estimated to create more column axial forces than unidirectional loads (angles of 0^0 and 90^0).

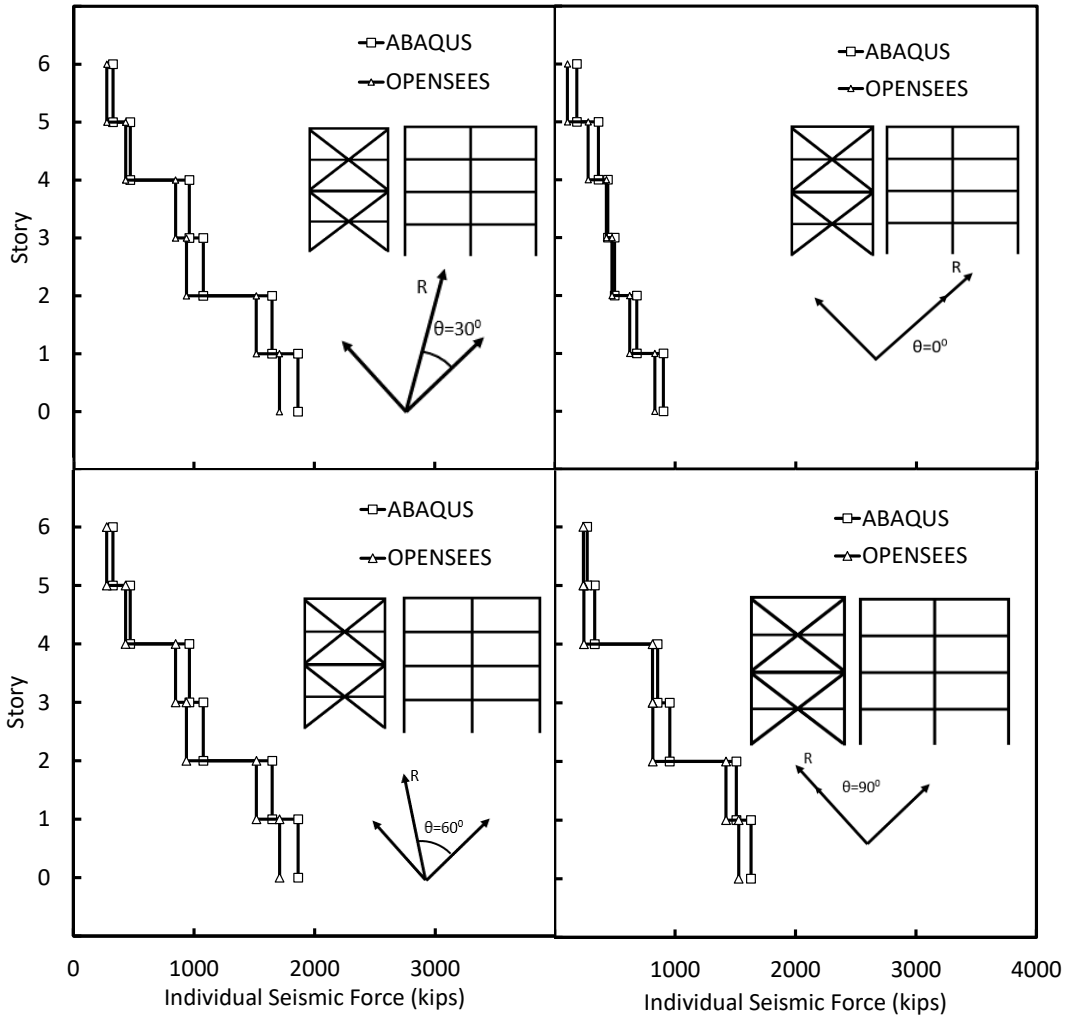

Figure 48. Seismic Forces in the Columns for 6- Uncoupled Frames (BF-MF). (OpenSEES and ABAQUS).

5.7 Summary and conclusions from ABAQUS investigations

An investigation of the column requirements and their demands was conducted in this chapter to evaluate the current design rule (100+30% rule) followed by the existing specifications to design structures in seismically active areas. The finite element commercial software ABAQUS was used to model four finite elements considering special moment frames and buckling-restrained braced frames under the combination of coupled and uncoupled steel systems. The finite elements models were fabricated as shell elements with four-node element (S4R), and the middle parts of beams and columns were modeled as wires to reduce the time of dynamic analysis. A wire gravity column was added to the main model to consider P-Δ effects, and was connected to the main models using links that allowed it to have the same displacement and rotation as the original model as well as the same boundary conditions.

The location of the models was assumed to be in the same directions as the OpenSEES models in chapter three, where the SMF has to be built at the E-W direction (X-axis), while the BRBF is to be located at the N-S direction (Y-axis). The angle of 0^0 is identical to X-axis and moves counter clockwise until it reaches 90^0, which is perpendicular to the previous axis. This approach allows results to be compared with the previous outcomes (Ch. 4).

Based on the AISC provisions, column axial loads and lateral displacement are connected under the term P-Δ effect, where increasing the axial load leads to the amplification of lateral and flexural displacement, which could affect the column fatigue life. The increase of axial loads in columns caused by the orthogonal shaking might produce plastic strains that go beyond the ultimate strains of steel members. Moreover, this increase in the column demands beyond design demand leads to column local buckling.

From this study it is concluded that column axial forces are correlated with the interaction angle between the lateral loads and the building. Seismic loads with the orientation of 30 degrees show development of the column demands by rate of 42.3 % compared to the direction of zero degree (0.0^0). The noticeable increase in the column axial loads was shown by moving the effect of lateral forces forward the BRBF (y-direction) until it reached the angle of 60 degrees, which resulted the in the largest rate of increase at 51.5%. Choosing the direction of seismic loads (E-W and/or N-S) and the locations of the steel frames (SMF and BRBF) has considerable effect on the results. Using symmetrical frames (BF-BF or SMS-SMF) at the end of the configuration (the corner of building) gives the same results; whereas, in the case of building a structure with unsymmetrical ends (SMF-BF) (as proposal in this chapter), defining the main orientations has a considerable effect on the outcomes.

CHAPTER 6: SUMMARY, CONCLUSIONS, CONTRIBUTIONS, AND AREAS FOR FUTURE RESEARCH

6.1 Summary and Conclusions

In this study, axial demands within shared columns of orthogonally connected seismic systems were investigated using nonlinear time-history analysis. Interaction effects from coupled seismic system demands were compared with column demand additions from independent (uncoupled) frame analyses as typically assumed in design. A total of 800 nonlinear time-history analyses were performed in this study, representing both BRBF and SMF configurations in uncoupled and coupled frames, 10 scaled earthquake ground motions, and four incident angles (0, 30, 60, and 90 degrees). In addition to the dynamic time-history analyses, two advanced finite element analyses using shell elements within crucial connection regions were performed. Key conclusions related to orthogonality effects in shared seismic columns are as follows:

1- Column demand estimations using the 100+30 rule are consistently non-conservative in the upper building stories of the 6, 9, and 12 story analyses conducted. Resulting orthogonality effects produced shared column demands that exceeded code estimations by nearly 50% on average.

2- Increasing to a 100+50 demand rule appears warranted for columns within the upper 1/3 building height.

3- Column demand summations from uncoupled frame analyses are conservative when compared to coupled system analyses having interaction effects. Demands from coupled BRBF system analyses were lower than those for uncoupled demand summations.

4- The current 100+30 rule results in conservative demand estimations for the lower building stories having higher lateral seismic demands. In lower building stories, estimated demands

exceeded measured demands by more than 40% for the coupled BRBF-BRBF configurations. Adding the additional 30% column demand within the bottom 1/3 of building height appears overly conservative and unwarranted.

6.2 Contributions to the Field of Structural Engineering

Based on the results of this investigation, the contributions from the dissertation work are listed as follows:

1) Evaluation of the current design rules that have been adapted by existing provisions and design requirements of the steel systems in seismically active areas.
2) Quantify the seismic column demands in uncoupled and connected steel systems under the composition (BF-MF) and (BF-BF).
3) Demonstration of the orthogonal effects of cyclic loading on corner steel columns.
4) Introducing a new rule to AISC provisions to design structures in seismic areas, which could be an alternative to the current rule.
5) Showing 800 inelastic analysis on various SMFs and BRBFs under several compositions.
6) Providing a comparative (parametric) study for configurations that have the same properties and seismic coefficients but in different locations.

6.3 Recommendations for Future Work

In this dissertation work, a new rule to design structures in seismic zones using numerical investigation was provided. However, experimental work on steel frames designed using the proposed method is needed. In addition, using other design coefficients such as R, I, and Cd in new studies could enhance the understanding of the orthogonal effects of seismic loads on

structures. Moreover, considering non-linear dynamic analyses with ground motions having probabilities of exceeding of 10% in 50 years instead of 2% in 50 years might be useful to cover in a comprehensive study related to this dissertation.

REFERENCES

[1] AISC (2016)."ANSI/AISC 358-16: Prequalified connections for special and intermediate steel moment frames for seismic applications." American Institute of Steel Construction, Chicago, IL.

[2] Sesigur, H., Celik, O. C., & Cili, F. (2004, August). Review and evaluation of combination rules for structures under bidirectional earthquake excitations. In *13th World conference on earthquake engineering, Vancouver, BC, August* (pp. 1-6).

[3] Menun, C., & Der Kiureghian, A. (1998). A replacement for the 30%, 40%, and SRSS rules for multicomponent seismic analysis. *Earthquake Spectra*, *14*(1), 153-163.

[4] Rahnavard, R., Hassanipour, A., & Siahpolo, N. (2015). Analytical study on new types of reduced beam section moment connections affecting cyclic behavior. *Case Studies in Structural Engineering*, *3*, 33-51.

[5] Richards, P. W., and Uang, C.-M. (2005). "Effect of flange width-thickness ratio on eccentrically braced frames link cyclic rotation capacity." *J. Struct. Eng.*, 10.1061/(ASCE)0733-9445(2005)131:10(1546), 1546–1552.

[6] Prinz, G. S. (2007). "Effect of beam splicing on seismic response of buckling-restrained braced frames." Thesis and Dissertations, Brigham Young University, Provo, UT.

[7] Desrochers, C. (2017). "Effect of column axial load on skewed SMF RBS connection demands." Thesis and Dissertations, University of Arkansas, Fayetteville, AR

[8] Kamyar, K., Rasoul, M., & Iradje Mahmoudzadeh, K. (2012). The Efficiency of Reduced Beam Section Connections for Reducing Residual Drifts in Moment Resisting Frames. *Open Journal of Civil Engineering*, *2012*.

[9] Swati, A. K., & Gaurang, V. (2014). Study of steel moment connection with and without reduced beam section. *Case Studies in Structural Engineering*, *1*, 26-31

[10] Desrochers, C., Prinz, G. S., and Richards, P. W. (2018). "Column axial load effects on the performance of skewed SMF RBS connections" Journal of Constructional Steel Research, 150(505-513.

[11] Chen, S. J., Yeh, C. H., & Chu, J. M. (1996). Ductile steel beam-to-column connections for seismic resistance. *Journal of Structural Engineering*, *122*(11), 1292-1299.

[12] Prinz, G. S., and Richards, P. W. (2016). "Demands on reduced beam section connections with out-of-plane skew." J. of Structural Engineering, 10.1061/(ASCE)ST.1943-41X.0001360,04015095.

[13] Prinz, G. S., and de Castro-e-Sousa, A. (2014). "Effect of slab stiffness on EBF link rotation demands and implications for link ultralow-cycle fatigue susceptibility." In Structures Congress 2014, 2664-2674.

[14] Kaufmann, E., Metrovich, B., and Pense, A. (2001). "Characterization of cyclic inelastic strain behavior on properties of A572 Gr. 50 and A913 Gr. 50 rolled sections." National Center for Engineering Research on Advanced Technology for Large Structural Systems, ATLSS Rep. No. 01-13, Lehigh University, Bethlehem, PA.

[15] Prinz, G. S., & Richards, P. W. (2012). Seismic performance of buckling-restrained braced frames with eccentric configurations. *Journal of Structural Engineering*, *138*(3), 345-353.

[16] Bisadi, V., & Head, M. (2011). Evaluation of combination rules for orthogonal seismic demands in non-linear time history analysis of bridges. *Journal of Bridge Engineering*, *16*(6), 711-717.

[17] ASCE 7. Minimum Design Loads for Buildings and Other Structures, ASCE 7-10. Virginia: American Society of Civil Engineers; 2010.

[18] Menun, C., & Der Kiureghian, A. (1998). A replacement for the 30%, 40%, and SRSS rules for multicomponent seismic analysis. *Earthquake Spectra*, *14*(1), 153-163.

[19] MacRae, G. A., & Mattheis, J. (2000). Three-dimensional steel building response to near-fault motions. *Journal of Structural Engineering*, *126*(1), 117-126.

[20] Stevens, D., & Wiebe, L. (2019). Experimental Testing of a Replaceable Brace Module for Seismically Designed Concentrically Braced Steel Frames. *Journal of Structural Engineering*, *145*(4), 04019012.

[21] Shen, J., Wen, R., Akbas, B., Doran, B., & Uckan, E. (2014). Seismic demand on brace-intersected beams in two-story X-braced frames. *Engineering Structures*, *76*, 295-312.

[22] Prinz, G. S. (2010). "Using buckling-restrained braced frames in eccentric configurations." Ph.D. Dissertation, Brigham Young University, Provo, UT.

[23] Hamburger, R. O., & Malley, J. O. (2009). Seismic design of steel special moment frames. *NEHRP seismic design technical brief*, (2).

[24] Asimakopoulos, A. V., Karabalis, D. L., & Beskos, D. E. (2007). Inclusion of P–Δ effect in displacement-based seismic design of steel moment resisting frames. *Earthquake engineering & structural dynamics*, *36*(14), 2171-2188.

[25] Prinz, G. S., & de Castro-e-Sousa, A. (2014). Effect of Slab Stiffness on EBF Link Rotation Demands and Implications for Link Ultra Low-Cycle Fatigue Susceptibility. In *Structures Congress 2014* (pp. 2664-2674).

[26] Tremblay, R., & Robert, N. (2001). Seismic performance of low-and medium-rise chevron braced steel frames. *Canadian Journal of Civil Engineering*, *28*(4), 699-714.

[27] Richards, P. W. (2009). Seismic column demands in ductile braced frames. *Journal of Structural Engineering*, *135*(1), 33-41

[28] Gupta, A., and Krawinkler, H. (1999). "Prediction of seismic demands for SMRFs with ductile connections and elements." SAC Joint Venture, Report No. SAC/BD-99/06, Sacramento, CA.

[29] Zhang, X., & Ricles, J. M. (2006). Seismic behavior of reduced beam section moment connections to deep columns. *Journal of structural engineering*, *132*(3), 358-367.

[30] Faghihmaleki, H., Nejati, F., Zarkandy, S., & Masoumi, H. (2017). Evaluation of progressive collapse in steel moment frame with different braces. *Jordan Journal of Civil Engineering*, *11*(2), 290-298.

[31] Okazaki, T., Engelhardt, M. D., Nakashima, M., & Suita, K. (2006). Experimental performance of link-to-column connections in eccentrically braced frames. *Journal of Structural Engineering*, *132*(8), 1201-1211.

[32] Sabelli, R., Mahin, S., & Chang, C. (2003). Seismic demands on steel braced frame buildings with buckling-restrained braces. *Engineering Structures*, *25*(5), 655-666.

[33] Prinz, G. S., Coy, B., & Richards, P. W. (2014). Experimental and numerical investigation of ductile top-flange beam splices for improved buckling-restrained braced frame behavior. *Journal of Structural Engineering*, *140*(9), 04014052.

[34] ASCE (2016)."Minimum design loads for buildings and other structures." ASCE/SEI 7-16, American Society of Civil Engineers, Reston, VA.

[35] Talebi, E., Tahir, M. M., Zahmatkesh, F., Yasreen, A., & Mirza, J. (2014). Thermal behavior of cylindrical buckling restrained braces at elevated temperatures. *The Scientific World Journal*, *2014*.

[36] Sahoo, D. R., & Chao, S. H. (2010). Performance-based plastic design method for buckling-restrained braced frames. *Engineering Structures*, *32*(9), 2950-2958.

[37] Zhang, X., & Ricles, J. M. (2006). Seismic behavior of reduced beam section moment connections to deep columns. Journal of structural engineering, 132(3), 358-367.

[38] Shin, S., & Engelhard, M. D. (2013). Experimental study on panel zone behavior in steel moment resisting frames. In Proceedings of the 7th International Symposium on Steel Structures.

[39] Imanpour, A., & Tremblay, R. (2017). Analysis methods for the design of special concentrically braced frames with three or more tiers for in-plane seismic demand. *Journal of Structural Engineering*, *143*(4), 04016213.

[40] Hsiao, J. K., Schultz, W., Petersen, T., & Vaicik, S. (2008). Computation of story drifts considering panel zone deformations for multistory steel moment frames with welded flange plate connections. *The Structural Design of Tall and Special Buildings*, *17*(2), 419-443.

[41] Richards, P. W. (2009). Seismic column demands in ductile braced frames. *Journal of Structural Engineering*, *135*(1), 33-41.

[42] Jones, S. L., Fry, G. T., & Engelhardt, M. D. (2002). Experimental evaluation of cyclically loaded reduced beam section moment connections. *Journal of Structural Engineering*, *128*(4), 441-451.

[43] Ariyaratana, C., & Fahnestock, L. A. (2011). Evaluation of buckling-restrained braced frame seismic performance considering reserve strength. *Engineering Structures*, *33*(1), 77-89.

[44] Norwood, J., & Prinz, G. S. (2019). Effect of continuity-plate alignment on the capacity of welded beam-to-column moment connections. *Engineering Structures*, *198*, 109550.

[45] Lee, C. H., Jeon, S. W., Kim, J. H., & Uang, C. M. (2005). Effects of panel zone strength and beam web connection method on seismic performance of reduced beam section steel moment connections. *Journal of Structural Engineering*, *131*(12), 1854-1865.

[46] Menegotto, M. (1973). Method of analysis for cyclically loaded RC plane frames including changes in geometry and non-elastic behavior of elements under combined normal force and bending. In *Proc. of IABSE symposium on resistance and ultimate deformability of structures acted on by well defined repeated loads* (pp. 15-22).

[47] Ibarra, L. F., & Krawinkler, H. (2005). *Global collapse of frame structures under seismic excitations*. Berkeley, CA: Pacific Earthquake Engineering Research Center.

[48] Lignos, D. G., & Krawinkler, H. (2011). Deterioration modeling of steel components in support of collapse prediction of steel moment frames under earthquake loading. *Journal of Structural Engineering*, *137*(11), 1291-1302.

[49] Mazzoni, S., McKenna, F., Scott, M.H., and Fenves, G.L. (2006). "The Open System for Earthquake Engineering Simulation (OpenSEES) User Command-Language Manual." *Pacific Earthquake Eng. Research Center*, Univ. Calif., Berkeley, CA, (http://OpenSEES.berkeley.edu).

[50] Bosco, M., & Marino, E. M. (2013). Design method and behavior factor for steel frames with buckling restrained braces. *Earthquake Engineering & Structural Dynamics*, *42*(8), 1243-1263.

[51] Makrup, L., & Jamal, A. U. (2016). The Earthquake Ground Motion and Response Spectra Design for Sleman, Yogyakarta, Indonesia with Probabilistic Seismic Hazard Analysis and Spectral Matching in Time Domain. *American Journal of Civil Engineering*, *4*(6), 298-305.

[52] Chen, R., Qiu, C., & Hao, D. (2020). Seismic Response Analysis of Multi-Story Steel Frames Using BRB and SCB Hybrid Bracing System. *Applied Sciences*, *10*(1), 284.

[53] Chao, S. H., Karki, N. B., & Sahoo, D. R. (2013). Seismic behavior of steel buildings with hybrid braced frames. *Journal of Structural Engineering*, *139*(6), 1019-1032.

[54] Dominguez, D. (2020). "On the Seismic Performance of Skewed Special Moment Frame Reduced Beam Section Connections" *Ph. D Dissertation*, University of Arkansas, Fayetteville, AR.

[55] CorBrace. The center of design and fabricate BRBs. https://corebrace.com

[56] Lee, D., Cotton, S. C., Hajjar, J. F., Dexter, R. J., Ye, Y., & Ojard, S. D. (2005). Cyclic behavior of steel moment-resisting connections reinforced by alternative column stiffener

details I. Connection performance and continuity plate detailing. *ENGINEERING JOURNAL-AMERICAN INSTITUTE OF STEEL CONSTRUCTION*, *42*(4), 189.

[57] Shin, S., & Engelhard, M. D. (2013). Experimental study on panel zone behavior in steel moment resisting frames. In *Proceedings of the 7th International Symposium on Steel Structures*.

[58] HKS (2014). ABAQUS Standard User's Manual, Version 6.14. Hibbitt, Karlsson, and Sorensen, Inc., Providence, RI.

[59] Richards, P. W., and Prinz, G. S. (2007). "Non-linear time history analysis of refined mesh steel structures." 9 the Canadian Conference on Earthquake Engineering, Ottawa, Ontario, Canada.

[60] Prinz, G. S., & Nussbaumer, A. (2012). Fatigue analysis of liquid-storage tank shell-to-base connections under multi-axial loading. *Engineering Structures*, *40*, 75-82.

[61] Qu, B., Liu, X., Hou, H., Qiu, C., & Hu, D. (2018). Testing of buckling-restrained braces with replaceable steel angle fuses. *Journal of Structural Engineering*, *144*(3), 04018001.

[62] Pachoumis, D. T., Galoussis, E. G., Kalfas, C. N., & Christitsas, A. D. (2009). Reduced beam section moment connections subjected to cyclic loading: Experimental analysis and FEM simulation. *Engineering Structures*, *31*(1), 216-223.

[63] Berde, N. K., Awari, U. R., & Kulkarni, S. A. (2017). Behavior of reduced beam section moment connection with varying thickness of continuity plate. *International Journal of Sustainable Construction Engineering and Technology*, *8*(1), 77-83.

[64] AISC (2012)."Seismic Design Manual." American Institute of Steel Construction, Chicago, IL.

[65] ABAQUS V6.7. 2007. User's manual. Dassault Syst`emes Simulia, Providence RI, USA.

[66] AASHTO. (2010). AASHTO LRFD bridge design specifications, 5th Ed., AASHTO, Washington, DC.

[67] Okazaki, T., Lignos, D. G., Hikino, T., & Kajiwara, K. (2013). Dynamic response of a chevron concentrically braced frame. *Journal of structural engineering*, *139*(4), 515-525.

[68] PEER strong motion database (peer.berkeley.edu/sm cat). Berkeley: Pacific Earthquake Engineering Research Center, University of California: 2000 https://peer.berkeley.edu

[69] Prinz, G. S., Nussbaumer, A., & Cortes, G. (2012). "Fatigue analysis of unanchored steel liquid storage tank shell-to-base connections during earthquake induced uplift." *15th World Conference on Earthquake Engineering*, Lisbon, Portugal.

[70] Chi, W. M., El-Tawil, S., Deierlein, G. G., & Abel, J. F. (1998). Inelastic analyses of a 17-story steel framed building damaged during Northridge. *Engineering Structures*, *20*(4-6), 481-495.

[71] Dehghani, M., & Tremblay, R. (2018). Design and full-scale experimental evaluation of a seismically endurant steel buckling-restrained brace system. *Earthquake Engineering & Structural Dynamics*, *47*(1), 105-129.

[72] Chi, B., & Uang, C. M. (2002). Cyclic response and design recommendations of reduced beam section moment connections with deep columns. *Journal of Structural Engineering*, *128*(4), 464-473.

[73] Mashayekh, A., and Uang, C. M. (2019). "Cyclic response of sloped steel moment connections" Journal of Structural Engineering, 145(7), 04019058.

APPENDICES

APPENDIX A: FULL DESIGN EXAMPLE FOR SIX STORY STEEL CONFIGURATIONS

The following are example calculations that demonstrate the procedure for design of beams, columns, reduced beam sections, doubler plates, and continuity plates for the 6-story special moment frame located in Los Angeles, California. The same approach has followed to design the other structures in LA, CA and SLC, UT. The ASCE 7-16 and AISC 341-16 requirements were followed to define the gravity loads, seismic loads and the structural element sizes.

Design ot 6-Story Special Moment Frame
Location: Los Angeles, California

1. Geometry of the structure

Number of Bays in Long Direction	$NBL := 6$
Number of Bays in Short Direction	$NBS := 4$
Length of Bay	$L_b := 30 \cdot ft$
Structure Length	$L := NBL \cdot L_b = 180\ ft$
Structure Width	$W := NBS \cdot L_b = 120\ ft$
Height of the First Floor	$h_1 := 13$ ft
Height of the Upper Floors	$h_2 := 13$ ft
Number of the Upper Stories	$NUS := 5$
Number of the all Stories	$NS := NUS + 1 = 6$
Height of the Structure	$HS := NUS \cdot h_1 + h_2 = 78$
Slab Area for L.L	$SA_L := L \cdot W = 21600\ ft^2$
Slab Area for D.L	$SA_D := (L + 2 \cdot ft) \cdot (W + 2 \cdot ft) = 22204\ ft^2$
Building Envelope	$BE := (L + 4 \cdot ft) + (W + 4 \cdot ft) = 308\ ft$
Perimeter	$P := 2 \cdot BE = 616\ ft$

Properties of Material

Yield Strength of Steel	$F_y := 50 \cdot ksi$
Modulus of Elasticity	$E := 29000 \cdot ksi$
Ultimate Strength of Steel	$F_u := 65 \cdot ksi$

Proporties of the Location

Site Class C

Risk Category II

Importance Parameter	$I := 1$	
Accidental Torsion	$AT := 5\%$	
Responce Modification Factor	$R := 8$	
Risk-Target MCE	$S_S := 1.978$	g
Risk-Target MCE	$S_1 := 0.705$	g
Site Coefficent	$F_v := 1.4$	
Site Coefficent	$F_a := 1.2$	

$S_{M1} := F_v \cdot S_1 = 0.99$

$S_{MS} := F_a \cdot S_S = 2.37$

$S_{DS} := \left(\frac{2}{3}\right) \cdot S_{MS} = 1.58$ g

$S_{D1} := \left(\frac{2}{3}\right) \cdot S_{M1} = 0.66$ g

Loads

Dead Load	$DL := 85 \cdot psf$
Dead Load for Roof	$DL_R := 95 \cdot psf$
Live Load	$LL := 50 \cdot psf$
Live Load for Roof	$LL_R := 20 \cdot psf$
Weight of the Exterior Wall	$WW := 25 \cdot psf$

The seismic Weight

$SW := DL \cdot (NS-1) \cdot SA_D + WW \cdot (h_1 \cdot ft + (NS-1) \cdot h_2 \cdot ft) \cdot P + DL_R \cdot SA_D = 12747.28\ kip$

$SWT := 1.5 \cdot SW = 19120.92\ kip$

From AICA

$C_u := 1.4 \qquad C_d := 5.5 \qquad C_t := 0.028 \qquad x := 0.8$

$T := C_u \cdot C_t \cdot (h_1 + (NS-1) \cdot h_2)^x = 1.28$

$C_{S1} := \frac{S_{DS}}{R} \cdot I = 0.2$

$C_{s2} := \frac{S_{D1}}{T} \cdot \frac{I}{R} = 0.06$

$k := \begin{cases} \text{if } T < 0.5 \\ \quad 1 \\ \text{if } T \geq 2.5 \\ \quad 2 \\ \text{if } T > 0.5 \wedge T < 2.5 \\ \quad 0.5 \cdot T + 0.75 \end{cases} \qquad k = 1.39$

$CS := \begin{cases} \text{if } C_{s2} > 0.01 \vee C_{s2} < C_{S1} \\ \quad C_{s2} \\ \text{if } C_{S1} < C_{s2} \\ \quad C_{S1} \end{cases} \qquad CS = 0.06$

$C_{s3} := 0.044 \cdot S_{DS} \cdot I = 0.07$

$C_s := \begin{cases} \text{if } CS < C_{s3} \\ \quad C_{s3} \\ \text{if } CS > C_{s3} \\ \quad CS \end{cases}$

$C_s = 0.07$

$V := C_s \cdot SWT = 1331.31\ kip$

$W_1 := (SA_D \cdot DL) + WW \cdot \frac{(h_1 \cdot ft + h_2 \cdot ft)}{2} \cdot P = 2087.54\ kip$

$W_2 := (SA_D \cdot DL) + WW \cdot h_2 \cdot ft \cdot P = 2087.54\ kip$

$W_3 := (SA_D \cdot DL) + WW \cdot h_2 \cdot ft \cdot P = 2087.54\ kip$

$W_4 := (SA_D \cdot DL) + WW \cdot h_2 \cdot ft \cdot P = 2087.54\ kip$

$W_5 := (SA_D \cdot DL) + WW \cdot h_2 \cdot ft \cdot P = 2087.54\ kip$

$W_6 := (SA_D \cdot DL) + WW \cdot h_2 \cdot ft \cdot P = 2087.54\ kip$

$h_1^{\ k} = 35.32$ $\quad (h_1 + h_2)^k = 92.53$ $\quad (h_1 + 2 \cdot h_2)^k = 162.55$

$(h_1 + 3 \cdot h_2)^k = 242.45$ $\quad (h_1 + 4 \cdot h_2)^k = 330.59$ $\quad (h_1 + 5 \cdot h_2)^k = 425.91$

$M_1 := W_1 \cdot h_1^{\ k} \cdot ft = 73723.97\ kip \cdot ft$

$M_2 := W_2 \cdot (h_1 + h_2)^k \cdot ft = 193165.84\ kip \cdot ft$

$M_3 := W_3 \cdot (h_1 + 2 \cdot h_2)^k \cdot ft = 339338.22\ kip \cdot ft$

$M_4 := W_4 \cdot (h_1 + 3 \cdot h_2)^k \cdot ft = 506118.18\ kip \cdot ft$

$M_5 := W_5 \cdot (h_1 + 4 \cdot h_2)^k \cdot ft = 690114.91\ kip \cdot ft$

$M_6 := W_6 \cdot (h_1 + 5 \cdot h_2)^k \cdot ft = 889107.74\ kip \cdot ft$

$C_{v1} := \frac{M_1}{M_1 + M_2 + M_3 + M_4 + M_5 + M_6} = 0.03$

$C_{v2} := \frac{M_2}{M_1 + M_2 + M_3 + M_4 + M_5 + M_6} = 0.07$

$C_{v3} := \frac{M_3}{M_1 + M_2 + M_3 + M_4 + M_5 + M_6} = 0.13$

$$C_{v4} := \frac{M_4}{M_1+M_2+M_3+M_4+M_5+M_6} = 0.19$$

$$C_{v5} := \frac{M_5}{M_1+M_2+M_3+M_4+M_5+M_6} = 0.26$$

$$C_{v6} := \frac{M_6}{M_1+M_2+M_3+M_4+M_5+M_6} = 0.33$$

Check

$C_{v1}+C_{v2}+C_{v3}+C_{v4}+C_{v5}+C_{v6}=1$ Good

OR

$$SC_{vi} := \left\| \begin{array}{l} \text{if } C_{v1}+C_{v2}+C_{v3}+C_{v4}+C_{v5}+C_{v6}=1 \\ \quad 1 \\ \text{if } C_{v1}+C_{v2}+C_{v3}+C_{v4}+C_{v5}+C_{v6}\neq 1 \\ \quad 0 \end{array} \right.$$

$SC_{vi}=1$

Good

Accidental Torsion $AT := 5\%$

$Exc := AT \cdot L = 9\ ft$

Reaction $R_1 := \frac{V \cdot \left(\frac{L}{2}+Exc\right)}{L} = 732.22\ kip$

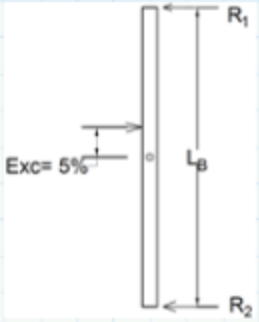

Tle Lateral Forces at Each Level

$F_1 := R_1 \cdot C_{v1} = 20.06\ kip$

$F_2 := R_1 \cdot C_{v2} = 52.55\ kip$

$F_3 := R_1 \cdot C_{v3} = 92.31\ kip$

$F_4 := R_1 \cdot C_{v4} = 137.69\ kip$

$F_5 := R_1 \cdot C_{v5} = 187.74\ kip$

$F_6 := R_1 \cdot C_{v6} = 241.87\ kip$

Check

$F_1+F_2+F_3+F_4+F_5+F_6=732.22\ kip$

2. Design of the Structure

2.1 Floor 1 and 2

$V_{UT12}:=F_2+F_3+F_4+F_5+F_6=712.16\ kip$

$V_{LT12}:=F_1+F_2+F_3+F_4+F_5+F_6=732.22\ kip$

$I_c:=1.\ in^4$ $I_b:=1\ in^4$

Number of All Columns $NAC:=7$

Number of External Columns $NEC:=2$

Number of Internal Columns $NIC:=NAC-NEC=5$

$$K_{e12}:=\frac{6\cdot E}{\left(0.5\cdot h_1\cdot ft+0.5\cdot h_2\cdot ft\right)^2}\left(\frac{1}{\frac{\left(0.5\cdot h_1\cdot ft+0.5\cdot h_2\cdot ft\right)}{2\cdot I_c}+\frac{L_b}{I_b}}\right)=0.02\ \frac{kip}{in}$$

$$K_{i12}:=\frac{12\cdot E}{\left(0.5\cdot h_1\cdot ft+0.5\cdot h_2\cdot ft\right)^2}\left(\frac{1}{\frac{\left(0.5\cdot h_1\cdot ft+0.5\cdot h_2\cdot ft\right)}{I_c}+\frac{L_b}{I_b}}\right)=0.03\ \frac{kip}{in}$$

$$K_{T12}:=2\cdot\left(K_{e12}\right)+NIC\cdot\left(K_{i12}\right)=0.17\ \frac{kip}{in}$$

$$V_{Ue12}:=\frac{K_{e12}}{K_{T12}}\cdot V_{UT12}=67.9\ kip$$

$$V_{Ui12}:=\frac{K_{i12}}{K_{T12}}\cdot V_{UT12}=115.27\ kip$$

$$V_{Le12}:=\frac{K_{e12}}{K_{T12}}\cdot V_{LT12}=69.81\ kip$$

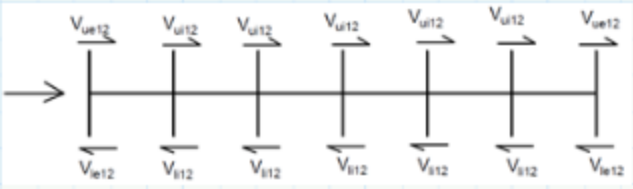

$$V_{Li12} := \frac{K_{i12}}{K_{T12}} \cdot V_{LT12} = 118.52\ kip$$

Drift Calculation $I_c := 1$ $I_c := 1$

$$\Delta_{e12} := \frac{\left(\frac{V_{Ue12} + V_{Le12}}{2}\right) \cdot \left(0.5 \cdot h_1 \cdot ft + 0.5 \cdot h_2 \cdot ft\right)^2}{6 \cdot E} \cdot \left(\frac{\left(0.5 \cdot h_1 \cdot ft + 0.5 \cdot h_2 \cdot ft\right)}{2 \cdot I_c} + \frac{L_b}{I_c}\right) = 4218.106\ in^4 \cdot in$$

The allowAbal drift (ASCE)

$$\Delta_a := 0.02\ \left(0.5 \cdot h_1 \cdot ft + 0.5 \cdot h_2 \cdot ft\right) = 3.12\ in$$

$$\Delta_{ae} := \frac{\Delta_a}{C_d} = 0.57\ in$$

$$I_{req} := \frac{\Delta_{e12}}{\Delta_{ae}} = 7435.764\ in^4$$

Column and Beam Sizes

Column W14×550

$d_{c12} := 19.6 \cdot in$ $b_{cf12} := 17 \cdot in$ $t_{cw12} := 2.19 \cdot in$ $t_{cf12} := 3.5 \cdot in$

$k_{cdes} := 4.1 \cdot in$ $h_c := d_{c12} - 2 \cdot k_{cdes} = 11.4\ in$

Beam W24*250

$d_{b12} := 26.7 \cdot in$ $b_{bf12} := 13.3 \cdot in$ $t_{bw12} := 1.16 \cdot in$ $t_{bf12} := 2.09 \cdot in$

$k_{bdes} := 2.59 \cdot in$ $h_b := d_{b12} - 2 \cdot k_{bdes} = 21.52\ in$

Check the Column

$$CC_f := \begin{cases} 1 & \text{if } \frac{b_{cf12}}{2 \cdot b_{cf12}} \le 0.56 \cdot \sqrt{\frac{E}{F_y}} \\ 0 & \text{if } \frac{b_{cf12}}{2 \cdot b_{cf12}} > 0.56 \cdot \sqrt{\frac{E}{F_y}} \end{cases}$$

$CC_f = 1$ For Flange

$$CC_w := \begin{cases} \text{if } \frac{h_c}{t_{cw12}} \le 1.49 \cdot \sqrt{\frac{E}{F_y}} \\ \quad 1 \\ \text{if } \frac{h_c}{t_{cw12}} > 1.49 \cdot \sqrt{\frac{E}{F_y}} \\ \quad 0 \end{cases} \qquad CC_w = 1 \qquad \text{For Web}$$

The Column is Compact

Check the Beam

$$CB_f := \begin{cases} \text{if } \frac{b_{bf12}}{2 \cdot b_{bf12}} \le 0.38 \cdot \sqrt{\frac{E}{F_y}} \\ \quad 1 \\ \text{if } \frac{b_{bf12}}{2 \cdot b_{bf12}} > 0.38 \cdot \sqrt{\frac{E}{F_y}} \\ \quad 0 \end{cases} \qquad CC_f = 1 \qquad \text{For Flange}$$

$$CB_w := \begin{cases} \text{if } \frac{h_b}{t_{bw12}} \le 3.76 \cdot \sqrt{\frac{E}{F_y}} \\ \quad 1 \\ \text{if } \frac{h_b}{t_{bw12}} > 3.76 \cdot \sqrt{\frac{E}{F_y}} \\ \quad 0 \end{cases} \qquad CB_w = 1 \qquad \text{For Web}$$

The Beam is Compact

2.2 Floor 3 and 4

$V_{UT34} := F_4 + F_5 + F_6 = 567.3$ ***kip***

$V_{LT34} := F_3 + F_4 + F_5 + F_6 = 659.61$ ***kip***

$I_c := 1.\ in^4 \qquad I_b := 1\ in^4$

$$K_{e34} := \frac{6 \cdot E}{(h_2 \cdot ft)^2} \left(\frac{1}{\frac{h_2 \cdot ft}{2 \cdot I_c} + \frac{L_b}{I_b}} \right) = 0.02\ \frac{kip}{in}$$

$$K_{i34} := \frac{12 \cdot E}{(h_2 \cdot ft)^2} \left(\frac{1}{\frac{h_2 \cdot ft}{I_c} + \frac{L_b}{I_b}} \right) = 0.03\ \frac{kip}{in}$$

$$K_{T34} := 2 \cdot (K_{e34}) + NIC \cdot (K_{i34}) = 0.17\ \frac{kip}{in}$$

$$V_{Ue34} := \frac{K_{e34}}{K_{T34}} \cdot V_{UT34} = 54.09\ kip$$

$$V_{Ui34} := \frac{K_{i34}}{K_{T34}} \cdot V_{UT34} = 91.82\ kip$$

$$V_{Le34} := \frac{K_{e12}}{K_{T12}} \cdot V_{LT34} = 62.89\ kip$$

$$V_{Li34} := \frac{K_{i12}}{K_{T12}} \cdot V_{LT34} = 106.77\ kip$$

Drift Calculation

$I_c := 1 \qquad I_b := 1$

$$\Delta_{e34} := \frac{\left(\frac{V_{Ue34} + V_{Le34}}{2} \right) \cdot (h_2 \cdot ft)^2}{6 \cdot E} \cdot \left(\frac{h_2 \cdot ft}{2 \cdot I_c} + \frac{L_b}{I_b} \right) = 3583.021\ in^4 \cdot in$$

The allowAbal drift (ASCE)

$$\Delta_a := 0.02\ (h_2 \cdot ft) = 3.12\ in$$

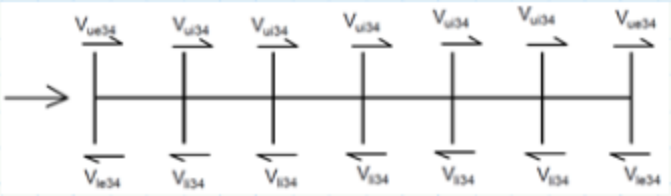

$$\Delta_{ae} := \frac{\Delta_a}{C_d} = 0.57\ in$$

$$I_{req} := \frac{\Delta_{e34}}{\Delta_{ae}} = 6316.223\ in^4$$

Column and Beam Sizes

Column W14×426

$d_{c34} := 18.7 \cdot in$ $b_{cf34} := 16.7 \cdot in$ $t_{cw34} := 1.88 \cdot in$ $t_{cf34} := 3.04 \cdot in$

$k_{cdes34} := 3.63 \cdot in$ $h_{c34} := d_{c34} - 2 \cdot k_{cdes34} = 11.44\ in$

Beam W24*192 $I := 6260 \cdot in^4$

$d_{b34} := 25.5 \cdot in$ $b_{bf34} := 13 \cdot in$ $t_{bw34} := 0.81 \cdot in$ $t_{bf34} := 1.46 \cdot in$

$k_{bdes34} := 1.96 \cdot in$ $h_{b34} := d_{b34} - 2 \cdot k_{bdes34} = 21.58\ in$

Check the Column

$$CC_{f34} := \begin{cases} 1 & \text{if } \frac{b_{cf34}}{2 \cdot b_{cf34}} \le 0.56 \cdot \sqrt{\frac{E}{F_y}} \\ 0 & \text{if } \frac{b_{cf34}}{2 \cdot b_{cf34}} > 0.56 \cdot \sqrt{\frac{E}{F_y}} \end{cases}$$

$CC_{f34} = 1$ For Flange

$$CC_{w34} := \begin{cases} 1 & \text{if } \frac{h_{c34}}{t_{cw34}} \le 1.49 \cdot \sqrt{\frac{E}{F_y}} \\ 0 & \text{if } \frac{h_{c34}}{t_{cw34}} > 1.49 \cdot \sqrt{\frac{E}{F_y}} \end{cases}$$

$CC_{w34} = 1$ For Web

The Column is Compact

Check the Beam

$$CB_{f34} := \begin{cases} 1 & \text{if } \frac{b_{bf34}}{2 \cdot b_{bf34}} \le 0.38 \cdot \sqrt{\frac{E}{F_y}} \\ 0 & \text{if } \frac{b_{bf34}}{2 \cdot b_{bf34}} > 0.38 \cdot \sqrt{\frac{E}{F_y}} \end{cases}$$

$CC_{f34} = 1$ For Flange

$$CB_{w34} := \begin{cases} \text{if } \frac{h_{b34}}{t_{bw34}} \le 3.76 \cdot \sqrt{\frac{E}{F_y}} \\ \quad 1 \\ \text{if } \frac{h_{b34}}{t_{bw34}} > 3.76 \cdot \sqrt{\frac{E}{F_y}} \\ \quad 0 \end{cases} \qquad CB_{w34} = 1 \qquad \text{For Web}$$

The Beam is Compact

2.3. Floor 5 and 6

$V_{UT56} := F_6 = 241.87\ kip$

$V_{LT56} := F_5 + F_6 = 429.61\ kip$

$I_c := 1.\ in^4 \qquad I_b := 1\ in^4$

$$K_{e56} := \frac{6 \cdot E}{(h_2 \cdot ft)^2} \left(\frac{1}{\frac{h_2 \cdot ft}{2 \cdot I_c} + \frac{L_b}{I_b}} \right) = 0.02\ \frac{kip}{in}$$

$$K_{i56} := \frac{12 \cdot E}{(h_2 \cdot ft)^2} \left(\frac{1}{\frac{h_2 \cdot ft}{I_c} + \frac{L_b}{I_b}} \right) = 0.03\ \frac{kip}{in}$$

$$K_{T56} := 2 \cdot (K_{e56}) + NIC \cdot (K_{i34}) = 0.17\ \frac{kip}{in}$$

$$V_{Ue56} := \frac{K_{e56}}{K_{T56}} \cdot V_{UT56} = 23.06\ kip$$

$$V_{Ui56} := \frac{K_{i56}}{K_{T56}} \cdot V_{UT56} = 39.15\ kip$$

$$V_{Le56} := \frac{K_{e56}}{K_{T56}} \cdot V_{LT56} = 40.96\ kip$$

$$V_{Li56} := \frac{K_{i56}}{K_{T56}} \cdot V_{LT56} = 69.54\ kip$$

Drift Calculation

$I_c := 1$ $I_b := 1$

$$\Delta_{e56} := \frac{\left(\frac{V_{Ue56} + V_{Le56}}{2}\right) \cdot (h_2 \cdot ft)^2}{6 \cdot E} \cdot \left(\frac{h_2 \cdot ft}{2 \cdot I_c} + \frac{L_b}{I_b}\right) = 1960.985\ in^4 \cdot in$$

The allowAbal drift (ASCE)

$$\Delta_a := 0.02\ (h_2 \cdot ft) = 3.12\ in$$

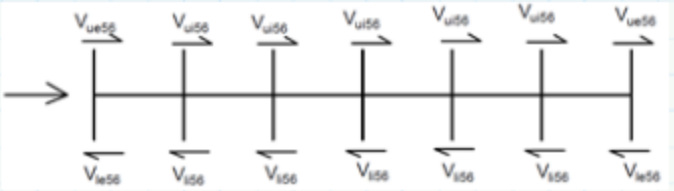

$$\Delta_{ae} := \frac{\Delta_a}{C_d} = 0.57\ in$$

$$I_{req} := \frac{\Delta_{e56}}{\Delta_{ae}} = 3456.864\ in^4$$

Column and Beam Sizes

Column W14×342

$d_{c56} := 17.5 \cdot in$ $b_{cf56} := 16.4 \cdot in$ $t_{cw56} := 1.54 \cdot in$ $t_{cf56} := 2.47 \cdot in$

$k_{cdes56} := 3.07 \cdot in$ $h_{c56} := d_{c56} - 2 \cdot k_{cdes56} = 11.36\ in$

Beam W24*162

$d_{b56} := 25 \cdot in$ $b_{bf56} := 13 \cdot in$ $t_{bw56} := 0.705 \cdot in$ $t_{bf56} := 1.22 \cdot in$

$k_{bdes56} := 1.72 \cdot in$ $h_{b56} := d_{b56} - 2 \cdot k_{bdes56} = 21.56\ in$

Check the Column

$$CC_{f56} := \begin{cases} 1 & \text{if } \frac{b_{cf56}}{2 \cdot b_{cf56}} \le 0.56 \cdot \sqrt{\frac{E}{F_y}} \\ 0 & \text{if } \frac{b_{cf56}}{2 \cdot b_{cf56}} > 0.56 \cdot \sqrt{\frac{E}{F_y}} \end{cases}$$

$CC_{f34} = 1$ For Flange

$$CC_{w56} := \begin{cases} \text{if } \frac{h_{c56}}{t_{cw56}} \le 1.49 \cdot \sqrt{\frac{E}{F_y}} \\ \quad 1 \\ \text{if } \frac{h_{c56}}{t_{cw56}} > 1.49 \cdot \sqrt{\frac{E}{F_y}} \\ \quad 0 \end{cases}$$

$CC_{w56} = 1$ For Web

The Column is Compact

Check the Beam

$$CB_{f56} := \begin{cases} \text{if } \frac{b_{bf56}}{2 \cdot b_{bf56}} \le 0.38 \cdot \sqrt{\frac{E}{F_y}} \\ \quad 1 \\ \text{if } \frac{b_{bf56}}{2 \cdot b_{bf56}} > 0.38 \cdot \sqrt{\frac{E}{F_y}} \\ \quad 0 \end{cases}$$

$CC_{f56} = 1$ For Flange

$$CB_{w56} := \begin{cases} \text{if } \frac{h_{b56}}{t_{bw56}} \le 3.76 \cdot \sqrt{\frac{E}{F_y}} \\ \quad 1 \\ \text{if } \frac{h_{b56}}{t_{bw56}} > 3.76 \cdot \sqrt{\frac{E}{F_y}} \\ \quad 0 \end{cases}$$

$CB_{w34} = 1$ For Web

The Beam is Compact

3. Design of Reduced Beam Section (RBS)

3.1 RBS for Floor 1 and 2

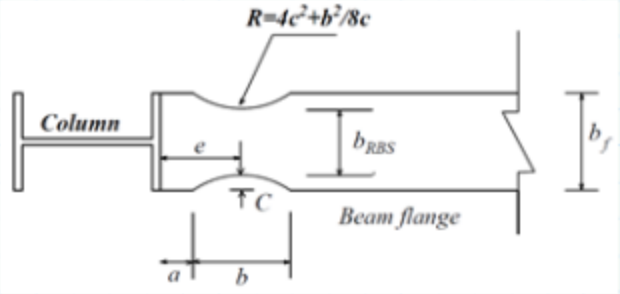

$d_{c12} := 19.6 \cdot in$ $b_{cf12} := 17 \cdot in$ $t_{cw12} := 2.19 \cdot in$ $t_{cf12} := 3.5 \cdot in$

Beam W24*279

$d_{b12} := 26.7 \cdot in$ $b_{bf12} := 13.3 \cdot in$ $t_{bw12} := 1.16 \cdot in$ $t_{bf12} := 2.09 \cdot in$ $Z_{b12} := 835 \cdot in^3$

Limitations if the RBS According to AISC

$a := 0.75 \cdot b_{bf12} = 9.98\ in$ Use $a_{12} := 9 \cdot in$

$b := 0.65 \cdot d_{b12} = 17.36\ in$ Use $b_{12} := 17 \cdot in$

$c := 0.2 \cdot b_{bf12} = 2.66\ in$ Use $c_{12} := 2.5 \cdot in$

$Z_{RBS12} := Z_{b12} - 2 \cdot c_{12} \cdot t_{bf12} \cdot (d_{b12} - t_{bf12}) = 577.83\ in^3$

$C_{pr} := \frac{F_y + F_u}{2 \cdot F_y} = 1.15$ Cpr<1.2

Use $C_{pr} := 1.2$ $R_y := 1.1$

$M_{pr12} := C_{pr} \cdot R_y \cdot Z_{RBS12} \cdot F_y = 38136.483\ kip \cdot in$

$V_{p12} := \frac{M_{pr12}}{\left(L_b - d_{c12} - 2 \cdot \left(a_{12} + \frac{b_{12}}{2}\right)\right)} \cdot 2 = 249.75\ kip$

$M_{f12} := M_{pr12} + V_{p12} \cdot \left(a_{12} + \frac{b_{12}}{2}\right) = 42507.069\ kip \cdot in$

The Capacity of the Column Face

$M_{pe12} := R_y \cdot Z_{b12} \cdot F_y = 45925\ kip \cdot in$

Check the Moments

$$CM_{12} := \begin{cases} \text{if } M_{pe12} \geq M_{f12} \\ \quad 1 \\ \text{if } M_{pe12} < M_{f12} \\ \quad 0 \end{cases} \qquad CM_{12} = 1$$

Good

The Percentage

$$\frac{M_{pe12}}{M_{f12}} = 1.08$$

-==========-

2. RBS for Floor 3 and 4

Column W14×426

$d_{c34} := 18.7 \cdot in$ $b_{cf34} := 16.7 \cdot in$ $t_{cw34} := 1.88 \cdot in$ $t_{cf34} := 3.04 \cdot in$

Beam W24*192

$d_{b34} := 25.5 \cdot in$ $b_{bf34} := 13 \cdot in$ $t_{bw34} := 0.81 \cdot in$ $t_{bf34} := 1.46 \cdot in$ $Z_{b34} := 559 \cdot in^3$

Limitations if the RBS According to AISC

$a := 0.75 \cdot b_{bf34} = 9.75\ in$ Use $a_{34} := 9 \cdot in$

$b := 0.65 \cdot d_{b34} = 16.58\ in$ Use $b_{34} := 16 \cdot in$

$c := 0.2 \cdot b_{bf34} = 2.6\ in$ Use $c_{34} := 2.5 \cdot in$

$$Z_{RBS34} := Z_{b34} - 2 \cdot c_{34} \cdot t_{bf34} \cdot (d_{b34} - t_{bf34}) = 383.51\ in^3$$

$$M_{pr34} := C_{pr} \cdot R_y \cdot Z_{RBS34} \cdot F_y = 25311.528\ kip \cdot in$$

$$V_{p34} := \frac{M_{pr34}}{\left(L_b - d_{c34} - 2 \cdot \left(a_{34} + \frac{b_{34}}{2}\right)\right)} \cdot 2 = 164.73\ kip$$

$$M_{f34} := M_{pr34} + V_{p34} \cdot \left(a_{34} + \frac{b_{34}}{2}\right) = 28112.022\ kip \cdot in$$

The Capacity of the Column Face

$M_{pe34} := R_y \cdot Z_{b34} \cdot F_y = 30745\ kip \cdot in$

Check the Moments

$$CM_{34} := \begin{cases} \text{if } M_{pe34} \geq M_{f34} \\ \quad 1 \\ \text{if } M_{pe34} < M_{f34} \\ \quad 0 \end{cases} \qquad CM_{34} = 1$$

Good

The Percentage

$$\frac{M_{pe34}}{M_{f34}} = 1.09$$

==========

3. RBS for Floor 5 and 6

Column W14×342

$d_{c56} := 17.5 \cdot in$ $b_{cf56} := 16.4 \cdot in$ $t_{cw56} := 1.54 \cdot in$ $t_{cf56} := 2.47 \cdot in$

Beam W24*162

$d_{b56} := 25 \cdot in$ $b_{bf56} := 13 \cdot in$ $t_{bw56} := 0.705 \cdot in$ $t_{bf56} := 1.22 \cdot in$ $Z_{b56} := 468 \cdot in^3$

Limitations if the RBS According to AISC

$a := 0.75 \cdot b_{bf56} = 9.75\ in$	Use	$a_{56} := 9 \cdot in$
$b := 0.65 \cdot d_{b56} = 16.25\ in$	Use	$b_{56} := 16 \cdot in$
$c := 0.2 \cdot b_{bf56} = 2.6\ in$	Use	$c_{56} := 2.5 \cdot in$

$Z_{RBS56} := Z_{b56} - 2 \cdot c_{56} \cdot t_{bf56} \cdot (d_{b56} - t_{bf56}) = 322.94\ in^3$

$M_{pr56} := C_{pr} \cdot R_y \cdot Z_{RBS56} \cdot F_y = 21314.172\ kip \cdot in$

$$V_{p56} := \frac{M_{pr56}}{\left(L_b - d_{c56} - 2 \cdot \left(a_{56} + \frac{b_{56}}{2}\right)\right)} \cdot 2 = 138.18 \ kip$$

$$M_{f56} := M_{pr56} + V_{p56} \cdot \left(a_{56} + \frac{b_{56}}{2}\right) = 23663.222 \ kip \cdot in$$

The Capacity of the Column Face

$$M_{pe56} := R_y \cdot Z_{b56} \cdot F_y = 25740 \ kip \cdot in$$

Check the Moments

$$CM_{56} := \begin{cases} \text{if } M_{pe56} \geq M_{f56} \\ \quad 1 \\ \text{if } M_{pe56} < M_{f56} \\ \quad 0 \end{cases} \qquad CM_{56} = 1$$

Good

The Percentage

$$\frac{M_{pe56}}{M_{f56}} = 1.09$$

==========

4. Design of Panel Zones

4.1. Stories 1 and 2

4.1.1 Design the Panel Zones for the Exterior Column

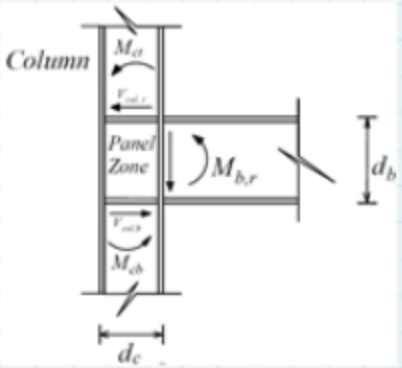

$$M_{f12} := M_{pr12} + V_{p12} \cdot \left(a_{12} + \frac{b_{12}}{2} \right) = 42507.069 \ kip \cdot in$$

Column W14×550

$d_{c12} := 19.6 \cdot in$ $b_{cf12} := 17 \cdot in$ $t_{cw12} := 2.19 \cdot in$ $t_{cf12} := 3.5 \cdot in$ $A_{c12} := 162 \cdot in^2$

Beam W24*279

$d_{b12} := 26.7 \cdot in$ $b_{bf12} := 13.3 \cdot in$ $t_{bw12} := 1.16 \cdot in$ $t_{bf12} := 2.09 \cdot in$

$$V_{ce1} := \frac{M_{f12}}{\frac{h_1 \cdot ft}{2} + \frac{h_2 \cdot ft}{2}} = 272.481 \ kip$$

$$R_u := \frac{M_{f12}}{d_{b12} - t_{bf12}} - V_{ce1} = 1454.746 \ kip$$

The capacity of Panel Zone

Assume $\phi_v := 1$

$$\phi R_n := \phi_v \cdot 0.6 \cdot F_y \cdot d_{c12} \cdot t_{cw12} \cdot \left(1 + \frac{3 \cdot b_{cf12} \cdot t_{cf12}^2}{d_{b12} \cdot d_{c12} \cdot t_{cw12}} \right) = 1989.686 \ kip$$

Check

$$CR_{n1.12} := \begin{cases} \text{if } \phi R_n < 0.75 \cdot F_y \cdot A_{c12} \\ \quad 1 \\ \text{if } \phi R_n \geq 0.75 \cdot F_y \cdot A_{c12} \\ \quad 0 \end{cases} \qquad CR_{n1.12} = 1$$

Good

$$CR_{n2.12} := \begin{cases} \text{if } \phi R_n < R_u \\ \quad 1 \\ \text{if } \phi R_n \geq R_u \\ \quad 0 \end{cases} \qquad CR_{n2.12} = 0$$

Not Good

Doubler Plate Design

For Column W14×550 $\frac{d_z}{90} = 0.14\ in$

$w_z := 0.14 \cdot in \cdot 90 = 12.6\ in$

For Beam W24×279 $\frac{d_z}{90} = 0.25\ in$

$d_z := 0.25 \cdot in \cdot 90 = 22.5\ in$

$t_w := \frac{(d_z + w_z)}{90} = 0.39\ in$

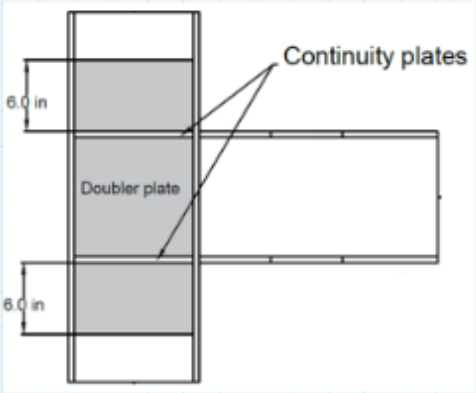

$$t_p := \left(R_u - \frac{0.6 \cdot F_y \cdot \left(3 \cdot b_{cf12} \cdot t_{cf12}^{\ 2}\right)}{d_{b12}}\right) \cdot \left(\frac{1}{0.6 \cdot F_y \cdot d_{c12}}\right) - t_w = 0.89\ in$$

Continuaty Plate Design

$R_{yb} := 1.1$ $R_{yc} := 1$ $t_{cf12} := 0.4 \cdot \left(1.8 \cdot b_{bf12} \cdot t_{bf12} \cdot \frac{R_{yb} \cdot F_y}{R_{yc} \cdot F_y}\right)^{0.5} = 2.97\ in$

$$t_{cf12} := \begin{cases} \text{if } t_{cf12} \geq 0.4 \cdot \left(1.8 \cdot b_{bf12} \cdot t_{bf12} \cdot \frac{R_{yb} \cdot F_y}{R_{yc} \cdot F_y}\right)^{0.5} \\ \quad 1 \\ \text{if } t_{cf12} < 0.4 \cdot \left(1.8 \cdot b_{bf12} \cdot t_{bf12} \cdot \frac{R_{yb} \cdot F_y}{R_{yc} \cdot F_y}\right)^{0.5} \\ \quad 0 \end{cases} \qquad t_{cf12} = 1$$

Good

$b_{bf12} := 13.3$

$$t_{cf12} := \begin{cases} \text{if } t_{cf12} \geq \frac{b_{bf12}}{6} \\ \quad 1 \\ \text{if } t_{cf12} < \frac{b_{bf12}}{6} \\ \quad 0 \end{cases} \qquad t_{cf12} = 0$$

Continuaty Plates are needed

According to AISC, 50% of the flange beam thickness is used

The thickness of the continuaty plates is $t_{cp12} := 0.5 \cdot t_{bf12} = 1.05\ in$

4.1.2 Design the Panel Zones for the Interior Column

$$V_{ci1} := \frac{2 \cdot M_{f12}}{\frac{h_1 \cdot ft}{2} + \frac{h_2 \cdot ft}{2}} = 544.962\ kip$$

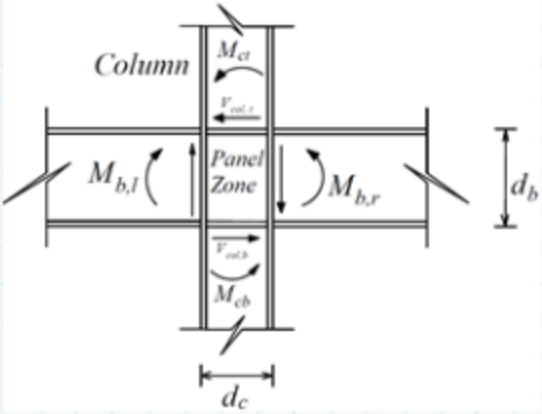

$$R_{ui12} := \frac{2 \cdot M_{f12}}{d_{b12} - t_{bf12}} - V_{ci1} = 2909.493\ kip$$

capacity of Panel Zone

Assume $\phi_v := 1$

$d_{c12} := 19.6 \cdot in$ $b_{cf12} := 17 \cdot in$ $t_{cw12} := 2.19 \cdot in$ $t_{cf12} := 3.5 \cdot in$

$A_{c12} := 162 \cdot in^2$

Beam W24*279

$d_{b12} := 26.7 \cdot in$ $b_{bf12} := 13.3 \cdot in$ $t_{bw12} := 1.16 \cdot in$ $t_{bf12} := 2.09 \cdot in$

$$\phi R_{ni12} := \phi_v \cdot 0.6 \cdot F_y \cdot d_{c12} \cdot t_{cw12} \cdot \left(1 + \frac{3 \cdot b_{cf12} \cdot t_{cf12}^2}{d_{b12} \cdot d_{c12} \cdot t_{cw12}}\right) = 1989.686\ kip$$

Check

$$CR_{ni.12} := \begin{cases} \text{if } \phi R_n < 0.75 \cdot F_y \cdot A_{c12} \\ \quad 1 \\ \text{if } \phi R_n \geq 0.75 \cdot F_y \cdot A_{c12} \\ \quad 0 \end{cases} \qquad CR_{ni.12} = 1$$

Good

$$CR_{ni.12} := \begin{cases} \text{if } \phi R_n < R_u \\ \quad 1 \\ \text{if } \phi R_n \geq R_u \\ \quad 0 \end{cases} \qquad CR_{ni.12} = 0$$

Not Good

Doubler Plate Design

For Column W14×550 $\frac{d_z}{90} = 0.14\ in$

$w_z := 0.14 \cdot in \cdot 90 = 12.6\ in$

For Beam W24×279

$\frac{d_z}{90} = 0.25\ in$

$d_z := 0.25 \cdot in \cdot 90 = 22.5\ in$

$t_w := \frac{(d_z + w_z)}{90} = 0.39\ in$

$t_p := \left(R_{ui12} - \frac{0.6 \cdot F_y \cdot \left(3 \cdot b_{cf12} \cdot t_{cf12}^{\ 2}\right)}{d_{b12}}\right) \cdot \left(\frac{1}{0.6 \cdot F_y \cdot d_{c12}}\right) - t_w = 3.36\ in$

Continuaty Plate Design

$R_{yb} := 1.1 \qquad R_{yc} := 1 \qquad t_{cfi12} := 0.4 \cdot \left(1.8 \cdot b_{bf12} \cdot t_{bf12} \cdot \frac{R_{yb} \cdot F_y}{R_{yc} \cdot F_y}\right)^{0.5} = 2.97\ in$

$$t_{cf12} := \begin{cases} \text{if } t_{cfi12} \geq 0.4 \cdot \left(1.8 \cdot b_{bf12} \cdot t_{bf12} \cdot \frac{R_{yb} \cdot F_y}{R_{yc} \cdot F_y}\right)^{0.5} \\ \quad 1 \\ \text{if } t_{cfi12} < 0.4 \cdot \left(1.8 \cdot b_{bf12} \cdot t_{bf12} \cdot \frac{R_{yb} \cdot F_y}{R_{yc} \cdot F_y}\right)^{0.5} \\ \quad 0 \end{cases} \qquad t_{cf12} = 1$$

Good

$b_{bf12} := 13.3$

$$t_{cfi12} := \begin{cases} \text{if } t_{cf12} \geq \frac{b_{bf12}}{6} \\ \quad 1 \\ \text{if } t_{cf12} < \frac{b_{bf12}}{6} \\ \quad 0 \end{cases} \qquad t_{cfi12} = 0$$

Continuaty Plates are needed

According to AISC, 75% of the flange beam thickness is used

The thickness of the continuaty plates is

$t_{cp12} := 0.75 \cdot t_{bf12} = 1.57\ in$

==========

4.2. Stories 3 and 4

4.2.1 Design the Panel Zones for the Exterior Column

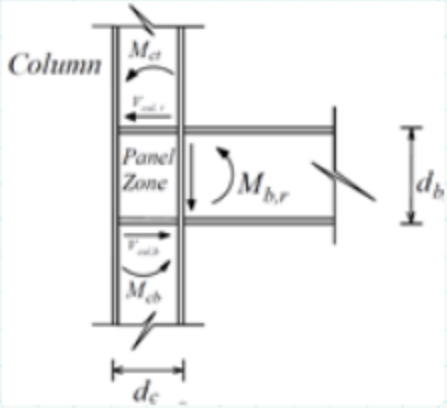

$$M_{f34} := M_{pr34} + V_{p34} \cdot \left(a_{34} + \frac{b_{34}}{2} \right) = 28112.022 \ kip \cdot in$$

Column W14×426

$d_{c34} := 18.7 \cdot in$ $b_{cf34} := 16.7 \cdot in$ $t_{cw34} := 1.88 \cdot in$ $t_{cf34} := 3.04 \cdot in$ $A_{c34} := 125 \cdot in^2$

Beam W24*192

$d_{b34} := 25.5 \cdot in$ $b_{bf34} := 13 \cdot in$ $t_{bw34} := 0.81 \cdot in$ $t_{bf34} := 1.46 \cdot in$

$$V_{ce34} := \frac{M_{f34}}{\frac{h_1 \cdot ft}{2} + \frac{h_2 \cdot ft}{2}} = 180.205 \ kip$$

$$R_{u34} := \frac{M_{f34}}{d_{b34} - t_{bf34}} - V_{ce34} = 989.18 \ kip$$

The capacity of Panel Zone

Assume $\phi_v := 1$

$$\phi R_{n34} := \phi_v \cdot 0.6 \cdot F_y \cdot d_{c34} \cdot t_{cw34} \cdot \left(1 + \frac{3 \cdot b_{cf34} \cdot t_{cf34}^2}{d_{b34} \cdot d_{c34} \cdot t_{cw34}} \right) = 1599.391 \ kip$$

Check

$$CR_{n1.34} := \begin{cases} \text{if } \phi R_{n34} < 0.75 \cdot F_y \cdot A_{c34} \\ \quad 1 \\ \text{if } \phi R_{n34} \geq 0.75 \cdot F_y \cdot A_{c34} \\ \quad 0 \end{cases} \qquad CR_{n1.34} = 1$$

Good

$$CR_{n2.34} := \begin{cases} \text{if } \phi R_{n34} < R_{u34} \\ \quad 1 \\ \text{if } \phi R_{n34} \geq R_{u34} \\ \quad 0 \end{cases} \qquad CR_{n2.34} = 0$$

Not Good

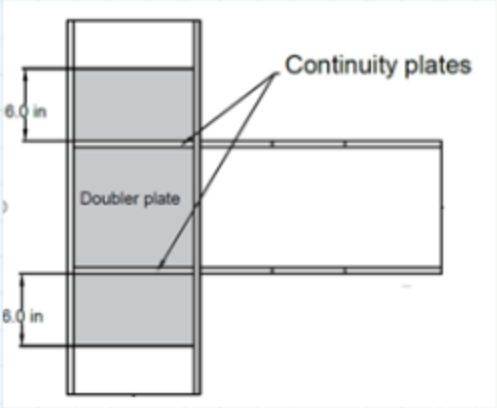

Doubler Plate Design

For Column W14×426

$$\frac{d_z}{90} = 0.14\ in$$

$$w_{z34} := 0.14 \cdot in \cdot 90 = 12.6\ in$$

For Beam W24×192

$$\frac{d_z}{90} = 0.251\ in$$

$$d_{z34} := 0.251 \cdot in \cdot 90 = 22.59\ in$$

$$t_{w34} := \frac{(d_{z34} + w_{z34})}{90} = 0.39\ in$$

$$t_{p3} := \left(R_{u34} - \frac{0.6 \cdot F_y \cdot \left(3 \cdot b_{cf34} \cdot t_{cf34}^{\ 2}\right)}{d_{b34}}\right) \cdot \left(\frac{1}{0.6 \cdot F_y \cdot d_{c34}}\right) - t_{w34} = 0.4\ in$$

Continuaty Plate Design

$$R_{yb} := 1.1 \qquad R_{yc} := 1 \qquad t_{cfi34} := 0.4 \cdot \left(1.8 \cdot b_{bf34} \cdot t_{bf34} \cdot \frac{R_{yb} \cdot F_y}{R_{yc} \cdot F_y}\right)^{0.5} = 2.45\ in$$

$$t_{cfi34} := \begin{cases} \text{if } t_{cf34} \geq 0.4 \cdot \left(1.8 \cdot b_{bf34} \cdot t_{bf12} \cdot \frac{R_{yb} \cdot F_y}{R_{yc} \cdot F_y}\right)^{0.5} \\ \quad 1 \\ \text{if } t_{cf34} < 0.4 \cdot \left(1.8 \cdot b_{bf34} \cdot t_{bf34} \cdot \frac{R_{yb} \cdot F_y}{R_{yc} \cdot F_y}\right)^{0.5} \\ \quad 0 \end{cases} \qquad t_{cfi34} = 1$$

Good

$b_{bf34} := 13.\ in$

$$t_{cf34} := \begin{cases} \text{if } t_{cf34} \geq \frac{b_{bf34}}{6} \\ \quad 1 \\ \text{if } t_{cf34} < \frac{b_{bf34}}{6} \\ \quad 0 \end{cases} \qquad t_{cf34} = 1$$

Continuaty Plates are not needed

According to AISC, 50% of the flange beam thickness is used

The thickness of the continuaty plates is

$t_{cp34} := 0.5 \cdot t_{bf34} = 0.73\ in$

4.1.2 Design the Panel Zones for the Interior Column

$$V_{ci34} := \frac{2 \cdot M_{f34}}{\frac{h_1 \cdot ft}{2} + \frac{h_2 \cdot ft}{2}} = 360.411\ kip$$

$$R_{ui34} := \frac{2 \cdot M_{f34}}{d_{b34} - t_{bf34}} - V_{ci34} = 1978.36\ kip$$

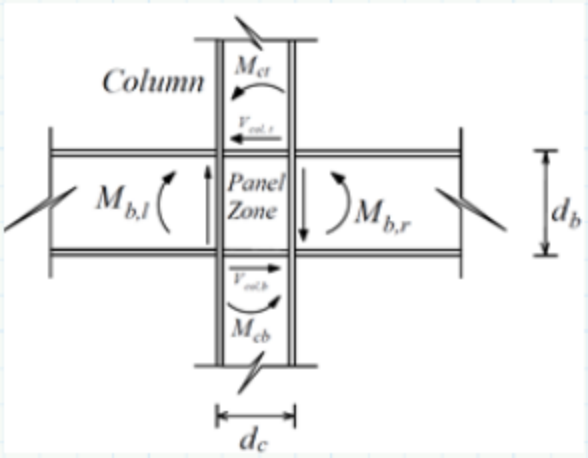

capacity of Panel Zone

Assume $\phi_v := 1$

Beam W14*426

$d_{c34} := 18.7 \cdot in$ $b_{cf34} := 16.7 \cdot in$ $t_{cw34} := 1.88 \cdot in$ $t_{cf34} := 3.04 \cdot in$

$A_{c34} := 125 \cdot in^2$

Beam W24*192

$d_{b34} := 25.5 \cdot in$ $b_{bf34} := 13 \cdot in$ $t_{bw34} := 0.81 \cdot in$ $t_{bf34} := 1.46 \cdot in$

$$\phi R_{ni34} := \phi_v \cdot 0.6 \cdot F_y \cdot d_{c34} \cdot t_{cw34} \cdot \left(1 + \frac{3 \cdot b_{cf34} \cdot t_{cf34}^{\,2}}{d_{b34} \cdot d_{c34} \cdot t_{cw34}}\right) = 1599.391 \ kip$$

Check

$$CR_{ni.34} := \begin{cases} \text{if } \phi R_{ni34} < 0.75 \cdot F_y \cdot A_{c34} \\ \quad 1 \\ \text{if } \phi R_{ni34} \geq 0.75 \cdot F_y \cdot A_{c34} \\ \quad 0 \end{cases} \qquad CR_{ni.12} = 0$$

Not Good

$$CR_{ni.34} := \begin{cases} \text{if } \phi R_{ni34} < R_{ui34} \\ \quad 1 \\ \text{if } \phi R_{ni34} \geq R_{ui34} \\ \quad 0 \end{cases} \qquad CR_{ni.12} = 0$$

Not Good

Doubler Plate Design

For Column W14×426 $\quad \frac{d_z}{90} = 0.14 \ in$

$$w_{z34} := 0.14 \cdot in \cdot 90 = 12.6 \ in$$

For Beam W24×192 $\quad \frac{d_z}{90} = 0.251 \ in$

$$d_{z34} := 0.251 \cdot in \cdot 90 = 22.59 \ in$$

$$t_{w34} := \frac{\left(d_{z34} + w_{z34}\right)}{90} = 0.39 \ in$$

$$t_{p34} := \left(R_{ui34} - \frac{0.6 \cdot F_y \cdot \left(3 \cdot b_{cf34} \cdot t_{cf34}^{\,2}\right)}{d_{b34}}\right) \cdot \left(\frac{1}{0.6 \cdot F_y \cdot d_{c34}}\right) - t_{w34} = 2.16 \ in$$

Continuaty Plate Design

$$R_{yb} := 1.1 \qquad R_{yc} := 1$$

$$t_{cfi34} := 0.4 \cdot \left(1.8 \cdot b_{bf34} \cdot t_{bf34} \cdot \frac{R_{yb} \cdot F_y}{R_{yc} \cdot F_y}\right)^{0.5} = 2.45 \ in$$

$$t_{cf34} := \begin{cases} \text{if } t_{cfi34} \geq 0.4 \cdot \left(1.8 \cdot b_{bf34} \cdot t_{bf34} \cdot \frac{R_{yb} \cdot F_y}{R_{yc} \cdot F_y}\right)^{0.5} \\ \quad 1 \\ \text{if } t_{cfi34} < 0.4 \cdot \left(1.8 \cdot b_{bf34} \cdot t_{bf34} \cdot \frac{R_{yb} \cdot F_y}{R_{yc} \cdot F_y}\right)^{0.5} \\ \quad 0 \end{cases} \qquad t_{cf12} = 1$$

Not Good

$b_{bf34} := 13$

$$t_{cfi34} := \begin{cases} \text{if } t_{cf34} \geq \frac{b_{bf34}}{6} \\ \quad 1 \\ \text{if } t_{cf34} < \frac{b_{bf34}}{6} \\ \quad 0 \end{cases} \qquad t_{cfi34} = 0$$

Continuaty Plates are needed

According to AISC, 75% of the flange beam thickness is used

The thickness of the continuaty plates is

$t_{cp12} := 0.75 \cdot t_{bf34} = 1.1\ in$

==========

4.3. Stories 5 and 6

4.3.1 Design the Panel Zones for the Exterior Column

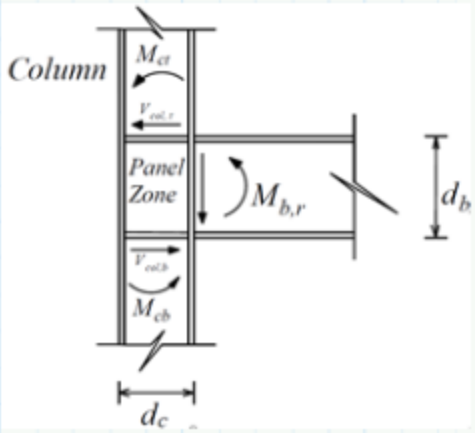

$M_{f56} := M_{pr56} + V_{p56} \cdot \left(a_{56} + \frac{b_{56}}{2}\right) = 23663.222\ kip \cdot in$

Column W14×342

$d_{c56} := 17.5 \cdot in$ $b_{cf56} := 16.4 \cdot in$ $t_{cw56} := 1.54 \cdot in$ $t_{cf56} := 2.47 \cdot in$ $A_{c56} := 101 \cdot in^2$

Beam W24*162

$d_{b56} := 25 \cdot in \qquad b_{bf56} := 13 \cdot in \qquad t_{bw56} := 0.705 \cdot in \qquad t_{bf56} := 1.22 \cdot in$

$$V_{ce56} := \frac{M_{f56}}{\frac{h_1 \cdot ft}{2} + \frac{h_2 \cdot ft}{2}} = 151.687\ kip$$

$$R_{u56} := \frac{M_{f56}}{d_{b56} - t_{bf56}} - V_{ce56} = 843.402\ kip$$

The capacity of Panel Zone

Assume $\phi_v := 1$

$$\phi R_{n56} := \phi_v \cdot 0.6 \cdot F_y \cdot d_{c56} \cdot t_{cw56} \cdot \left(1 + \frac{3 \cdot b_{cf56} \cdot t_{cf56}^{\ 2}}{d_{b56} \cdot d_{c56} \cdot t_{cw56}}\right) = 1168.697\ kip$$

Check

$$CR_{n1.56} := \begin{cases} \text{if } \phi R_{n56} < 0.75 \cdot F_y \cdot A_{c56} \\ \quad 1 \\ \text{if } \phi R_{n56} \geq 0.75 \cdot F_y \cdot A_{c56} \\ \quad 0 \end{cases} \qquad CR_{n1.56} = 1$$

Good

$$CR_{n2.56} := \begin{cases} \text{if } \phi R_{n56} < R_{u56} \\ \quad 1 \\ \text{if } \phi R_{n56} \geq R_{u56} \\ \quad 0 \end{cases} \qquad CR_{n2.56} = 0$$

Not Good

Doubler Plate Design

For Column W14×342 $\frac{d_z}{90} = 0.14\ in$

$w_z := 0.14 \cdot in \cdot 90 = 12.6\ in$

For Beam W24×162 $\frac{d_z}{90} = 0.251\ in$

$d_z := 0.251 \cdot in \cdot 90 = 22.59\ in$

$$t_w := \frac{(d_z + w_z)}{90} = 0.39\ in$$

$$t_p := \left(R_{u56} - \frac{0.6 \cdot F_y \cdot \left(3 \cdot b_{cf56} \cdot t_{cf56}^{\,2}\right)}{d_{b56}}\right) \cdot \left(\frac{1}{0.6 \cdot F_y \cdot d_{c56}}\right) - t_w = 0.53\ in$$

Continuaty Plate Design

$R_{yb} := 1.1$ $\quad R_{yc} := 1$ $\quad t_{cfi56} := 0.4 \cdot \left(1.8 \cdot b_{bf56} \cdot t_{bf56} \cdot \frac{R_{yb} \cdot F_y}{R_{yc} \cdot F_y}\right)^{0.5} = 2.24\ in$

$$t_{cfi56} := \begin{cases} \text{if } t_{cf56} \geq 0.4 \cdot \left(1.8 \cdot b_{bf56} \cdot t_{bf56} \cdot \frac{R_{yb} \cdot F_y}{R_{yc} \cdot F_y}\right)^{0.5} \\ \quad 1 \\ \text{if } t_{cf56} < 0.4 \cdot \left(1.8 \cdot b_{bf56} \cdot t_{bf56} \cdot \frac{R_{yb} \cdot F_y}{R_{yc} \cdot F_y}\right)^{0.5} \\ \quad 0 \end{cases} \qquad t_{cfi56} = 1$$

Good

$b_{bf34} := 13$

$$t_{cf56} := \begin{cases} \text{if } t_{cf56} \geq \frac{b_{bf56}}{6} \\ \quad 1 \\ \text{if } t_{cf56} < \frac{b_{bf56}}{6} \\ \quad 0 \end{cases} \qquad t_{cf12} = 1$$

Continuaty Plates are needed

According to AISC, 50% of the flange beam thickness is used

The thickness of the continuaty plates is

$t_{cp56} := 0.5 \cdot t_{bf56} = 0.61\ in$

4.1.2 Design the Panel Zones for the Interior Column

$$V_{ci56} := \frac{2 \cdot M_{f56}}{\frac{h_1 \cdot ft}{2} + \frac{h_2 \cdot ft}{2}} = 303.375\ kip$$

$$R_{ui56} := \frac{2 \cdot M_{f56}}{d_{b56} - t_{bf56}} - V_{ci56} = 1686.804\ kip$$

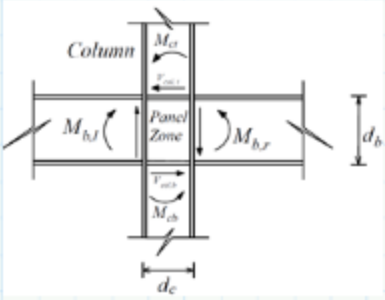

The Capacity of Panel Zone

Assume $\phi_v := 1$

Column W14*342

$d_{c56} := 17.5 \cdot in$ $b_{cf56} := 16.4 \cdot in$ $t_{cw56} := 1.54 \cdot in$ $t_{cf56} := 2.47 \cdot in$

$A_{c56} := 101 \cdot in^2$

Beam W24*162

$d_{b56} := 25 \cdot in$ $b_{bf56} := 13 \cdot in$ $t_{bw56} := 0.705 \cdot in$ $t_{bf56} := 1.22 \cdot in$

$$\phi R_{ni56} := \phi_v \cdot 0.6 \cdot F_y \cdot d_{c56} \cdot t_{cw56} \cdot \left(1 + \frac{3 \cdot b_{cf56} \cdot t_{cf56}^2}{d_{b56} \cdot d_{c56} \cdot t_{cw56}}\right) = 1168.697\ kip$$

Check

$$CR_{ni.56} := \begin{cases} \text{if } \phi R_{ni56} < 0.75 \cdot F_y \cdot A_{c56} \\ \quad 1 \\ \text{if } \phi R_{ni56} \geq 0.75 \cdot F_y \cdot A_{c56} \\ \quad 0 \end{cases} \qquad CR_{ni.56} = 1$$

Good

$$CR_{ni.56} := \begin{cases} \text{if } \phi R_{ni56} < R_{ui56} \\ \quad 1 \\ \text{if } \phi R_{ni56} \geq R_{ui56} \\ \quad 0 \end{cases} \qquad CR_{ni.56} = 1$$

Good

No Need for Doubler Plates

Continuaty Plate Design

$R_{yb} := 1.1$ $R_{yc} := 1$ $t_{cfi56} := 0.4 \cdot \left(1.8 \cdot b_{bf56} \cdot t_{bf56} \cdot \frac{R_{yb} \cdot F_y}{R_{yc} \cdot F_y}\right)^{0.5} = 2.24\ in$

$$t_{cf56} := \begin{cases} \text{if } t_{cfi56} \geq 0.4 \cdot \left(1.8 \cdot b_{bf56} \cdot t_{bf56} \cdot \frac{R_{yb} \cdot F_y}{R_{yc} \cdot F_y}\right)^{0.5} \\ \quad 1 \\ \text{if } t_{cfi56} < 0.4 \cdot \left(1.8 \cdot b_{bf56} \cdot t_{bf56} \cdot \frac{R_{yb} \cdot F_y}{R_{yc} \cdot F_y}\right)^{0.5} \\ \quad 0 \end{cases} \qquad t_{cf56} = 1$$

Good

$b_{bf56} := 13$

$$t_{cfi56} := \begin{cases} \text{if } t_{cf56} \geq \frac{b_{bf56}}{6} \\ \quad 1 \\ \text{if } t_{cf56} < \frac{b_{bf56}}{6} \\ \quad 0 \end{cases} \qquad t_{cfi56} = 0$$

Continuaty Plates are needed

According to AISC, 75% of the flange beam thickness is used

The thickness of the continuaty plates is

$t_{cp56} := 0.75 \cdot t_{bf56} = 0.92\ in$

==========

Summary

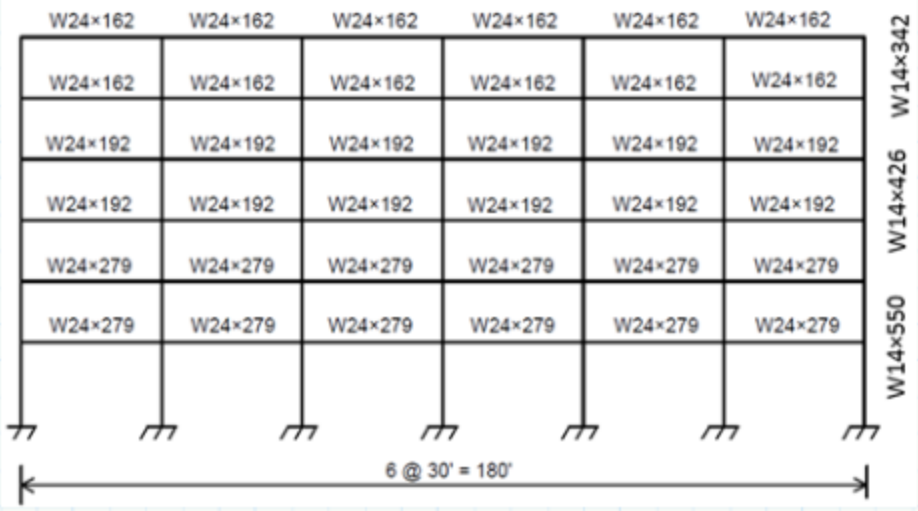

Level	Beam	Beam RBS dimensions (in)			M_{pe}/M_f
		a	b	c	ratio
1&2	W24×279	9	17	2.5	1.08
3&4	W24×192	9	16	2.5	1.09
5&6	W24×162	9	16	2.5	1.09

Thickness of Doubler Plates (in)		
Level	Exterior Columns	Interior Columns
1&2	1	3 3/8
3&4	1/2	2 2/8
5&6	5/8	1/2

Thickness of Continuity Plates (in)		
Level	Exterior Columns	Interior Columns
1&2	1 1/8	1 5/8
3&4	3/4	1 1/8
5&6	6/8	1

APPENDIX B: OPENSEES EXAMPLE FOR NINE-STORY MODEL

The following is one example of the twenty models that were under the consideration for the structures 6-, and 9-story SMFs and 6-, 9- , and 12-story BRBFs under the combinations coupled and uncoupled frames; and the investigation included two sites LA, CA and SLC, UT [2(5*2)]=20. The script could be copied and pasted directly into a text editor and saved it as a .tcl file for use in OpenSEES.

```
# MF with Panel Zone and RBS (6-Story and 6-Bay


# SET UP
wipe;
model BasicBuilder -ndm 2 -ndf 3;
set dataDir MF_Data;
set dataFor MF_Data;

source LibUnits.tcl;
source DisplayPlane.tcl;
source DisplayModel2D.tcl;
source Wsection.tcl;
source rotSpring2DModIKModel.tcl;
source rotLeaningCol.tcl;
source rotPanelZone2D.tcl;
source elemPanelZone2D.tcl;
set analysisType "dynamic";
if {$analysisType == "dynamic"} {

#set dataDir 1_RSN767_LOMAP_G03090-Output;
file mkdir $dataDir;
}

# define GEOMETRY
set IDctrlNode 1705;
set IDctrlDOF 1;
set NStory 6;
set NBay 2;
set LBuilding 996;
set g 386.2;

node 1 0.0 0.0;
node 8 360.0 0.0;
node 31 720.0 0.0;
node 117 0.0 0.0;
node 217 360.0 0.0;
node 317 720.0 0.0;
```

```
node 125 0.0 202.65;
node 225 360.0 202.65;
node 325 720.0 202.65;
node 128 0.0 229.35;
node 228 360.0 229.35;
node 328 720.0 229.35;
node 135 0.0 358.65;
node 235 360.0 358.65;
node 335 720.0 358.65;
node 138 0.0 385.35;
node 238 360.0 385.35;
node 338 720.0 385.35;
node 145 0.0 515.25;
node 245 360.0 515.25;
node 345 720.0 515.25;
node 148 0.0 540.75;
node 248 360.0 540.75;
node 348 720.0 540.75;
node 155 0.0 671.25;
node 255 360.0 671.25;
node 355 720.0 671.25;
node 158 0.0 696.75;
node 258 360.0 696.75;
node 358 720.0 696.75;
node 165 0.0 827.5;
node 265 360.0 827.5;
node 365 720.0 827.5;
node 168 0.0 852.5;
node 268 360.0 852.5;
node 368 720.0 852.5;
node 175 0.0 983.5;
node 275 360.0 983.5;
node 375 720.0 983.5;
node 121 27.6 216;
node 122 27.6 216;
node 123 332.4 216;
node 124 332.4 216;
node 221 387.6 216;
node 222 387.6 216;
node 223 692.4 216;
node 224 692.4 216;
node 131 27.6 372;
node 132 27.6 372;
node 133 332.4 372;
node 134 332.4 372;
node 231 387.6 372;
node 232 387.6 372;
node 233 692.4 372;
node 234 692.4 372;
node 141 26.35 528;
node 142 26.35 528;
node 143 333.65 528;
node 144 333.65 528;
node 241 386.35 528;
```

```
node 242 386.35 528;
node 243 693.65 528;
node 244 693.65 528;
node 151 26.35 684;
node 152 26.35 684;
node 153 333.65 684;
node 154 333.65 684;
node 251 386.35 684;
node 252 386.35 684;
node 253 693.65 684;
node 254 693.65 684;
node 161 25.75 840;
node 162 25.75 840;
node 163 334.25 840;
node 164 334.25 840;
node 261 385.75 840;
node 262 385.75 840;
node 263 694.25 840;
node 264 694.25 840;
node 171 25.75 996;
node 172 25.75 996;
node 173 334.25 996;
node 174 334.25 996;
node 271 385.75 996;
node 272 385.75 996;
node 273 694.25 996;
node 274 694.25 996;

# Calculate panel zone dimensions
node 1201 -10.1 229.35;
node 1202 -10.1 229.35;
node 1203  10.1 229.35;
node 1204  10.1 229.35;
node 1205  10.1 216;
node 1206  10.1 202.65;
node 1207  10.1 202.65;
node 1208 -10.1 202.65;
node 1209 -10.1 202.65;
node 1210 -10.1 216;
node 126  0.0 202.65;
node 127  0.0 229.35;
node 2201 349.9 229.35;
node 2202 349.9 229.35;
node 2203 370.1 229.35;
node 2204 370.1 229.35;
node 2205 370.1 216;
node 2206 370.1 202.65;
node 2207 370.1 202.65;
node 2208 349.9 202.65;
node 2209 349.9 202.65;
node 2210 349.9 216;
node 226 360 202.65;
node 227 360 229.35;
node 3201 709.9 229.35;
```

```
node 3202 709.9 229.35;
node 3203 730.1 229.35;
node 3204 730.1 229.35;
node 3205 730.1 216;
node 3206 730.1 202.65;
node 3207 730.1 202.65;
node 3208 709.9 202.65;
node 3209 709.9 202.65;
node 3210 709.9 216;
node 326 720 202.65;
node 327 720 229.35;
node 1301 -10.1 385.35;
node 1302 -10.1 385.35;
node 1303  10.1 385.35;
node 1304  10.1 385.35;
node 1305  10.1 372;
node 1306  10.1 358.65;
node 1307  10.1 358.65;
node 1308 -10.1 358.65;
node 1309 -10.1 358.65;
node 1310 -10.1 372;
node 136   0.0 358.65;
node 137   0.0 385.35;
node 2301 349.9 385.35;
node 2302 349.9 385.35;
node 2303 370.1 385.35;
node 2304 370.1 385.35;
node 2305 370.1 372;
node 2306 370.1 358.65;
node 2307 370.1 358.65;
node 2308 349.9 358.65;
node 2309 349.9 358.65;
node 2310 349.9 372;
node 236 360 358.65;
node 237 360 385.35;
node 3301 709.9 385.35;
node 3302 709.9 385.35;
node 3303 730.1 385.35;
node 3304 730.1 385.35;
node 3305 730.1 372;
node 3306 730.1 358.65;
node 3307 730.1 358.65;
node 3308 709.9 358.65;
node 3309 709.9 358.65;
node 3310 709.9 372;
node 336 720 358.65;
node 337 720 385.35;
node 1401 -9.35 540.75;
node 1402 -9.35 540.75;
node 1403  9.35 540.75;
node 1404  9.35 540.75;
node 1405  9.35 528;
node 1406  9.35 515.25;
node 1407  9.35 515.25;
```

```
node 1408 -9.35 515.25;
node 1409 -9.35 515.25;
node 1410 -9.35 528;
node 146   0.0 515.25;
node 147   0.0 540.75;
node 2401 350.65 540.75;
node 2402 350.65 540.75;
node 2403 369.35 540.75;
node 2404 369.35 540.75;
node 2405 369.35 528;
node 2406 369.35 515.25;
node 2407 369.35 515.25;
node 2408 350.65 515.25;
node 2409 350.65 515.25;
node 2410 350.65 528;
node 246  360 515.25;
node 247  360 540.75;
node 3401 710.65 540.75;
node 3402 710.65 540.75;
node 3403 729.35 540.75;
node 3404 729.35 540.75;
node 3405 729.35 528;
node 3406 729.35 515.25;
node 3407 729.35 515.25;
node 3408 710.65 515.25;
node 3409 710.65 515.25;
node 3410 710.65 528;
node 346  720 515.25;
node 347  720 540.75;
node 1501 -9.35 696.75;
node 1502 -9.35 696.75;
node 1503 9.35 696.75;
node 1504 9.35 696.75;
node 1505 9.35 684;
node 1506 9.35 671.25;
node 1507 9.35 671.25;
node 1508 -9.35 671.25;
node 1509 -9.35 671.25;
node 1510 -9.35 684;
node 156 0.0 671.25;
node 157 0.0 696.75;
node 2501 350.65 696.75;
node 2502 350.65 696.75;
node 2503 369.35 696.75;
node 2504 369.35 696.75;
node 2505 369.35 684;
node 2506 369.35 671.25;
node 2507 369.35 671.25;
node 2508 350.65 671.25;
node 2509 350.65 671.25;
node 2510 350.65 684;
node 256 360 671.25;
node 257 360 696.75;
node 3501 710.65 696.75;
```

```
node 3502 710.65 696.75;
node 3503 729.35 696.75;
node 3504 729.35 696.75;
node 3505 729.35 684;
node 3506 729.35 671.25;
node 3507 729.35 671.25;
node 3508 710.65 671.25;
node 3509 710.65 671.25;
node 3510 710.65 684;
node 356 720 671.25;
node 357 720 696.75;
node 1601 -8.75 852.5;
node 1602 -8.75 852.5;
node 1603  8.75 852.5;
node 1604  8.75 852.5;
node 1605  8.75 840;
node 1606  8.75 827.5;
node 1607  8.75 827.5;
node 1608 -8.75 827.5;
node 1609 -8.75 827.5;
node 1610 -8.75 840;
node 166   0.0 827.5;
node 167   0.0 852.5;
node 2601 351.25 852.5;
node 2602 351.25 852.5;
node 2603 368.75 852.5;
node 2604 368.75 852.5;
node 2605 368.75 840;
node 2606 368.75 827.5;
node 2607 368.75 827.5;
node 2608 351.25 827.5;
node 2609 351.25 827.5;
node 2610 351.25 840;
node 266  360 827.5;
node 267  360 852.5;
node 3601 711.25 852.5;
node 3602 711.25 852.5;
node 3603 728.75 852.5;
node 3604 728.75 852.5;
node 3605 728.35 840;
node 3606 728.35 827.5;
node 3607 728.35 827.5;
node 3608 711.25 827.5;
node 3609 711.25 827.5;
node 3610 711.25 840;
node 366  720 827.5;
node 367  720 852.5;
node 1701 -8.75 1008.5;
node 1702 -8.75 1008.5;
node 1703  8.75 1008.5;
node 1704  8.75 1008.5;
node 1705  8.75 996;
node 1706  8.75 983.5;
node 1707  8.75 983.5;
```

```
node 1708 -8.75 983.5;
node 1709 -8.75 983.5;
node 1710 -8.75 996;
node 176   0.0 983.5;
node 177   0.0 1008.5;
node 2701 351.25 1008.5;
node 2702 351.25 1008.5;
node 2703 368.75 1008.5;
node 2704 368.75 1008.5;
node 2705 368.75 996;
node 2706 368.75 983.5;
node 2707 368.75 983.5;
node 2708 351.25 983.5;
node 2709 351.25 983.5;
node 2710 351.25 996;
node 276 360 983.5;
node 277 360 1008.5;
node 3701 711.25 1008.5;
node 3702 711.25 1008.5;
node 3703 728.75 1008.5;
node 3704 728.75 1008.5;
node 3705 728.75 996;
node 3706 728.75 983.5;
node 3707 728.75 983.5;
node 3708 711.25 983.5;
node 3709 711.25 983.5;
node 3710 711.25 996;
node 376 720 983.5;
node 377 720 1008.5;
node 505 800 0.0;
node 526 800 216;
node 506 800 216;
node 527 800 216;
node 536 800 372;
node 507 800 372;
node 537 800 372;
node 546 800 528;
node 508 800 528;
node 547 800 528;
node 556 800 684;
node 509 800 684;
node 557 800 684;
node 566 800 840;
node 510 800 840;
node 567 800 840;
node 576 800 996;
node 511 800 996;

# BOUNDARY CONDITIONS
fix 1 1 1 1;           # Fixed support nodes
fix 8 1 1 1;           # Fixed support nodes
fix 31 1 1 1;          # Fixed support nodes
fix 505 1 1 0;         # P-delta column is pinned
```

```
# define MATERIAL properties
# $R0, $cR1, $cR2 control the transition from elastic to plastic branches.
# Recommended values:
# $R0=between 10 and 20, $cR1=0.925, $cR2=0.15
set R0_BC 20;
set cR1_BC 0.925;
set cR2_BC 0.15;
# Beam and Column Materials
set b_BC 0.01;
set Fy 50;
set Es 29000;
set BCMat 10;
uniaxialMaterial Steel02 $BCMat $Fy $Es $b_BC $R0_BC $cR1_BC $cR2_BC

# ELEMENT properties

#column 1-2 sections: W14x550
#set ColSecTag 1
set Acol_12 162;
set Icol_12 9430;
set Mycol_12 64900;

set d [expr 20.2*$in]; # depth
set bf [expr 17.2*$in];      # flange width
set tf [expr 3.82*$in];      # flange thickness
set tw [expr 2.38*$in];      # web thickness
set nfdw 16;           # number of fibers along dw
set nftw 2;      # number of fibers along tw
set nfbf 16;           # number of fibers along bf
set nftf 4;            # number of fibers along tf
Wsection 1 $BCMat $d $bf $tf $tw $nfdw $nftw $nfbf $nftf;

# Column 3-4 sections: W14x426
#set ColSecTag 2
set Acol_34 125;
set Icol_34 6600;
set Mycol_34 47795;
set d [expr 18.7*$in];
set bf [expr 16.7*$in];
set tf [expr 3.04*$in];
set tw [expr 1.88*$in];
set nfdw 16;
set nftw 2;
set nfbf 16;
set nftf 4;
Wsection 2 $BCMat $d $bf $tf $tw $nfdw $nftw $nfbf $nftf;
# Column 5-6 sections: W14x342
set ColSecTag 3
set Acol_56 101;
set Icol_56 4900;
set Mycol_56 36960;
```

```
set d [expr 17.5*$in]; # depth
set bf [expr 16.4*$in];
set tf [expr 2.47*$in];
set tw [expr 1.54*$in];
set nfdw 16;
set nftw 2;
set nfbf 16;
set nftf 4;
Wsection 3 $BCMat $d $bf $tf $tw $nfdw $nftw $nfbf $nftf
# beam 1-2 sections: W24x279
#set BeamSecTag 4
set Abeam_23 81.9;
set Ibeam_23 9600;
set Mybeam_23 45925;
set d [expr 26.7*$in];
set bf [expr 13.3*$in];
set tf [expr 2.09*$in];
set tw [expr 1.16*$in];
set nfdw 16;
set nftw 2;
set nfbf 16;
set nftf 4;
Wsection 4 $BCMat $d $bf $tf $tw $nfdw $nftw $nfbf $nftf
# beam 3-4 sections: W24x192
#set BeamSecTag 5
set Abeam_45 56.5;
set Ibeam_45 6260;
set Mybeam_45 30745;
set d [expr 25.5*$in];
set bf [expr 13.0*$in];
set tf [expr 1.46*$in];
set tw [expr 0.81*$in];
set nfdw 16;
set nftw 2;
set nfbf 16;
set nftf 4;
Wsection 5 $BCMat $d $bf $tf $tw $nfdw $nftw $nfbf $nftf
# beam 5-6 sections: W24x162
#BeamSecTag 6
set Abeam_67 47.8;
set Ibeam_67 5170;
set Mybeam_67 25740;
set d [expr 25.0*$in];
set bf [expr 13.0*$in];
set tf [expr 1.22*$in];
set tw [expr 0.705*$in];
set nfdw 16;
set nftw 2;
set nfbf 16;
set nftf 4;
Wsection 6 $BCMat $d $bf $tf $tw $nfdw $nftw $nfbf $nftf

set n 10.0;   # stiffness multiplier for rotational spring
```

```
# calculate modified moment of inertia for elastic elements
############################################################
# modified moment of inertia for columns in Story 1 & 2
set Icol_12mod  [expr $Icol_12*($n+1.0)/$n];  # modified moment of inertia
for columns in Story 1 & 2
set Icol_34mod  [expr $Icol_34*($n+1.0)/$n];  # modified moment of inertia
for columns in Story 3 & 4
set Icol_56mod  [expr $Icol_56*($n+1.0)/$n];  # modified moment of inertia
for columns in Story 5 & 6
# modified moment of inertia for beams in Floor 2 & 3
set Ibeam_23mod [expr $Ibeam_23*($n+1.0)/$n];
set Ibeam_45mod [expr $Ibeam_45*($n+1.0)/$n];
set Ibeam_67mod [expr $Ibeam_67*($n+1.0)/$n];
# calculate modified rotational stiffness for plastic hinge springs
set HStory1 216;
set WBay 360;
set HStoryTyp 156;
# for columns
set Ks_col_1   [expr $n*6.0*$Es*$Icol_12mod/$HStory1];    # rotational
stiffness of Story 1 column springs
set Ks_col_2   [expr $n*6.0*$Es*$Icol_12mod/$HStoryTyp]; # rotational
stiffness of Story 2 column springs
set Ks_col_3   [expr $n*6.0*$Es*$Icol_34mod/$HStoryTyp]; # rotational
stiffness of Story 3 column springs
set Ks_col_4   [expr $n*6.0*$Es*$Icol_34mod/$HStoryTyp]; # rotational
stiffness of Story 4 column springs
set Ks_col_5   [expr $n*6.0*$Es*$Icol_56mod/$HStoryTyp]; # rotational
stiffness of Story 5 column springs
set Ks_col_6   [expr $n*6.0*$Es*$Icol_56mod/$HStoryTyp]; # rotational
stiffness of Story 6 column springs
# for beams
set Ks_beam_23 [expr $n*6.0*$Es*$Ibeam_23mod/$WBay];      # rotational
stiffness of Floor 2 & 3 beam springs
set Ks_beam_45 [expr $n*6.0*$Es*$Ibeam_45mod/$WBay];      # rotational
stiffness of Floor 4 & 5 beam springs
set Ks_beam_67 [expr $n*6.0*$Es*$Ibeam_67mod/$WBay];      # rotational
stiffness of Floor 6 & 7 beam springs
# set up geometric transformation of elements
set PDeltaTransf 1;
geomTransf PDelta $PDeltaTransf;  # PDelta transformation

# define ELEMENTS -----
set IDColTransf 101;            # all columns
set IDBeamTransf 102;           # all beams
set ColTransfType Corotational;
geomTransf $ColTransfType $IDColTransf;
geomTransf $ColTransfType $IDBeamTransf;
set np 5;

# COLUMNS
element non-linearBeamColumn 111 117 125 $np 1 $IDColTransf;
element non-linearBeamColumn 112 128 135 $np 1 $IDColTransf;
element non-linearBeamColumn 113 138 145 $np 2 $IDColTransf;
```

```
element non-linearBeamColumn 114 148 155 $np 2 $IDColTransf;
element non-linearBeamColumn 115 158 165 $np 3 $IDColTransf;
element non-linearBeamColumn 116 168 175 $np 3 $IDColTransf;
element non-linearBeamColumn 121 217 225 $np 1 $IDColTransf;
element non-linearBeamColumn 122 228 235 $np 1 $IDColTransf;
element non-linearBeamColumn 123 238 245 $np 2 $IDColTransf;
element non-linearBeamColumn 124 248 255 $np 2 $IDColTransf;
element non-linearBeamColumn 125 258 265 $np 3 $IDColTransf;
element non-linearBeamColumn 126 268 275 $np 3 $IDColTransf;
element non-linearBeamColumn 131 317 325 $np 1 $IDColTransf;
element non-linearBeamColumn 132 328 335 $np 1 $IDColTransf;
element non-linearBeamColumn 133 338 345 $np 2 $IDColTransf;
element non-linearBeamColumn 134 348 355 $np 2 $IDColTransf;
element non-linearBeamColumn 135 358 365 $np 3 $IDColTransf;
element non-linearBeamColumn 136 368 375 $np 3 $IDColTransf;
# Gravity Column
element elasticBeamColumn 60 505 526 98.9 29000 4060 $IDColTransf;
element elasticBeamColumn 61 527 536 98.9 29000 4060 $IDColTransf;
element elasticBeamColumn 62 537 546 56.0 29000 2130 $IDColTransf;
element elasticBeamColumn 63 547 556 56.0 29000 2130 $IDColTransf;
element elasticBeamColumn 64 557 566 32.9 29000 716 $IDColTransf;
element elasticBeamColumn 65 567 576 32.9 29000 716 $IDColTransf;
# BEAMS
element non-linearBeamColumn 2121 1205 121 $np 4 $IDBeamTransf;
element non-linearBeamColumn 211 122 123 $np 4 $IDBeamTransf;
element non-linearBeamColumn 2122 124 2210 $np 4 $IDBeamTransf;
element non-linearBeamColumn 2123 2205 221 $np 4 $IDBeamTransf;
element non-linearBeamColumn 221 222 223 $np 4 $IDBeamTransf;
element non-linearBeamColumn 2124 224 3210 $np 4 $IDBeamTransf;
element non-linearBeamColumn 2131 1305 131 $np 4 $IDBeamTransf;
element non-linearBeamColumn 212 132 133 $np 4 $IDBeamTransf;
element non-linearBeamColumn 2132 134 2310 $np 4 $IDBeamTransf;
element non-linearBeamColumn 2133 2305 231 $np 4 $IDBeamTransf;
element non-linearBeamColumn 222 232 233 $np 4 $IDBeamTransf;
element non-linearBeamColumn 2134 234 3310 $np 4 $IDBeamTransf;
element non-linearBeamColumn 2141 1405 141 $np 5 $IDBeamTransf;
element non-linearBeamColumn 213 142 143 $np 5 $IDBeamTransf;
element non-linearBeamColumn 2142 144 2410 $np 5 $IDBeamTransf;
element non-linearBeamColumn 2143 2405 241 $np 5 $IDBeamTransf;
element non-linearBeamColumn 223 242 243 $np 5 $IDBeamTransf;
element non-linearBeamColumn 2144 244 3410 $np 5 $IDBeamTransf;
element non-linearBeamColumn 2151 1505 151 $np 5 $IDBeamTransf;
element non-linearBeamColumn 214 152 153 $np 5 $IDBeamTransf;
element non-linearBeamColumn 2152 154 2510 $np 5 $IDBeamTransf;
element non-linearBeamColumn 2153 2505 251 $np 5 $IDBeamTransf;
element non-linearBeamColumn 224 252 253 $np 5 $IDBeamTransf;
element non-linearBeamColumn 2154 254 3510 $np 5 $IDBeamTransf;
element non-linearBeamColumn 2161 1605 161 $np 6 $IDBeamTransf;
element non-linearBeamColumn 215 162 163 $np 6 $IDBeamTransf;
element non-linearBeamColumn 2162 164 2610 $np 6 $IDBeamTransf;
element non-linearBeamColumn 2163 2605 261 $np 6 $IDBeamTransf;
element non-linearBeamColumn 225 262 263 $np 6 $IDBeamTransf;
element non-linearBeamColumn 2164 264 3610 $np 6 $IDBeamTransf;
element non-linearBeamColumn 2171 1705 171 $np 6 $IDBeamTransf;
```

```
element non-linearBeamColumn 216 172 173 $np 6 $IDBeamTransf;
element non-linearBeamColumn 2172 174 2710 $np 6 $IDBeamTransf;
element non-linearBeamColumn 2173 2705 271 $np 6 $IDBeamTransf;
element non-linearBeamColumn 226 272 273 $np 6 $IDBeamTransf;
element non-linearBeamColumn 2174 274 3710 $np 6 $IDBeamTransf;

# Define Rotational Springs for Plastic Hinges, Panel Zones, and Gravity
Column
set pzlat23 [expr 20.2/2.0];
set pzlat45 [expr 18.7/2.0];
set pzlat67 [expr 17.5/2.0];
set phvert23 [expr $pzlat23+9 + 17/2.0];
set phvert45 [expr $pzlat45+9 + 16/2.0];
set phvert67 [expr $pzlat67+9 + 16/2.0];

# define rotational spring properties and create spring elements using
"rotSpring2DModIKModel" procedure
# rotSpring2DModIKModel creates a uniaxial material spring with a bilinear
response based on Modified Ibarra Krawinkler Deterioration Model
# references provided in rotSpring2DModIKModel.tcl
# input values for Story 1 column springs
set McMy12 1.04;
set LS 1000.0;
set LK 1000.0;
set LA 1000.0;
set LD 1000.0;
set cS 1.0;
set cK 1.0;
set cA 1.0;
set cD 1.0;
set th_pP 0.025;
set th_pN 0.025;
set th_pcP 0.3;
set th_pcN 0.3;
set ResP 0.4;
set ResN 0.4;
set th_uP 0.4;
set th_uN 0.4;
set DP 1.0;
set DN 1.0;
set a_mem [expr ($n+1.0)*($Mycol_12*($McMy12-1.0)) / ($Ks_col_1*$th_pP)];
set b [expr ($a_mem)/(1.0+$n*(1.0-$a_mem))];
# define beam springs
set th_pP 0.02;
set th_pN 0.02;
set th_pcP 0.16;
set th_pcN 0.16;
set a_mem [expr ($n+1.0)*($Mybeam_23*($McMy12-1.0)) /
($Ks_beam_23*$th_pP)];
set b [expr ($a_mem)/(1.0+$n*(1.0-$a_mem))];

#beam springs at Floor 2
```

```
rotSpring2DModIKModel 4121 121 122 $Ks_beam_23 $b $b $Mybeam_23 [expr -
$Mybeam_23] $LS $LK $LA $LD $cS $cK $cA $cD $th_pP $th_pN $th_pcP $th_pcN
$ResP $ResN $th_uP $th_uN $DP $DN;

rotSpring2DModIKModel 4122 123 124 $Ks_beam_23 $b $b $Mybeam_23 [expr -
$Mybeam_23] $LS $LK $LA $LD $cS $cK $cA $cD $th_pP $th_pN $th_pcP $th_pcN
$ResP $ResN $th_uP $th_uN $DP $DN;

rotSpring2DModIKModel 4221 221 222 $Ks_beam_23 $b $b $Mybeam_23 [expr -
$Mybeam_23] $LS $LK $LA $LD $cS $cK $cA $cD $th_pP $th_pN $th_pcP $th_pcN
$ResP $ResN $th_uP $th_uN $DP $DN;

rotSpring2DModIKModel 4222 223 224 $Ks_beam_23 $b $b $Mybeam_23 [expr -
$Mybeam_23] $LS $LK $LA $LD $cS $cK $cA $cD $th_pP $th_pN $th_pcP $th_pcN
$ResP $ResN $th_uP $th_uN $DP $DN;
#beam springs at Floor 3
rotSpring2DModIKModel 4131 131 132 $Ks_beam_23 $b $b $Mybeam_23 [expr -
$Mybeam_23] $LS $LK $LA $LD $cS $cK $cA $cD $th_pP $th_pN $th_pcP $th_pcN
$ResP $ResN $th_uP $th_uN $DP $DN;

rotSpring2DModIKModel 4132 133 134 $Ks_beam_23 $b $b $Mybeam_23 [expr -
$Mybeam_23] $LS $LK $LA $LD $cS $cK $cA $cD $th_pP $th_pN $th_pcP $th_pcN
$ResP $ResN $th_uP $th_uN $DP $DN;

rotSpring2DModIKModel 4231 231 232 $Ks_beam_23 $b $b $Mybeam_23 [expr -
$Mybeam_23] $LS $LK $LA $LD $cS $cK $cA $cD $th_pP $th_pN $th_pcP $th_pcN
$ResP $ResN $th_uP $th_uN $DP $DN;

rotSpring2DModIKModel 4232 233 234 $Ks_beam_23 $b $b $Mybeam_23 [expr -
$Mybeam_23] $LS $LK $LA $LD $cS $cK $cA $cD $th_pP $th_pN $th_pcP $th_pcN
$ResP $ResN $th_uP $th_uN $DP $DN;

set a_mem [expr ($n+1.0)*($Mybeam_45*($McMy34-1.0)) /
($Ks_beam_45*$th_pP)];
set b45 [expr ($a_mem)/(1.0+$n*(1.0-$a_mem))];
#beam springs at Floor 4
rotSpring2DModIKModel 4141 141 142 $Ks_beam_45 $b45 $b45 $Mybeam_45 [expr
-$Mybeam_45] $LS $LK $LA $LD $cS $cK $cA $cD $th_pP $th_pN $th_pcP $th_pcN
$ResP $ResN $th_uP $th_uN $DP $DN;

rotSpring2DModIKModel 4142 143 144 $Ks_beam_45 $b45 $b45 $Mybeam_45 [expr
-$Mybeam_45] $LS $LK $LA $LD $cS $cK $cA $cD $th_pP $th_pN $th_pcP $th_pcN
$ResP $ResN $th_uP $th_uN $DP $DN;

rotSpring2DModIKModel 4241 241 242 $Ks_beam_45 $b45 $b45 $Mybeam_45 [expr
-$Mybeam_45] $LS $LK $LA $LD $cS $cK $cA $cD $th_pP $th_pN $th_pcP $th_pcN
$ResP $ResN $th_uP $th_uN $DP $DN;

rotSpring2DModIKModel 4242 243 244 $Ks_beam_45 $b45 $b45 $Mybeam_45 [expr
-$Mybeam_45] $LS $LK $LA $LD $cS $cK $cA $cD $th_pP $th_pN $th_pcP $th_pcN
$ResP $ResN $th_uP $th_uN $DP $DN;
#beam springs at Floor 5
```

```
rotSpring2DModIKModel 4151 151 152 $Ks_beam_45 $b45 $b45 $Mybeam_45 [expr
-$Mybeam_45] $LS $LK $LA $LD $cS $cK $cA $cD $th_pP $th_pN $th_pcP $th_pcN
$ResP $ResN $th_uP $th_uN $DP $DN;

rotSpring2DModIKModel 4152 153 154 $Ks_beam_45 $b45 $b45 $Mybeam_45 [expr
-$Mybeam_45] $LS $LK $LA $LD $cS $cK $cA $cD $th_pP $th_pN $th_pcP $th_pcN
$ResP $ResN $th_uP $th_uN $DP $DN;

rotSpring2DModIKModel 4251 251 252 $Ks_beam_45 $b45 $b45 $Mybeam_45 [expr
-$Mybeam_45] $LS $LK $LA $LD $cS $cK $cA $cD $th_pP $th_pN $th_pcP $th_pcN
$ResP $ResN $th_uP $th_uN $DP $DN;

rotSpring2DModIKModel 4252 253 254 $Ks_beam_45 $b45 $b45 $Mybeam_45 [expr
-$Mybeam_45] $LS $LK $LA $LD $cS $cK $cA $cD $th_pP $th_pN $th_pcP $th_pcN
$ResP $ResN $th_uP $th_uN $DP $DN;
#beam springs at Floor 6 & 7
set a_mem [expr ($n+1.0)*($Mybeam_67*($McMy56-1.0)) /
($Ks_beam_67*$th_pP)];
set b67 [expr ($a_mem)/(1.0+$n*(1.0-$a_mem))];
#beam springs at Floor 6
rotSpring2DModIKModel 4161 161 162 $Ks_beam_67 $b67 $b67 $Mybeam_67 [expr
-$Mybeam_67] $LS $LK $LA $LD $cS $cK $cA $cD $th_pP $th_pN $th_pcP $th_pcN
$ResP $ResN $th_uP $th_uN $DP $DN;

rotSpring2DModIKModel 4162 163 164 $Ks_beam_67 $b67 $b67 $Mybeam_67 [expr
-$Mybeam_67] $LS $LK $LA $LD $cS $cK $cA $cD $th_pP $th_pN $th_pcP $th_pcN
$ResP $ResN $th_uP $th_uN $DP $DN;

rotSpring2DModIKModel 4261 261 262 $Ks_beam_67 $b67 $b67 $Mybeam_67 [expr
-$Mybeam_67] $LS $LK $LA $LD $cS $cK $cA $cD $th_pP $th_pN $th_pcP $th_pcN
$ResP $ResN $th_uP $th_uN $DP $DN;

rotSpring2DModIKModel 4262 263 264 $Ks_beam_67 $b67 $b67 $Mybeam_67 [expr
-$Mybeam_67] $LS $LK $LA $LD $cS $cK $cA $cD $th_pP $th_pN $th_pcP $th_pcN
$ResP $ResN $th_uP $th_uN $DP $DN;
#beam springs at Floor 7
rotSpring2DModIKModel 4171 171 172 $Ks_beam_67 $b $b $Mybeam_67 [expr -
$Mybeam_67] $LS $LK $LA $LD $cS $cK $cA $cD $th_pP $th_pN $th_pcP $th_pcN
$ResP $ResN $th_uP $th_uN $DP $DN;

rotSpring2DModIKModel 4172 173 174 $Ks_beam_67 $b $b $Mybeam_67 [expr -
$Mybeam_67] $LS $LK $LA $LD $cS $cK $cA $cD $th_pP $th_pN $th_pcP $th_pcN
$ResP $ResN $th_uP $th_uN $DP $DN;

rotSpring2DModIKModel 4271 271 272 $Ks_beam_67 $b $b $Mybeam_67 [expr -
$Mybeam_67] $LS $LK $LA $LD $cS $cK $cA $cD $th_pP $th_pN $th_pcP $th_pcN
$ResP $ResN $th_uP $th_uN $DP $DN;

rotSpring2DModIKModel 4272 273 274 $Ks_beam_67 $b $b $Mybeam_67 [expr -
$Mybeam_67] $LS $LK $LA $LD $cS $cK $cA $cD $th_pP $th_pN $th_pcP $th_pcN
$ResP $ResN $th_uP $th_uN $DP $DN;
# create region for beam springs
region 2 -ele 4121 4122 4221 4222 4131 4132 4231 4232 4141 4142 4241 4242
4151 4152 4251 4252 4161 4162 4261 4262 4171 4172 4271 4272;
```

```
#define panel zone springs
##########################
source rotPanelZone2D.tcl
set Ry 1.2;
set as_PZ 0.03;
set dcol_12 20.2;
set bfcol_12 17.2;
set tfcol_12 3.82;
set twcol_12 2.38;
set dbeam_23 26.7;
rotPanelZone2D 41200 1203 1204 $Es $Fy $dcol_12 $bfcol_12 $tfcol_12
$twcol_12 $dbeam_23 $Ry $as_PZ;
rotPanelZone2D 42200 2203 2204 $Es $Fy $dcol_12 $bfcol_12 $tfcol_12
$twcol_12 $dbeam_23 $Ry $as_PZ;
rotPanelZone2D 43200 3203 3204 $Es $Fy $dcol_12 $bfcol_12 $tfcol_12
$twcol_12 $dbeam_23 $Ry $as_PZ;
#3nd Floor PZ springs
rotPanelZone2D 41300 1303 1304 $Es $Fy $dcol_12 $bfcol_12 $tfcol_12
$twcol_12 $dbeam_23 $Ry $as_PZ;
rotPanelZone2D 42300 2303 2304 $Es $Fy $dcol_12 $bfcol_12 $tfcol_12
$twcol_12 $dbeam_23 $Ry $as_PZ;
rotPanelZone2D 43300 3303 3304 $Es $Fy $dcol_12 $bfcol_12 $tfcol_12
$twcol_12 $dbeam_23 $Ry $as_PZ;
set dcol_34 18.7;
set bfcol_34 16.7;
set tfcol_34 3.04;
set twcol_34 1.88;
set dbeam_45 25.5;
#4nd Floor PZ springs
rotPanelZone2D 41400 1403 1404 $Es $Fy $dcol_34 $bfcol_34 $tfcol_34
$twcol_34 $dbeam_45 $Ry $as_PZ;
rotPanelZone2D 42400 2403 2404 $Es $Fy $dcol_34 $bfcol_34 $tfcol_34
$twcol_34 $dbeam_45 $Ry $as_PZ;
rotPanelZone2D 43400 3403 3404 $Es $Fy $dcol_34 $bfcol_34 $tfcol_34
$twcol_34 $dbeam_45 $Ry $as_PZ;
#5nd Floor PZ springs
rotPanelZone2D 41500 1503 1504 $Es $Fy $dcol_34 $bfcol_34 $tfcol_34
$twcol_34 $dbeam_45 $Ry $as_PZ;
rotPanelZone2D 42500 2503 2504 $Es $Fy $dcol_34 $bfcol_34 $tfcol_34
$twcol_34 $dbeam_45 $Ry $as_PZ;
rotPanelZone2D 43500 3503 3504 $Es $Fy $dcol_34 $bfcol_34 $tfcol_34
$twcol_34 $dbeam_45 $Ry $as_PZ;
set dcol_56 17.5;
set bfcol_56 16.4;
set tfcol_56 2.47;
set twcol_56 1.54;
set dbeam_67 25.0;
#6nd Floor PZ springs
rotPanelZone2D 41600 1603 1604 $Es $Fy $dcol_56 $bfcol_56 $tfcol_56
$twcol_56 $dbeam_67 $Ry $as_PZ;
rotPanelZone2D 42600 2603 2604 $Es $Fy $dcol_56 $bfcol_56 $tfcol_56
$twcol_56 $dbeam_67 $Ry $as_PZ;
rotPanelZone2D 43600 3603 3604 $Es $Fy $dcol_56 $bfcol_56 $tfcol_56
$twcol_56 $dbeam_67 $Ry $as_PZ;
```

```
#7nd Floor PZ springs
rotPanelZone2D 41700 1703 1704 $Es $Fy $dcol_56 $bfcol_56 $tfcol_56
$twcol_56 $dbeam_67 $Ry $as_PZ;
rotPanelZone2D 42700 2703 2704 $Es $Fy $dcol_56 $bfcol_56 $tfcol_56
$twcol_56 $dbeam_67 $Ry $as_PZ;
rotPanelZone2D 43700 3703 3704 $Es $Fy $dcol_56 $bfcol_56 $tfcol_56
$twcol_56 $dbeam_67 $Ry $as_PZ;
# define elastic panel zone elements (assume rigid)


# elemPanelZone2D creates 8 elastic elements that form a rectangular panel
zone
set Apz 1000.0;                          # area of panel zone element (make
much larger than A of frame elements)
set Ipz 1.0e5;                          # moment of inertia of panel zone
element (make much larger than I of frame elements)
set PDeltraTransf 401;
geomTransf PDelta $PDeltraTransf;        # PDelta transformation
# elemPanelZone2D eleID  nodeR E  A_PZ I_PZ transfTag
elemPanelZone2D   500121 1201 $Es $Apz $Ipz $PDeltraTransf;
elemPanelZone2D   500221 2201 $Es $Apz $Ipz $PDeltraTransf;
elemPanelZone2D   500321 3201 $Es $Apz $Ipz $PDeltraTransf;
elemPanelZone2D   500131 1301 $Es $Apz $Ipz $PDeltaTransf;
elemPanelZone2D   500231 2301 $Es $Apz $Ipz $PDeltaTransf;
elemPanelZone2D   500331 3301 $Es $Apz $Ipz $PDeltaTransf;
elemPanelZone2D   500141 1401 $Es $Apz $Ipz $PDeltaTransf;
elemPanelZone2D   500241 2401 $Es $Apz $Ipz $PDeltaTransf;
elemPanelZone2D   500341 3401 $Es $Apz $Ipz $PDeltaTransf;
elemPanelZone2D   500151 1501 $Es $Apz $Ipz $PDeltaTransf;
elemPanelZone2D   500251 2501 $Es $Apz $Ipz $PDeltaTransf;
elemPanelZone2D   500351 3501 $Es $Apz $Ipz $PDeltaTransf;
elemPanelZone2D   500161 1601 $Es $Apz $Ipz $PDeltaTransf;
elemPanelZone2D   500261 2601 $Es $Apz $Ipz $PDeltaTransf;
elemPanelZone2D   500361 3601 $Es $Apz $Ipz $PDeltaTransf;
elemPanelZone2D   500171 1701 $Es $Apz $Ipz $PDeltaTransf;
elemPanelZone2D   500271 2701 $Es $Apz $Ipz $PDeltaTransf;
elemPanelZone2D   500371 3701 $Es $Apz $Ipz $PDeltaTransf;
# display the model with the node numbers
DisplayModel2D NodeNumbers;

# Assign masses to nodes
mass 127 0.684 1e-9 1e-9
mass 227 0.684 1e-9 1e-9
mass 227 0.684 1e-9 1e-9
mass 137 0.674 1e-9 1e-9
mass 237 0.674 1e-9 1e-9
mass 237 0.674 1e-9 1e-9
mass 147 0.674 1e-9 1e-9
mass 247 0.674 1e-9 1e-9
mass 247 0.674 1e-9 1e-9
mass 157 0.674 1e-9 1e-9
mass 257 0.674 1e-9 1e-9
mass 257 0.674 1e-9 1e-9
mass 167 0.674 1e-9 1e-9
```

```
mass 267 0.674 1e-9 1e-9
mass 267 0.674 1e-9 1e-9
mass 177 0.72 1e-9 1e-9
mass 277 0.72 1e-9 1e-9
mass 277 0.72 1e-9 1e-9
set dof1 1;          # constrain movement in dof 1 (x-direction)
equalDOF 1205 2205 $dof1;      # Floor 2:  Pier 1 to pair 2
equalDOF 1205 3205 $dof1;      # Floor 2:  Pier 1 to pair 3
equalDOF 1305 2305 $dof1;      # Floor 3:  Pier 1 to pair 2
equalDOF 1305 3305 $dof1;      # Floor 3:  Pier 1 to pair 3
equalDOF 1405 2405 $dof1;      # Floor 4:  Pier 1 to pair 2
equalDOF 1405 3405 $dof1;      # Floor 4:  Pier 1 to pair 3
equalDOF 1505 2505 $dof1;      # Floor 5:  Pier 1 to pair 2
equalDOF 1505 3505 $dof1;      # Floor 5:  Pier 1 to pair 3
equalDOF 1605 2605 $dof1;      # Floor 6:  Pier 1 to pair 2
equalDOF 1605 3605 $dof1;      # Floor 6:  Pier 1 to pair 3
equalDOF 1705 2705 $dof1;      # Floor 7:  Pier 1 to pair 2
equalDOF 1705 3705 $dof1;      # Floor 7:  Pier 1 to pair 3
# Attachment of Gravity Column to Frame
equalDOF 3210 506 1 3
equalDOF 3310 507 1 3
equalDOF 3410 508 1 3
equalDOF 3510 509 1 3
equalDOF 3610 510 1 3
equalDOF 3710 511 1 3
# Gravity Load & Gravity Analysis
pattern Plain 1 Linear {
load 506 0.0 -548.25 0.0;
load 507 0.0 -538.5  0.0;
load 508 0.0 -538.5  0.0;
load 509 0.0 -538.5  0.0;
load 510 0.0 -538.5  0.0;
load 511 0.0 -582.75 0.0;
}
constraints Plain;
numberer RCM;
system BandGeneral;
test NormDispIncr 1.0e-8 6;
integrator LoadControl 0.1;
analysis Static;
analyze 10;
loadConst -time 0.0;
puts "Model Built"

#Eigenvalue Analysis
set pi [expr 2.0*asin(1.0)];
set nEigenI 1;
set nEigenJ 2;
set lambdaN [eigen [expr $nEigenJ]];
set lambdaI [lindex $lambdaN [expr $nEigenI-1]];
set lambdaJ [lindex $lambdaN [expr $nEigenJ-1]];
set w1 [expr pow($lambdaI,0.5)];
set w2 [expr pow($lambdaJ,0.5)];
set T1 [expr 2.0*$pi/$w1];
```

```
set T2 [expr 2.0*$pi/$w2];
puts "T1 = $T1 s";
puts "T2 = $T2 s";

#Recorders
recorder Drift -file $dataDir/Drift-Story1.out -time -iNode 1 -jNode 1205
-dof 1 -perpDirn 2;
recorder Drift -file $dataDir/Drift-Story2.out -time -iNode 1205 -jNode
1305 -dof 1 -perpDirn 2;
recorder Drift -file $dataDir/Drift-Story3.out -time -iNode 1305 -jNode
1405 -dof 1 -perpDirn 2;
recorder Drift -file $dataDir/Drift-Story4.out -time -iNode 1405 -jNode
1505 -dof 1 -perpDirn 2;
recorder Drift -file $dataDir/Drift-Story5.out -time -iNode 1505 -jNode
1605 -dof 1 -perpDirn 2;
recorder Drift -file $dataDir/Drift-Story6.out -time -iNode 1605 -jNode
1705 -dof 1 -perpDirn 2;
recorder Drift -file $dataDir/Drift-Roof.out -time -iNode 1 -jNode 1705 -
dof 1 -perpDirn 2;

# record floor displacements
recorder Node -file $dataDir/NodeDisp.out -time -node 1205 1305 1405 1505
1606 1705 -dof 1 disp;
# record base shear reactions
recorder Node -file $dataDir/Vbase.out -time -node 117 217 317 -dof 1
reaction;

# record story 1 column forces in global coordinates
recorder Element -file $dataDir/Fcol-Lef.out -time -ele 111 112 113 114
115 116 force;      #Column Demands (story 1 Left)

#Time History/Dynamic Analysis

if {$analysisType == "dynamic"} {
puts "Running dynamic analysis..."
set ViewScale 5;
DisplayModel2D DeformedShape $ViewScale;
set zeta 0.02;
set a0 [expr $zeta*2.0*$w1*$w2/($w1 + $w2)];
set a1 [expr $zeta*2.0/($w1 + $w2)];
et a1_mod [expr $a1*(1.0+$n)/$n];
set g 386.2;
# define ground motion parameters

set patternID 400;     # load pattern ID
set GMdirection 1;     # ground motion direction (1 = x)
set GMfile "1_X_RSN767_LOMAP_G03090.tcl";  # ground motion filename
set dt 0.005;                              # timestep of input GM file
set TotalNumberOfSteps 7998;           # number of steps in ground motion
set Scalefact 1.68;                    # ground motion scaling factor
set TmaxAnalysis [expr $dt*$TotalNumberOfSteps + 10.0];
source LibAnalysisDynamicParameters.tcl
pattern UniformExcitation $patternID $GMdirection -accel $accelSeries;
```

```
# define dynamic analysis parameters
set DtAnalysis [expr 0.01*$sec];
wipeAnalysis;
constraints Plain;
numberer RCM;
system UmfPack;
test NormDispIncr 1.e-8 10;
set algorithmTypeDynamic Newton;
algorithm $algorithmTypeDynamic;
integrator Newmark 0.5 0.25;
analysis Transient;
set Nsteps [expr int(($TmaxAnalysis + 0.0)/$DtAnalysis)];
set ok [analyze $Nsteps $DtAnalysis];
if {$ok == 0} {
puts "Dynamic analysis complete";
} else {
puts "Dynamic analysis did not converge";
}
set currentTime [getTime];
puts "The current time is: $currentTime";
}
if {$ok != 0} { ;
set ok 0;
set controlTime [getTime];
while {$controlTime < $TmaxAnalysis && $ok == 0} {
set controlTime [getTime];
set ok [analyze 1 $DtAnalysis]
if {$ok != 0} {
puts "Trying Newton with Initial Tangent .."
test NormDispIncr   $Tol 1000  0
algorithm Newton -initial
set ok [analyze 1 $DtAnalysis]
test $testTypeDynamic $TolDynamic $maxNumIterDynamic  0
algorithm $algorithmTypeDynamic
}
if {$ok != 0} {
puts "Trying Broyden .."
algorithm Broyden 8
set ok [analyze 1 $DtAnalysis]
algorithm $algorithmTypeDynamic
}
f {$ok != 0} {
puts "Trying NewtonWithLineSearch .."
algorithm NewtonLineSearch .8;
set ok [analyze 1 $DtAnalysis];
algorithm $algorithmTypeDynamic
}
}
};      # end if ok !0

puts "Ground Motion Done. End Time: [getTime]"
wipe all;
```

APPENDIX C: INDIVIDUAL SMF AND BRBF AXIAL COLUMN DEMANDS FROM CHAPTER 3

Individual axial column forces for 6-, and 9-story SMF and 6-, 9-, and 12-story BRBF under the combination coupled and uncoupled frames for LA and SLC sites performed in Chapter 3 are provided in Figure C-5 through Figure C-45. Ten earthquakes were used to consider the orthogonal effects of seismic loads on the building for directions 0.0^0, 30^0, 60^0, and 90^0. [(2*(5*2) (10) (4) =800 dynamic analysis]. Figures C-1 through C-4 show the average maximum axial column demand for SMF and BRBF with 6-, 9-, and 12-story frames under the combinations coupled and uncoupled structures.

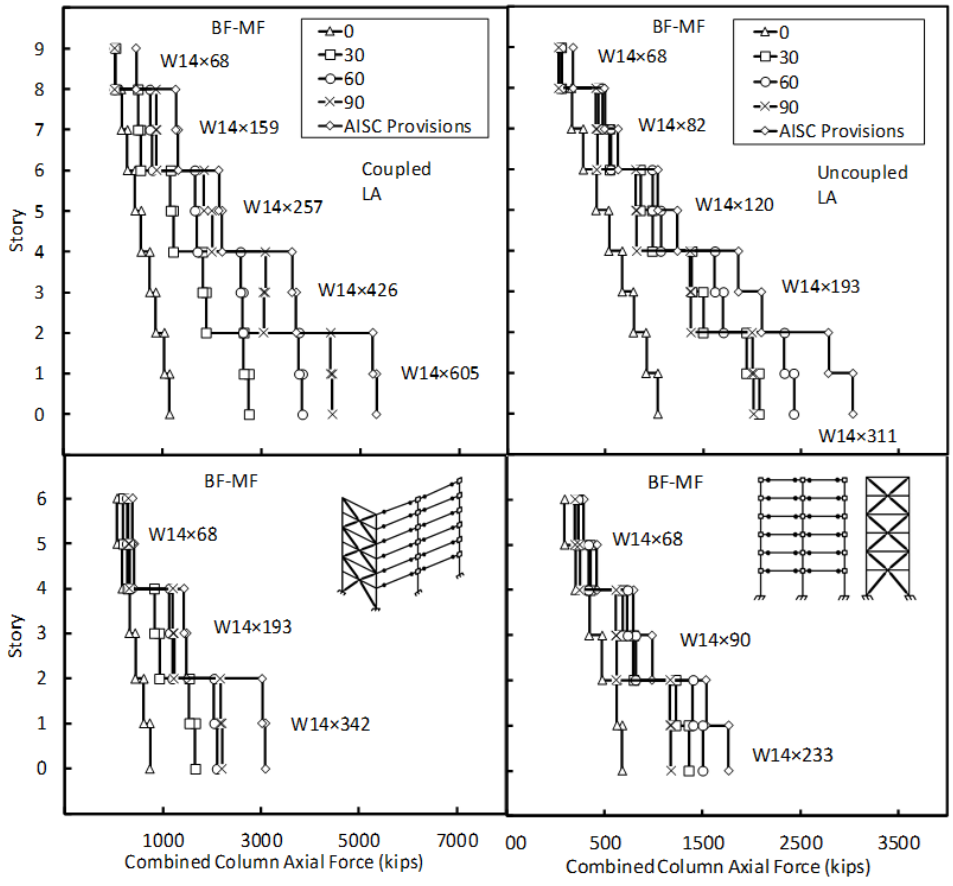

Figure C- 1. Seismic Forces in the Columns with the Column Demands for 6- and 9-Story Uncoupled and Coupled Frames (BF-MF) [LA].

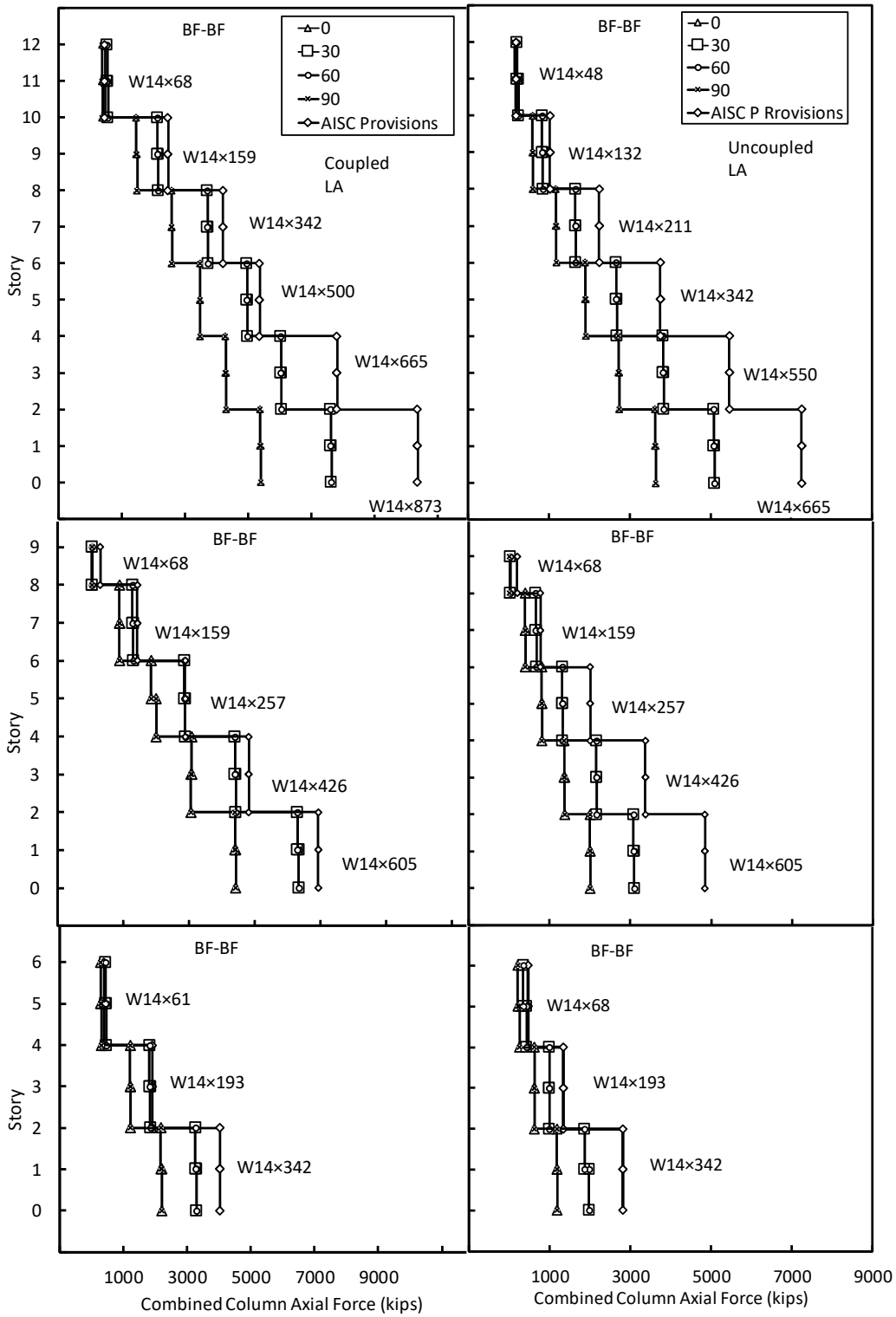

Figure C- 2. Seismic Forces in the Columns with the Column Demands for 6- and 9- and 12-Story Uncoupled and Coupled Frames (BF-BF) [LA].

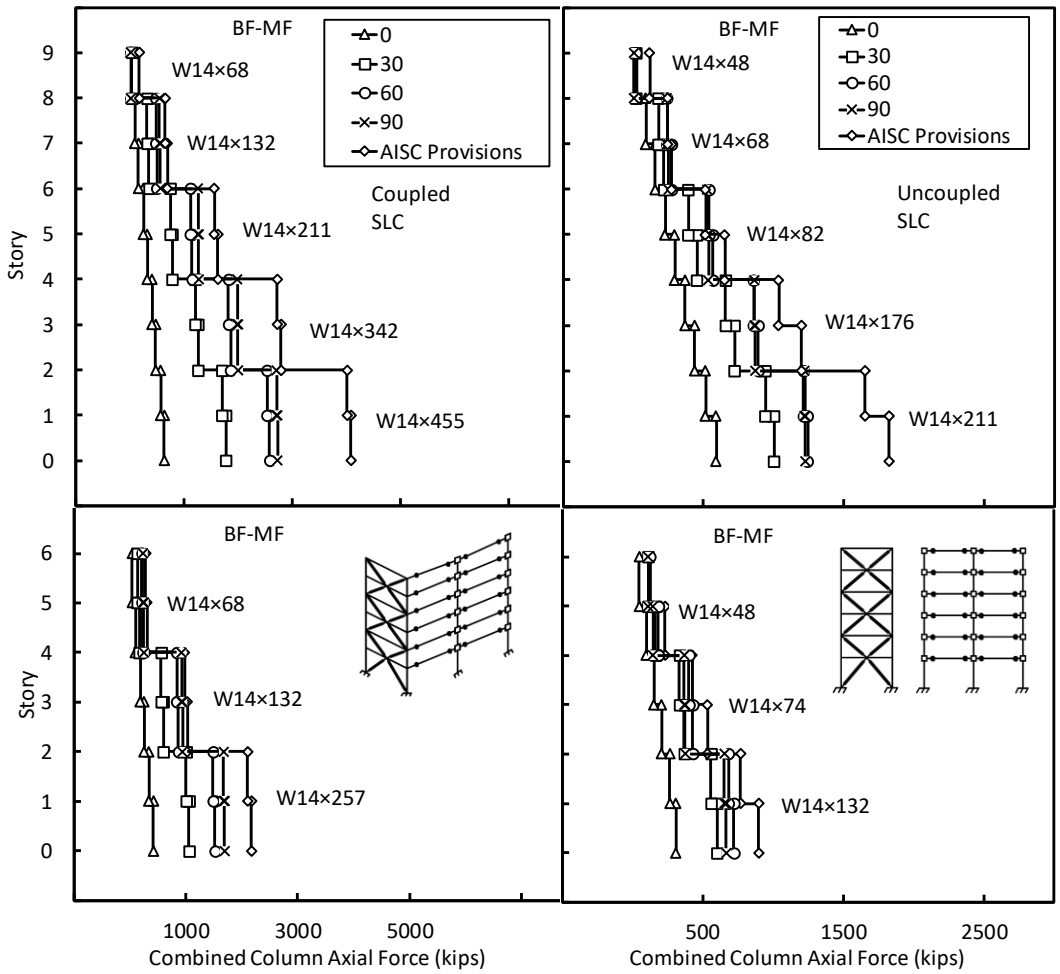

Figure C- 3. Seismic Forces in the Columns with the Column Demands for 6- and 9-Story Uncoupled and Coupled Frames (BF-MF) [SLC].

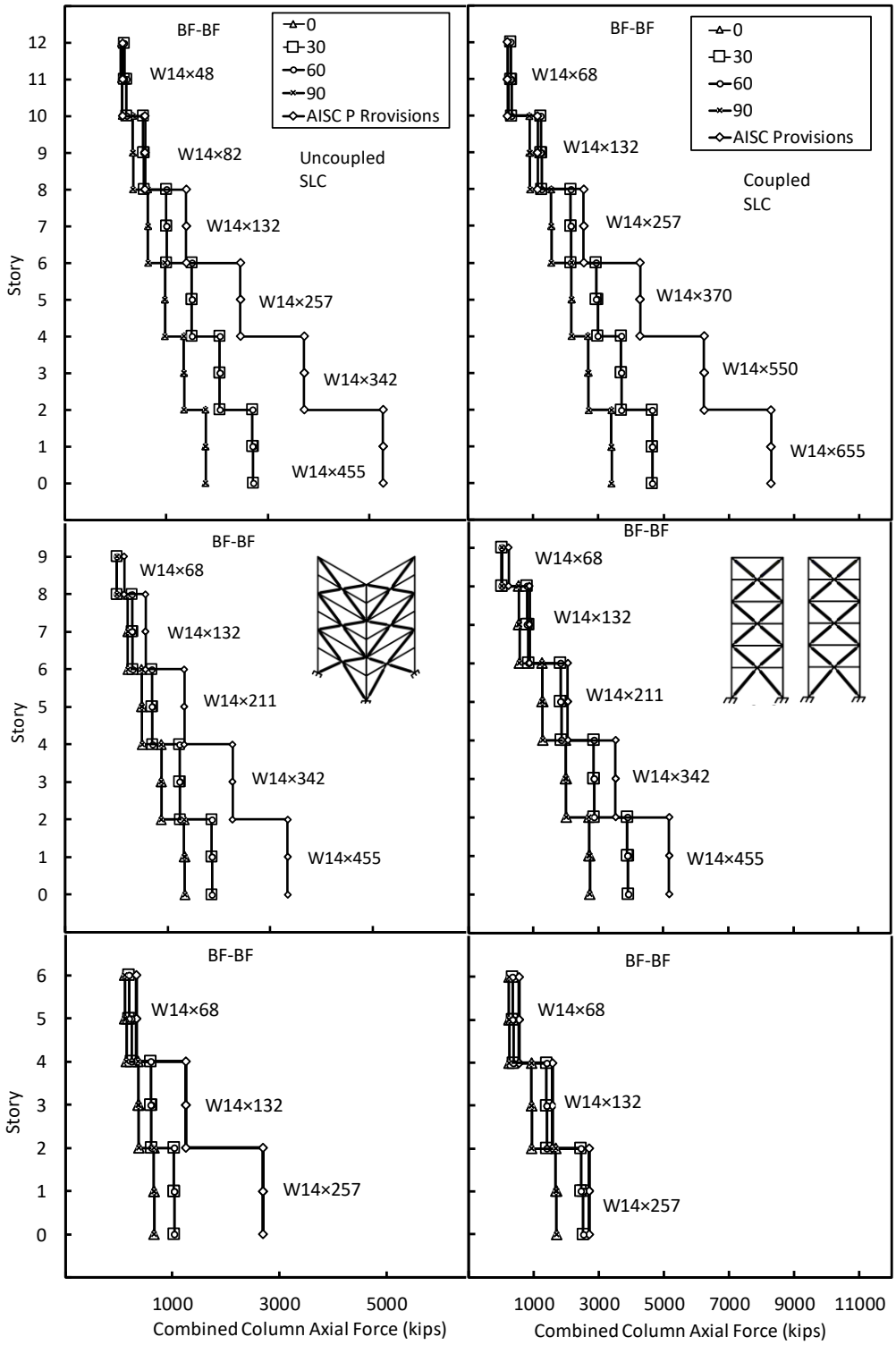

Figure C- 4. Seismic Forces in the Columns with the Column Demands for 6- and 9- and 12-Story Uncoupled and Coupled Frames (BF-BF) [SLC].

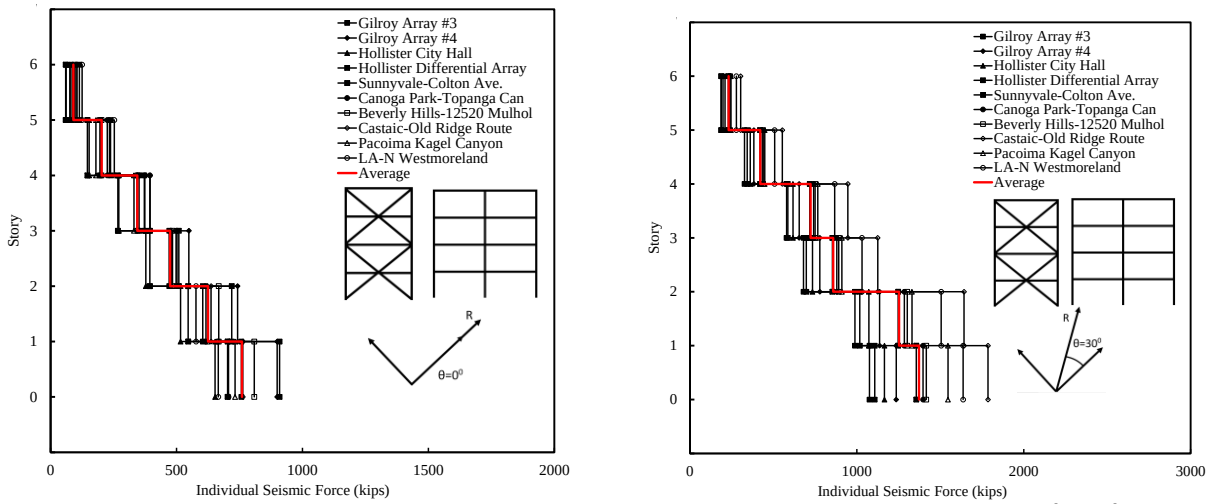

Figure C- 5. Individual Seismic Force for 6-Story Uncoupled Frames (BF-MF) [0^0, 30^0] [LA].

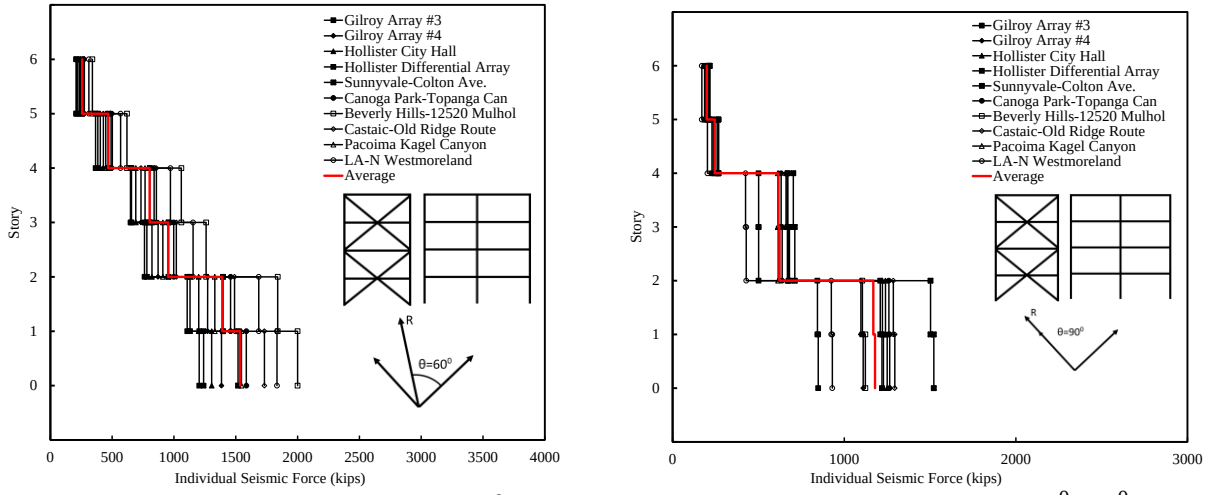

Figure C- 6. Individual Seismic Force for 6-Story Uncoupled Frames (BF-MF) [60^0, 90^0] [LA].

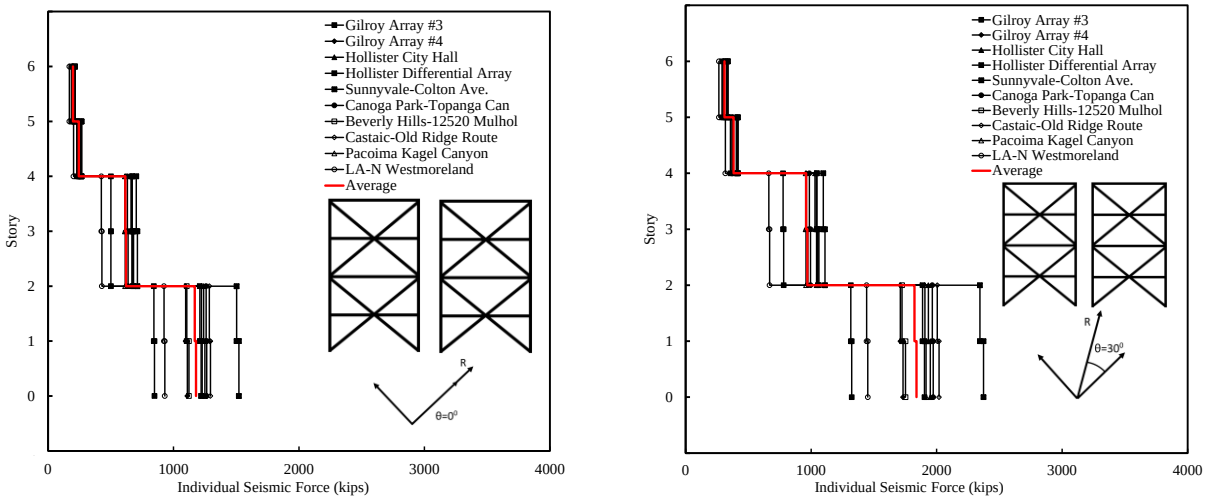

Figure C- 7. Individual Seismic Force for 6-Story Uncoupled Frames (BF-BF) [0^0, 30^0] [LA].

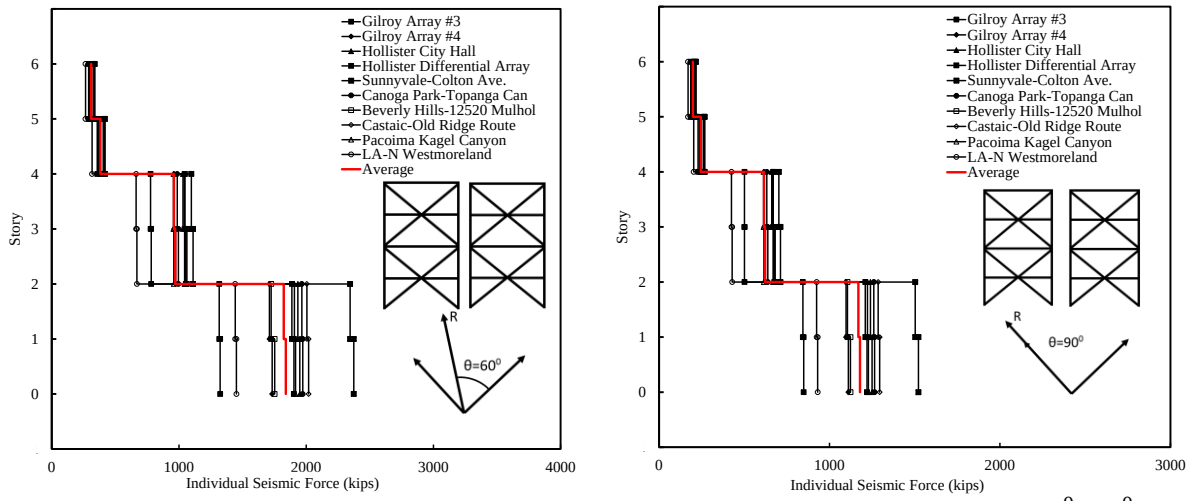

Figure C- 8. Individual Seismic Force for 6-Story Uncoupled Frames (BF-BF) [60^0, 90^0] [LA].

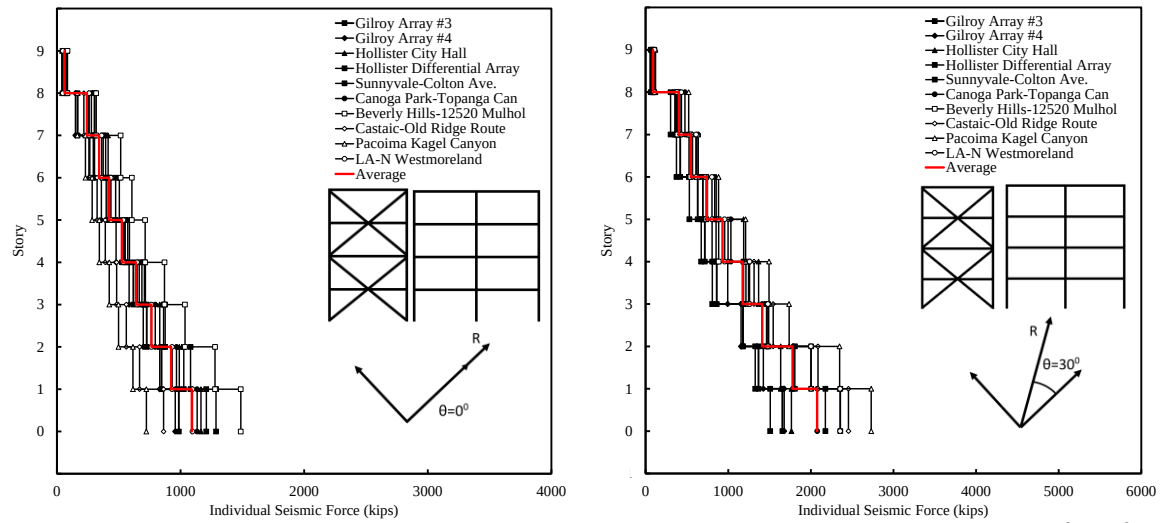

Figure C- 9. Individual Seismic Force for 9-Story Uncoupled Frames (BF-MF) [0^0, 30^0] [LA].

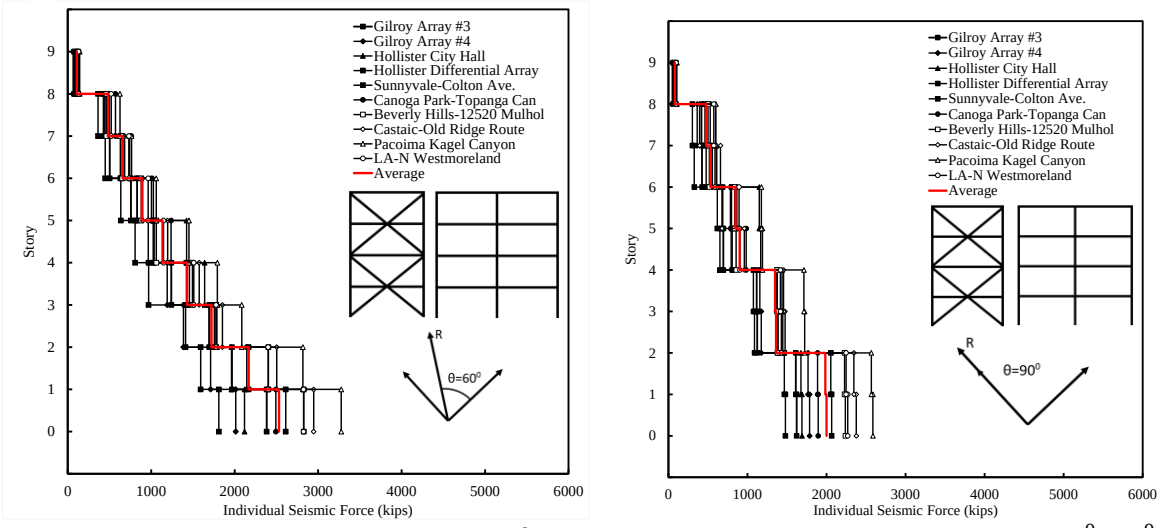

Figure C- 10. Individual Seismic Force for 9-Story Uncoupled Frames (BF-MF) [60^0, 90^0] [LA].

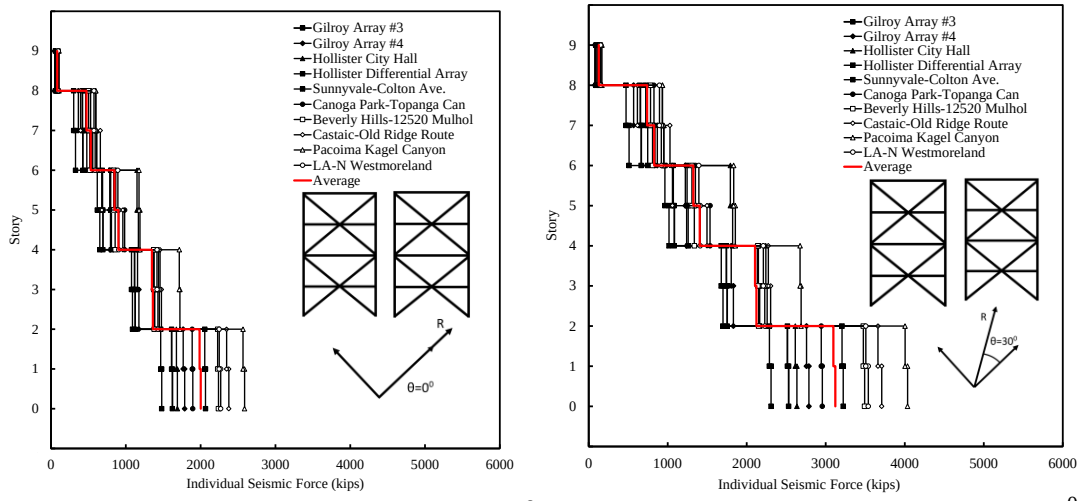

Figure C- 11. Individual Seismic Force for 9-Story Uncoupled Frames (BF-BF) [0^0, 30^0] [LA].

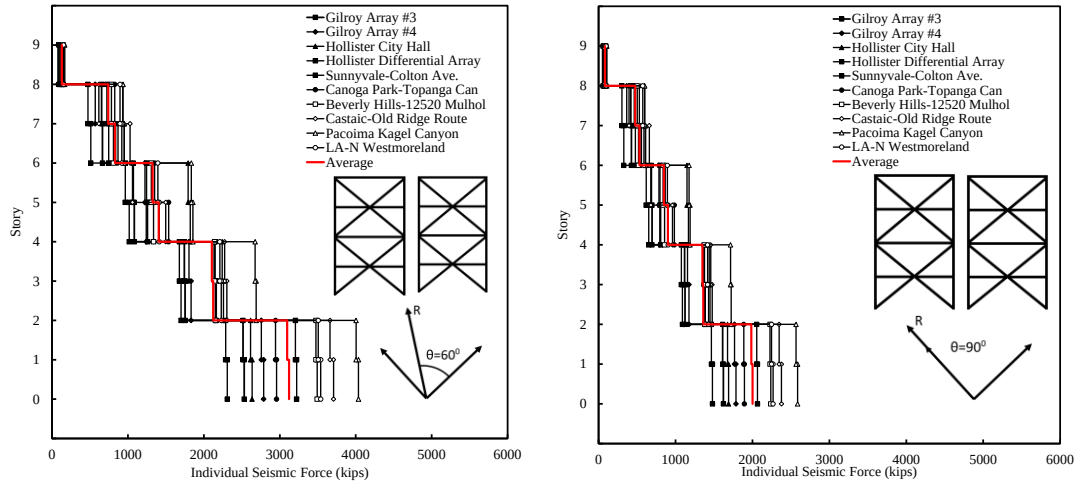

Figure C- 12. Individual Seismic Force for 9-Story Uncoupled Frames (BF-BF) [60^0, 90^0] [LA].

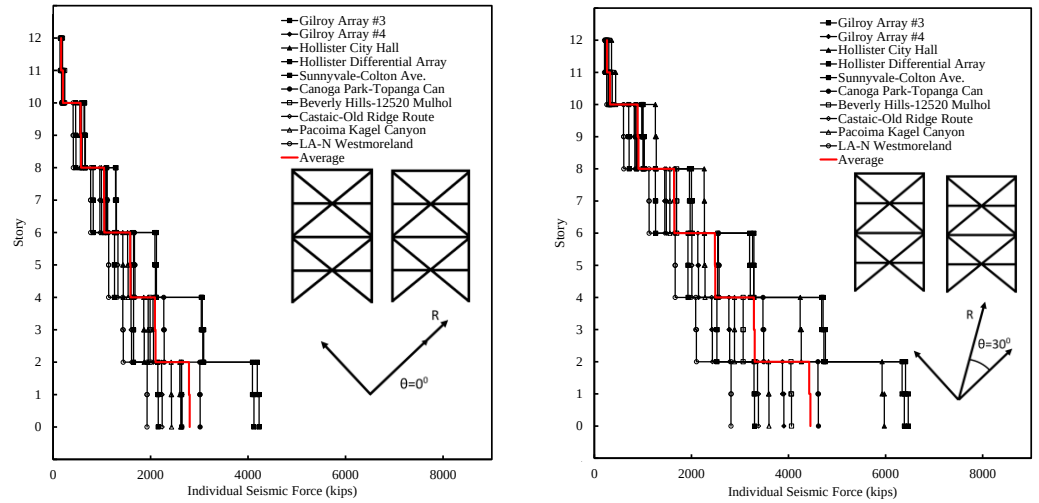

Figure C- 13. Individual Seismic Force for 12-Story Uncoupled Frames (BF-BF) [0^0, 30^0] [LA].

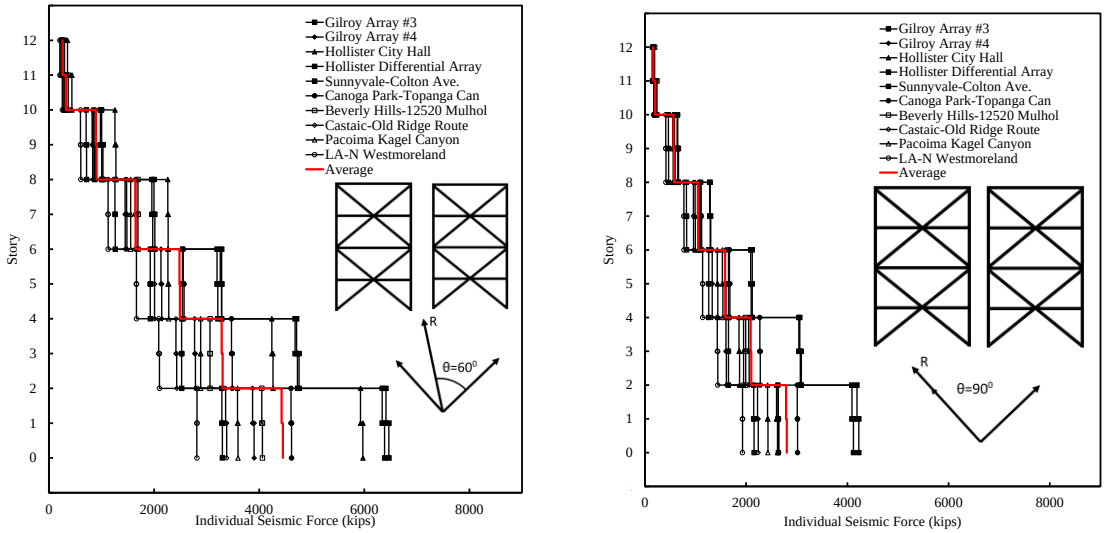

Figure C- 14. Individual Seismic Force for 12-Story Uncoupled Frames (BF-BF) [60^0, 90^0] [LA].

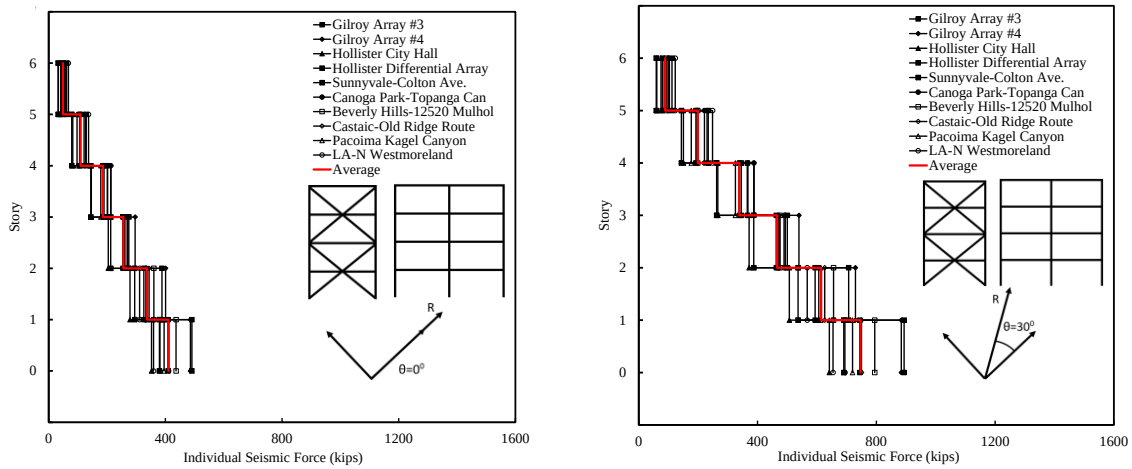

Figure C- 15. Individual Seismic Force for 6-Story Uncoupled Frames (BF-MF) [0^0, 30^0] [SLC].

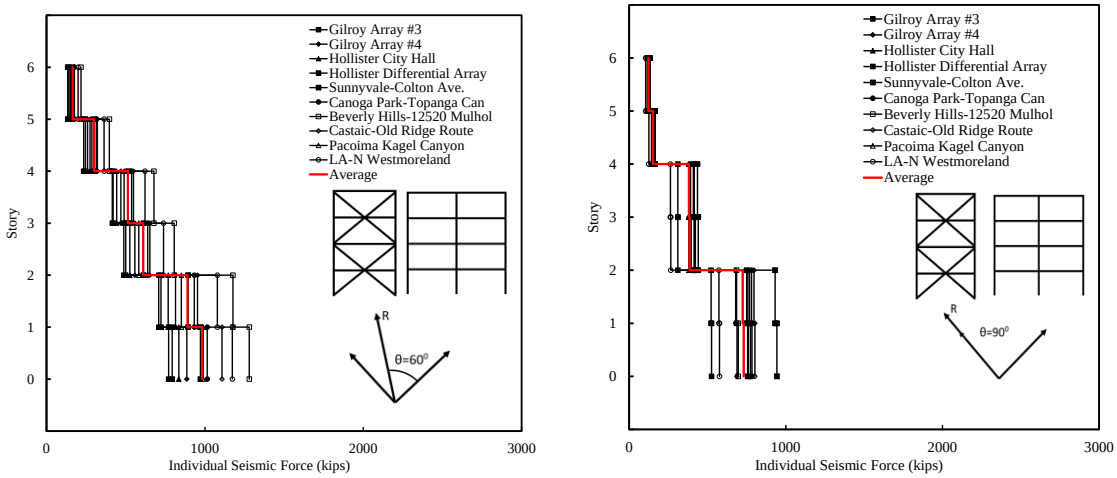

Figure C- 16. Individual Seismic Force for 6-Story Uncoupled Frames (BF-MF) [60^0, 90^0] [SLC]

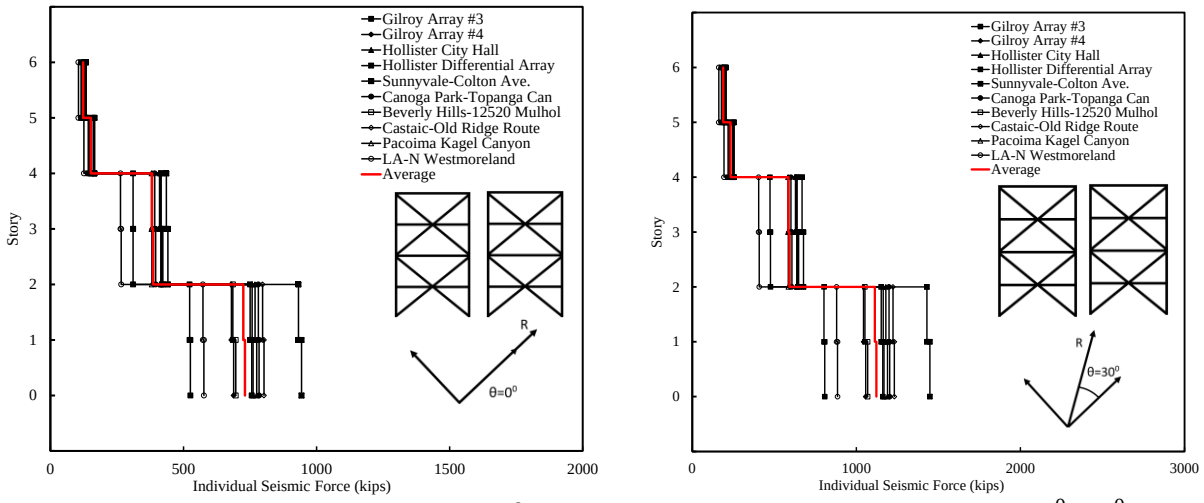

Figure C- 17. Individual Seismic Force for 6-Story Uncoupled Frames (BF-BF) [0^0, 30^0] [SLC].

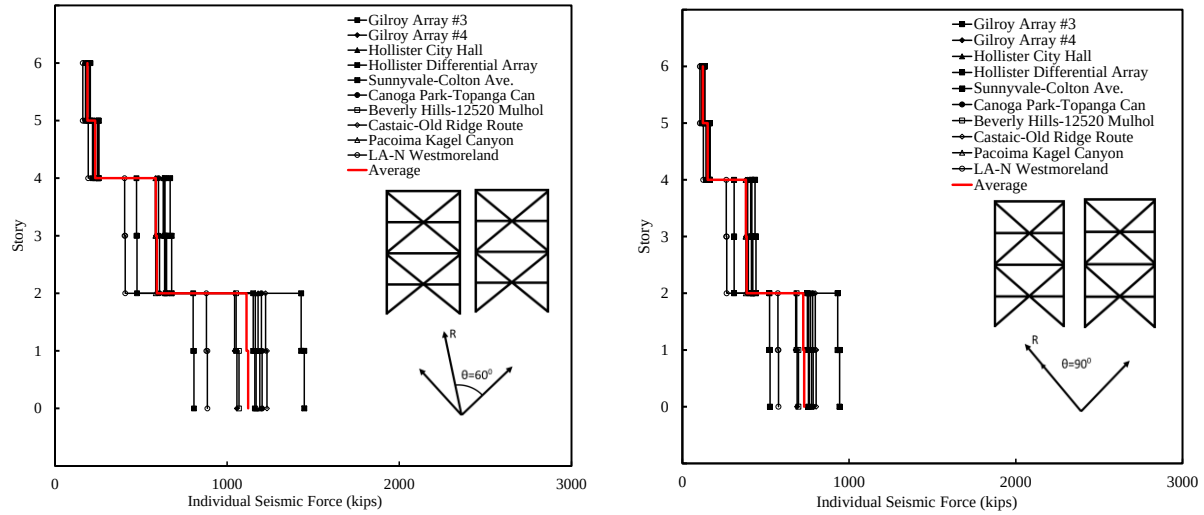

Figure C- 18. Individual Seismic Force for 6-Story Uncoupled Frames (BF-BF) [60^0, 90^0] [SLC].

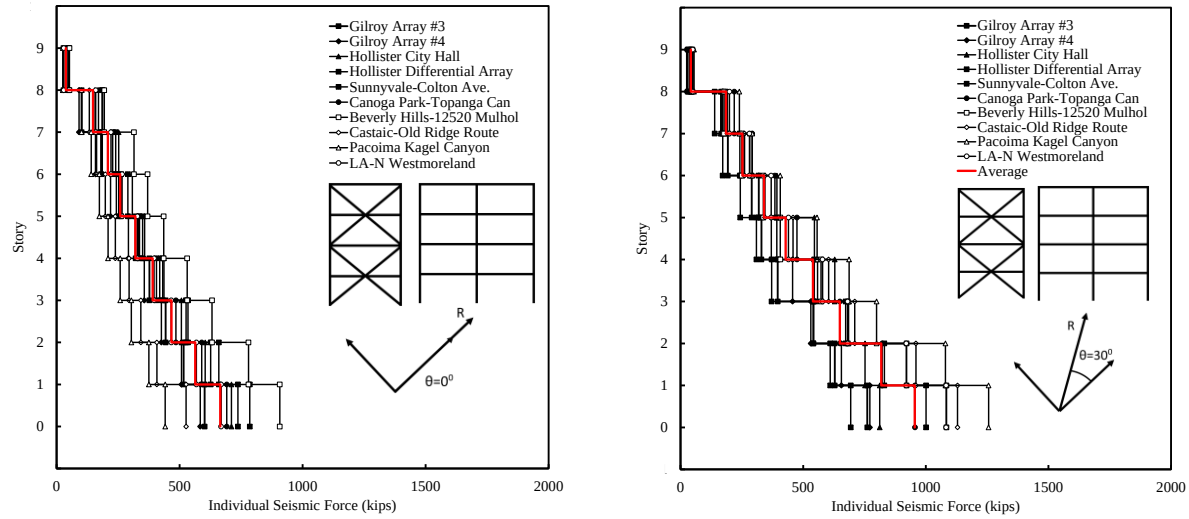

Figure C- 19. Individual Seismic Force for 6-Story Uncoupled Frames (BF-MF) [0^0, 30^0] [SLC].

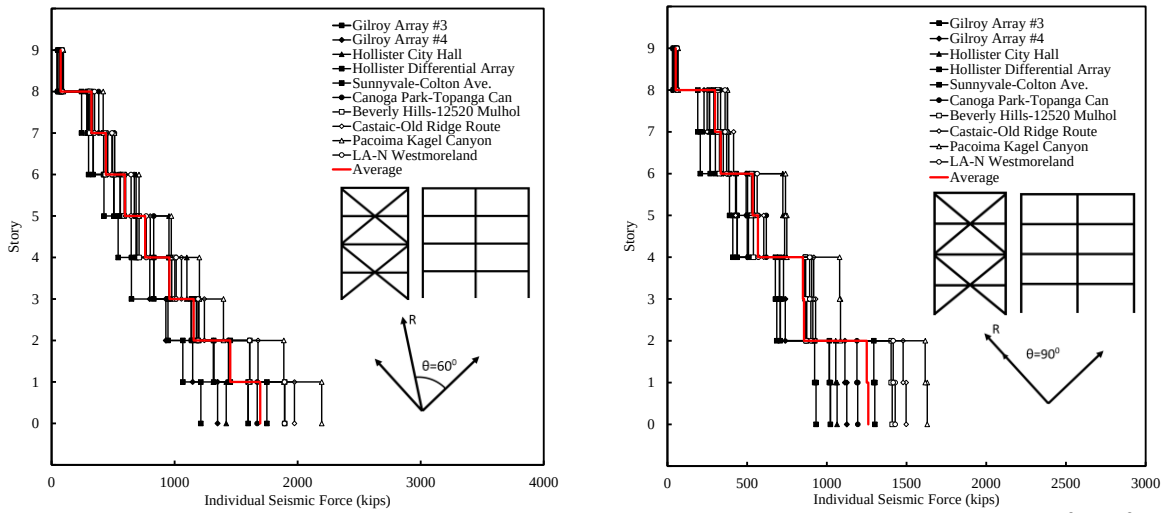

Figure C- 20. Individual Seismic Force for 9-Story Uncoupled Frames (BF-MF) [60^0, 90^0] [SLC]

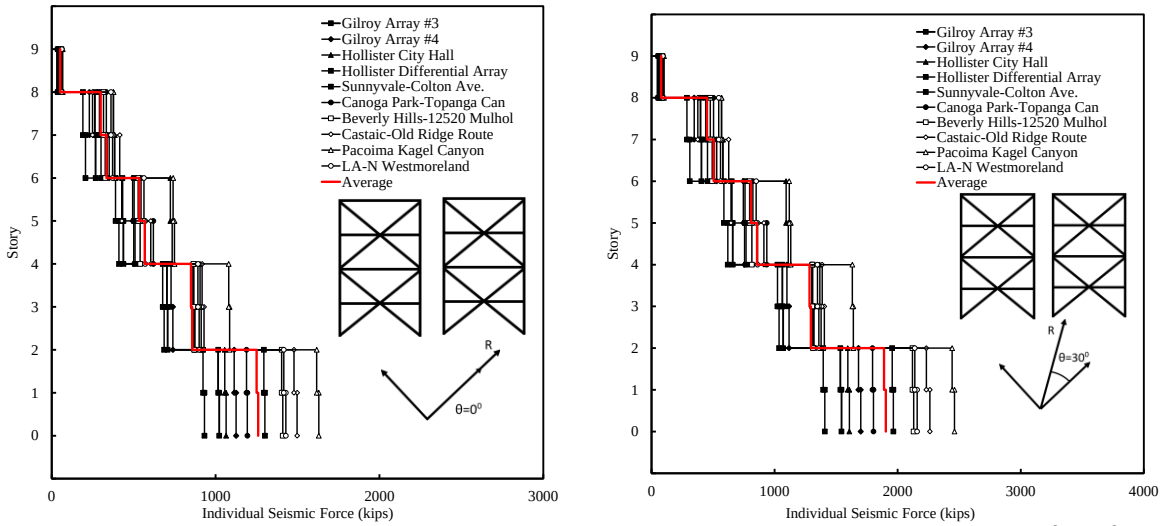

Figure C- 21. Individual Seismic Force for 9-Story Uncoupled Frames (BF-BF) [0^0, 30^0] [SLC].

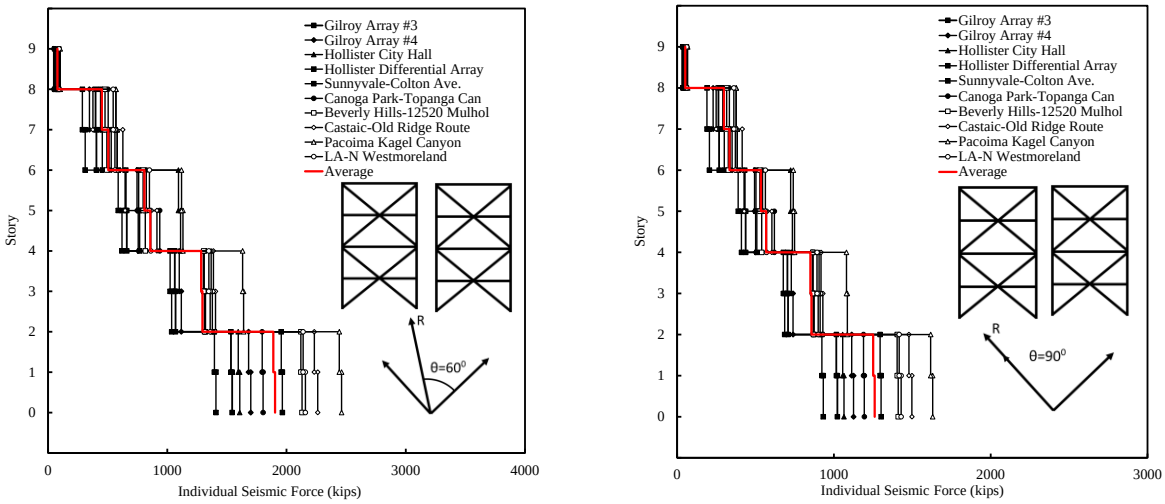

Figure C- 22. Individual Seismic Force for 9-Story Uncoupled Frames (BF-BF) [90^0, 60^0] [SLC].

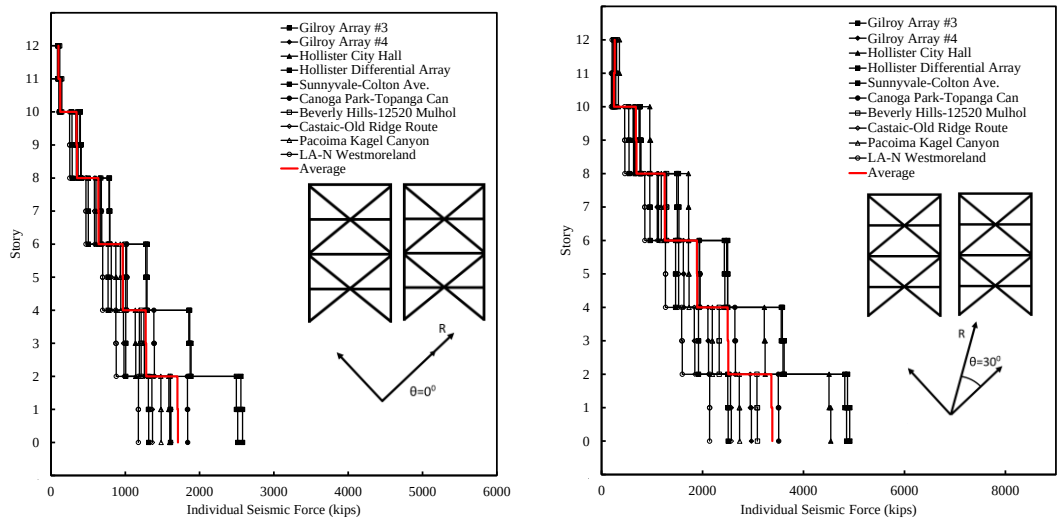

Figure C- 23. Individual Seismic Force for 12-Story Uncoupled Frames (BF-BF) [0^0, 30^0] [SLC].

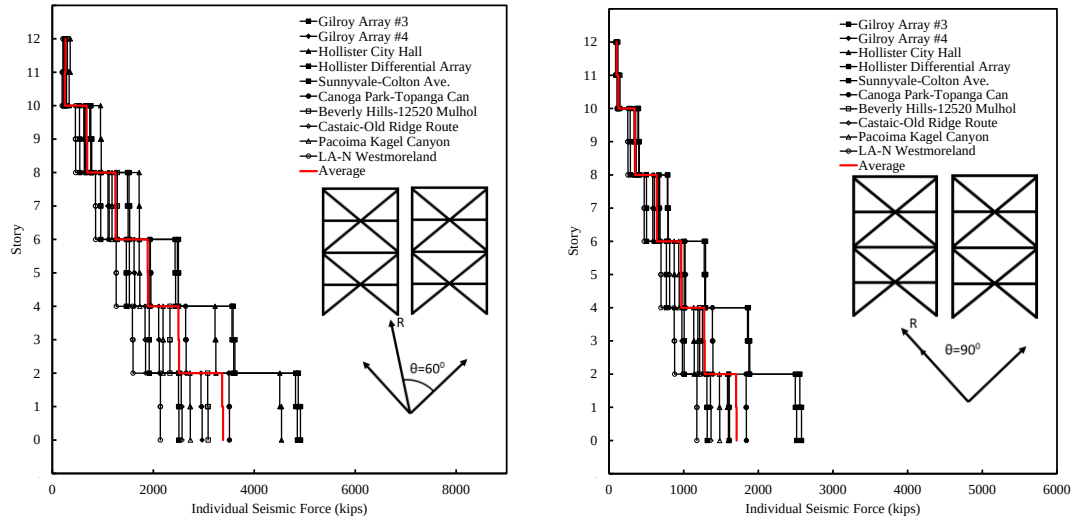

Figure C- 24. Individual Seismic Force for 12-Story Uncoupled Frames (BF-BF) [60^0, 90^0][SLC]

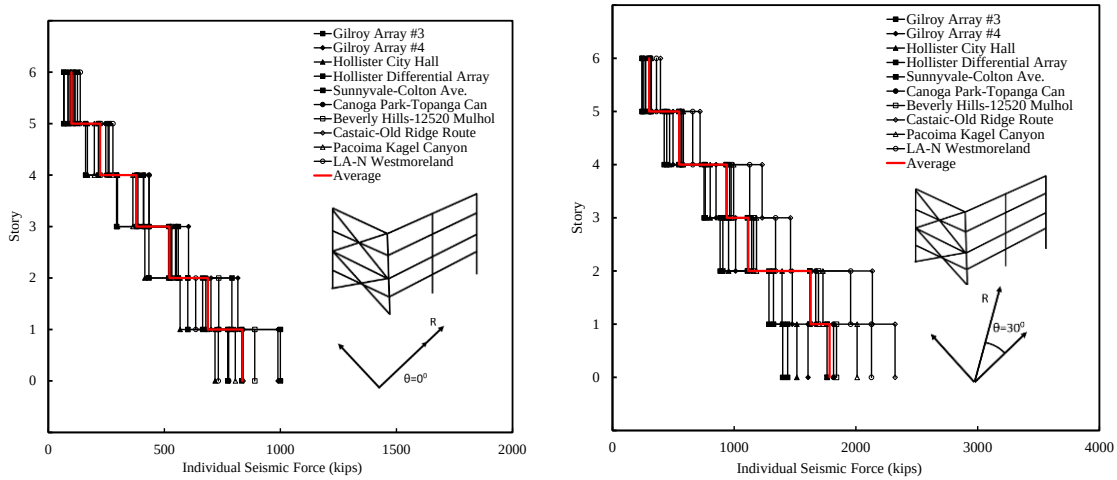

Figure C- 25. Individual Seismic Force for 6-Story Coupled Frames (BF-MF) [0^0, 30^0] [LA].

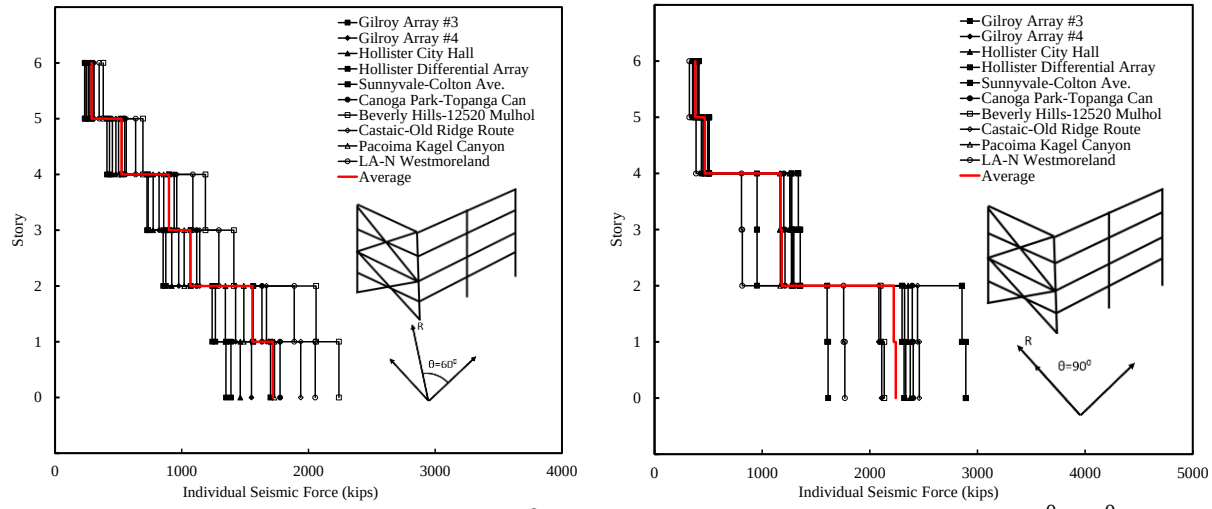

Figure C- 26. Individual Seismic Force for 6-Story Coupled Frames (BF-MF) [6^0, 90^0] [LA].

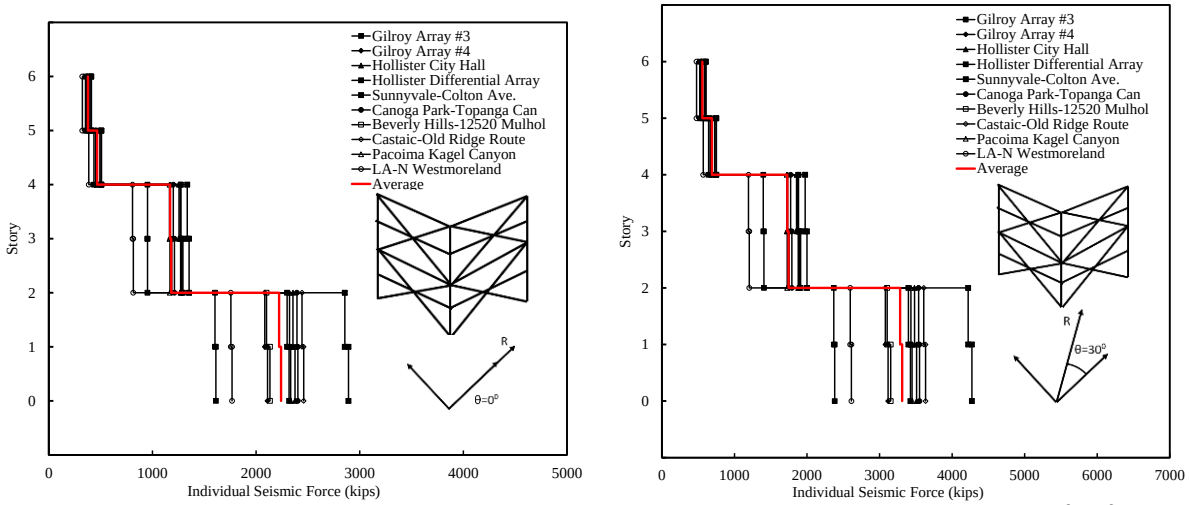

Figure C- 27. Individual Seismic Force for 6-Story Coupled Frames (BF-BF) [30^0, 0^0] [LA].

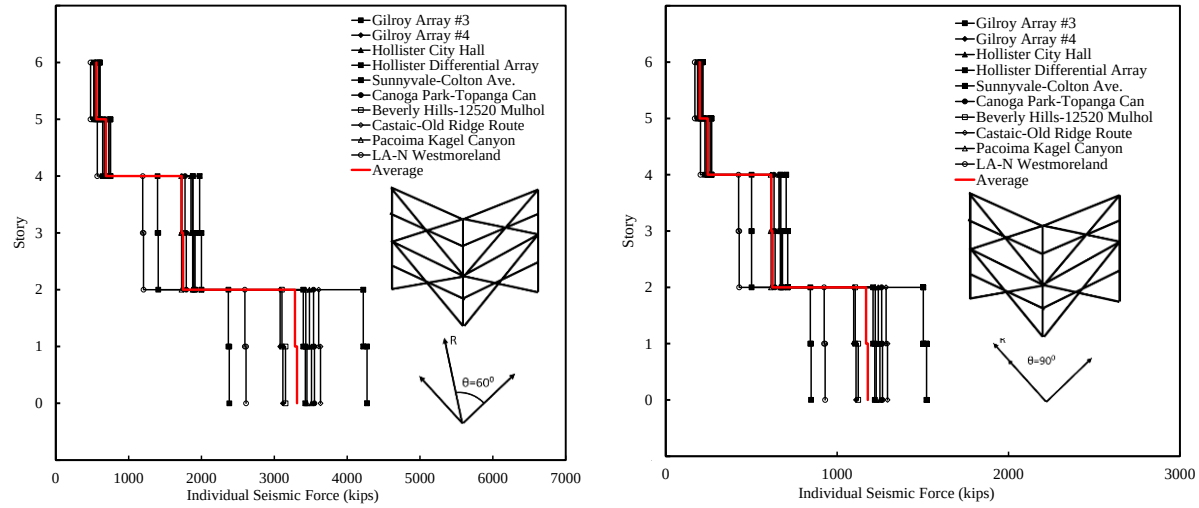

Figure C- 28. Individual Seismic Force for 6-Story Coupled Frames (BF-BF) [60^0, 90^0] [LA].

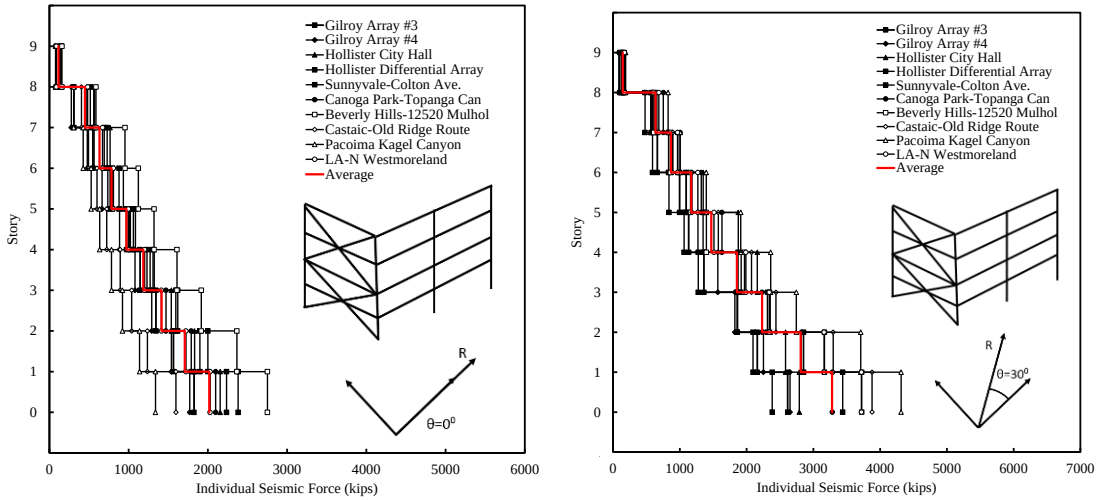

Figure C- 29. Individual Seismic Force for 9-Story Coupled Frames (BF-MF) [0^0, 30^0] [LA].

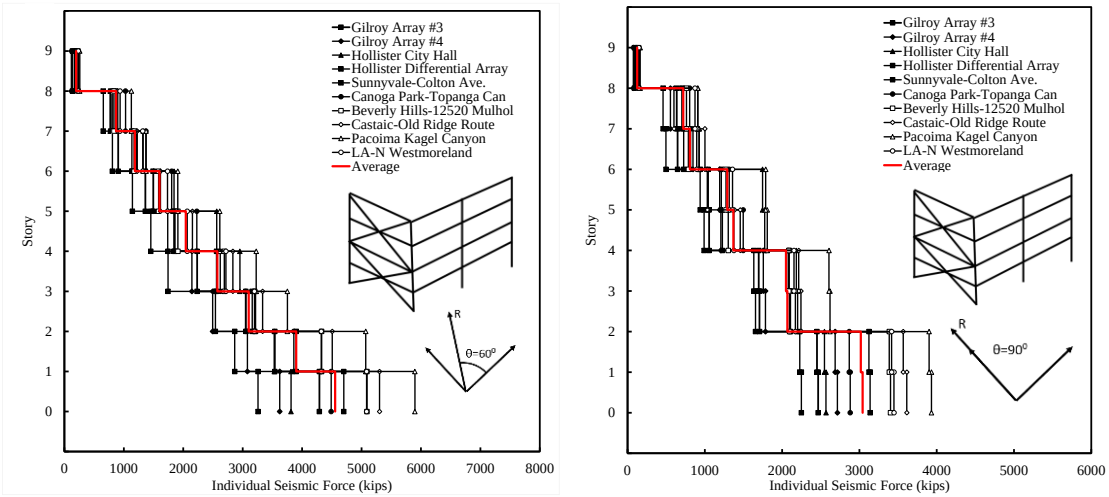

Figure C- 30. Individual Seismic Force for 9-Story Coupled Frames (BF-MF) [60^0, 90^0] [LA].

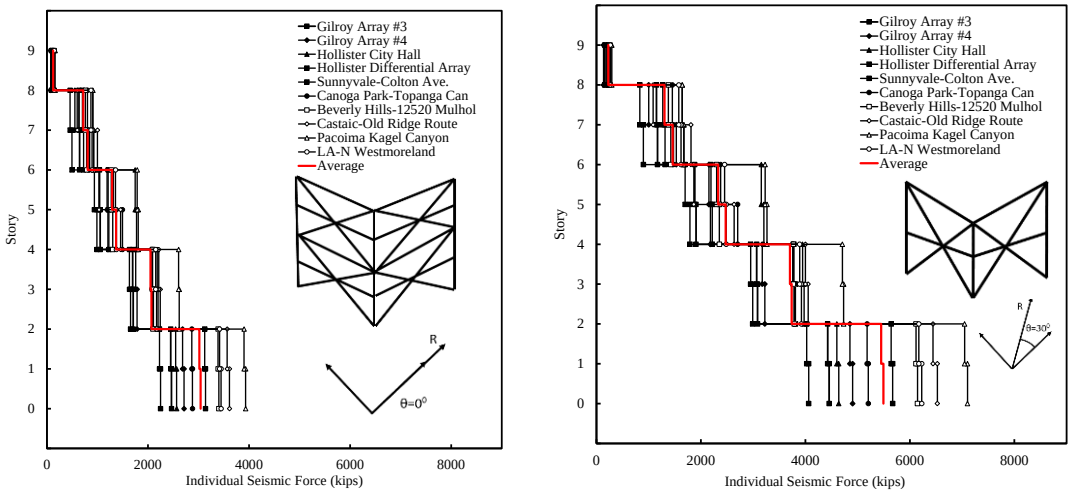

Figure C- 31. Individual Seismic Force for 9-Story Coupled Frames (BF-BF) [0^0, 30^0] [LA].

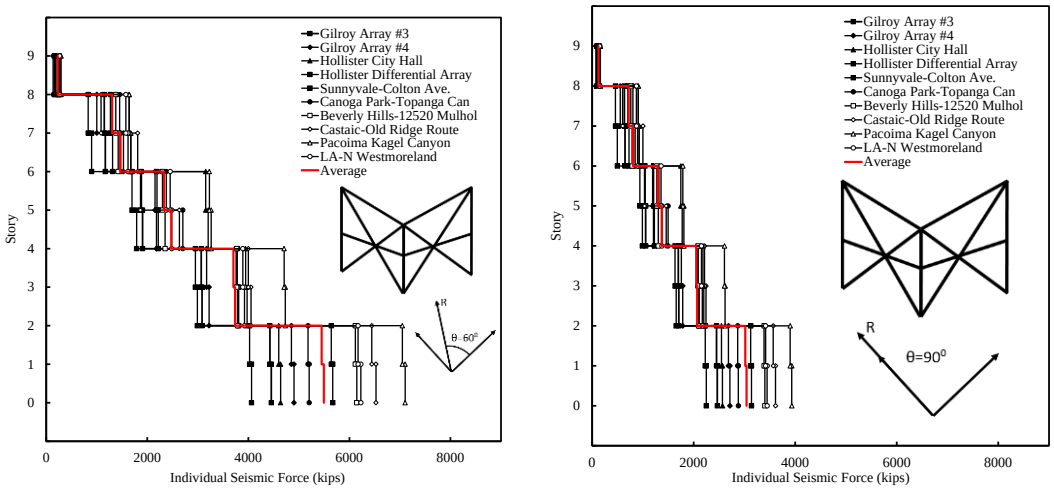

Figure C- 32. Individual Seismic Force for 9-Story Coupled Frames (BF-BF) [60^0, 90^0] [LA].

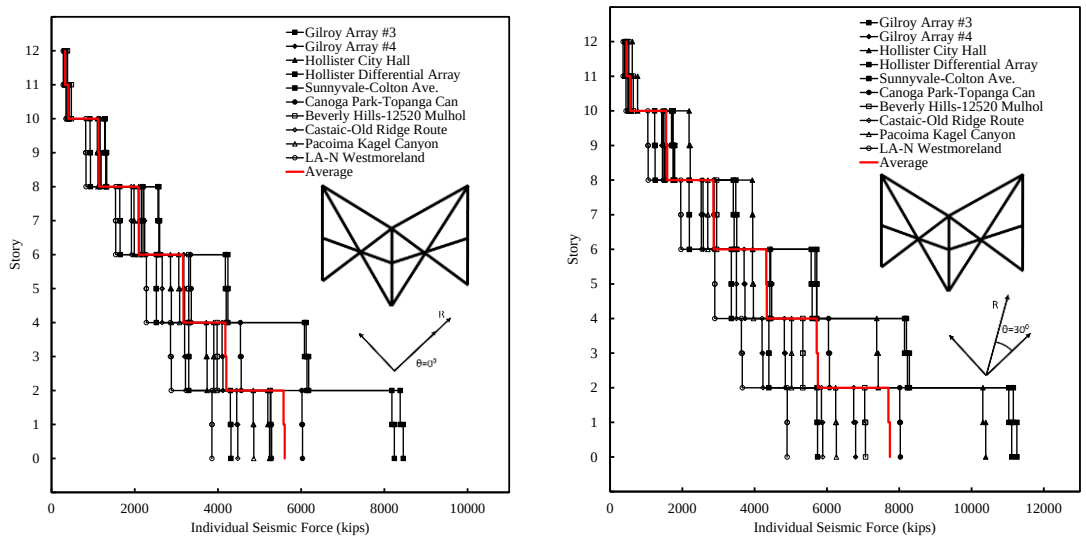

Figure C- 33. Individual Seismic Force for 12-Story Coupled Frames (BF-BF) [0^0, 30^0] [LA].

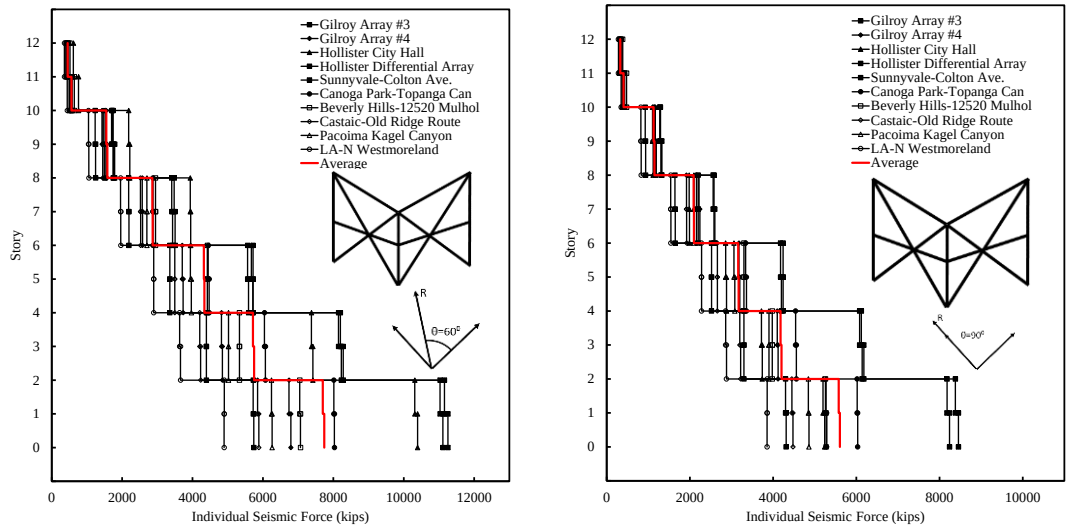

Figure C- 34. Individual Seismic Force for 12-Story Coupled Frames (BF-BF) [60^0, 90^0] [LA].

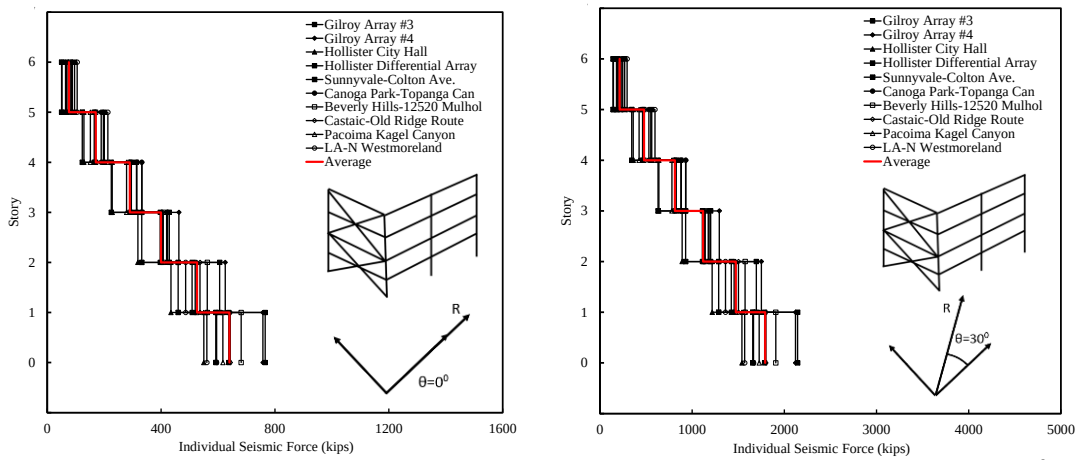

Figure C- 35. Individual Seismic Force for 6-Story Coupled Frames (BF-MF) [0^0, 30^0] [SLC].

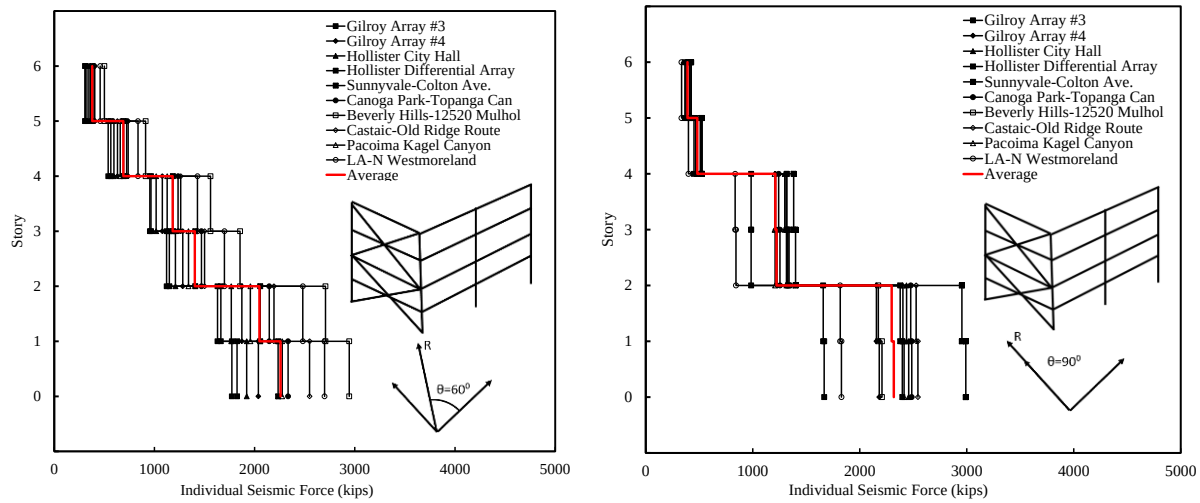

Figure C- 36 Individual Seismic Force for 6-Story Coupled Frames (BF-MF) [60^0, 90^0] [SLC].

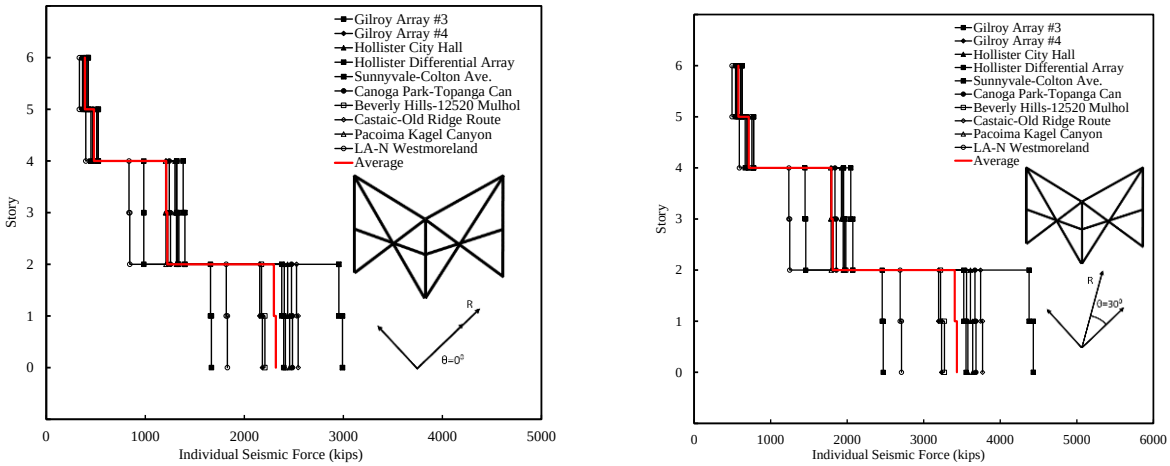

Figure C- 37F. Individual Seismic Force for 6-Story Coupled Frames (BF-BF) [0^0, 30^0] [SLC].

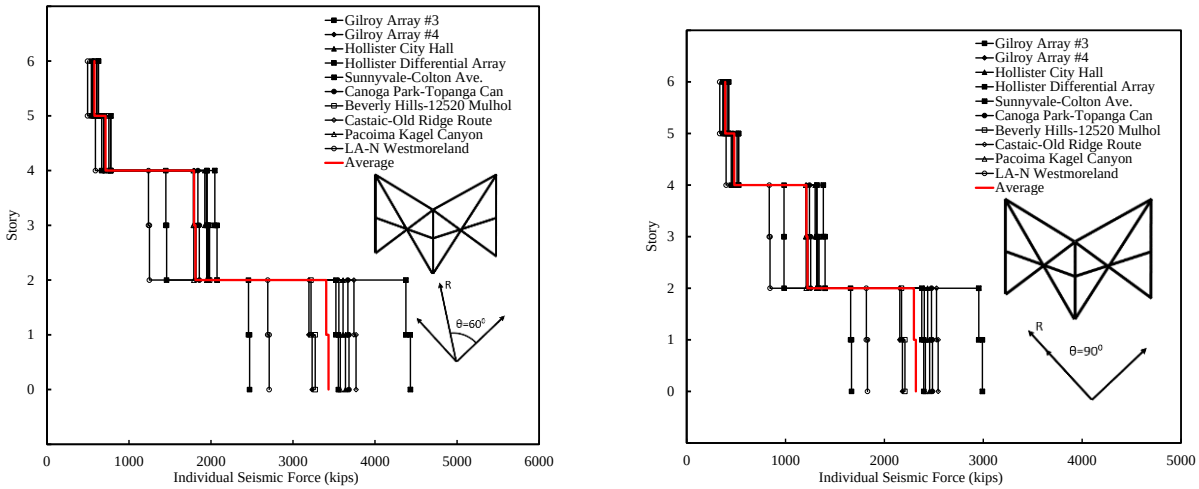

Figure C- 38. Individual Seismic Force for 6-Story Coupled Frames (BF-BF) [60^0, 90^0] [SLC].

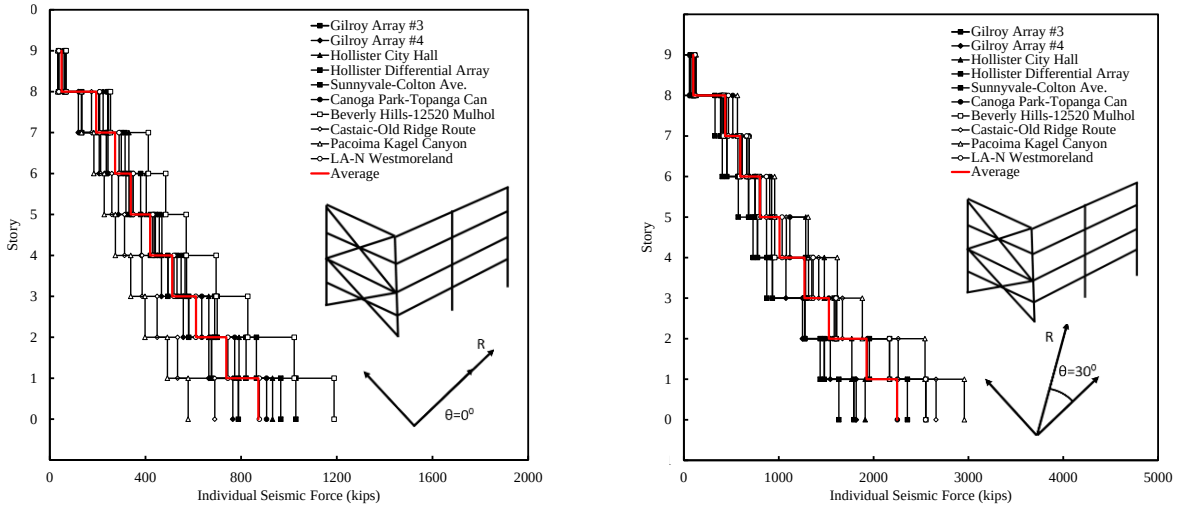

Figure C- 39. Individual Seismic Force for 9-Story Coupled Frames (BF-MF) [0^0, 30^0] [SLC].

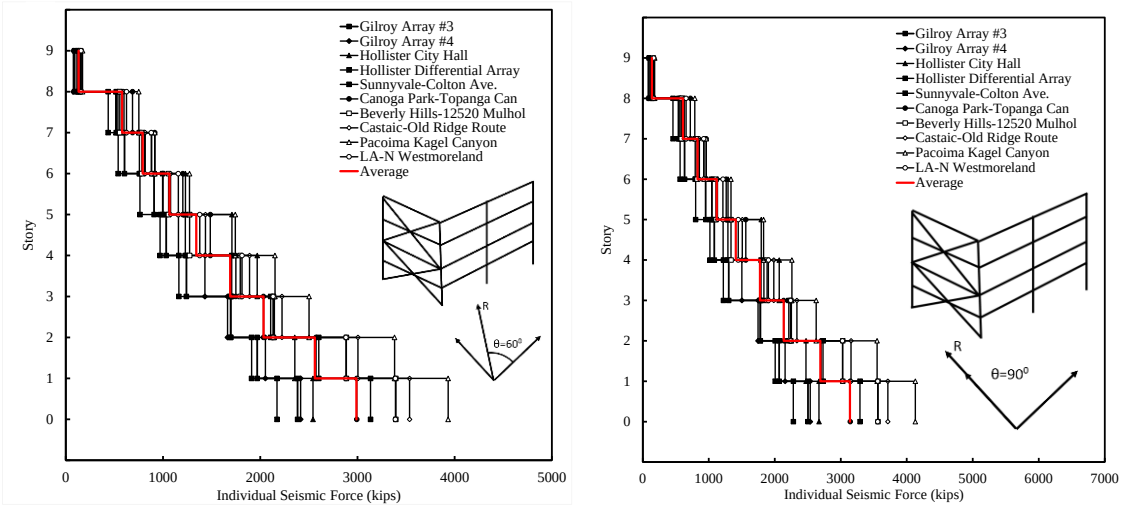

Figure C- 40. Individual Seismic Force for 9-Story Coupled Frames (BF-MF) [60^0, 90^0] [SLC].

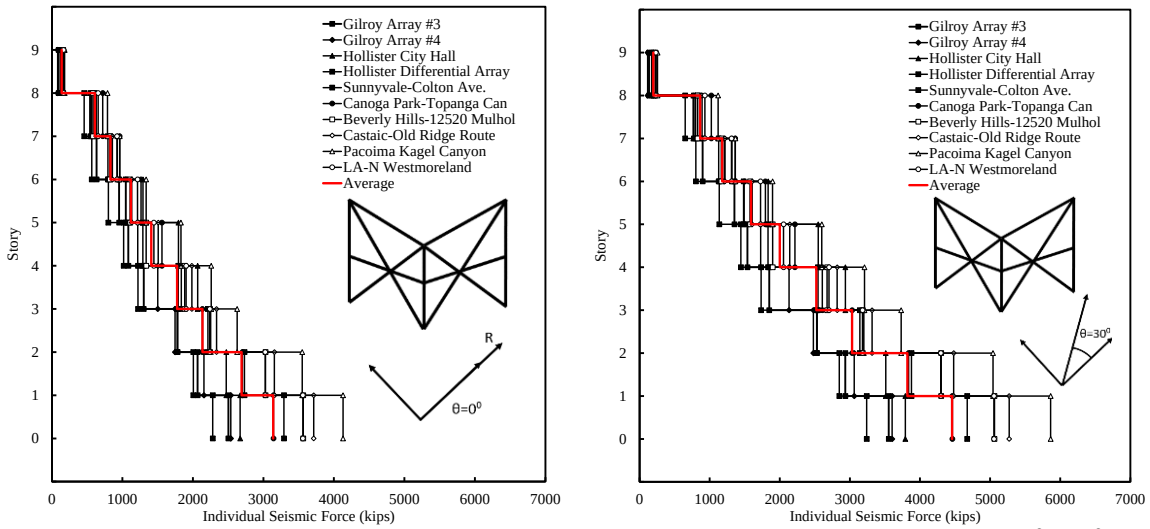

Figure C- 41. Individual Seismic Force for 9-Story Coupled Frames (BF-BF) [0^0, 30^0] [SLC].

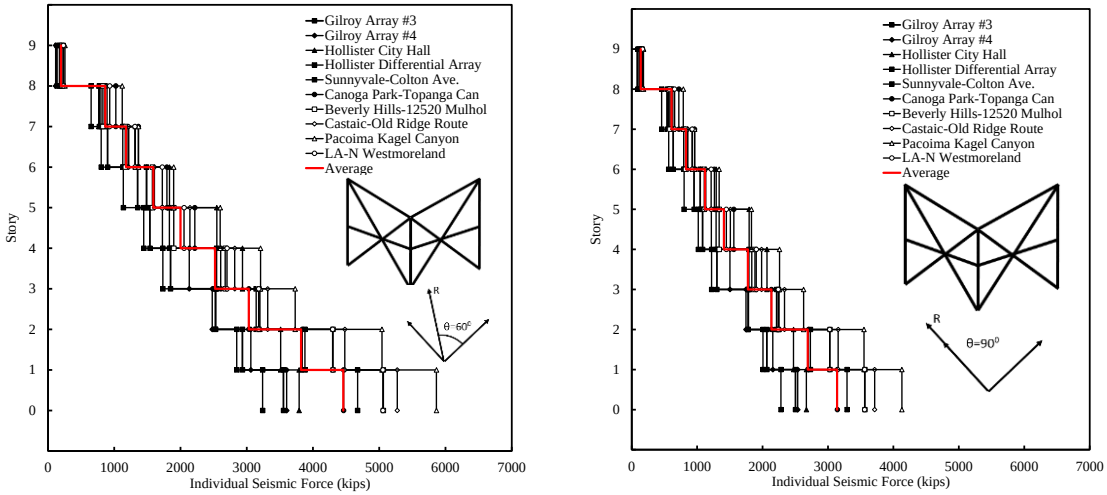

Figure C- 42. Individual Seismic Force for 9-Story Coupled Frames (BF-BF) [60^0, 90^0] [SLC].

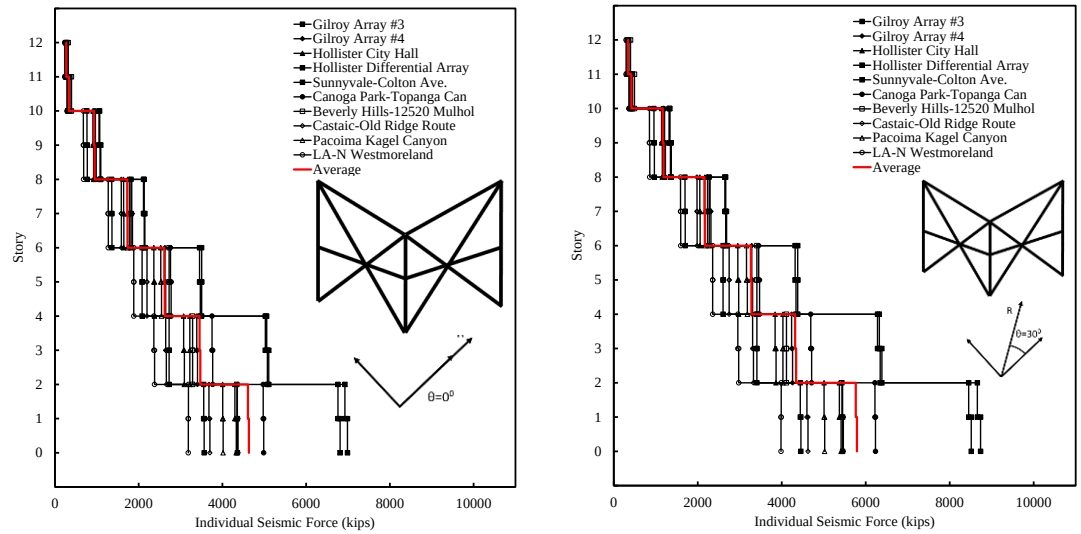

Figure C- 43. Individual Seismic Force for 12-Story Coupled Frames (BF-BF) [0^0, 30^0] [SLC].

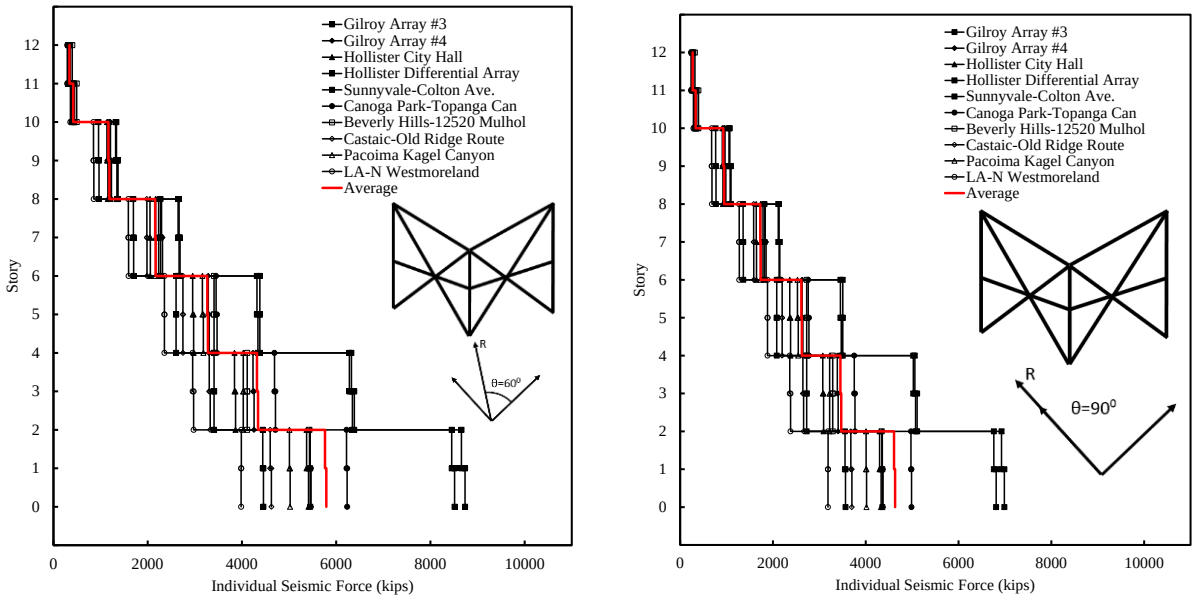

Figure C- 44. Individual Seismic Force for 12-Story Coupled Frames (BF-BF) [60^0, 90^0] [SLC].

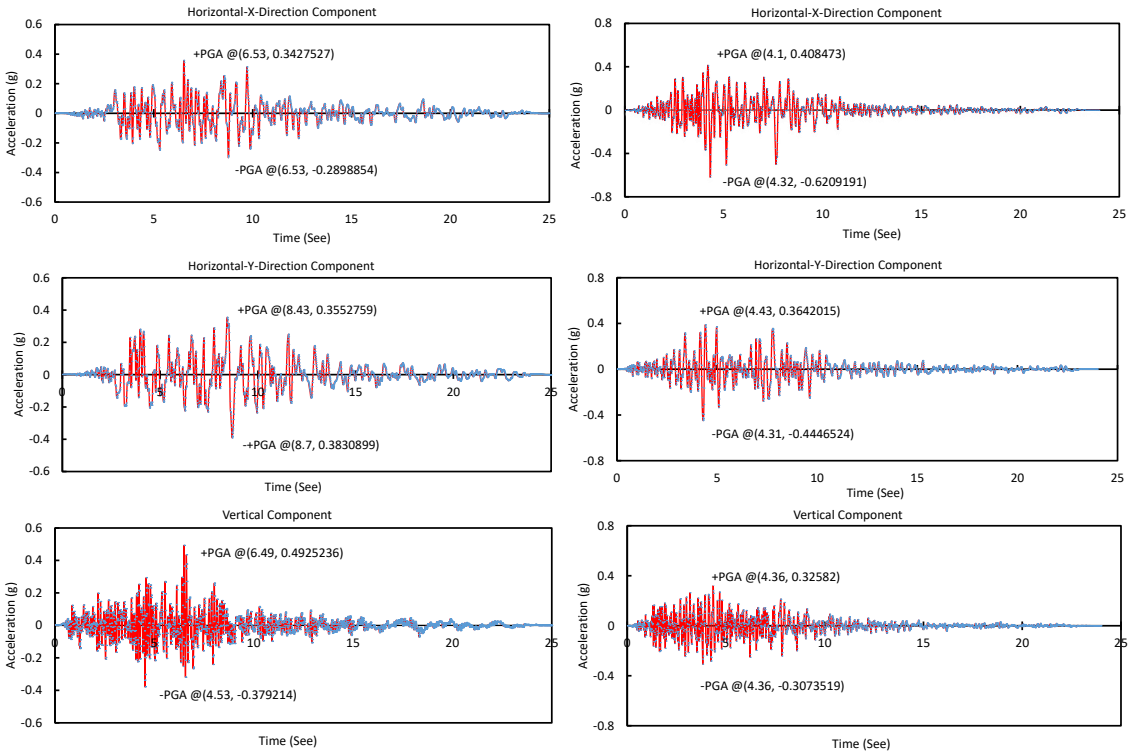

Figure C- 45. Horizontal and vertical directions of Northridge (Beverly Hills, Canoga Park).

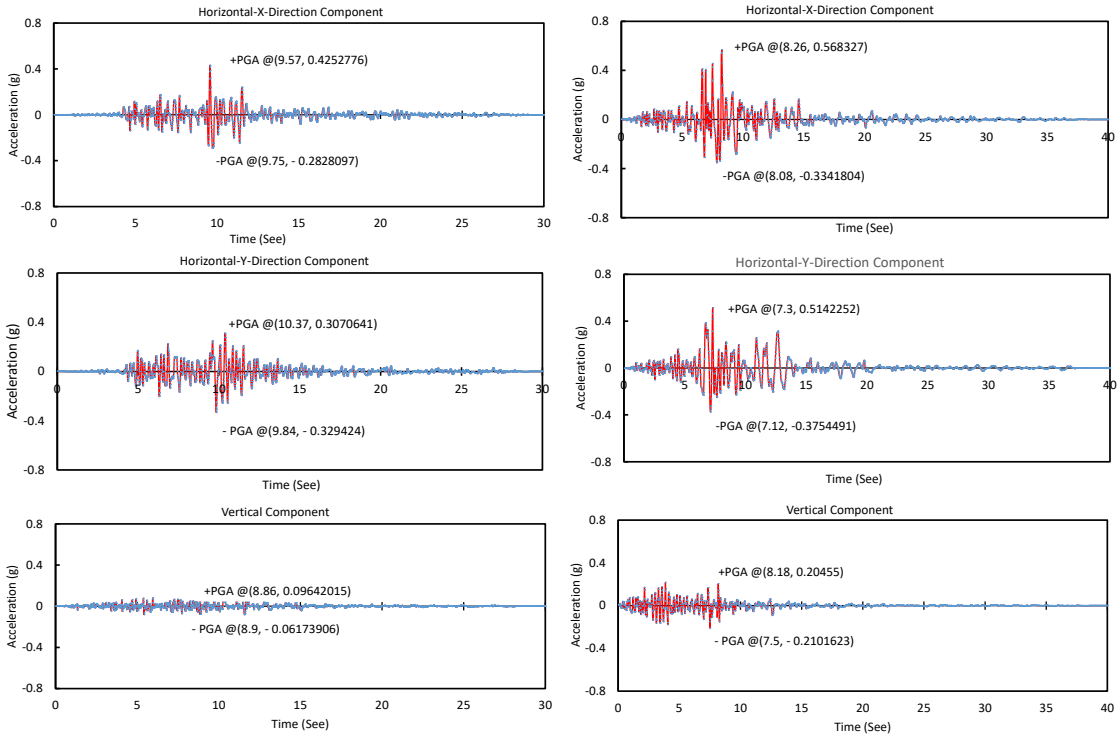

Figure C- 46. Horizontal and vertical directions of Northridge (Castaic-Old Ridge Route, LA-N Westmoreland).

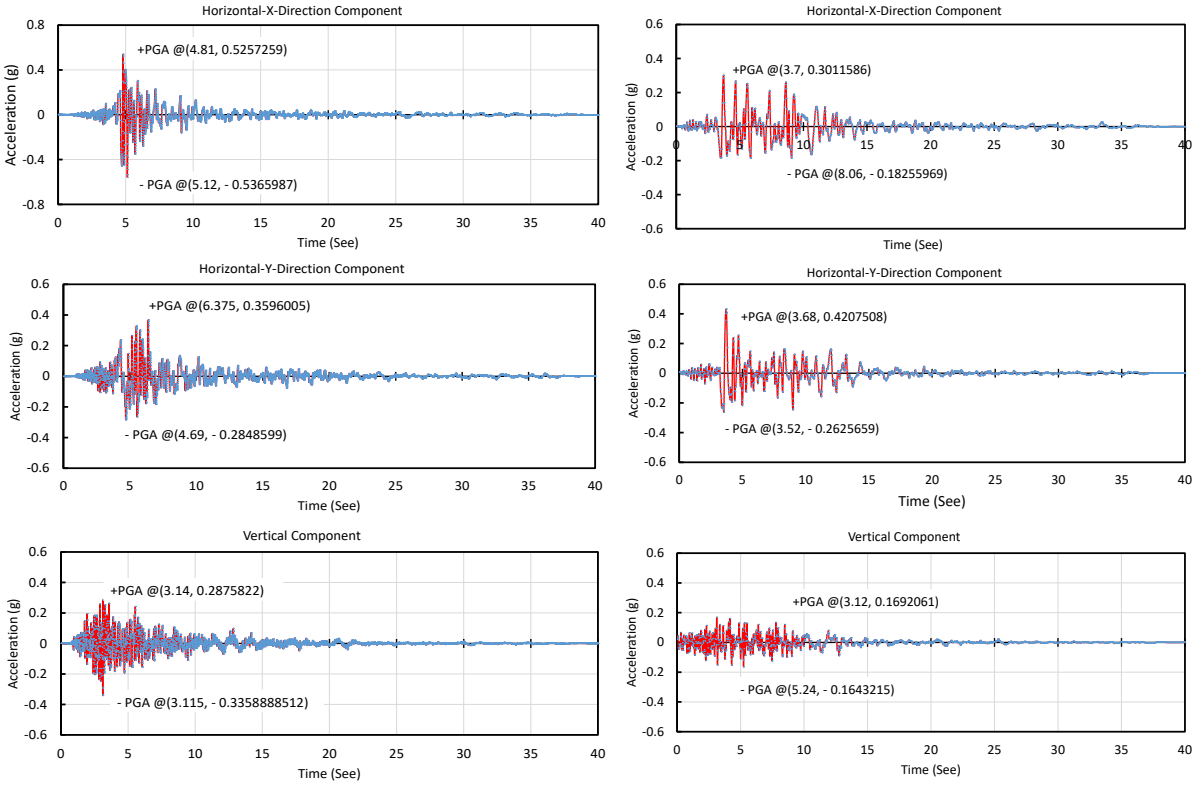

Figure C- 47. Horizontal and vertical directions of Northridge and Loma Prieta (Pacoima Kagel Canyon, Gilroy Array #3).

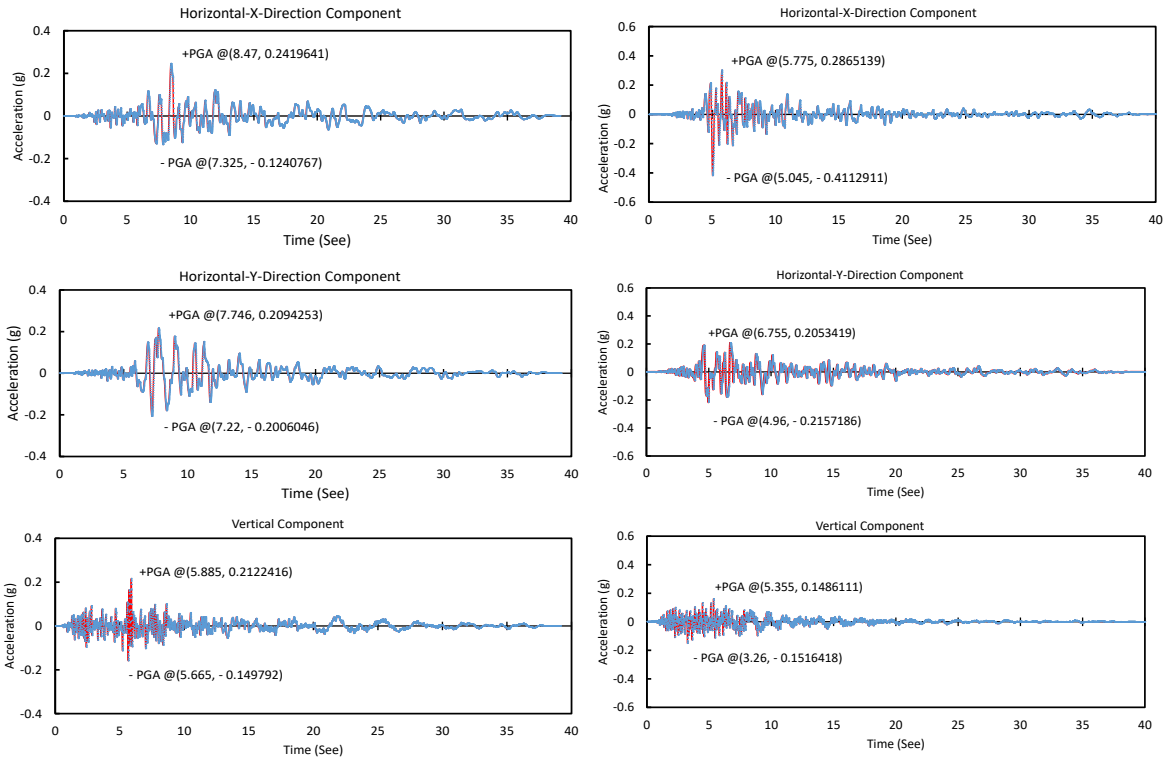

Figure C- 48. Horizontal and vertical directions of Loma Prieta (Gilroy Array #4, Hollister City Hall).

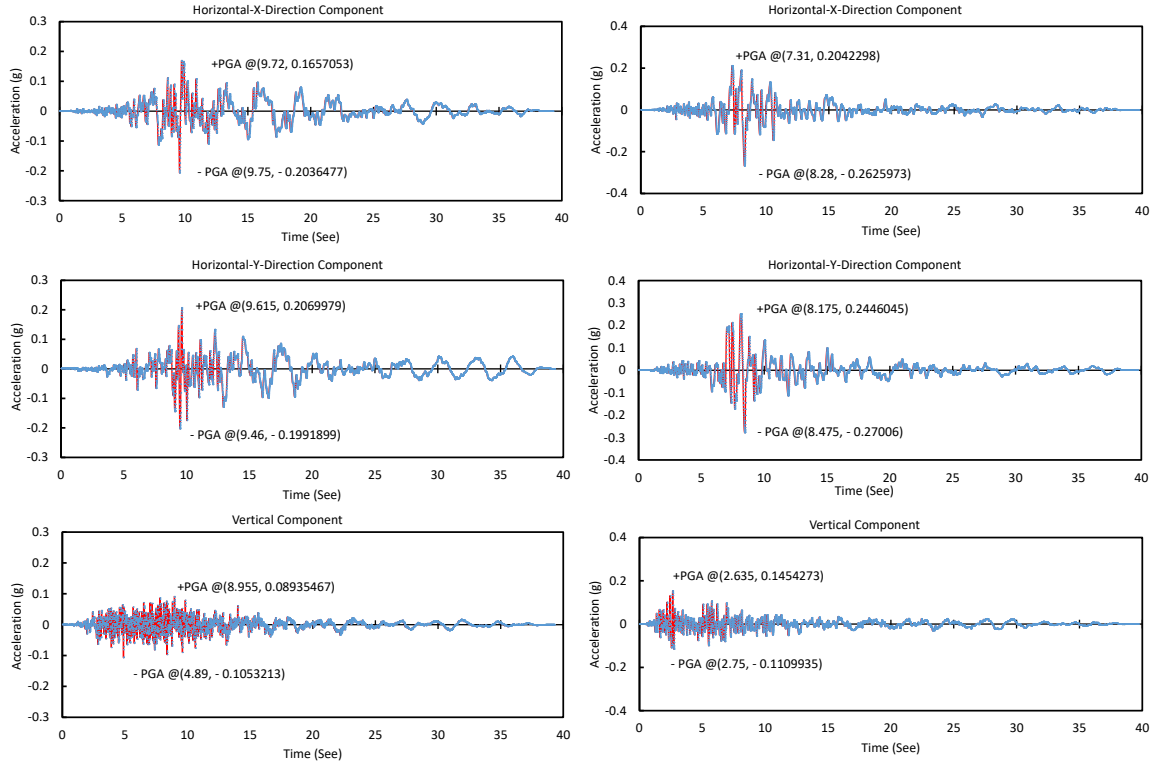

Figure C- *49.* Horizontal and vertical directions of Loma Prieta (Hollister Differential Array, Hollister Differential Array).